An investigation of the performance of a free-piston engine using Miller cycle and renewable fuels

LI, CHENGQIAN

An investigation of the performance of a free-piston engine using Miller cycle and renewable fuels

Thesis by

Chengqian Li

In Partial Fulfilment of the Requirements

for the Degree of

Doctor of Philosophy

Durham University

Durham

United Kingdom

February 2022

Abstract

A dual-piston type two-stroke spark-ignition free-piston engine prototype has been developed. A comprehensive review on recent published researches and patent documents from academia and industrial organizations on free-piston engine, especially the application of renewable fuels such as hydrogen and ethanol, was conducted. Relevant parameters affecting the operating performance and a number of challenges had been identified as the common denominator for this technology. Modelling and simulations using one-dimensional tools were conducted in parallel with the development activities. Three main simulation models for the crankshaft engines were developed, validated and optimised before converted into the free-piston engine model. This was done by using imposed-piston motion sub-model. The two-stroke free-piston engine model had undergone parametric study for valve timing optimisation. By using similar methods, a two-stroke hydrogen free-piston engine was developed from the prototype and it was validated by experimental data. Emission performance, along with the relationship between equivalent ratio, in-cylinder temperature and NOx emission on the hydrogen FPE was investigated. Series of ethanol-gasoline blend free-piston engine were developed, essential parameters such as compression ratio, air/fuel ratio and valve timing, etc., were amended for each model and both engine performance and emission performance were analysed. Miller cycle has been applied on three types of free-piston engine models: gasoline FPE, hydrogen FPE and ethanol FPE. Two types of Miller cycle (LIVC and EIVC) were both applied and analysed, and different late/early intake valve closing angles (from 5°CA to 35°CA) have been converted to specific time to apply on the free-piston engine. Engine performance and emission performance of Miller cycle free-piston engines have been obtained and individually presented. It turns out that large late/early intake valve closing angles (time) are not suitable in renewable free-piston engines due to the efficiency reduction.

Acknowledgements

I have been through a long journey, nineteen and a half years of study, and here, comes to the end.

I have been pursuing the dream, but failed; I have dreamt about being a poet, being the star that flashing in the sombre sky, being someone who contributes the entire race, but failed. Fortunately, I have never stopped. There's a saying that all your experience is study. Say not the struggle nought availeth, the labour and the wounds are vain, the enemy faints not, nor faileth, and as things have been, things remain.

I was born in a small southern city in China, and my parents are just conscientious worker and primary school teacher, but they tried to make me the luckiest boy in the world. They offered me a better life and a better brain for the past twenty-five years but never asked any payment, which I could never pay. No word is enough for presenting my gratitude, but only an indebted heart that never die.

Thank to Durham University, this beautiful historical university offered me this opportunity to complete my research and provided almost everything I need.

Three-and-a-half-year struggle in England, my supervisor, professor Tony Roskilly, has given me great support on the research. And Dr Yaodong Wang, who has been providing me for any support nor just in study but life always. For me, he is no longer a supervisor only, but also a kinsfolk, a guide in life. I also have to thank Boru Jia, who was a member of our research group, were always kind and helped me a lot.

I am also grateful for my girlfriend, Ying Zhong, who was a master student in Durham University as well. Thank to her company, meticulous love and care, I have been always able to keep happy, energetic and highly focus towards every-day tough research.

I must thank Shi Chen, another hard-working intelligent PhD student, my colleague, private driver, accompanier on the road of research, and the best friend in England, who has brought me countless happiness and meticulous care during the darkest moment.

I must thank my close friends, Yu Huang and Tinghao Mao. They brought me countless happiness and meticulous care and made me feel like home in this far away-from-home place.

I am appreciating to every staff in the college of engineering, my every email was responded in

extremely short time, every problem was solved in time. This thesis would not be completed without their help.

Sincere wish to everyone who has ever helped me.

Publication

Chengqian, Yaodong, Boru, Application of Miller cycle with turbocharger and ethanol to reduce NOx and particulates emissions from diesel engine – A numerical approach with model validations, Applied Thermal Engineering 150(2019)904-911

Content

Abstract I

Acknowledgements III

Publication VI

Content VII

List of figures XII

List of Tables XX

Chapter 1. Introduction 1

1.1 Background 1

1.2 The free-piston engine 2

1.3 Miller cycle 3

1.4 Renewable fuels 4

1.5 Aims and objectives 4

1.6 Methodology and thesis outline 5

Chapter 2. Literature review 7

2.1 The free-piston engine 7

2.1.1 History of the free-piston engine 7

2.1.2 Recent advances and application of the FPE 9

2.1.2.1 Free-piston engine linear generator 9

2.1.3 Different fuels on the FPE 25

2.1.3.1 Fossil fuel 25

2.1.3.2 Hydrogen 30

2.1.3.3 Biofuel 42

2.2 Miller cycle 47

2.2.1 Atkinson cycle 47

2.2.2 Miller cycle 50

2.3 Summary 59

Chapter 3. Single-cylinder gasoline FPE modelling and simulation 61

3.1 Theoretical review....61
3.2 Modelling approach and sub-models....63
3.2.1 Sub-models....64
3.2.1.1 Crank/slider piston motion....65
3.2.1.2 Imposed piston sub-model....66
3.2.1.3 Friction....67
3.2.1.4 Woschni heat transfer....68
3.2.1.5 SI Wiebe combustion....68
3.3 Modelling and simulation implementation....69
3.3.1 Baseline modelling, simulation and validations....71
3.3.2 Crankshaft engine model optimisation....73
3.3.2.1 Four-stroke model up-scaling and validation....73
3.3.3 Two-stroke model performance optimisation....75
3.3.3.1 Parametric study....76
3.3.3.2 Final optimisation....80
3.3.4 Two-stroke optimization results and discussions....81
3.3.4.1 The effect of intake boost pressure....81
3.3.4.2 The effect of intake and exhaust valves anchor....84
3.3.4.3 The effect of intake and exhaust valves duration....85
3.3.5 Summary....87
3.4 The free-piston engine modelling and validations....88
3.4.1 Dynamic balance equation of motion....88
3.4.1.1 Linear electrical machine....90
3.4.1.2 Cogging force....91
3.4.1.3 Frictional force....92
3.4.1.4 Compression-expansion process....93
3.4.2 The imposed piston motion modelling....93
3.4.3 Valve timing optimisation....94
3.5 Discussion....95

3.5.1 Effect of piston motion....95
3.5.2 Valve timings....98
3.5.3 In-cylinder pressure....102
3.6 Simulation results....104
3.7 Summary....106
Chapter 4. Single-cylinder hydrogen FPE modelling and simulation....108
4.1 Theoretical review....108
4.2 Hydrogen FPE modelling/validation and simulation implementation....110
4.2.1 Hydrogen FPE modelling....110
4.2.2 Model performance optimisation....117
4.3 Hydrogen free-piston engine model validation....119
4.3.1 Indicated power....119
4.4 Emission performance analysis....120
4.4.1 NOx emission....120
4.4.2 Regulation between NOx emission and equivalent ratio....123
4.5 Summary....125
Chapter 5. Single-cylinder Ethanol FPE modelling and simulation....127
5.1 Theoretical review....127
5.1.1 Ethanol effects of engine parameters....129
5.1.1.1 Effect of compression ratio....129
5.1.1.2 Effect of engine load....132
5.1.1.3 Effect of equivalence ratio....133
5.1.1.4 Effect of engine frequency (speed)....134
5.1.2 Ethanol-gasoline blend....135
5.1.3 Formation of NOx....140
5.1.3.1 Thermal NOx....141
5.1.3.2 Prompt NOx....141
5.1.3.3 Intermediate $\boldsymbol{N2O}$....142
5.1.3.4 Fuel NOx....143

5.2 Ethanol free-piston engine modelling and simulation implementation 143
5.2.1 Base parameters setting 143
5.2.2 Parametric study 147
5.3 Modelling results 151
5.3.1 Engine performance 151
5.3.2 Emission performance 154
5.4 Summary 157
Chapter 6. Miller cycle and its application on the FPE 158
6.1 Theoretical review 158
6.1.1 Concept of Miller cycle 158
6.2 Engine modelling 164
6.2.1 Miller cycle on the free-piston engine 164
6.3 Simulation results 165
6.3.1 Simulation results on the free-piston engine 165
6.3.1.1 Engine performance 166
6.3.1.1.1 Gasoline free-piston engine 166
6.3.1.1.2 Hydrogen free-piston engine 170
6.3.1.1.3 Ethanol free-piston engine 173
6.3.2.1 Emission performance 175
6.3.2.1.1 Gasoline free-piston engine 175
6.3.2.1.2 Hydrogen free-piston engine 178
6.3.2.1.3 Ethanol free-piston engine 178
6.4 Summary 181
Chapter 7. Conclusions and future research 183
7.1 Summary of the findings 183
7.2 Significant contributions and findings 185
7.3 Recommendations for further research 185
7.3.1 Practice experiment 185
7.3.2 Co-simulation 186

7.3.3 Miller cycle valve timing 186
Reference 187
Appendix 216

List of figures

Figure 2.1 Schematic representation of free-piston gas compressor and free-piston gas generator [25] 9
Figure 2.2 Schematic representations of three typical structures of FPELG [6,17] 10
Figure 2.3 The piston operation characteristic and Linear generator performance from FPEC [68] 14
Figure 2.4 FPELG performance of 2-stroke and 4-stroke from Newcastle University [80]. .. 15
Figure 2.5 FPELG performance in the SI-HCCI transition from Ulsan University [97] 19
Figure 2.6 The performance of FPELG at Toyota Central R&D Labs Inc [100,101] 19
Figure 2.7 The performance of FPELG at National Taiwan University of Science & Technology [102]. 20
Figure 2.8 P-V diagram and combustion process of FPELG from Chongqing Jiaotong University [116,117] 22
Figure 2.9 The natural frequency characteristic of FPELG from Shanghai Jiaotong University [118] 23
Figure 2.10 The combustion process of FPELG from Beijing Institute of Technology [42] .. 25
Figure 2.11 Predicated in-cylinder gas pressure [131] 26
Figure 2.12 Mean in-cylinder gas temperature [131] 26
Figure 2.13 Exhaust gas emissions for FPE and TCE [131] 28
Figure 2.14 Concentration of nitrogen oxide (NO) in the in-cylinder gases [132] 29
Figure 2.15 Effects of reductions in in-cylinder heat transfer losses on engine indicated efficiency and NO formation [132] 30
Figure 2.16 NO concentrations of the engines [145] 33
Figure 2.17 Combustion heat releases of the engines [145] 33
Figure 2.18 NO mass fractions [156] 35
Figure 2.19 NO mass fractions [157] 36
Figure 2.20 Formation of NO [157] 37
Figure 2.21 Soot mass fractions [157] 38

Figure 2.22 Pressure development in a mean two-stroke and four-stroke cycle [158] 39
Figure 2.23 NOx emissions from FPEG [158].....40
Figure 2.24 Work output along asymmetric piston trajectories, indicated by two Ωs (H2, AFR = 2, CR = 22, (b) is the zoom-in view of (a)) [159] 41
Figure 2.25 NOx emission along asymmetric piston trajectories, indicated by two Ωs (H2, AFR = 2, CR = 22) [159].....41
Figure 2.26 U.S. production, consumption and trade of ethanol [165].....45
Figure 2.27 The internal configuration of the Atkinson engine [170].....48
Figure 2.28 Working comparison of the Atkinson cycle with the standard cycle 48
Figure 2.29 P-V diagrams of the Miller cycle engine [181].....52
Figure 2.30 NOx comparison between Diesel cycle, Miller cycle and T-Miller cycle [221]..55
Figure 2.31 (a) p–V diagram; (b) T–S diagram for the air standard Miller cycle [119].....56
Figure 2.32 (a) The heat leakage percentage affected by the maximum cycle temperature;(b) the heat leakage percentage affected by the excess air coefficient [119] 57
Figure 2.33 Comparison of optimal and conventional piston motion curves for the STD case [119] 58
Figure 2.34 Comparison of optimal and conventional thermodynamic curves for the STD case [119] 59
Figure 3.1 Cylinder geometry definitions for an engine with a flat top piston (Without the bowl) 62
Figure 3.2 Three primary sub-programs in Ricardo WAVE programs suite employed in this research. 63
Figure 3.3 Basic model variables and initial conditions 64
Figure 3.4 Crank-slider mechanism schematic [225].....65
Figure 3.5 Profile editor for piston motion profile to model free-piston engine.....67
Figure 3.6 SI Wiebe combustion sub-model 69
Figure 3.7 Types of models developed for the research.....70
Figure 3.8 Baseline model of 31cc Stihl 4MIX engine in Ricardo WAVE. 72
Figure 3.9 Power curves comparison from experimental result and as obtained from Ricardo

WAVE simulation....72
Figure 3.10 HC+NOx emissions comparison from experimental result and as obtained from Ricardo WAVE simulation....73
Figure 3.11 Fitted power curve of the four-stroke 65cc engine as obtained from Ricardo WAVE simulation....75
Figure 3.12 General timing diagram for two-stroke cycle....76
Figure 3.13 The experiments panel in Ricardo WAVE which was used during the parametric investigations for model tuning....77
Figure 3.14 The experiment analysis panel showed-up at the end of the experiments in Ricardo WAVE....79
Figure 3.15 The sweep case generator panel used for refined optimizations....80
Figure 3.16 Boost pressure effect on brake thermal efficiency(bte)....82
Figure 3.17 Boost pressure effect on brake power....83
Figure 3.18 Boost pressure effect on brake mean effective pressure(bmep)....83
Figure 3.19 Valves anchor positions effect on brake thermal efficiency(bte)....84
Figure 3.20 Valves anchor positions effect on brake power....85
Figure 3.21 Valves anchor positions effect on brake mean effective pressure(bmep)....85
Figure 3.22 Valves duration effect on brake thermal efficiency(bte)....86
Figure 3.23 Valves duration effect on brake power....86
Figure 3.24 Valves duration effect on brake mean effective pressure(bmep)....87
Figure 3.25 Final valves timings for the 65cc two-stroke crankshaft engine....88
Figure 3.26 Free-body diagram of the dual piston free-piston engine generator dynamic model....89
Figure 3.27 Typical profile of cogging force vs. position of a linear motor....92
Figure 3.28 The input panel for imposed piston sub-model....94
Figure 3.29 Piston position against crank angle comparison for free-piston engine (FPE) and crankshaft engine (CSE)(a)At 50 Hz and (b) At 10Hz....96
Figure 3.30 Piston velocity against piston position comparison for FPE and CSE(a) At 50Hz and (b) At 10Hz....98

Figure 3.31 Optimised intake and exhaust valves timing for FPE and CSE(a) Crank angle-based(b) Piston position-based....99
Figure 3.32 Variation of valve opening and closing timing at different speeds for the free-piston engine model(a) Exhaust valve(b) Intake valve....101
Figure 3.33 Valve opening and closing positions for free-piston engine....102
Figure 3.34 P-V diagram comparison between (a)FPE and (b)CSE at 80Hz....103
Figure 3.35 Brake power comparison for both models....104
Figure 3.36 HC emission comparison for both models....105
Figure 3.37 NOx emission comparison for both models....105
Figure 4.1 Piston motion vs min time in Hydrogen FPE model....111
Figure 4.2 Pre-set piston motion data in Ricardo WAVE....112
Figure 4.3 Fuel and air properties panel in Ricardo WAVE....113
Figure 4.4 Fuel Property Tag Selector in Ricardo WAVE....114
Figure 4.5 Cylinder panel in Ricardo WAVE....115
Figure 4.6 Air/fuel ratio pre-set in the injector panel....117
Figure 4.7 The experiment analysis panel showed-up at the end of the experiments in Ricardo WAVE....118
Figure 4.8 Indicated power for four-stroke FPE....119
Figure 4.9 Indicated power comparison between WAVE model and experimental data....120
Figure 4.10 NOx emission of two-stroke hydrogen free-piston engine model....121
Figure 4.11 NOx emission comparison between three models....122
Figure 4.12 Highest in-cylinder temperature of Gasoline FPE and hydrogen FPE....123
Figure 4.13 NOx emission with different equivalent ratio....124
Figure 4.14 Highest mean in-cylinder temperature with equivalent ratio....125
Figure 5.1 Relation between compression ratio accumulator pressure Pc, injection timing $tinj$ and the effective compression ratio ε [247]....130
Figure 5.2 The influences of the compression accumulator pressure and the start of fuel injection [247]....131
Figure 5.3 Correlation of NOx and HC emission with ethanol percentage at 2000 rpm [265]

.....138
Figure 5.4 Correlation of NOx and HC with the percentage of ethanol at 3500 rpm [258]..140
Figure 5.5 Fuel panel in Ricardo WAVE.....144
Figure 5.6 Simulink model for the ethanol FPE model.....145
Figure 5.7 Parameters in MATLAB.....146
Figure 5.8 Piston motion pre-set in Ricardo WAVE.....147
Figure 5.9 The experiments panel in Ricardo WAVE which was used during the parametric investigations for model tuning.....148
Figure 5.10 The experiment analysis panel simulation processes and results.....150
Figure 5.11 Brake power of different ethanol-gasoline blend concentration.....152
Figure 5.12 BSFC of different ethanol-gasoline blend concentration.....153
Figure 5.13 Brake thermal efficiency of different ethanol-gasoline blend concentration.....153
Figure 5.14 In-cylinder temperature comparison.....154
Figure 5.15 NOx emission of different ethanol-gasoline blend concentration and gasoline.155
Figure 5.16 CO emission of different ethanol-gasoline blend concentration and gasoline...156
Figure 5.17 HC emission of different ethanol-gasoline blend concentration and gasoline...157
Figure 6.1 P-V diagram compared between LIVC Miller cycle and Diesel cycle. 159
Figure 6.2 EIVC Miller cycle P-V Diagram 161
Figure 6.3 Turbocharger fixed compressor panel.....162
Figure 6.4 Turbo shaft panel 163
Figure 6.5 Turbocharger fixed turbine panel.....164
Figure 6.6 Different Miller cycle intake valve timing on hydrogen FPE.....165
Figure 6.7 Indicated power comparison of different LIVC angles.....166
Figure 6.8 BSFC of different turbo-charged LIVC comparison 168
Figure 6.9 Indicated power of different turbo-charged EIVC comparison 169
Figure 6.10 Indicated power comparison of different types of Miller cycle.....171
Figure 6.11 BSFC comparison of different types of Miller cycle.....172
Figure 6.12 Indicated efficiency of different types of Miller cycle.....172
Figure 6.13 Indicated power comparison of different Miller cycle.....173

Figure 6.14 BSFC comparison of EIVC and LIVC 174
Figure 6.15 Indicated efficiency comparison of EIVC and LIVC 175
Figure 6.16 NOx emission comparison of different EIVC and LIVC.....176
Figure 6.17 HC emission comparison of different EIVC and LIVC.....177
Figure 6.18 CO emission comparison of different EIVC and LIVC.....177
Figure 6.19 NOx emission comparison of different LIVC angles 178
Figure 6.20 NOx emission comparison of different EIVC and LIVC.....179
Figure 6.21 HC emission comparison of different EIVC and LIVC.....180
Figure 6.22 CO emission comparison of different EIVC and LIVC.....180

List of Tables

Table 2.1 Advantages and disadvantages of different typical types of FPELG [6,17] 11

Table 2.2 The influence of the parameters on the performance of FPELG [11] 12

Table 2.3 Performance comparison of 2–4 stroke FPELG [80] 15

Table 2.4 The performance of FPELG under SI and HCCI combustion mode respectively [88] 16

Table 2.5 Measurement Data ZK02 SI-HCCI mode [89] 17

Table 2.6 Comparison of the prototype and the simulation results of FPELG [120] 23

Table 3.1 Empirical design data for valve capacity and head design in relation to the actual design for the 31cc and 65cc Stihl 4MIX engines 74

Table 4.1 Hydrogen FPE prototype specifications 108

Table 4.2 Baseline model operating parameters 109

Table 5.1 Comparison of gasoline and ethanol fuel properties [246] 128

Table 5.2 Properties of different ethanol–gasoline blended fuels [246] 135

Table 6.1 Indicated power of different turbo-charged LIVC comparison 166

Table 6.2 BSFC of different turbo-charged LIVC comparison 167

Table 6.3 Indicated power of different EIVC comparison 169

Chapter 1. Introduction

1.1 Background

Under the current trend of serious shortage of electric energy and serious air pollution, basic automobile engines with uneconomical scale and high emission can no longer meet the obvious requirements of energy saving and consumption reduction [1,2]. The key to the operation of traditional gas turbines is the ignition of hydrocarbons in the cylinder, and the incineration of hydrocarbons will cause a lot of industrial waste gas, such as carbon monoxide (CO), carbon dioxide (CO2), nitrogen oxides, etc. (NOx), smoke and fine particulate matter (PM) and other harmful metallic materials [3,4]. These unclean ignited substances create many environmental pollution problems, thus posing a threat to the earth and people. In addition, the increase in the total number of vehicles has accelerated the rate of fossil fuel consumption. Therefore, there is a strong motivation to find a replacement for an environmentally friendly and energy-saving engine or a gas turbine. A recent report by the New Energy Technology Institute (ETI) highlighted those light vehicles contribute about 16% of France's CO2 consumption [5]. Some have suggested that a radical way to reduce such emissions is to use new energy electric vehicles and phased out internal combustion engines. The less risky route is by using a combination of different fuel types such as bio-fuel and ethanol as well as increasing hybrid vehicle use on the road. And also, as a potential renewable fuel, hydrogen has great advantages of ultra-low pollution and high efficiency for internal combustion engine, as well as long-term availability [6-9].

At the same time, the free-piston engine (FPE) was born in such a situation [10]. The new engine revolutionizes the crank and connecting mechanism of the traditional gas turbine, thereby reducing friction damage, improving thermal efficiency, and exercising with a variable compression ratio, giving a flexible scope of application of natural materials and the possibility of new cleaning and ignition methods [11-13]. This potential advantage of FPE creates a broad range of primary uses. It can not only be used as the propulsion system hardware of hybrid new energy electric vehicles or

electric vehicles, but also can be used as auxiliary driving force for mechanical equipment [14].

1.2 The free-piston engine

A free-piston engine is an automobile engine that operates without an engine crankshaft or any other rotating mechanism. As a common power system, tubular gas turbines with engine crankshaft system hardware are widely used. However, this kind of engine crankshaft system hardware automobile engine has the defects of complicated structure, long mechanical equipment transmission chain, large friction damage, high heat transfer efficiency and inferior [15]. Consequently, scientific researchers are still diligently improving the characteristics of rotating gas turbines containing engine crankshaft system hardware [16]. At the same time, they are also actively promoting new power electronic devices [17]. For rotary table gas turbines, the engine crankshaft system hardware significantly compromises the characteristics and high efficiency of the gear transmission. High friction damage is caused by piston side forces caused by the engine crankshaft system hardware. In addition to this, this automotive engine has an extremely complex configuration caused by the engine crankshaft system hardware [18]. Therefore, in the search for a new powertrain, the engine crankshaft system hardware was eliminated. For the new power system, the free-piston engine is the classic means of linear power system [19]. The reciprocating motion of the FPE is "free" because it is not limited by the engine crankshaft system hardware. Therefore, FPEs have the advantages of simple structure, high heat transfer efficiency, extremely low friction damage, various engine compression ratios, and feasibility analysis of various natural materials [6]. In addition, the type of power can be changed by coupling the FPICE with different heat transfer equipment. For example, electromagnetic energy [4], hydraulic function [20], or mechanical energy [15,21] is generated when FPEs are individually coupled to linear generator sets, hydraulic transmission systems, or specialized mechanical structures.

The definition of the free-piston engine has a long history, and its definition originated from the Otto-Langen air free piston engine in 1867 [8,9]. These early prototypes of free-piston engines were dedicated to the use of rack-and-pinion and transmission gear mechanisms to complete rotational applications. One of the main problems with this type of equipment is the inability to keep the circulatory system operational. Afterwards, this problem was solved by using the crank-slider

mechanism for the actual operation of the circulation system and the gears as the energy storage technical equipment to maintain the actual operation of the circulation system. This type of equipment forms the basis for cranking automotive engines for engines used in gas turbine (IC) applications. With increasing concern on global warming and sustainability, crankshaft IC engine technology has been under intense scrutiny due to its relatively low efficiency and poor exhaust gas emissions. The efficiency of modern internal combustion engines for HEV applications is reported to be 30-37% SI and 40% CI [22]. Accordingly, there has been a search for a replacement prime mover, especially one that can impart more efficiency and lower emissions for hybrid vehicle applications; namely, a free-piston engine generator set. The allure of the free-piston engine depends on its great advantages, such as high power-to-weight ratio, high working capacity, low cost of manufacturing, low maintenance (because of few components and simplicity of mechanical equipment) [6],[23]-[25]. When closely combined with linear generator sets and energy storage systems, this technology can meet the main requirements of new energy electric vehicles or auxiliary power systems [26]. In addition, the lack of a crankshaft and gears in the engine can result in higher thermal efficiency and can operate at different engine compression ratios. In tests of rapidly scaled centrifugal compressors, it has been reported that the stated thermal efficiency can reach 56% [27].

1.3 Miller cycle

Traditional reciprocating IC engines use four strokes, two of which can be considered powerful: the compression stroke (the high-power flow from the engine crankshaft to the pump) and the power stroke (the high-power flow from the ignition gas to the engine crankshaft).

In the Miller cycle, the intake valve is open longer or shorter than in the Otto cycle of a car engine. In fact, the compression stroke is a cyclic system of two discrete variables: the original part when the intake valve opens and the last part when the intake valve closes. These two-stage intake four-strokes contributed to the introduction of the Miller Cycle into a "fifth" four-stroke. When the piston initially moves up on the traditional compression stroke, part of the pumping is expelled through the still-open bypass valve. Often, the loss of such pressure-increasing gas results in a loss of output power. Nevertheless, in the Miller cycle, this can be compensated according to the application of the supercharger. The supercharger usually has to be of the positive displacement (Roots or screw)

type as it can cause increased pressure at relatively low car revs. Otherwise, the low-speed ratio output power will be compromised. Or, if you don't need to operate at low rpm, or with a motor, you can use a supercharger to improve work efficiency.

In a Miller cycle car engine, the piston gradually shrinks the gasoline-diesel-gas mixture only after the intake valve is closed; and the bypass valve closes after the piston has moved a certain distance above its bottom end: Probably 20% to 30% of the total piston travel that should go up the four-stroke. Thus, in a Miller cycle automotive engine, the piston actually shrinks the gas-gas mixture only during the last 70% to 80% of the compression stroke. At the beginning of the compression stroke, the piston pushes a portion of the gas-fuel mixture through the still-open bypass valve, and then back into the intake manifold.

1.4 Renewable fuels

Ethanol is a renewable natural material made from various plant raw materials, commonly known as "biomass fuel". "More than 98% of American motor gasoline contains ethanol, usually E10 (10% ethanol, 90% motor gasoline), which is used for air oxidation of the fuel to reduce environmental pollution. hydrogen (H2) is an alternative fuel that can be produced from diverse renewable resources. Although the sales market for hydrogen as a natural material is still in its infancy, government departments and fields have made efforts to create hydrogen production for clean, economic development and safety Manufacture and distribution for general use in hydrogen fuel cell new energy electric vehicles (FCEVs). Light-duty FCEVs are currently in limited market demand in China and parts of the world. Buses, raw material equipment handling (such as electric forklifts), road support equipment, small and medium-sized and heavy trucks, boats and stationary applications sales markets are also developing [28]. The use of renewable natural materials in FPE has hardly been mentioned in past discussions. Therefore, in this thesis, ethanol and hydrogen are considered as the replacement renewable natural materials introduced into FPE, and the characteristics and exhaust characteristics of the automobile engine are described.

1.5 Aims and objectives

This research will focus on a spark-ignited dual piston type FPE, and aims to analyse the basic

emission performance of the spark-ignited dual piston type FPE prototype developed in Durham University, optimise the emission performance and identify the best emission performance condition. The main objectives of the study are as follow:

- To develop a detailed numerical model for the engine;
- To calibrate and validate the model against test results from the prototype;
- To apply Miller cycle into the FPE and analyse the emission performance to identify factors and variables that will influence the engine emission characteristics;
- To identify the best valve timing of the Miller-FPE that produce the least emission
- To utilise renewable fuel (ethanol and hydrogen) in both conventional FPE and Miller-FPE, and to analyse their emission performance and identify the best operating condition

1.6 Methodology and thesis outline

The content of the thesis was organized according to the methodology of the research and comprised of the following chapters:

Chapter 2 introduces the free-piston engine generator fundamental principles and then presents literature review on the parameters and challenges in the area as reported by major research groups worldwide. In addition, this chapter includes the introduction of Miller cycle, presents literature review on previous work on Miller cycle research and achievements till now. Also presents literature review on renewable fuel (ethanol and hydrogen) application in both conventional engines and the FPE.

Chapter 3 describes the development of four main simulation models using one-dimensional simulation tools. All models were a single cylinder engine. Both four-stroke crankshaft engine models had been validated while the two-stroke crankshaft engine model was optimised for performance through parametric investigations. The final optimised two-stroke crankshaft engine model was converted into the two-stroke free-piston engine model by using the imposed-piston motion (IPM) sub-model. The free-piston engine model was optimised for maximum performance and the findings are discussed.

Chapter 4 describes a Ricardo WAVE hydrogen free-piston engine developed from the baseline model. This chapter presents the whole process of modelling, validation, implementation and simulation. The hydrogen free-piston engine model is validated by existing experimental data, and both engine output performance and emission performance were analysed.

Chapter 5 presents series of ethanol-gasoline blend free-piston engine models developed from the baseline model. Essential parameters such as compression ratio, equivalence ratio, etc., were amended, and piston motion file was obtained from a MATLAB/Simulink model. Ethanol blends from 5% to 100% were all simulated, and both engine performance and emission performance of this ethanol-gasoline blend free-piston engine were analysed.

Chapter 6 describes the whole process of Miller cycle application on the conventional diesel engine and free-piston engines that presented in the above chapters. Both possibilities of late intake valve closure (LIVC) and early intake valve closure (EIVC) were tested and applied, and different late/early intake valve closing angle from 5°CA to 35°CA were analysed. Miller cycle application on different types of conventional engine and free-piston engine was investigated, and the advantages and disadvantages were discussed on the basis of the engine performance and emission performance results.

Chapter 7 summarised the main process, contributions and findings over the above six chapters, and several recommendations and concerns for further researches were raised.

Chapter 2. Literature review

This chapter presents a literature review of the free-piston engine fundamental information and recent research development on the free-piston engine (FPE). From the recent patents and publications, the previous work on numerical modelling, prototype design and test, emission performance analysis, as well as emission characteristic of different fuel are summarised and presented in this chapter. This review aims to provide an overview of previous research in this area, and identify the challenges to be acknowledged to the prototype development in Durham University.

2.1 The free-piston engine

The free-piston engine is a linear heat transfer system hardware, the technical term "free-piston" is commonly used to distinguish its linear characteristics from traditional reciprocating automobile engines [6]. Not limited by the engine crankshaft organization already known for conventional car engines, the piston can sway freely in the middle of its dead centers. The piston component is the only major moving component of the FPE, and its movement is due to the exhaust gas and load forces acting on it [29]. In this section, the basic information of FPE is introduced in detail, and the possible FPE loads and different FPE equipment are briefly described as well as the future development of FPE by various international teams.

2.1.1 History of the free-piston engine

FPICE started with a free piston engine (FPE). In order to better get rid of the many pitfalls caused by the engine crankshaft and crankshaft system hardware of automobile engines, FPE was scientifically researched. Pescara [29] is generally credited as the inventor of the free piston engine, and his exclusiveness dates to 1928, but other distributors, mainly Junkers in France, were also researching free piston machinery at this time. Since then, many patents have been issued describing or relating to the free-piston machinery. Pescara's original patent described a single-piston- flame-fired air compressor, but the patent was dedicated to maintaining the standard of use for many applications with free piston s. Pescara gradually researched free piston engines around 1922 and developed prototypes with flame ignition (1925) and diesel ignition (1928). The latter has resulted

in the development trend of Pescara free piston air compressors [30]. Pescara again worked at the level of free piston machinery and in 1941 patented a multi-level free piston air compressor for automotive engines [31]. The prototype of the FPE was designed in 1925 as a spark ignition (SI) FPE, and in 1928, the design was a reduced ignition FPE [32]. Various FPEs have been developed since the 1930s. According to the main use, it can be divided into two types: free piston engine gas compressors and free piston engine gas generators, as shown in Figure 2.1 below [25]. Free piston air compressors are derived from Pescara's compression ignition FPE. Next, the four-stage free piston engine gas compressor was developed by the French Junkers company in the middle and late 1930s and was used in German submarines during World War II [30]. After World War II, the analytical staff in Worthington, England, carried out scientific research on the free piston gas compressor of the opposed piston engine, and chose the compression ignition method. The test results show that the engine compression ratio of the free piston engine gas compressor of the opposed piston engine can reach 40 under the promotion of the air compression of the multi-component reduction equipment.

Gradually the whole process. In addition, the volume of the opposed-piston free-piston air compressor is about half of that of the traditional electric air compressor. Therefore, the opposed-piston free-piston gas compressor is particularly suitable for submarine applications [33,34]. Nevertheless, the free piston air compressor has not been widely used because of its narrow scope of use and the fact that it can use a lower motor to drive the refrigeration compressor [35]. Regarding the free piston engine gas generator, the key principle is the same as that of the free piston engine gas compressor. However, the principle is slightly different in that the compressed air of the free piston engine gas generator does not work immediately. Free piston engine gas generators coupled with gas turbines have high power [6]. The GS-34 free piston engine gas generator of the French SIGMA design has been used in power plants for many years. The CS-75 free piston engine gas generator was developed and designed by the British free piston engine company [36]. In addition, General Electric Vehicles and Ford Motor Company developed and designed prototypes of free piston engine gas generators [37,38]. Nevertheless, FPE (including free piston engine gas compressors and free piston engine gas generators) were discontinued in the 1960s due to their lower rationality and stability of gasoline and diesel compared to rotary disk gas turbines [6].

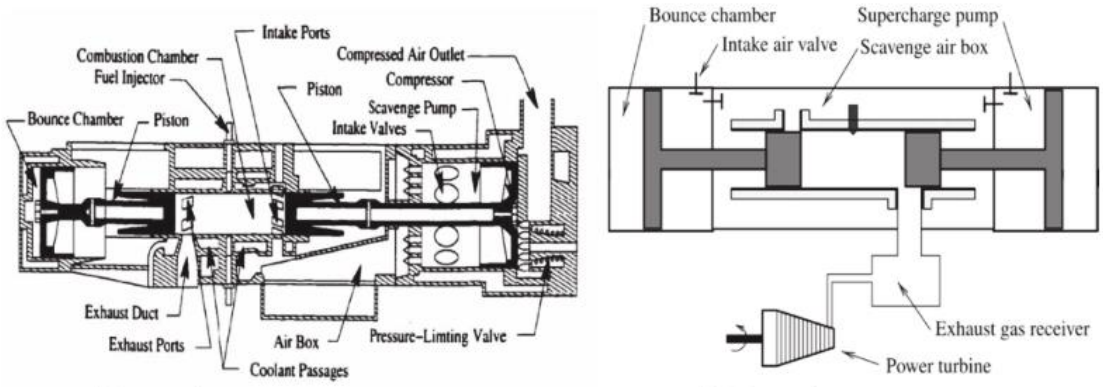

Figure 2.1 Schematic representation of free-piston gas compressor and free-piston gas generator [25]

2.1.2 Recent advances and application of the FPE

Advances in machine building technology, control methods, and gas turbine characteristics in recent decades have led to a new interest in FPICE, especially in new FPE categories: FPE Linear Generator Sets (FPELG) and Hydraulic Press FPE (HFPE). In addition to this, free piston centrifugal compressor linear generator sets (Linear Joule automotive engine generator sets) and small FPICE have been scientifically researched on a global scale. Each class of FPICEs has benefited from important research results over the past few decades [39].

2.1.2.1 Free-piston engine linear generator

FPELGs that combine FPICEs with linear generators instantly have been explored since the 1990s. The specific principle of FPELG is as follows: The ultra-high pressure and high temperature gas formed in the whole process of ignition in the FPICE cylinder pushes the mover (the piston part rigidly connected with the moving rod of the parallel line generator set). Subsequently, the linear generator set converts the kinetic energy of the mover into electromagnetic energy [6,40-42]. In principle, FPELG has three typical models and specifications of double-cylinder single-piston, two-cylinder double-piston and opposed piston, as shown in Figure 2.2 below. The specific rationale for the specifications of the three models of FPELGs is the same, as previously described, although there are some minor differences. Their advantages and disadvantages are shown in Table 2.1.

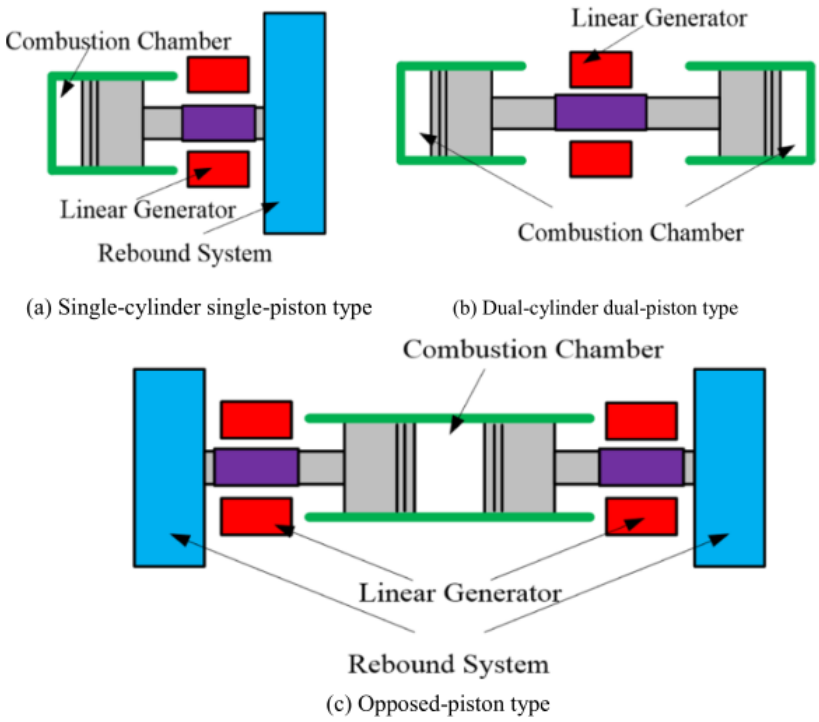

Figure 2.2 Schematic representations of three typical structures of FPELG [6,17]

(1) Two-cylinder single-piston FPELG is composed of engine combustion chamber, linear generator set and rebound force system hardware, and must get rid of the compression force of reactive power four-stroke.

(2) The two-cylinder two-piston engine contains two engine combustion chambers and a linear generator set. The whole process of ignition occurs alternately in each cylinder. When the car engine is in the two-stroke thermodynamic cycle, the resilience device is deactivated in this configuration. In contrast, for the automobile engine under the four-stroke thermal cycle, the working mode of the linear generator set should be switched from the power generation mode to the electric mode during the reactive power four-stroke period [6,17].

(3) The third type is composed of two opposing piston s with one engine combustion chamber, two linear generator sets and two rebound force system hardware. The ultra-high pressure and high temperature gas formed in the whole process of ignition drives two pistons to reciprocate synchronously. Similar to the double-cylinder single-piston machine, the resilience device is indispensable. Since FPELG was explicitly proposed, it has caused great interest in many scientific research institutions. Nevertheless, until now, no FPELG variety has been successful in the industry.

Fortunately, according to recent reports, FPELG has made a major breakthrough in technology. Therefore, in the next section, a brief description of previous scientific findings on FPELG will be detailed.

Table 2.1 Advantages and disadvantages of different typical types of FPELG [6,17]

FPELG type	Advantage	Disadvantage
Single-piston (Fig.2 a)	Easy to control	Rebound device required; Low power density
Dual-cylinder dual-piston (Fig.2 b)	High working frequency; compact structure; High power density; Elimination of the rebound device	Relatively difficult to control; Unbalanced
Opposed-piston (Fig.2 c)	Intrinsically balanced; Vibration free with equal piston masses	Complex design; Piston synchronization required

Walters and his elite team at West Virginia colleges and universities have been working on the practical operating characteristics and characteristics of the FPELG's piston since the 1990s [43-45]. For the SI FPELG, the results show that with the improvement of the mover quality, the maximum working pressure of the master cylinder and the engine compression ratio are both improved. In turn, the output power and piston peak velocity are reduced. Along with the increase in the type of calorific value, the main parameters (including output power, master cylinder air pressure maximum value, piston maximum value speed and engine compression ratio) are also improved. When this primary parameter is reduced, the ignition delay time and load lift are shown in Table 2.2. Besides, the test results show that the power and output power of the SI vehicle gasoline FPELG sample can achieve 316 W and 23.1 Hz respectively [43,44]. Nevertheless, FPELG for automotive gasoline

often catches fire due to the instability of the entire ignition process in the work process. They applied a dimensionless solid model to analyze the influence of the main operating parameters (including bore ratio, equivalence ratio, load, ignition delay time) on the characteristics of the compression ignition FPELG [46]. The results show that the characteristics of this FPELG are high when the ratio of cylinder diameter is 1.3 [47]. Recently, scientific studies have investigated ignition engine timing and thermal damage with torsion spring-assisted FPELGs. Output power and power increased with an increase in stiffness coefficient, while various reductions from circulatory system to cycle [48]. It has been found that ignition timing of the engine has a significant effect on the master cylinder air pressure [49]. In addition, when the multi-reciprocating motion control method is selected, the conversion index of the engine compression ratio and the maximum working pressure is controlled below 5% [50].

Table 2.2 The influence of the parameters on the performance of FPELG [11]

	Heat input	**Combustion duration**	**Frictional force(load)**	**Mover mass**
Frequency	↑	↓	↓	↓
Peak pressure	↑	↓	↓	↑
Velocity	↑	↓	↓	↓
Displacement	↑	↓	↓	↑

The Peter Van Blarigan working group at Sandia National Laboratories in the US, explored the characteristics of the FPELG using the Homogeneous Pumped Ignition (HCCI) ignition method, which uses a hydrogen-rich fuel cell. The engine compression ratio and equivalence ratio are 30 and 0.3, respectively. The simulation results show that the working characteristics of the piston of FPELG are quite different from those of traditional rotary engines (TREs). For example, the FPELG has a fast expansion four-stroke, a slower compression stroke and more instantaneous piston speed. The NOx emission of FPELG was significantly smaller than that of TRE. In addition, the basic

theory indicates that the high efficiency can be achieved by 65% (according to the research results of rapidly shrinking-expanding equipment, the high efficiency is about 56%) [51-54]. In the whole process of lifting and scavenging, it was found that compared with the scavenging method of the circulating system and the scavenging method of the mixed circulating system, the scavenging characteristics of the single-flow scavenging method were the best. In addition, according to the application, the hierarchical scavenging equipment [55,56] can obtain a smooth ultra-low temperature and low voltage intake air supply (300 K, 1.2 bar). Recent studies have shown that under special conditions, the indicated thermal efficiency of the opposed piston hydrogen FPELG can reach 55% [57].

The new Free Piston Energy Converter (FPEC) project has been supported by EU countries since 2002. The indicated automotive engine high efficiency of FPEC under HCCI ignition mode is about 51% [58]. In addition to this, the overall target power and power density are about 23 kW and 0.6 kW/kg respectively, and the environmental protection standard can reach Euro V. TRE, as shown in Figure 2.3 [58] below. In addition to this, the results show that lower gasoline octane energy must have more engine compression ratio, which will improve the output power, power and high efficiency of FPEC [59]. And it was found that the transverse flux rare earth permanent magnet linear generator set becomes a good candidate for FPEC because of its low moving quality [60-63]. The linear generator set with quasi-Halbach magnetized configuration has high power and high efficiency, as shown in Figure 2.3 [64-67] below. In addition, it was found that the speed of the linear generator set was the most important factor that endangered the FPEC in the whole process of operation, and friction was the most important factor in the whole process of standby speed [68]. In addition to this, it can be seen that the fuel consumption of FPEC is reduced by 19% compared to diesel generators [69-71].

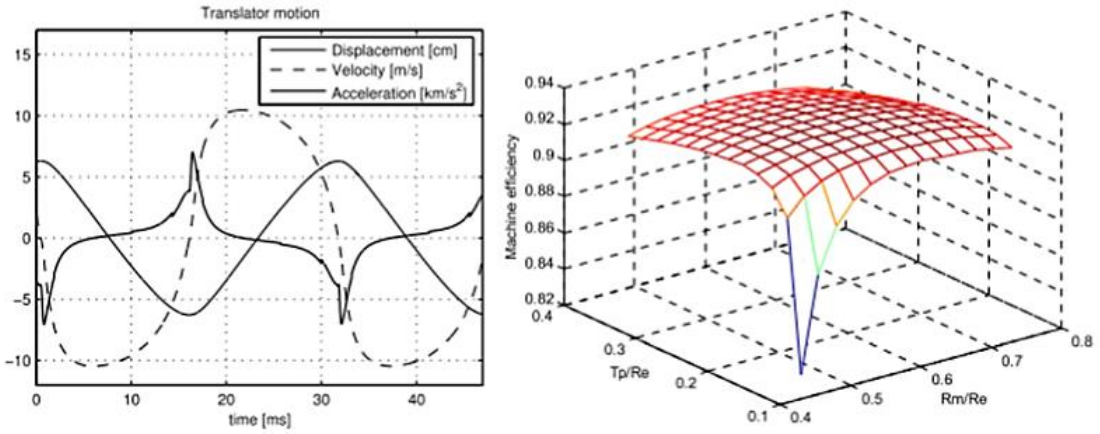

Figure 2.3 The piston operation characteristic and Linear generator performance from FPEC [68]

Analytical staff at the Swedish Institute of Technology applied MATLAB/Simulink and the dSPACE simulation service platform [72,73]. Based on the test results, they confirmed that the output power of the prototype LCE01 is about 27 Hz. In addition, the highest value power is only 650 W, and the high efficiency is less than 10% [74,75]. For the control method of FPELG, the sine curve is used as the overall target motion trajectory at first, and the current of the linear generator set and the position of the piston are used as the adjustment variables. The results show that after applying this control method, the FEPLG sample can complete the smooth and continuous operation [74,75].

The SI FPELG and the compression ignition FPLG were critically analyzed by Tony Roskilly's research group at Newcastle University. The results show that the basic parameters of FPELG are relatively highly coupled and optimally controlled. The high efficiency of FPELG is slightly higher than that of TRE. Besides, the friction damage of FPELG is only half of that of conventional engine crankshaft system hardware rotary engine, and its NOx emission is smaller than TREs [76-79]. Recently, Roskilly and Boru dissected the characteristics of 2-4-stroke and 4-stroke FPELG. The results show that the characteristics of the 2 four-stroke FPELG are quite different from those of the 4 four-stroke FPELG, for example, in the reciprocating motion curve, output power, the maximum working pressure of the master cylinder and the marked high efficiency level, as shown in Figure 2.4 below and Table 2.3. In addition, the control method of FPELG is designed, and the single-cycle ignition advance angle is used as the adjustment variable. Bottom dead center (TDC) of the piston is predicted from the piston velocity in the mid-section of the four-stroke. The results show that

when the control method is applied to FPELG [81-85], the maximum value of the in-cylinder air pressure is controllable. Recently, in order to better complete the smooth operation of SI FPELG, a cascade control optimization algorithm was explicitly proposed [85].

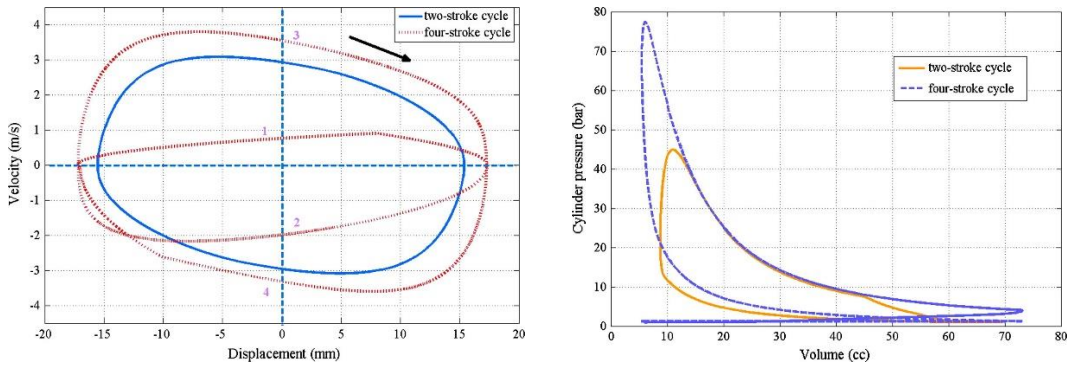

Figure 2.4 FPELG performance of 2-stroke and 4-stroke from Newcastle University [80].

Table 2.3 Performance comparison of 2–4 stroke FPELG [80]

	Two-stroke engine	**Four-stroke engine**
Mean equivalent crankshaft rotational speed(rpm)	2000	900
Maximum piston velocity(m/s)	3.1	3.8
Peak cylinder pressure(bar)	47	76
Fuel consumption(kg/kW.h)	0.22	0.2
Thermodynamic efficiency (%)	34.5	44.9
Indicated power(W)	3900	1230
Electric power output(W)	3760	640
Maximum efficiency compression ratio (-)	7.36	16.2

Engine power/weight ratio(W/kg)	0.07	0.022

From 2002, the analytical staff of the French Aerospace Core became interested in the two-stroke FPELG [86]. For the single-piston FPELG with a pneumatic spring device, the entire process of the intake port and exhaust pipe is controlled by a variable magnetic induction cylinder organization. During the whole scavenging process, the layout of 2 channel valves and one inlet and outlet valve was confirmed to be the best choice for FPELG [87]. Regarding the characteristics of FPELG under different ignition modes, it is noted that the indicated high efficiency of FPELG under HCCI ignition mode is higher than that of SI ignition mode, as shown in Table 2.4. Moreover, it is found that FPELG is particularly suitable for HCCI ignition due to the self-regulating effect of reciprocating motion, and the high efficiency can reach 38%. The main parameters of FPELG are listed in Table 2.4 [86,88,89]. Recently, computational fluid dynamics (CFD) simulations and precise measurements have shown that the two-stroke opposed- FPELG has a marked high efficiency of 38.8% and 27.3%, respectively, in the SI ignition mode. In addition to this, the successful transition from the SI ignition mode to the HCCI ignition mode was confirmed [90,91].

Table 2.4 The performance of FPELG under SI and HCCI combustion mode respectively [88]

	SI	**HCCI**
Stroke(mm)	80	80
Inlet pressure(bar)	2	2
Compression ratio (-)	9	9
IMEP (bar)	40.1	17.1
Injected fuel mass(mg)	13.1	5.76
Indicated efficiency (%)	33.3	34.4

Indicated power(kW)	11.3	5.0

Table 2.5 Measurement Data ZK02 SI-HCCI mode [89]

	1	**2**	**3**	**4**	**5**
Stroke(mm)	80	80	80	80	80
Boost pressure(bar)	2.0	2.2	2.3	2.4	2.5
Compression ratio (-)	12.8	11.3	11.5	10.5	11.6
Efficiency compression ratio (-)	9.5	8.8	8.7	7.9	8.6
Injected fuel mass(mg)	17.6	20.7	22.7	24.5	22.7
IMEP (bar)	6.7	7.7	8.2	8.7	8.4
Frequency (Hz)	18.1	18.9	19.6	19.5	19.9
Indicated power(kW)	38.1	37.3	36.3	35.6	37.4
Maximum pressure gradient(bar/CAD)	10.0	12.9	18.8	17.2	16.7

Pempek System Company designed an FPELG in 2003 called the Free Piston Drive Group (FP3). The FP3 contains eight two-stroke engines and a linear generator. The high-pressure gasoline and diesel direct injection engine system is applied to FP3 with SI ignition mode. Output power, peak power and power density are 30 Hz, 40 kW and 1 kW/kg respectively. The FP3 is extremely compact, highly efficient, and has low discharge. Its power can be increased by adjusting the total amount and size of FP3 control modules [92]. Unfortunately, there is very little coverage of FPE.

The Ocktaeck Lim working group at Ulsan University in South Korea has studied two-stroke SI FPELG based on butane [93,94]. The results show that FPELG can successfully switch from SI ignition mode to HCCI combustion mode when operating under special conditions. The equivalence ratio, external load, inlet temperature, inlet working pressure, ignition position and stiffness coefficient index are 0.7, 180 Ω, 400 K, 1.2 bar, 3 mm and 14.7 N/mm from the cylinder head, respectively, as shown in Figure 2.5 [95]. Changing the ignition position in the SI ignition mode is a beneficial strategy for the whole process of FPELG connection. For the whole scavenging process of FPELG, it is found that when the best output power is 33 Hz, the maximum collection efficiency is 83%. Moreover, with the improvement of the distance between the exhaust port and the reduction of the working pressure of the intake port, the collection efficiency is improved [96].

Japan's Toyota Central R&D Labs Inc. has scientifically researched the twin-cylinder single-piston FPELG. It consists of a twin-cylinder FPE, a linear generator set, and a vapor resilience device [98]. The results show that the power of FPELG for vehicle gasoline using the premixed charge compressor ignition (PCCI) ignition method can produce more than 10 kW, and the thermal efficiency is about 42%. However, compared with the SI ignition method, the ignition timing of the FPELG cannot be controlled under the PCCI ignition method [99]. At the same time, when the reciprocating motion graph is manipulated by the linear generator set, the bottom dead center, bottom dead center (BDC) and output power of the piston are manipulated, as shown in Figure 2.6 below [100,101]. FPELG samples can continue to run for more than 4 hours.

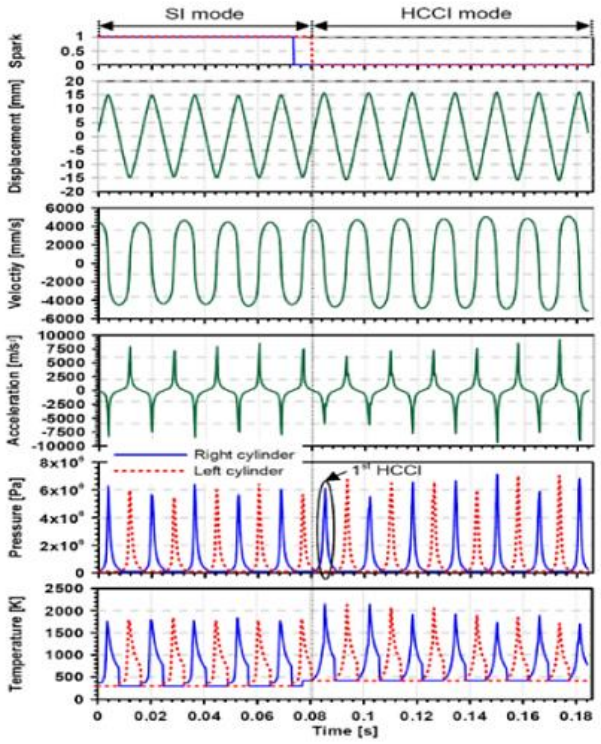

Figure 2.5 FPELG performance in the SI-HCCI transition from Ulsan University [97]

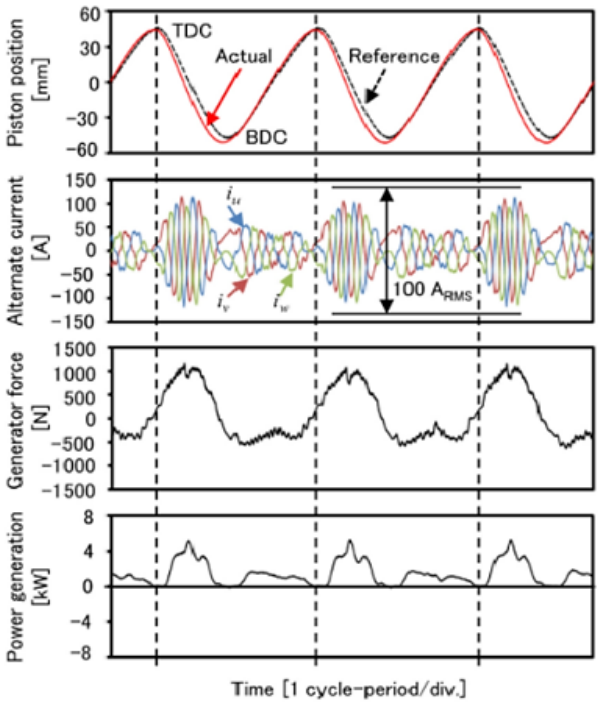

Figure 2.6 The performance of FPELG at Toyota Central R&D Labs Inc [100,101]

National Taiwan University of Science and Technology researchers have researched a two-cylinder,

double-piston- FPELG based on isooctane. The characteristics of FPELG under three different ignition modes were compared, namely SI ignition mode with an equivalence ratio of 1, lean SI ignition mode and HCCI ignition mode [102]. When operating in the SI ignition mode, the FPELG has high power, but also high fuel consumption, with an equivalence ratio of 1. FPELG has high efficiency, increased stroke schedule, and low output power during operation under HCCI ignition mode. In addition to this, FPELG can successfully transition from SI firing to HCCI firing. The FPELG should operate with lean gas mixture and moderate load, as shown in Figure 2.7 below [102].

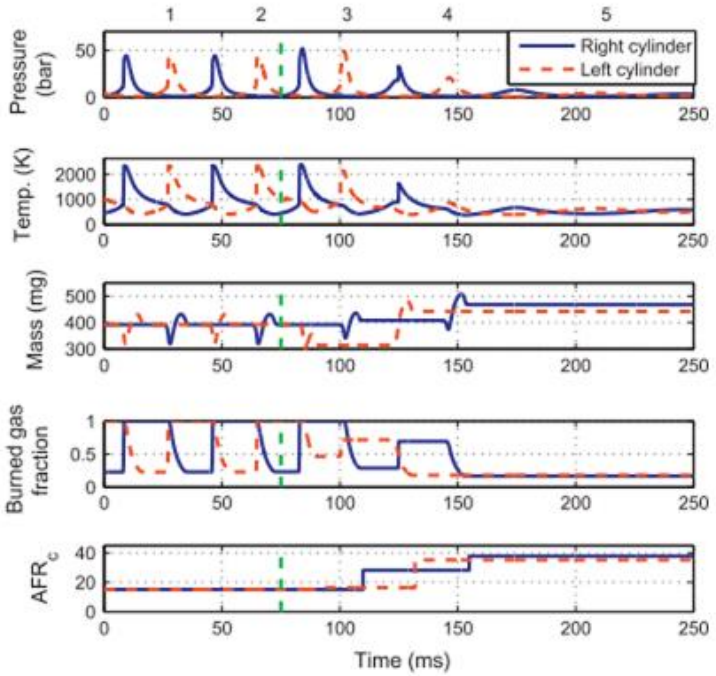

Figure 2.7 The performance of FPELG at National Taiwan University of Science & Technology [102].

Singapore scientific researchers' critical simulation SI FPELG. Note that the reciprocating motion graph is non-sinusoidal [103,105]. As the input energy increases, the piston speed increases and the four-stroke length decreases. Subsequently, the control method of FPELG in the whole process of operation is clearly proposed. When Hengli lifts during the whole process of operation, the frequency of the circulation system decreases [106]. In addition, the characteristics of FPELG and different DC servo motors are compared [107]. It was found that with the increase of the total number of rechargeable batteries, the maximum speed of the mover increased, and the working

pressure of the master cylinder also increased [108]. In addition, the results show that the highest value of the working pressure of the cylinder is achieved when the distance between the position of injection and the TDC of the hydrogen FPELG is 25 mm [109].

The Zhang Chi working group of the Chinese Academy of Sciences uses FPELG as a range extender for hybrid new energy electric vehicles [110]. FPELG chose a decoupled design approach for powers of 10 kW, 15 kW, 20 kW, and 25 kW, with an overall high efficiency exceeding 35% [111]. Apart from that, the reasonable power, peak power and total high efficiency of FPELG are about 5 kW, 47.5 kW and 38.2% respectively [112]. In addition to this, the control method (including running, smooth operation, common fault repair, and termination) is effective, and the delay time for unstable conditions is less than 20 ms when common fault repair countermeasures are applied [113,114].

Yuan from Chongqing Jiaotong University has researched a hydrogen-based FPELG [115]. Compared with the long four-stroke FPELG fueled by hydrogen, the short four-stroke FPELG mainly exhibits many advantages, such as the marked thermal efficiency, the maximum air pressure of the master cylinder and the output power, as shown in Figure 2.8(a) below [116]. In addition to this, increasing the hydrogen plus fraction is sufficiently detrimental to the ignition and exhaust characteristics of the FPELG, such as master cylinder air pressure peaks, temperature, and NOx exhaust. Compared with the pure diesel FPELG, the ignition rate of each ignition link decreases with the increase of hydrogen gas, as shown in Figure 2.8(b) below [117].

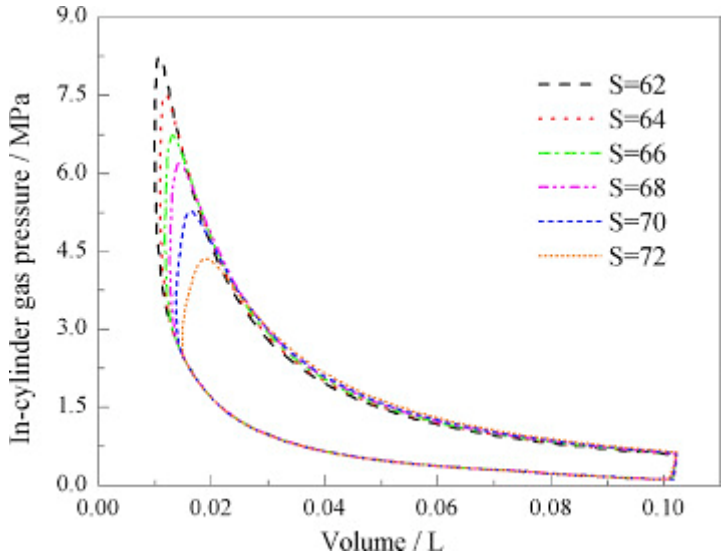

(a)

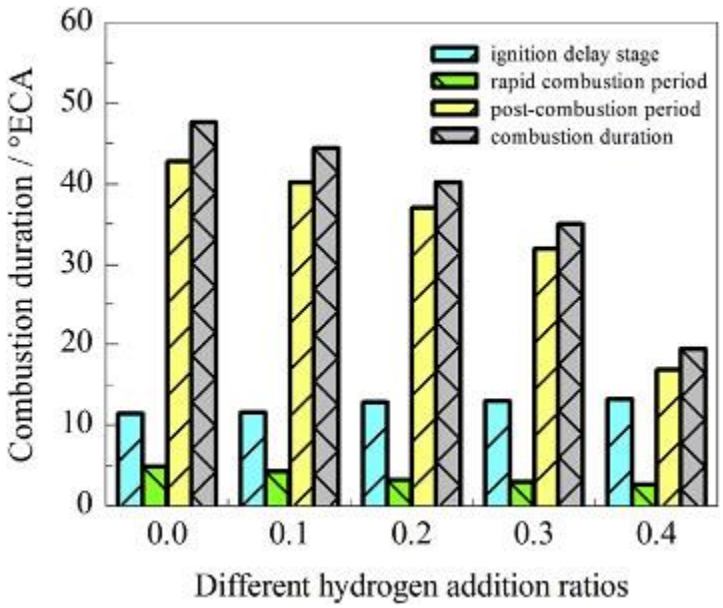

(b)

Figure 2.8 P-V diagram and combustion process of FPELG from Chongqing Jiaotong University [116,117]

The research group of Jin Xiao of Shanghai Jiaotong University has scientifically researched the dual-cylinder dual-piston FPELG. FPELG is simplified as a single playable discrete system with variable damping and strength. It is particularly noted that the natural output power of FPELG increases with the increase of the inlet working pressure, and decreases with the increase of the four-stroke length, as shown in Figure 2.9 below [118]. The characteristics and characteristics of the piston in the working of FPELG under the main parameters such as mover quality, automobile engine cylinder diameter, ignition timing, air inlet working pressure and equivalence ratio are analyzed. In addition, it was found that ignition timing was the main factor that compromised the characteristics of FPELG, and the subsequent circulation system was greatly affected by the previous cycle [118].

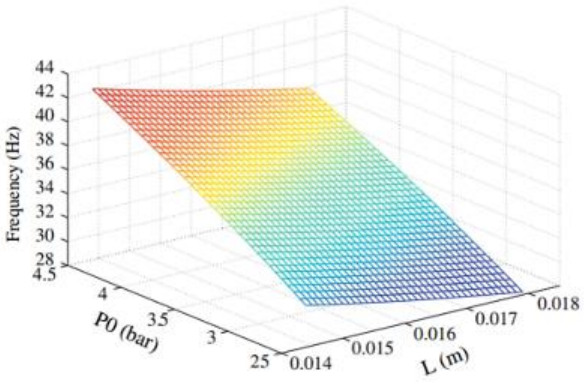

Figure 2.9 The natural frequency characteristic of FPELG from Shanghai Jiaotong University [118]

Xu Zhaoping of Nanjing University of Science and Technology has scientifically studied the twin-cylinder four-stroke FPELG under the SI ignition mode. The test results show a power of 2.2 kW and a thermal efficiency of 32%, as shown in Table 2.6 [119,120]. In addition, when the FPELG operates in the short-port 4-stroke and the full-expansion 4-stroke, the high efficiency of the generator set can be achieved 33.4%, and the power is improved [119]. For the control method of FPELG, the linear generator set is used as the control board to adjust the movement trajectory of the piston, and the parameters detected by the sensor are used to estimate the operation of the FPELG in the whole process of power generation. Then, the FPELG operation is adjusted according to the current flow of the linear generator set [121]. More recently, opposed-piston- four-stroke FPELGs have been scientifically studied. The study found a number of advantages for an opposed-piston four-stroke FPELG compared to a single-piston- four-stroke FPELG. For example, it has more power, less oscillation and stronger equalization [122].

Table 2.6 Comparison of the prototype and the simulation results of FPELG [120]

Items	Prototype	Simulation
Intake stroke	7-45	4-45
Compression ratio (-)	6.4	11.2
Expansion stroke(mm)	7-74	4-74

Expansion ratio (-)	10.6	18.5
Peak pressure(bar)	28	53
Output power(kW)	2.2	3.6
Generating efficiency (-)	32%	42%

Zhengxing Zuo and Huihua Feng of BIT developed and designed several types of FPELG, including SI FPELG based on gasoline for vehicles and compression-ignition FPELG based on gasoline. In the whole process of FPELG simulation, the coupling method of zero-dimensional dynamic solid model and 3D CFD ignition solid model and iterative program flow is used. The simulation results show that the afterburning condition is more severe than the corresponding TRE, as shown in Figure 2.10 below [42,123,125]. NOx emissions from FPELG are less than TRE [42,126]. At the same time, the test results of the vehicle gasoline FPELG show that the output power, the maximum value of the master cylinder air pressure, the maximum value of the piston speed is 24 Hz, 40 bar and about 4.5 m/s. According to the test results, for diesel engine FPELG, the best timing of gasoline and diesel injection engine is 7 mm from the cylinder head [127]. During the whole process of operation, the maximum air pressure of the master cylinder and the compression ratio of the engine increase with the increase of the thrust of the linear motor. When the electric motor pushing force is 125 N, the gasoline FPE for vehicles reaches the ignition standard after four cycles [128,129]. During the whole conversion process, no matter which control method is used (“asymptotic conversion strategy” or “immediate conversion strategy”), the operation characteristics of FPELG after the whole conversion process are the same, and the operating parameters are lower than the whole process before the conversion. Nevertheless, FPELG operates more smoothly in the whole process of transition according to the application of “progressive transition” control method [41]. During the whole process of power generation, when the FPELG oscillates or fluctuates regularly, the magnetic field force of the linear generator set will change [130]. The control method of the whole process of running and converting was successfully applied to the FPELG samples.

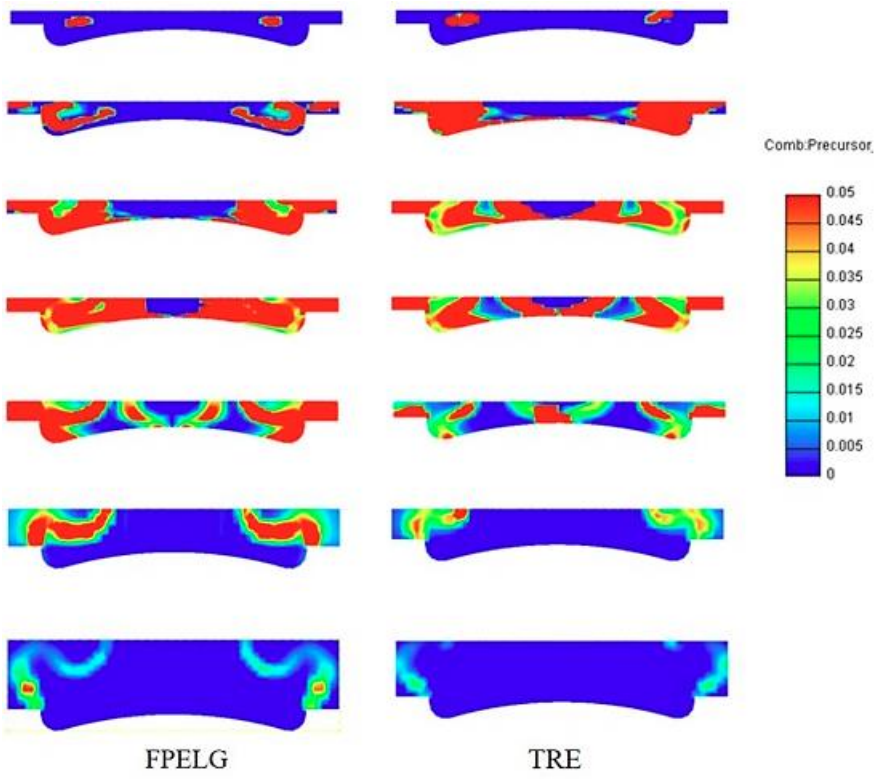

Figure 2.10 The combustion process of FPELG from Beijing Institute of Technology [42]

2.1.3 Different fuels on the FPE

2.1.3.1 Fossil fuel

Scientific research has been carried out on the discharge characteristics of FPE, and some studies have shown that FPE has the advantages of variable compression ratio, wide adaptability to materials, and less nitric oxide (NO) emissions, but some disadvantages have also been seen, such as high dust emissions [131]. Yuan et al., devoted themselves to the finite element analysis and scientific research on the ignition characteristics of free piston diesel generators. In the discussions of many people, an iterative finite element analysis method using zero-dimensional dynamic model, multi-dimensional scavenging and ignition coupled solid model is clearly proposed. According to the main parameters of the coupling in this mode, compared with the corresponding traditional gear automobile engine, the harm of the reciprocating motion to the whole ignition process is scientifically studied. The results show that, compared with the traditional automobile engine, the average speed of the piston in the ignition link of the free piston engine generator set is faster, and

the ignition delay time is longer. The exothermic reaction before the bottom dead center, the constant volume exothermic reaction, and the exothermic reaction in the premixed ignition period are all smaller than those of the traditional automobile engine. They also determined the master cylinder operating pressure, temperature of the FPE and crankshaft automotive engines, as shown in Figure 2.11 and Figure 2.12 below.

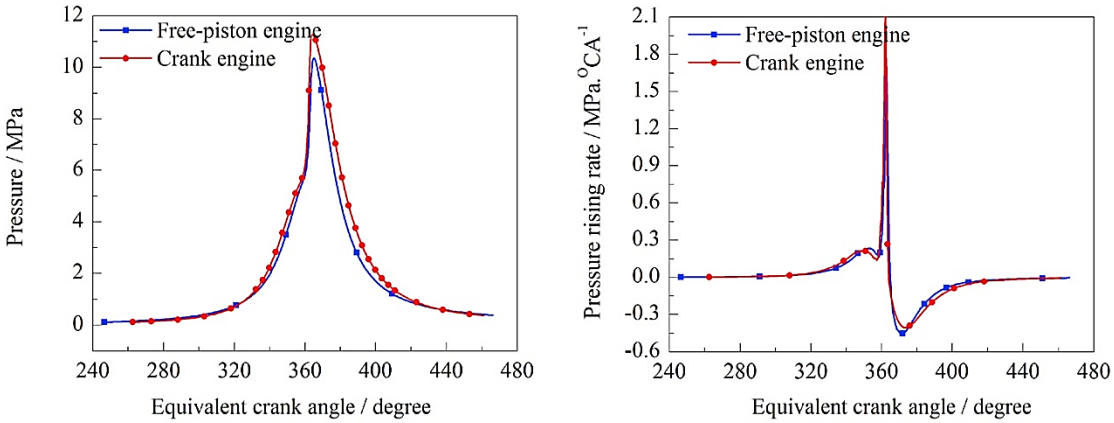

(a) In-cylinder pressure (b) Rate of pressure rising

Figure 2.11 Predicated in-cylinder gas pressure [131]

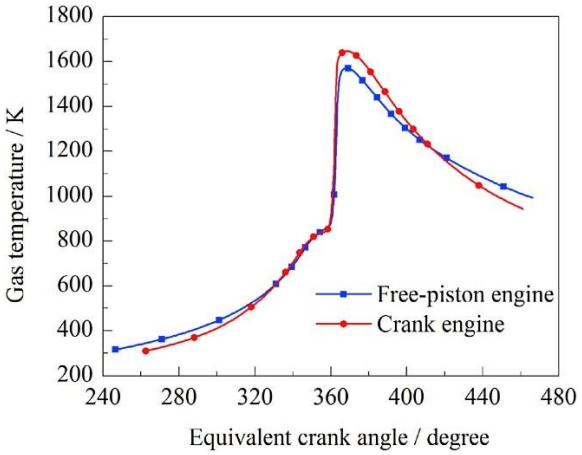

Figure 2.12 Mean in-cylinder gas temperature [131]

Figure 2.13 shows the predicted analytical master cylinder air pressure for a free piston engine and a conventional gear car engine at the same ejection site. The study found that the maximum ignition working pressure of the free piston engine is lower than that of the gear automobile engine, and the maximum working pressure of the free piston engine occurs later and the delay time is shorter. The positive pressure increase of the free piston engine in the combustion process is smaller than that of

the engine crankshaft automobile engine, but the negative pressure increase is slightly higher than that of the traditional automobile engine. Therefore, compared with the traditional automobile engine, the free piston engine has a slight disadvantage of high efficiency under the same working conditions. Figure 2.12 shows the transition of the mean master cylinder gas temperature for two automotive engines. It is obvious that the temperature of the main cylinder gas in the two car engines is similar throughout the downsizing process. However, in the burning process, there is a significant difference in the main cylinder gas temperature of the two automobile engines. The maximum ignition temperature of the free piston engine is significantly lower than that of the traditional automobile engine, and the maximum temperature difference is significant. is 97K. When the expansion process is gradual, the mean gas temperature of the master cylinder of the free piston engine is also lower than that of the gear automobile engine. Nevertheless, the free piston engine has a higher gas temperature in the final link of the expansion process. For diesel engines, the key industrial exhaust gases are nitrogen oxides and fine particulate matter, among which nitrogen oxides are generally considered to be the most important exhaust gases in automotive engines. Figure 2.13(a) shows the predicted analytical concentrations of in-cylinder nitrogen oxides NO for a free piston engine and a basic automobile engine with the same engine compression ratio and injection site. It clearly shows that the free piston engine has a significant development potential for NO emission reduction compared to the geared car engine. Nevertheless, the free piston engine has no advantage in the level of fine particulate matter discharge, as shown in Figure 2.13(b) below, from which it can be seen that the predicted analytical concentration value of fine particulate matter discharge in the free piston engine exceeds that of the traditional gear car engine [131].

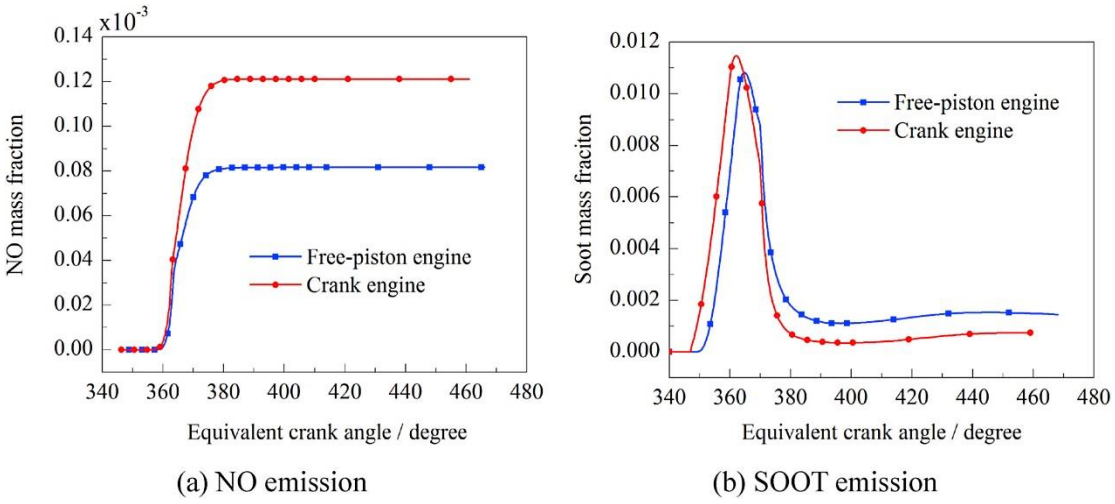

Figure 2.13 Exhaust gas emissions for FPE and TCE [131]

Prof. Tony and Mikalsen conducted experiments in 2009 on the fuel efficiency and industrial exhaust gas of a low heat dissipation free piston diesel engine [132]. Based on their scientific research, some major exhaust characteristics and heat transfer adjustments were clearly proposed. The production of nitrogen oxides in the combustion chamber of an engine depends to a large extent on the residence time at the vapor temperature and high temperature. Both suffer from the characteristics of free piston engine operation: increased master cylinder air fitness will increase the mixing of natural, gas and ignition substances, which in turn will reduce the total number of master cylinder high temperatures, while faster power stroke expansion will reduce time available for NOx generation. Typically, more than 90% of the nitrogen oxides in car engine ignitions and organic exhaust gases are present in the form of nitric oxide (NO), so their scientific studies only consider this exotic species. The key generation reflection of NO, the extended Zeldovich principle, is included in the organic chemistry solver, so it is possible to study the hazards of nitric oxide emission caused by the actual operating characteristics of the free piston. Figure 2.14 shows the predicted analytical NO concentration values in the master cylinder. The obvious advantage of the free piston engine can be seen, the NO concentration value in the cylinder body when the exhaust valve is opened is about 17% lower than that of the traditional car engine. This is also because of high-quality reverse extrusion, improved material-gas mixing in the middle and late stages of ignition, and its temperature reduction due to expansion, both of which are arbitrary - the instantaneous speed of the piston shortly after BDC higher result. Piston engine.

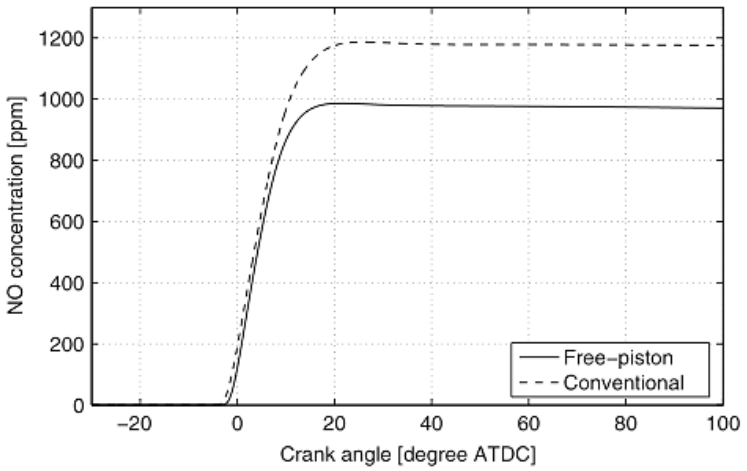

Figure 2.14 Concentration of nitrogen oxide (NO) in the in-cylinder gases [132]

Figure 2.15 shows the detrimental effects of reducing thermal convection damage in the master cylinder on vehicle engine performance and nitric oxide emissions in many discussions. They found that the low-radiation engine combustion chamber design improved the fuel efficiency of free piston engines and conventional car engines, the latter results consistent with those reported by other authors. The study found that free piston engines benefited slightly less from thermal insulation of the engine's combustion chamber than conventional car engines due to their inherently lower heat transfer damage. Nevertheless, some people feel that because the NO emission levels in free piston engines are lower, they can tolerate higher levels of engine combustion chamber insulation, so this type of automotive engine should be particularly suitable for low exhaust heat design. It was found that even with a 30% reduction in master cylinder heat transfer, the NO consumption of a free-piston engine would still be less than that of a conventional car engine originally equipped. It is predicted that this level of engine combustion chamber insulation will increase the stated efficiency by about 3%. In addition, the implementation and application of ceramic ceramics in the surface region of the engine combustion chamber in free piston engines should be easier because of the lower side forces on the piston.

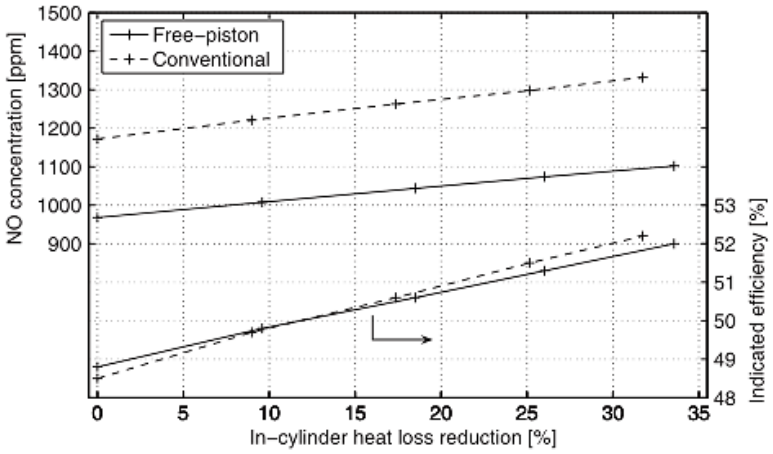

Figure 2.15 Effects of reductions in in-cylinder heat transfer losses on engine indicated efficiency and NO formation [132]

It is not too difficult to find that in most of the scientific research in the past, most people's attention has been focused on the scientific research carried out by FPE in the fields of ignition characteristics, control measures and high efficiency, but less attention is paid to the discharge industry, other emission characteristics scientific studies have highlighted its advantages at the level of NOx reduction and its disadvantages for soot particles.

2.1.3.2 Hydrogen

Hydrogen (H2) is a lighter element with extreme characteristics such as high heat transfer, rapid ignition rate, and very high gasoline octane [133]. As a natural material, H2 has the largest kinetic energy component per enterprise product quality, about 120 MJ/kg, and causes zero carbon emissions. In addition to this, because H2 is the most abundant element on earth, it is also considered as one of the boundless sources of electricity. At this stage, widespread analysis has already been carried out to scientifically produce hydrogen gas from biomass immediately. This overall process is usually divided into 2 groups: thermochemical transformation and biochemical transformation [134]. The former approach involves a series of thermochemical changes, such as steam reforming, thermal cracking, and biomass fuel vaporization. The latter one includes hydrogen production from alcohol, the whole process of plant photosynthesis, and the reaction of microbial blast furnace gas conversion [135]. Although biochemical conversion is more environmentally friendly and consumes less energy, biochemical conversion still needs to further improve the conversion efficiency and

reduce the associated costs [136]. In addition, if renewable resources such as solar power, wind turbines and wind power plants are used, hydrogen gas can also be produced from water electrolysis, which will be more sustainable. There are a number of obstacles preventing the large-scale use of hydrogen. The most obvious concern is the safety of hydrogen gas storage and delivery. Because of its small size of molecular structure and low ignition kinetic energy, H2 is very easy to disperse into the air and be ignited [137]. Although the sales market of hydrogen as a transport material is still in its infancy, government departments and fields have made efforts to create clean, economic development and safe hydrogen production and distribution for widespread use in hydrogen fuel cell new energy electric vehicles (FCEV) [138]. Lightweight FCEVs are currently in limited market demand in China and parts of the world. The sales market for buses, raw material equipment handling (such as electric forklifts), road supporting machinery and equipment, small and medium-sized and heavy trucks, boats and stationary applications is also developing.

Although hydrogen fuel cells used in traditional automobile engines have many of the above advantages, the further improvement of their characteristics and flexible control is limited by their mechanical equipment system. For these reasons, the fusion of FPE and hydrogen is increasingly of concern. Woo et al. of the Korea Electric Power Research Institute experimented with the characteristics of flame-ignited FPEG to ignite hydrogen fuel cells and compressed natural gas [139,140]. Their findings found that the non-traditional hydrogen car engine operates at 13 Hz and exhibits a somewhat higher peak exothermic response rate than under CNG conditions, but requires more accurate ignition control. This result is similar to that of conventional hydrogen car engines. Nevertheless, their experiments show that the scavenging efficiency of hydrogen FPEG is low, and it will produce a high intake dilution, which in turn causes the hydrogen fuel cell in the car engine to ignite at a slower rate.

Blarigan et al. performed experiments at Sandia National Laboratories on the HCCI characteristics of hydrogen fuel cells in a free piston shrinking and expanding linear generator set [141,142]. They found that under the low equivalence ratio of 0.319 and the high engine compression ratio of 37.1, the ignition delay time was only 20 ms, the thermal efficiency of the car engine was 54%, and the NO level was lower than 10 PPMM. The primary factor for such high conversion efficiency is the nearly stable volume ignition at high engine compression ratios. The test clearly demonstrates the

efficiency and potential of hydrogen fuel cell FPEG, including the development of clean energy, but it must be complicated to use.

Sun et al. from the University of Minnesota have scientifically investigated HCCI ignition manipulation according to the motion trajectory of renewable energy in FPEG [143,144]. Their simulations show that the minimum engine compression ratio to ignite a hydrogen fuel cell in this car engine is 22. Because of its perfect fuel operation flexibility, large tolerance of fuel residue and controllable piston motion trajectory, the thermal efficiency of non-traditional hydrogen vehicle engines can be improved according to the collaborative improvement of hydrogen fuel cells and vehicle engine operating motion trajectories to 48%. In addition, it can also improve the NO emission of the hydrogen vehicle engine according to the maneuvering trajectory. But they show that there is some disagreement between igniting high efficiency and low emissions.

Yuan et al. from Chongqing Jiaotong University studied the properties of flame-fired hydrogen fuel cell FPEG [145]. Their results showed that compared with the corresponding conventional hydrogen car engine, the hydrogen car engine exercised with better efficiency and instantaneous speed around the top dead center (TDC), because the available time was reduced, which would cause more Low heat conduction damage and less NO caused. They also found that compared with traditional car engines, the ignition rate of the hydrogen fuel cell in the new engine is slower and the ignition delay time is longer, resulting in more obvious afterburning and lower isovolumic exothermic reaction levels. They stress that the thermal efficiency of the new hydrogen car engine is very negative, and it must be properly ignited to incorporate its unique reciprocating motion. Figure 2.16 and Figure 2.17 show the comparative values of NO concentration and combustion heat release for a free piston hydrogen car engine, a free piston gasoline engine and a hydrogen conventional IC engine.

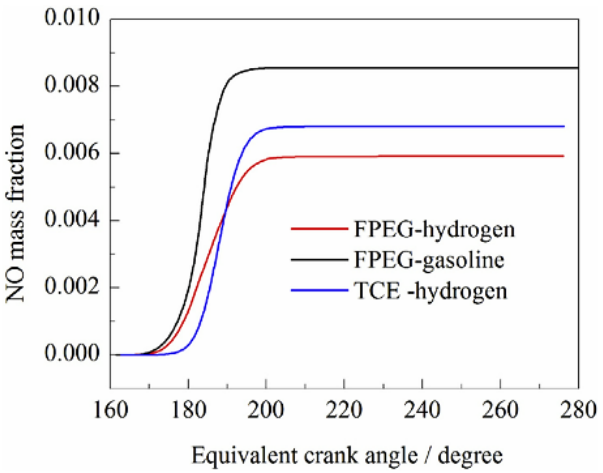

Figure 2.16 NO concentrations of the engines [145]

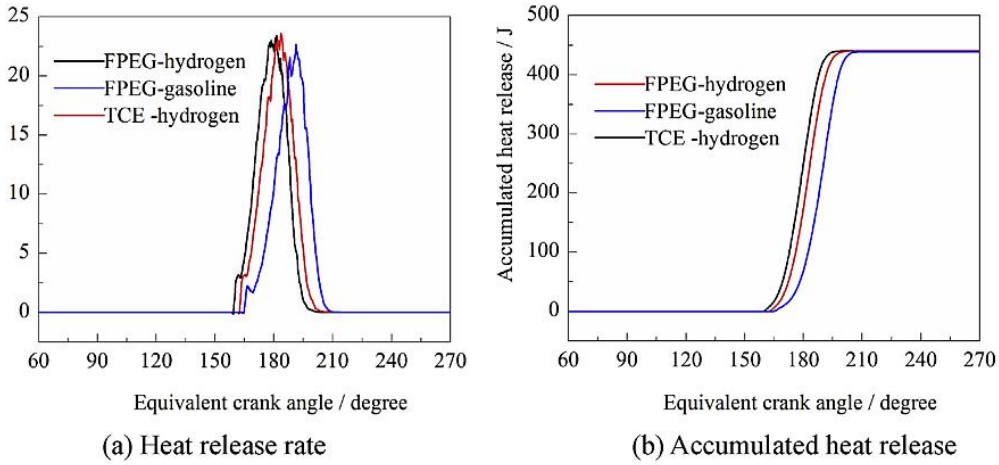

Figure 2.17 Combustion heat releases of the engines [145]

This result has also been extended to other natural FPEGs. Feng et al. of Beijing Institute of Technology compared the characteristics of FPEG and traditional gasoline engines based on the gasoline used for conventional gasoline engine [146]. It was found that, compared with the traditional automobile engine, the automobile gasoline ignited in FPEG reacted slowly, and the maximum exothermic reaction rate was lower. Thermal efficiency is lower due to less heat being released around the TDC. In addition, Yuan et al. conducted experiments on the ignition of diesel fuel in FPEG [147,148]. The characteristics of diesel FPEG are close to those of hydrogen. Diesel FPEG also has problems such as slow exothermic reaction, obvious secondary ignition, and poor thermal efficiency.

Worldwide, several investigations have reported ignition and rate deficiencies in hydrogen FPEGs.

Therefore, how to reasonably prevent this defect is a crucial issue to promote the progress of hydrogen FPEG technology. As a technology commonly used in gas engines to improve natural gas combustion, Diesel Engine Ignition (DPI) technology promises to accomplish the goal of accelerating ignition based on the use of "a little more ignition" [149,150]. A car engine with gas as the key fuel and diesel engine as the small fuel is called a diesel-ignited gas engine. In the intake four-stroke, a well-proportioned mixture of gas and atmosphere enters the cylinder; while in the compression stroke, when the piston is close to the bottom dead center, the injector sprays a small amount to ignite the diesel engine. The spontaneous ignition of a pilot diesel engine produces millions of ignition sources that ignite a homogeneous mixture of vapor and atmosphere [151,152]. The flame then spreads through the entire premixed gas and gas mixture. With a sufficient ignition diesel engine, the total number of ignition sources will be very considerable, which makes the whole ignition process close to the homogeneous charge reduction ignition [153]. Thus, dual-fuel operation with gas fuel can result in high thermal efficiency that is almost comparable to the same automotive engine operating with diesel fuel at higher loads [154].

Diesel engine ignition of automobile engines has been widely used to utilize various fossil fuel resources, and at the same time, compared with traditional diesel engines, it can minimize industrial exhaust gas without increasing the cost of automobile engines too much [155]. Combining the defects of hydrogen FPEG and the technical characteristics of DPI, it can be estimated that DPI not only alleviates the ignition of hydrogen FPEG, but also further completes the leaner ignition and reduces NO emission. Thus, DPI may be a potential ideal technology for igniting hydrogen FPEG. However, before applying it to a new hydrogen vehicle engine, a basic assessment of this technology must be carried out.

In order to better explore the new application of DPI technology in hydrogen FPEG and evaluate its application scope, Yuan et al. developed and designed a full cycle system operation model of two-stroke hydrogen FPEG [156], and applied a professional iterative simulation method to measure the hazard of DPI to hydrogen FPEG. At the same time, the results are compared with the corresponding traditional flame ignition (TSI) conditions, revealing the technical advantages and disadvantages of DPI. Figure 2.18 shows the NO mass concentrations in their study.

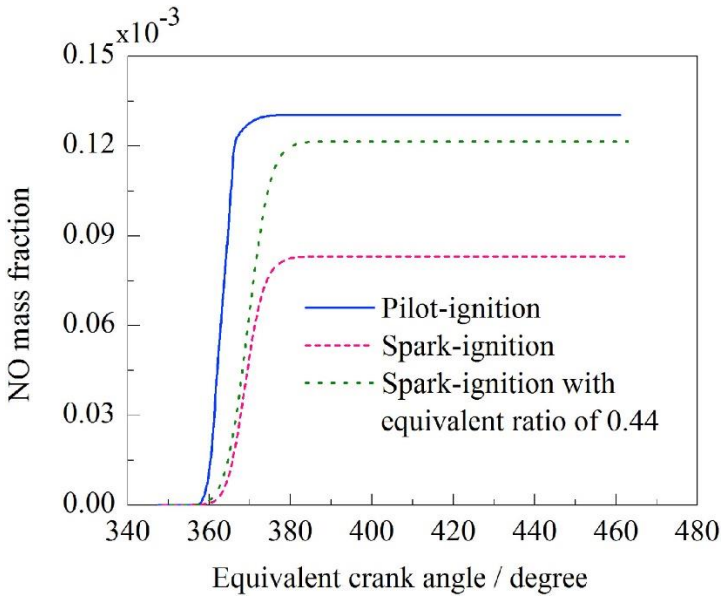

Figure 2.18 NO mass fractions [156]

They found that 1. Compared to TSI, DPI made hydrogen FPEG work faster, reducing circulatory system delay time, and at the same time resulting in higher reciprocation. As a result, the power generation of FPEG was significantly enhanced. 2. DPI can accelerate the ignition of the hydrogen fuel cell, causing a large number of exothermic reactions around the TDC, further improving the isovolumetric exothermic level of FPEG. Therefore, it produces a lot of nominal work and more nominal thermal efficiency for the car engine. 3. Using DPI, hydrogen vehicle engine has longer ignition delay time and shorter rapid ignition cycle time than TSI condition. Nevertheless, the calorific value released during the rapid ignition period is significantly large. At the same time, because of the greater rate of increase in the capacity of the engine's combustion chamber, the rapid spread of the flame becomes slower and the time period after ignition is slightly longer. 4. When the hydrogen vehicle engine using DPI technology is running, the maximum working pressure and temperature are relatively large, the maximum value occurs earlier than TSI, and the delay time is shorter. Higher ignition temperatures also produce more severe NO emissions. 5. Compared with TSI, DPI has slightly lower scavenging efficiency for hydrogen vehicle engines. However, due to the fact that the total gas quality of the main cylinder is slightly larger [156], the specific fresh air quality is almost the same as that under the TSI condition [156]. Besides, Yuan et al. In 2018, they tried to add different proportions of hydrogen to the FPE according to the air inlet, and obtained different piston offsets and initial conditions according to multiple iterations [157]. On the one hand,

hydrogen gas can accelerate the ignition rate of the mixture in the cylinder. On the other hand, the engine compression ratio, exercise frequency and residual organic waste gas index with the change of hydrogen gas composition also change the whole process of mixing and ignition. This element has different hazards to the ignition and discharge of FPE. Adding some hydrogen gas to the diesel engine FPE will cause harm to the whole process of diesel engine volatilization, crushing, impact and boundary layer interaction, and then change the whole process of ignition in the hydraulic cylinder. In addition, due to the ignition of hydrogen gas, the working pressure, temperature and oxygen concentration will have corresponding changes, and finally the exhaust characteristics under the variable RH2 standard are different from those under the pure diesel engine standard. In a diesel engine, the consumption of CO and HC is very small. In addition, due to the high diffusion of the hydrogen fuel cell, the agitation of the diesel engine and the atmosphere will be more uniform, and the combustion conditions in the cylinder will be further improved. As a result, the emissions of CO and HC are further reduced. So, the main emission would be NO and soot production only. Figure 2.19 and Figure 2.20 show the mass fraction and formation of NO emission.

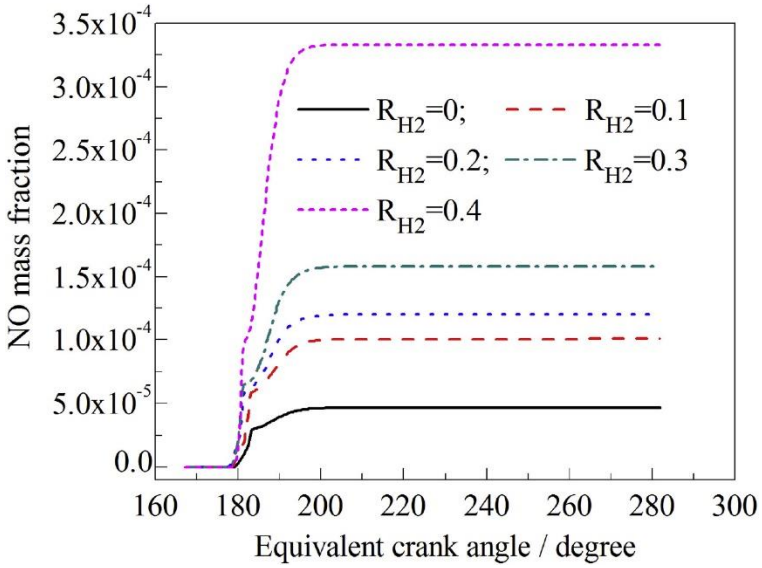

Figure 2.19 NO mass fractions [157]

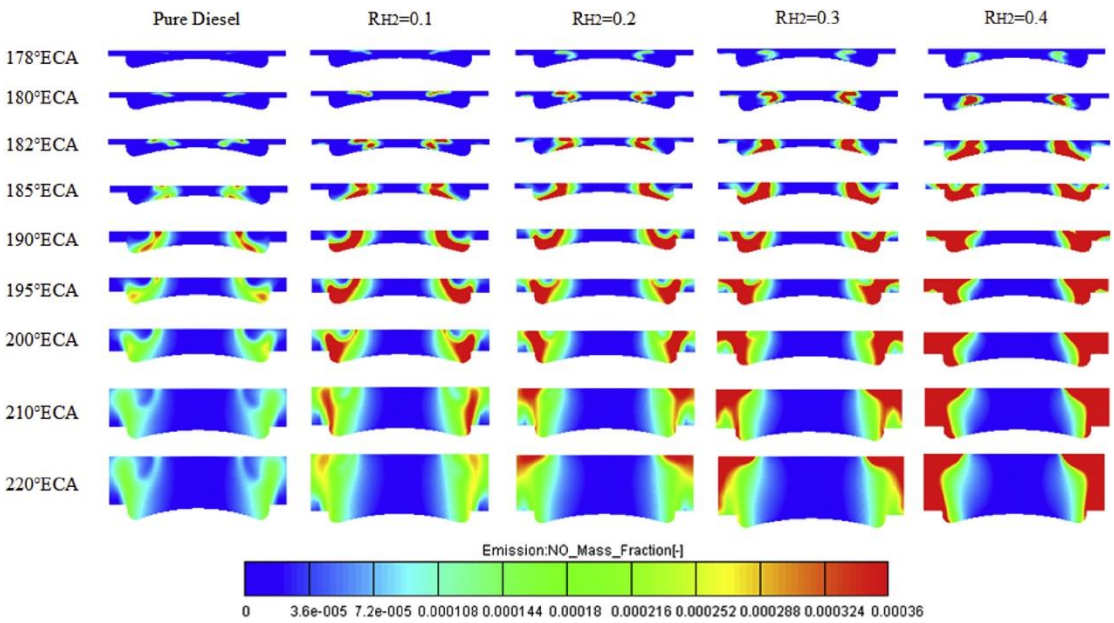

Figure 2.20 Formation of NO [157]

Figure 2.21 shows the hazard of RH2 on FPE soot formation. It can be seen that RH2 has an adverse effect on the dust of FPE. When RH2 is 0.4, the dust of FPE is 24 times lower than that of steel diesel engine. In addition, the whole process of the establishment of soot in Fig. 21 shows that under a large RH2 standard, ash is produced earlier and oxidized to a lower level. Factors leading to this may be some of the following levels. First of all, hydrogen has the advantages of faster ignition speed and good spreading characteristics. Therefore, adding hydrogen fuel cells to FPE can promote diesel engine ignition more comprehensively, and finally reduce soot. Secondly, in order to ensure that the total calorific value in the cylinder remains stable, with the increase of RH2, the quality of the diesel engine is correspondingly reduced, which in turn results in a reduction in the hydrocarbon content. Third, after adding hydrogen gas to FPE, because of the high temperature, nitrogen oxides are very easily oxidized, so the final ash is reduced. In addition, as mentioned above, when RH2 is increased, the frequency of FPE activity is also increased, which promotes a more homogeneous mixture. In addition, the increase of the engine compression ratio causes the main cylinder gas temperature and working pressure to increase, which is also beneficial to the mixing of natural materials and atmosphere.

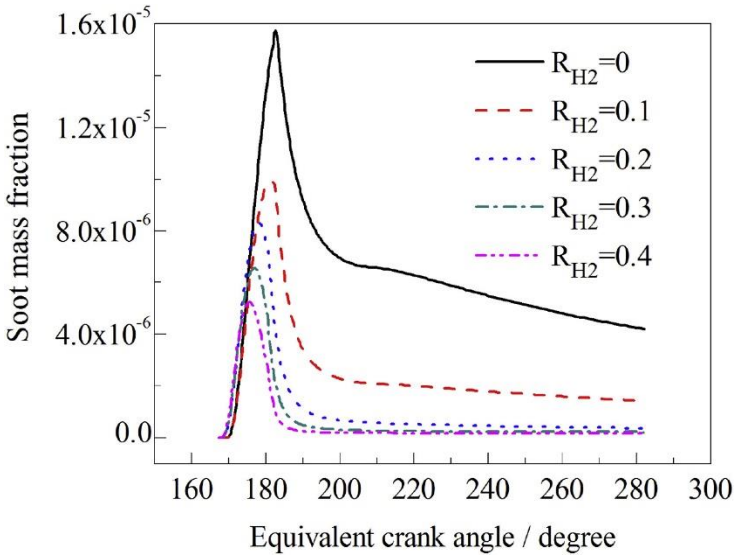

Figure 2.21 Soot mass fractions [157]

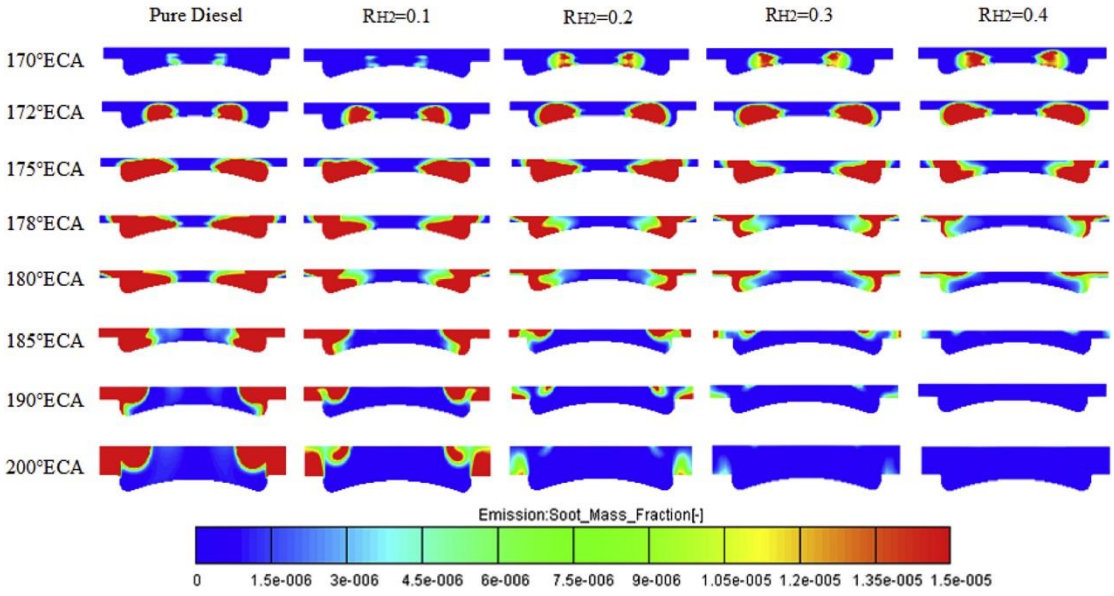

Fig 21. Formation of soot [157]

They found that, compared with the operation of pure diesel engine, the addition of hydrogen can increase the NO emission slowly. When the RH2 reaches 0.4, the amount of NO produced is larger. Nevertheless, soot consumption is inversely proportional to the hydrogen addition rate. When RH2 is 0.4, the dust of FPE is 24 times lower than that of steel diesel engine.

For the first time, Ugochukwu Ngwaka and an elite scientific research team have carried out a comprehensive test in the world: a pilot scientific study of the innovative hydrogen fuel cell dual piston FPEG in two-stroke and four-stroke thermal cycle systems [158]. It was found that compared

with the two-stroke cycle system, the four-stroke cycle system mainly showed a slightly higher maximum working pressure of the master cylinder and a higher overall master cylinder working pressure from the peak working pressure position to BDC. It can be seen that the ignition time of the four-stroke cycle system is longer than that of the two-stroke cycle, and the factor that the cylinder ignition working pressure is higher and the ignition time is longer in the four-stroke cycle system is because of charge mixing work capacity and longer ignition time. The high efficiency of scavenging is inherited from the whole process of the four-stroke cycle system. In the four-stroke mode, the indicated high efficiency due to FPEG is enhanced by 13% compared to the actual operation mode of the two-stroke, as shown in Figure 2.22 below. The NOx emission profile of FPEG at an actual operating frequency and equivalence ratio of 0.4365 at 5 Hz is shown in Figure 2.23 below for the emission fraction. The two-stroke mode of FPEG resulted in 44 ppm of NOx emissions and less than 84 ppm of NOx emissions for the four-stroke mode. This is mainly because of master cylinder temperature, a four-stroke cycle system has more cycles than a two-stroke cycle.

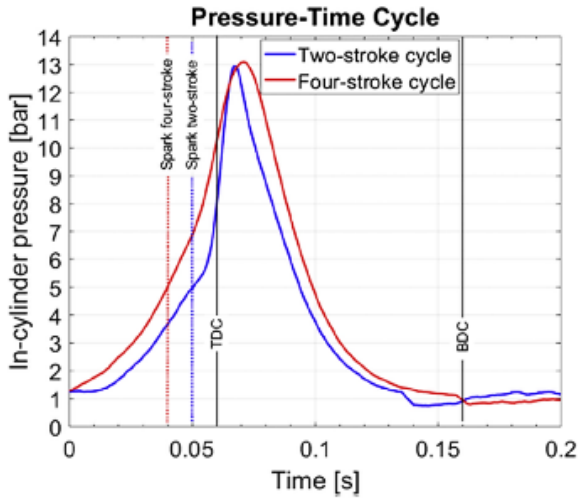

Figure 2.22 Pressure development in a mean two-stroke and four-stroke cycle [158]

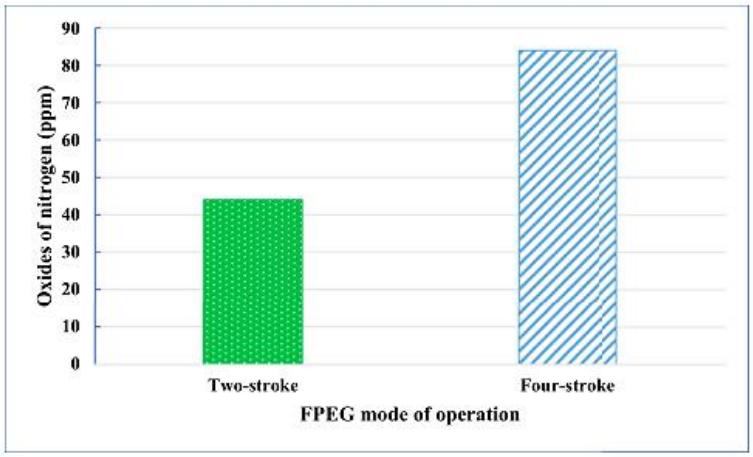

Figure 2.23 NOx emissions from FPEG [158]

Zhang and Sun created a trajectory-based ignition control measure to study the ignition characteristics and emissions of FPE. Their simulations took into account seven different types of renewable natural materials, including hydrogen gas, biogas slurry, syngas, and ethanol, dimethyl ether (DME), biodiesel and Fischer-Tropsch fuel. The scientific research takes into account the hazard of the engine compression ratio (CR) and the reciprocating motion mode between the two dead centers on the whole ignition process, confirming the extreme flexibility of fuel operation and the large tolerance of fuel residues of FPE. In addition, the simulation results show that under a fixed CR, the thermal efficiency of the FPE can still be improved by only changing the reciprocating motion (5% in the DME condition). In addition to this, a corresponding asymmetrical piston movement profile is generated to further increase the thermal efficiency of the car engine (8% in hydrogen conditions) and at the same time reduce NOx emissions (about 70% in hydrogen conditions). Due to its ultimate fuel flexibility, large tolerance of fuel impurity, and controllable piston trajectory, the FPE, with the trajectory-based combustion control, enables a co-optimization of renewable fuels and engine operation [159].

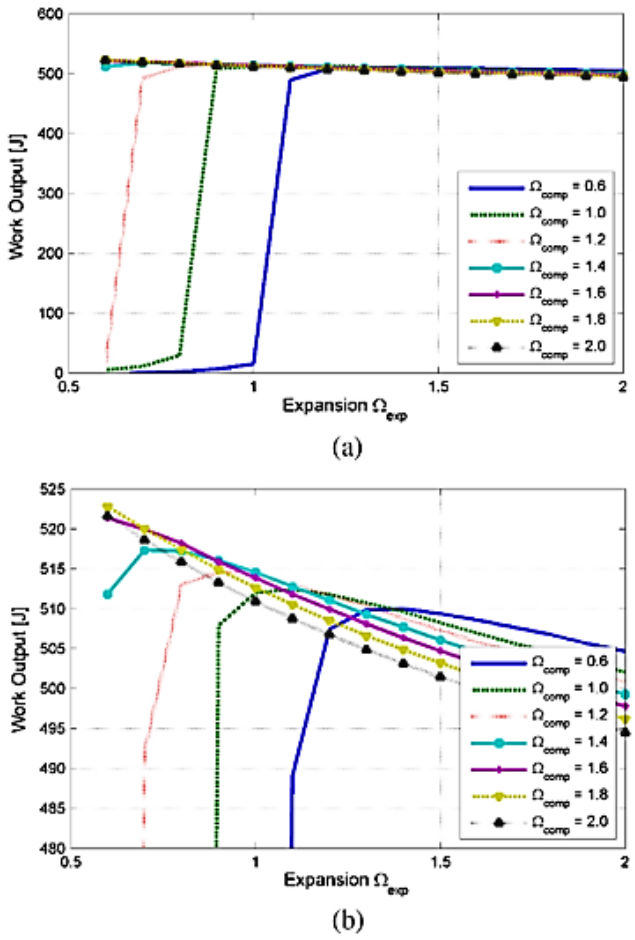

Figure 2.24 Work output along asymmetric piston trajectories, indicated by two Ωs (H2, AFR = 2, CR = 22, (b) is the zoom-in view of (a)) [159]

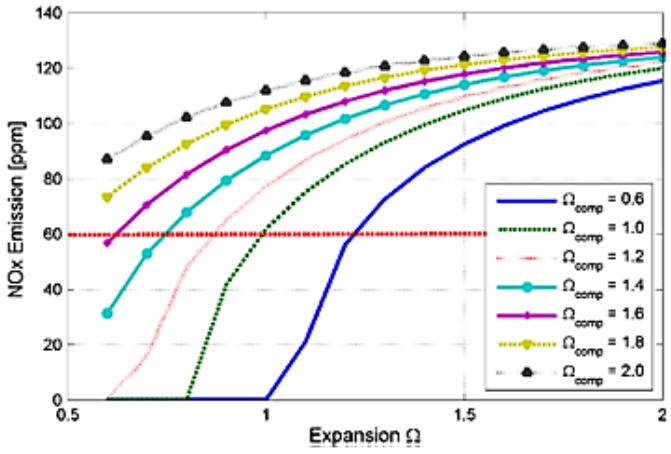

Figure 2.25 NOx emission along asymmetric piston trajectories, indicated by two Ωs (H2, AFR = 2, CR = 22) [159]

Figure 2.25 shows the corresponding NOx emissions after the same settings as in Figure 2.24. It can

be seen that NOx emissions are in the range of 30-140 ppm for all simulated examples, significantly less than the typical range of NOx emissions, 100-500 ppm, in conventional automotive engines (almost 70% reduction) [160][161]. In general, the least Nox expulsion is based on the least Ω_{exp} that can be done. This motion profile gives faster expansion, thus immediately reducing the master cylinder temperature and freezing NOx causing the reaction [162]. In the research of many people, it is found that the ignition control according to the motion trajectory performed by the FPE with the virtual engine crankshaft organization is applied to renewable materials. Seven renewable fuels, such as hydrogen, biogas slurry, syngas, ethanol, DME, biodiesel, and F-T fuels, are fully considered in the paper. The results show that FPE has the ultimate raw material operation flexibility. In addition, a suitable CR can also be selected, which can not only ensure ignition, but also expand the tolerance of poor components in renewable natural materials. In addition, a moderate reciprocation pattern between the 2 dead centers can be defined to reduce the CR required for each renewable material and further improve the high efficiency of the car engine (up to 5% in DME conditions). Ultimately, the best asymmetrically densified piston trajectory for a given renewable fuel design can significantly reduce NOx emissions (70% at H2 conditions) while increasing thermal efficiency (at H2 conditions) 8% increase). The ignition operation according to the motion trajectory realizes the cooperative improvement of the fuel and the operation of the automobile engine. Under such circumstances, both renewable and traditional natural materials can improve their production in terms of their own physicochemical and organic chemical characteristics, environmental hazards and marginal benefits. It is then also possible to improve car engine operation by maintaining the best possible piston trajectory in the FPE, which is generated according to the special characteristics of common materials, variable load regulations and stringent emission regulations, which may be the only scientific study of ethanol presently used in FPE [162].

In general, there are relatively few scientific studies on the discharge characteristics of FPE from renewable natural materials, so this study is devoted to a detailed and comprehensive report on the discharge results of FPE.

2.1.3.3 Biofuel

biofuel, is defined as any fuel that is derived from biomass—that is, plant or algae material or animal

waste. Because these raw materials can be replenished relatively easily, biomass is considered a renewable resource, as opposed to non-renewable resources such as crude oil, coal, and gas. Biomass is often seen as a cost-effective and green alternative to crude oil and other non-renewable resources, especially in light of rising crude oil prices and growing concerns about the contribution of non-renewable resources to global warming. Many critics have expressed concern about the expansion of some biomass, due to the socioeconomic and natural environment costs associated with the refining process and its potential to remove large areas of agricultural land from agricultural production [163].

The two most common biomasses are bioethanol and biodiesel.

1. Microbial ethanol is a kind of ethanol made from ethanol, which mainly comes from sugars and carbohydrates formed in glycogen or tapioca starch crops such as corn, sweet sorghum or sweet sorghum. Cellulosic biomass fuels derived from non-food sources such as flowers, trees and grasses have also been developed and designed as raw materials for ethanol production. Ethanol can be used as a car fuel in its pure form (E100), but is often used as a gasoline additive to raise gasoline octane and improve vehicle emissions. Microbial ethanol is widely used abroad and in Mexico.

2. Biodiesel is produced by transesterification of vegetable oils and fats, and is the most common biomass in Europe. It is available as a pure form (B100) vehicle feedstock, but is often used as a diesel additive to reduce fine particulate matter, carbon monoxide and nitrogen oxides in diesel powered vehicles.

In 2019, the world biomass production reached 161 billion liters (43 billion gallons in the UK), an increase of 6% over 2018 [164]. Biomass provides 3% of the world's road freight. The International Energy Agency expects that by 2050, biomass can address more than a quarter of the world's transportation demand, reducing dependence on crude oil [164]. Nevertheless, the manufacturing and trading of biomass has not stepped into the track of the IEA's concept of sustainable development. From 2020 to 2030, the world's biomass production must increase by 10% every year to achieve the overall goal of the IEA. It is expected to increase by only 3% each year for the next 5 years [164].

The high practical operational flexibility of the free-piston engine can give a significant probability of surprise. High automotive engine characteristics can be achieved with a variety of fuels, which allows operators to select fuels based on current fuel prices, overall emission goals, or other reasons. For example, ethanol-vehicle gasoline mixtures are becoming more widespread and widely used in many gasses filling stations in my country. Using modern engine technologies such as variable compression ratio and its electronic control, variable flame engine timing and precise knock sensors, it is possible to enhance car engine operation according to the characteristics of natural materials. However, the most important characteristics of the material are flame rate, engine knock limit and thermal composition. For example, ethanol has a flame rate that is about 30% higher than that of typical motor gasoline, in addition to having more engine knock limits. The fire rate of hydrogen gas is an order of magnitude higher than this natural gas [76].

Ethanol is a renewable natural material made from various plant raw materials commonly known as "biomass fuels". More than 98% of US motor gasoline contains ethanol, usually E10 (10% ethanol, 90% motor gasoline), which is used to air-oxidise the fuel and thereby reduce environmental pollution [165]. Ethanol has a slightly higher-octane number than motor gasoline, giving high-quality stirring characteristics. Minimum gasoline octane rating for motor gasoline to avoid engine knock and ensure safe driving characteristics. Low gasoline octane motor gasoline was blended with 10% ethanol to achieve a specification of 87 gasoline octane [165].

Ethanol contains less power per gallon than motor gasoline, and the level is different, the actual volume percentage of ethanol in the mixture. Denatured ethanol (98% ethanol) has about 30% less power per gallon of motor gasoline. The hazard of ethanol to the rationality of gasoline and diesel is whether the ethanol content in gasoline and diesel and whether the automobile engine is operated with automobile gasoline or ethanol through upgrading [165]. Figure 2.26 shows the manufacturing, trading and trading of ethanol in the US.

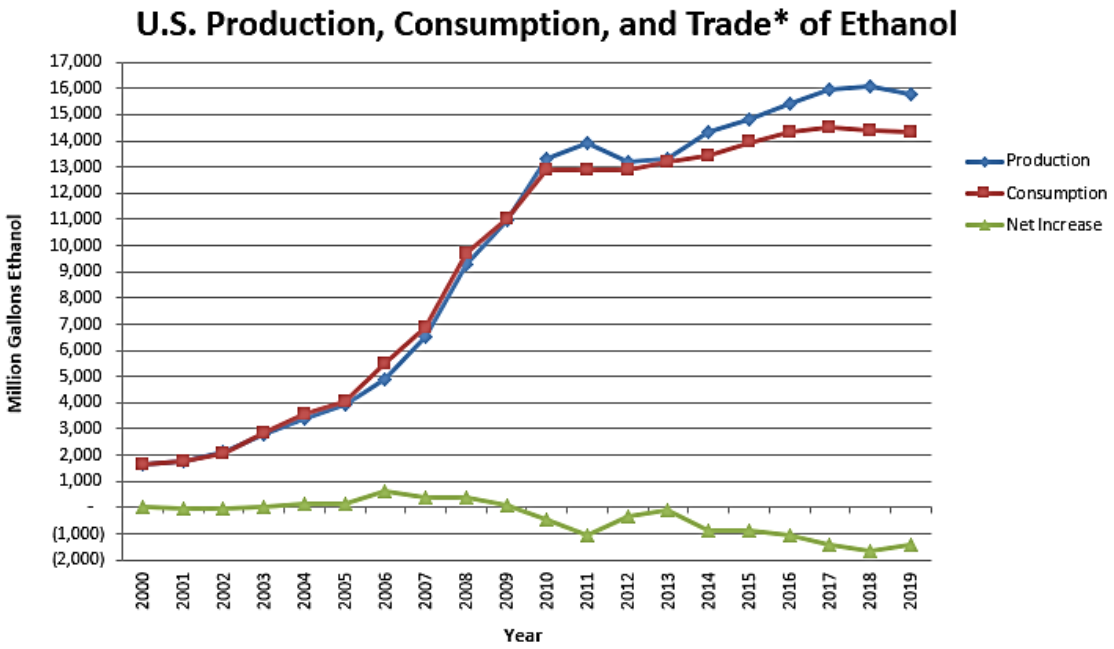

Figure 2.26 U.S. production, consumption and trade of ethanol [165]

Ethanol is mainly produced by renewable biomass fuel according to the whole process of alcohol production. Even before the advent of motor gasoline, it was accepted as a natural ingredient for ICE [166]. At this stage, ethanol is still a promising alternative due to its compatibility with current gas turbines. In addition, ethanol has more gasoline octane, which allows ICE to operate at more CR [167]. The use of ethanol in ICE also reduces emissions such as CO, unignited HC, SOx and NOx due to its higher oxygen content, almost zero sulfur content and lower calorific value (LHV) [166]. It is also known as ethanol, cereal ethanol and EtOH. Ethanol has the same chemical formula, whether it is produced from tapioca starch or sugar chain raw materials, such as corn (the key is abroad), sugarcane (the key in Mexico), or from fibrous raw materials such as wood residue or crop residues.

The production of ethanol is drastically increased from 4.5 billion gallons to 23.4 billion gallons in 2010 globally [168]. Conventionally, ethanol is produced from the food crops, which are easily transformed to simple sugar through milling, liquefaction, and saccharification. Then, the simple sugar is further fermented to ethanol via specific microorganisms. The corresponding chemical process is represented as follow:

$$(C_6H_{10}0_5)_n(sugar, cellulose) + nH_2O \rightarrow nC_6H_{12}0_6 \quad (2.1)$$

$$C_6H_{12}O_6 \rightarrow 2CH_3CH_2OH(ethanol) + 2CO_2 \quad (2.2)$$

Concerns are raised for this approach due to the food supply issues worldwide. Therefore, conversion of ethanol from the non-food lignocellulosic plant, or so-called "second generation feedstock", is extensively explored [169]. Consequently, besides reactions (6), (7), the conversion process of second-generation feedstock is also affected by following reactions:

$$(C_5H_8O_4)_n(hemicellulose) + nH_2O \rightarrow nC_5H_{10}O_5 \quad (2.3)$$

$$3C_5H_{10}O_5 \rightarrow 5CH_3CH_2OH(ethanol) + 5CO_2 \quad (2.4)$$

To date, how to extract simple sugar from these lignocellulosic materials in a cost-effective way, is still a bottleneck for this technology. Usually, such feedstock has been treated through acid hydrolysis and/or enzymatic hydrolysis before the fermentation process [169], which are very energy- and cost-intensive. Other conversion methods, e.g., thermochemical transformation of lignocellulosic materials and ethanol production from microalgae and seaweeds, are also proposed, which have not entered into practice yet.

Chen Zhang et al. studied the properties of different materials (such as hydrogen, biogas, syngas, ethanol, DME, biodiesel, and FT materials) used in free-piston engines using ignition control based on motion trajectories. He found that the results showed that FPE had greater flexibility in material handling. In addition, a suitable CR (engine compression ratio) can also be selected, which not only ensures ignition, but also expands the tolerance of poor components in renewable natural materials. In addition, a moderate reciprocation pattern between the 2 dead centers can be defined to reduce the CR required for each renewable material and further improve the high efficiency of the car engine (up to 5% in DME conditions). Ultimately, the best asymmetrical piston trajectory can be designed for special renewable fuels, which can significantly reduce NOx emissions (up to 70% in H2 conditions) while increasing thermal efficiency (in H2 conditions) 8% increase) [143].

Other than this, very few researches on biofuel of the free-piston has been carried out. In this thesis, both engine performance and emission performance of the ethanol-gasoline blend free-piston engine have been investigated.

2.2 Miller cycle

2.2.1 Atkinson cycle

There are many elements that are closely related to the characteristics of a car engine. Evaluating the characteristics of an automobile engine represents evaluating such different elements, in which dynamic characteristics and economic development characteristics are the two most important aspects. In order to better improve the driving force and economic development characteristics of automobile engines, the most common and traditional way or view is to increase the engine compression ratio [169]. Nevertheless, in all car engines, there is no limit to increase the engine compression ratio. With the increase in the engine compression ratio, some negative conditions occur. For example, the condition most associated with high engine compression ratios is "engine knock" [170]. Thus, in the early 19th century, scientific researchers gradually shifted their focus from engine compression ratios to expansion ratios. However, due to the technical limitations at that time, scientific research could not achieve a stronger increase in the expansion ratio, so it was difficult to improve the high efficiency of automobile engines. In 1882, French technical engineer LeBron James Atkinson based on the diesel cycle system automobile engine, based on a series of complicated crankshafts, the expansion of the four-stroke exceeds the four-stroke expression of the automobile engine. This kind of proper formulation can not only improve the high efficiency of the air intake of the car engine, but also make the expansion ratio exceed the expression ratio, and at the same time improve the high efficiency of the car engine. Thus, the basic principle of this type of automotive engine is hereafter referred to as the Atkinson cycle. Figure 2.27 shows the configuration and trajectories of the engine crankshaft system hardware within the Atkinson automotive engine.

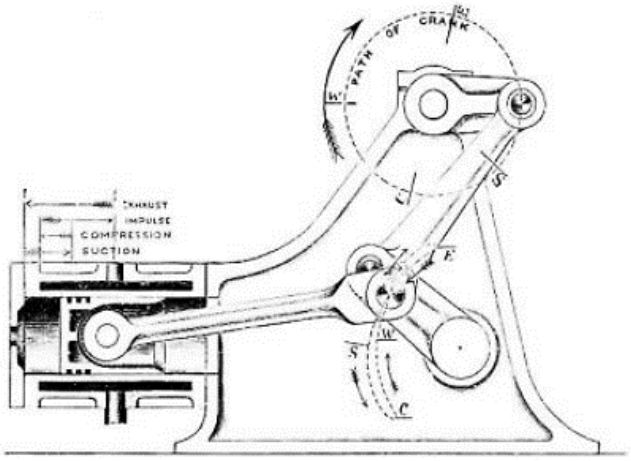

Figure 2.27 The internal configuration of the Atkinson engine [170]

Depending on the engine structure, a longer, expanded four-stroke can more reasonably utilize the high fuel pressure. Therefore, the fuel consumption and output power of the Atkinson cycle car engine are better than the standard cycle car engine of the same generation. Figure 2.28 shows the working comparison of the Atkinson cycle car engine with the standard cycle car engine.

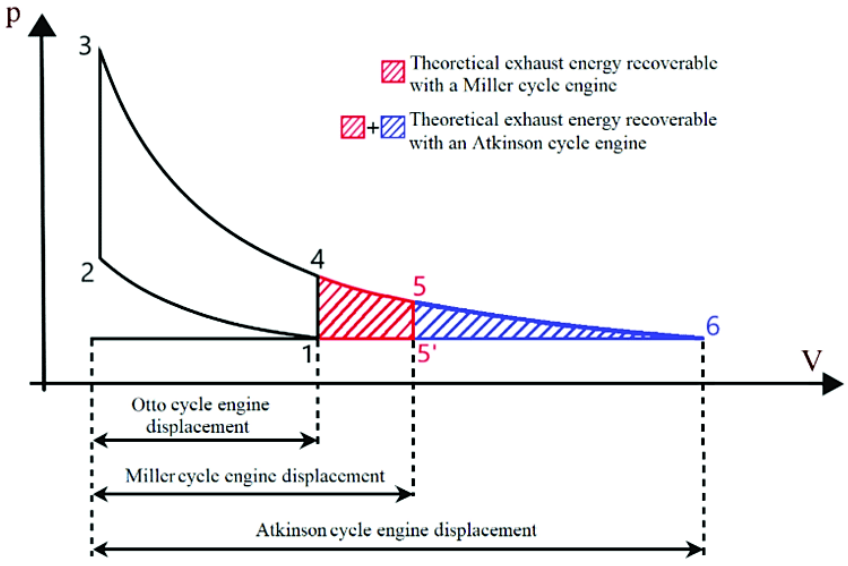

Figure 2.28 Working comparison of the Atkinson cycle with the standard cycle

At the same time, the Atkinson cycle also improves the discharge characteristics. Even so, because of the complicated internal linkage equipment, the volume of the car engine is usually larger than that of the standard car engine. In addition, the failure rate of mechanical equipment is high, which

means that the car engine is not stable. Therefore, the implementation of the Atkinson cycle automotive engine in the automotive industry is difficult. Nevertheless, at the beginning of the 20th century, many scientific studies on large and medium-sized diesel engines such as marine engines and first-generation automobile engines introduced the definition of the Atkinson cycle. All in all, the discussion and development of the Atkinson cycle has been going on since the early 19th century to the present day. In 1988, Ma and Rajabu created a solid model of the Atkinson cycle vehicle engine based on measured and simulated simulations [171]. This scientific study is about applying the Atkinson cycle to a diesel cycle car engine. The simulation data shows that different characteristic variable values show that, in a multi-inlet vehicle engine, different intake port engine timings match different engine compression ratios. In 1991, Blakey created the diesel Atkinson car engine in the laboratory. In the engine, there is a variable valve timing (VVT) automatic control system [172]. The control system can complete the delayed closing of the intake valve and obtain a variable compression ratio. However, the limitations of automatic control systems depend on the fact that the engine compression ratio cannot be precisely controlled, only within a rough range. In 1995, Boggs and Schechter's scientific research focused on gasoline and diesel rationality and exhaust pipe characteristics [173]. In the test, the Atkinson cycle automobile engine can achieve the higher power of the diesel engine cycle system automobile engine under the overload working condition under the partial load working condition. The results show that the fuel consumption of the Atkinson cycle car engine accounts for 85% of the value of the diesel cycle system car engine. At the same time, the NOx and CO consumption of Atkinson cycle automotive engines is only 50% of that of diesel cycle systems.

In 2006, Ge Yanlin deduced the relationship between the engine characteristics and the engine compression ratio in the gas specification Atkinson cycle automobile engine based on the finite element analysis [174]. In the analysis, both thermal conduction and internal friction damage are taken into account. In the following year, Ge Yanlin further scientifically researched the heat conduction of working fluid, frictional damage and its variable specific heat capacity on the operating characteristics of the Atkinson cycle automobile engine and gas specification that cannot pass through the regenerated Atkinson cycle automobile engine [175]. In the same year, Shuhn-Shyurng Hou addressed the comparison of the practical characteristics of the Atkinson cycle and

diesel cycle systems [176]. In the test, many main parameters are involved, such as engine compression ratio, inlet temperature and net output power derivation. The results show that, under the same working conditions, although the engine compression ratio of the diesel cycle system automobile engine is higher than that of the Atkinson cycle automobile engine. The thermal efficiency and power output of the Atkinson cycle are higher than those of the diesel cycle system. In 2009, J. Benajes [177] explicitly proposed the harm of the Atkinson cycle to super heavy duty diesel engines. In the study, the Atkinson cycle was used on an HD diesel engine and interacted with the EGR system hardware. Statistics show that, compared with traditional diesel engines, the thermal efficiency of the Atkinson cycle under low-load operating conditions (25%) is mainly manifested. At the same time, scientific research has also found that the concentration of oxygen in the intake of an Atkinson cycle vehicle engine is reduced, which in turn results in a reduction in NOx consumption.

In 2013, a new approach was explicitly proposed, fusing responsive neural system fuzzy inference system hardware and a variable intelligent bee optimization algorithm, the classic Atkinson cycle improved by Mozaffari Ahmad and Alireza Fathi [178]. As a comment on the new approach, practical improvements are clearly proposed. In the same year, Zhao Uranus and Xu Min used evolutionary algorithms to improve the fuel efficiency of Atkinson cycle automobile engines [179]. According to the scientific research of the ancestors, the optimal geometry engine compression ratio of the Atkinson cycle automobile engine is 12.5 under overloaded working conditions. The core of Zhao's analysis is part of the workload. The engine compression ratio is changed after the upgrade, and the fuel consumption is reduced by 7.67% under some load conditions. In 2014 Pietro Capaldi [180] designed and established a 10 KW microgenerator according to the Atkinson cycle.

2.2.2 Miller cycle

Since the invention of the Atkinson cycle, the definition of discrete variables of engine compression ratio and expansion ratio has gradually attracted the attention of scientific researchers. And clearly put forward the definition of overexpansion circulatory system. In the 1940s, the scientific study of the circulatory system of hyperinflation made great strides. The original Miller cycle was explicitly proposed by Ralph Steiger. Compared with the Atkinson cycle automobile engine, the Miller cycle

automobile engine eliminates the more complicated crankshaft system hardware, and can achieve the actual effect of over-expansion according to the adjustment of the air distribution opportunity. Some references claim that the Atkinson cycle also refers to Intake Delay Time Closure (LIVC) countermeasures. However, there is no established direct evidence to support this view.

In 1947, "High Output Supercharging and Internal Cooling Cycle" was published. In this article, the definition of the Miller cycle is explicitly proposed by Ralph Steiger, and the Miller cycle is understood as an intercooling circulatory system [181]. For a four-stroke engine, the original design was to close the intake valve before bottom dead center (BDC) and the end of the intake port. This countermeasure can reduce the gas output and its reasonable engine compression ratio. At the same time, tailpipe engine timing must not be compromised. In other words, the expansion ratio is consistent with the expansion ratio of the standard cycle system automobile engine. Therefore, the final practical effect of the Miller cycle is that the reasonable expansion ratio is likely to be higher than the reasonable engine compression ratio, thereby improving the high efficiency of the automobile engine.

In the early stage, the marketing promotion of the Miller cycle was obviously limited because the energy export damage of the Miller cycle automobile engine was mainly caused by the reduction of the input gas and its high fuel consumption and soot emission. at the level of automobile manufacturing. Since the 1970s and 1980s, with the development trend of turbocharging technology, the major problem of the air intake seems to have been solved, and then the concept of Miller cycle has been re-understood by scholars, and it has received more and more attention from us. According to the current scientific research, the integration of the two-stage turbocharger intercooling system hardware can achieve the intake port quality under the standard of early closing of the intake valve. In addition, according to the whole process of the intermediate cooling tower, the air temperature of the gas can be further reduced, which can reasonably result in a lower original ignition temperature. Finally, under the same gasoline and diesel injection standards, the maximum ignition temperature in the cylinder can be lower, and the NOx emission can be limited to a certain level. At this stage, there are two key ways to complete the Miller cycle. One is to close the intake valve early (EIVC). The other is the Bypass Valve Delay Time Off (LIVC). Figure 2.29 shows the P-V plots of the EIVC and LIVC Miller cycles.

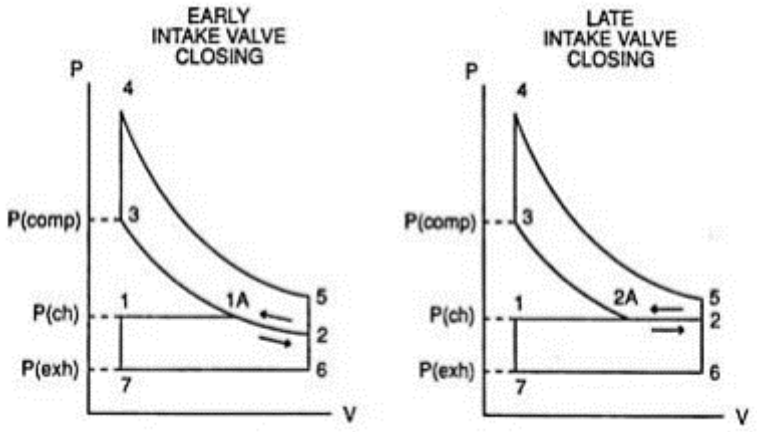

Figure 2.29 P-V diagrams of the Miller cycle engine [181]

At the 1957 Congress of the International Gas Turbine Consortium (CIMAC), Ralph Steiger further demonstrated the operation of the Miller cycle in diesel and natural gas engines. In the initial Miller cycle, the closing engine timing of the intake valve is retarded at the end of the intake four-stroke, which represents a portion of the intake port being expelled out of the cylinder. After closing the intake valve, the whole process is gradually and truly reduced. Therefore, a reasonable compression stroke is shorter than an expansion four-stroke [182]. In the 1960s, the invention of the variable valve timing automatic control system made the completion of the Miller cycle more convenient [183]. In 1978, Bradford Bates and D. H. Smith created a variable displacement car engine based on adjusting intake and exhaust valves. The engine has excellent gasoline-diesel rationality and exhaust pipe characteristics [184]. In 1982 Tommy released various VVT solutions for gasoline engines. W. Asmus. In the analysis, a comparison of different solutions for different car engines is also pointed out [185].

In 2009, more than 6 papers were published, all of which were related to the application of new technologies to Miller cycle automobile engines. In this graduation thesis, very professional valve engine timing, high pressure common rail injection system hardware, new increased pressure equipment, fully variable cylinder organization and new air inlets are all involved. This new composition is close to the active performance of the Miller cycle car engine. At the same time, relative statistical analysis methods are also clearly proposed to detect or apply new independent innovations. In addition, the use of Miller cycle involves many new automobile engines [186-189]. Lin Zhu applied the Miller cycle to a 12-cylinder medium speed car engine [190]. Federico Millo

applied the Miller cycle to a medium speed marine engine and evaluated the correlation of EGR ratio with Steiger engine timing [191]. In the analysis, NOx consumption was reduced by 90%, along with a magnitude increase in fuel usage. Since then, in the discussion of Li Zongfu, the function of different two-stage superchargers in the marine Miller cycle automobile engine has been analyzed [192].

The new J920 gas engine developed by Klaus Payrhuber is a fast and efficient Miller cycle automotive engine. The most obvious characteristic of this engine is that it operates very well in highland conditions [193]. The exhaust pipe characteristics of Jeffrey Blair's Rotax ACE Miller cycle car engine is better than BAT specifications because of the use of an excellent catalytic converter [194]. At the same stage, Stöber-Schmidt also pointed to the Miller cycle for medium-speed automobile engines. There is an EGR system hardware in the engine [195]. The calorific value of the Scuderi split-cycle automotive engine has been significantly improved according to the use of the Miller cycle [196]. In the same year, Michael Riess studied the use of the Miller cycle in the creation of seepage [197]. In 2012, the new increased pressure system hardware - Power2 and VCM (Gate Valve Operation Management Method) - was developed and designed by ABB LLC. The system hardware is aimed at a larger-scale Miller cycle diesel engine [198]. With the development of scientific research, the harm of Miller cycle to various detailed characteristic elements of automobile engine has been clearly put forward. A study by L Miklanek found a correlation between intake air temperature and Miller cycle automotive engines [199]. Rahim Ebrahimi discovered the effects of air-fuel ratio and four-stroke length on the characteristics of Miller-cycle automobile engines [200][201]. In addition to internal reasons, external factors also aroused the concern of scientific research staff.

In 2011, a Miller cycle diesel engine applying hydrocracking to address edible oil (HVO) to replace diesel achieved a substantial reduction in PM emissions [202]. Tests have shown that NOx consumption is also reduced by 50%. In 2012, the application of HVO to high pressure common rail Miller cycle automotive engines also reduced NOx consumption by 50% [203]. In the same year, Juha Heikkilä discussed the overall characteristics of HVO Miller cycle automotive engines under different loads. According to the analysis, the most significant reduction in the displacement of substituted hydrocarbons is at the moderate velocity level [204]. The core of Wang Chongming's

analysis is the comparison of the characteristics of gasoline and DMF in the Miller cycle automobile engine. The results show that the thermal efficiency and exhaust pipe characteristics of DMF are better than those of motor gasoline [205].

In 2013, Wolfram Gottschalk [206] further improved the working ability to avoid the engine knock problem in the incineration chain of the Miller cycle gasoline engine. At the same time, the analysis of the Miller cycle combined with the leaner ignition technique conforms to the US National Park Service (NPS) Best Available Technical (BAT) specification [207]. Based on CFD simulations, Guven Gonca and Carlo Alberto [208][210] each produced characteristic maps of the double Miller cycle in a fast direct injection (HSDI) automotive engine. In 2014, the application of ultra-low temperature ignition technology was closely combined with the hybrid automatic control system, and the NOx and PM emissions of ultra-heavy Miller cycle automobile engines were reduced to a certain extent [211,212]. In the analysis, the hazards of closing the intake valve delay time and closing the intake valve early in the Miller cycle are analyzed. The results show that EIVC has stronger characteristics under long-term load working conditions, and the fuel consumption is reduced by 12%, and LIVC has no improvement on the car engine. However, under low load operating conditions, the gasoline and diesel consumption of the LIVC Miller cycle vehicle engine is reduced by 7.8%, and the EIVC Miller cycle value is 6.8% [213]. Based on the introduction of the dominant gasoline and diesel injection system hardware into the Miller cycle automobile engine, Clemens Brückner further studied the hazards of the Miller cycle on the exhaust pipe characteristics of a 3.9-liter low-speed light-load diesel engine [214]. Based on the Apparent Exothermic Reaction Rate Analysis (AHRR), the EGR-checked hazards of NOx emissions from medium-speed heavy-duty Miller-cycle automotive engines were obtained [215]. Incorporating steam injection technology, the direct injection engine Miller cycle diesel engine reduces NOx emissions by 48% and HC emissions by 46% [216,217]. In 2015, Audi clearly proposed a new 2.0L flame ignition car engine. The use of the Miller cycle enables the maximum torque-speed derivation to be 320N.M, and the maximum speed ratio of the automobile engine is 4400 rpm [218].

Through 70 years of development trends, from the perspective of experiments and analysis, the analytical level of the basic theory of Miller's cycle has long been perfected [219]. With the increasing attention to the natural environment and the diversification of the automobile

manufacturing industry, the Miller cycle automobile engine will be widely promoted in the engine sales market [220]. Chengqian created a zero-dimensional simulation solid model in 2019 to study the exhaust characteristics of a Miller-cycle automobile engine using gasoline and ethanol as raw materials [221]. In this scientific study, the effects of the Miller cycle on NOx and other particulate emissions on diesel engines, and the use of ethanol as a substitute for NOx and other particulate emissions characteristics were investigated. The high temperature in ignition drives the formation of NOx, and the Miller cycle belongs to the ultra-low temperature cycle system in the automobile engine, so it is a reasonable way to reduce the NOx emission. And the reduction range of NOx was between 8.5% and 12.9% comparing with what produced by conventional Diesel cycle as shown in Figure 2.30. And the effectiveness gained by the combination of Miller cycle and ethanol was relatively prominent. To summarise the whole consequences, applying Miller cycle into diesel engine could effectively reduce NOx and other particulates emissions, and ethanol could bring a larger improvement to the emission performance as long as the demand of output power can be met.

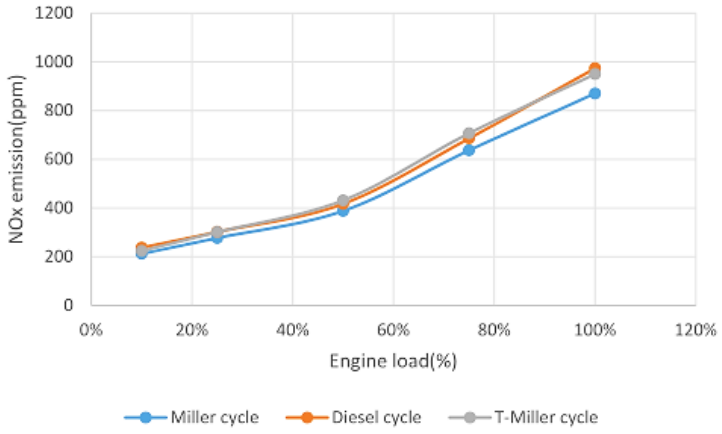

Figure 2.30 NOx comparison between Diesel cycle, Miller cycle and T-Miller cycle [221]

Lin et al. applied comparative finite-time thermal analysis to characterize the irreversible canonical Miller cycle in a four-stroke free piston engine [119]. In the solid model, the internal reversibility of the efficient description of shrinkage and expansion, the specific heat capacity of the substance in operation at its temperature, the heat conduction damage as a percentage of the kinetic energy of the natural material, and the friction damage based on the mean value of the interrelationships take into account the piston rate. In addition, according to the detailed calibration example, the damage of other engine compression ratios corresponding to excess air coefficient, original temperature,

engine compression ratio and expansion level to Miller cycle is analyzed. The results show that the high efficiency is enhanced with the reduction of the specific heat capacity of the steam parameter. Thermal conduction damage and frictional damage adversely affect properties. The comparison of Miller cycle and Otto cycle shows that Miller cycle has more high efficiency according to the additional expansion work. The results of this analysis have key practical implications for the evaluation and refinement of specific Steiger automotive engine characteristics.

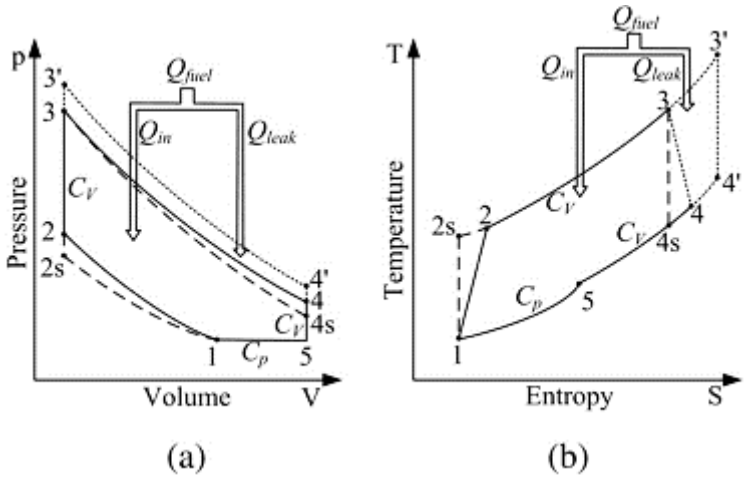

Figure 2.31 (a) p–V diagram; (b) T–S diagram for the air standard Miller cycle [119]

The working pressure-volume (pV) and temperature-entropy (TS) of a non-reversible four-stroke free piston are shown in Figure 2.31 above: Thermodynamic cycle 1-2s-3′-4′-5-1 shows ideal the reversible Miller cycle with no heat leakage, the thermodynamic cycle 1-2s-3-4s-5-1 shows the reversible Miller cycle with heat leakage, and the cycle system 1-2-3-4-5-1 Indicates an irreversible Miller cycle with thermal leakage. The internal reversibility originates from the heat transfer contraction and expansion process. Processes 1-2s are isentropic (reversible heat transfer) reductions, while overall processes 1-2 are irreversible adiabatic processes with internal reversibility taken into account in the specific reduction overall. Warming occurs in the overall process 2-3, which is also isovolumic. The general process of isentropic expansion 3-4s is a reversible heat transfer schedule, and the whole process 3-4 takes into account the reversibility generated during the specific expansion operation. This cycle is carried out by the adiabatic process 4-5 and the isobaric 5-1 heat dissipation process. In this analysis, the heat leakage in the ignition link is fully considered, and the temperature (T3) at which the titrant is ignited in the past depends on the thermal

input at the time of ignition and the heat leakage according to the cylinder wall. Heat leakage is considered as a percentage of the kinetic energy of the transport material [222]. If all heat leakage occurs, the maximum circulating system temperature T3 is still lower than the case of no heat leakage.

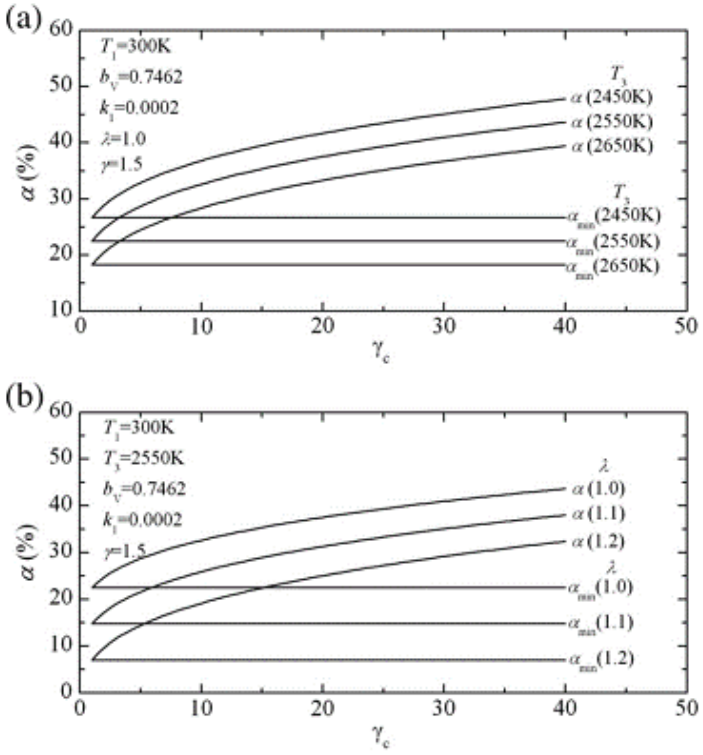

Figure 2.32 (a) The heat leakage percentage affected by the maximum cycle temperature;(b) the heat leakage percentage affected by the excess air coefficient [119]

The transformation of the heat leakage percentage α relative to the larger circulation system temperature T3, the excess air coefficient λ and the engine compression ratio γc is shown in Figure 2.32(a). In the same year, Lin et al. used the basic theory of adaptive control to simulate the adaptive control trajectory of a four-stroke Miller cycle FPE, derived from the Internet under different conditions of profit maximization. Figure 2.33 shows the reciprocating motion graph for the best STD condition compared to the conventional STD condition, and Figure 2.34 shows the working pressure and temperature graphs for the best STD condition compared to the conventional STD condition Graph. Figure 2.34 also shows that the thermal conduction damage is lower compared to the conventional condition. Combining the above observations, the heat conduction key appears in

the expansion stroke arrangement, and the expansion time t_p after the lift is significantly reduced, so the contact time between the high-temperature mixture and the cylinder wall is also reduced.

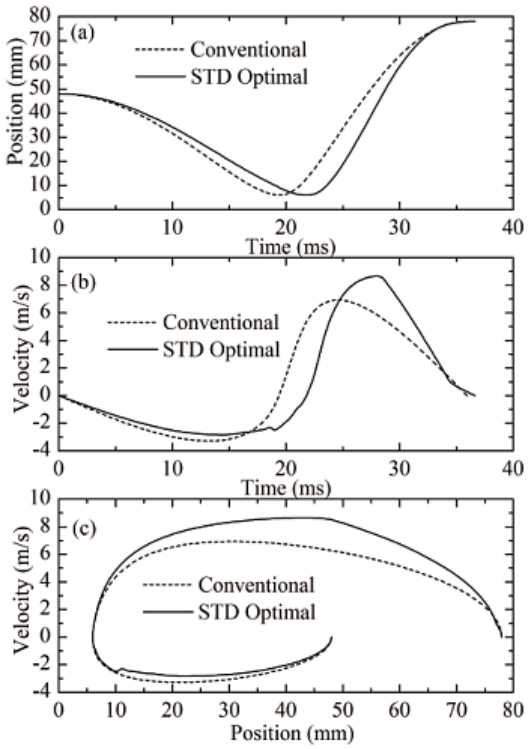

Figure 2.33 Comparison of optimal and conventional piston motion curves for the STD case [119]

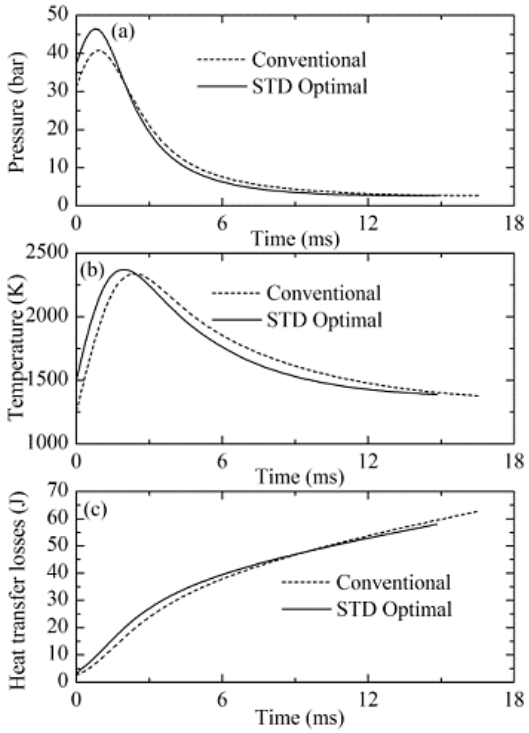

Figure 2.34 Comparison of optimal and conventional thermodynamic curves for the STD case [119]

The results show that optimizing the piston motion has the potential of improving the free-piston engine efficiency by more than 10%, which is primarily due to the increase of average pressure and reduction of the heat transfer losses on the power stroke. By optimizing the piston motion around the TDC, the in-cylinder gas pressure and temperature have a remarkable increment while the heat transfer losses have a remarkable descent. In addition to improving the network output there are other advantages that may result from optimizing the piston motion. The cooling demands are greatly reduced, because of the reduction of the heat transfer losses. Although the above researches have not studied the emission characteristics of Miller cycle free-piston engine, but the combustion characteristics and piston motion results are still helpful for the investigation in this paper.

2.3 Summary

This chapter covered the history, advanced findings and recent applications on the free-piston engine, along with a review of Miller cycle. These literatures gave me significant guidance towards this dissertation.

It could be found that there are relatively limited researches on the emission performance of no matter gasoline, diesel or hydrogen fueled free-piston engine and most of results existing are not

comprehensive, and ethanol has barely been applied on the free-piston engine. Moreover, there's only one example existing on the combination of the free-piston engine and Miller cycle; however, emission was not taken into account in that research. Therefore, this dissertation will complete the emission study on the conventional gasoline/hydrogen free-piston engine and Miller cycle free-piston engine as well as the best valve timing of Miller cycle.

Chapter 3. Single-cylinder gasoline FPE modelling and simulation

For the purpose of developing a free-piston engine, it is necessary to build up a simulation model. The model should be able to represent every detail including geometric and combustion properties and assist the design and development. Moreover, the model should be capable of pushing the boundaries in predicting the performance of the prototype without making any changes of the systems' hardware.

This chapter presented the whole process of modelling, validation, implementation and simulation of a two-stroke 65cc free-piston engine using Ricardo WAVE. Section 3.3 presented the prototype (a validated four-stroke crankshaft engine) of this two-stroke free-piston engine. Simulation results were used for different fuel free-piston engine prototype development in Chapter 4, Chapter 5 and Chapter 6.

3.1 Theoretical review

A one-dimensional (1D) model of a gas turbine is a step beyond standard automotive engine thermal profiling. The numbers contain basic thermal equations and work experience correlations that can adequately simulate the overall individual behavior of a car engine to give the basic characteristics and exhaust characteristics of a car engine that has been developed and designed.

1D models and simulation tools are used by key automotive groups in automotive engine development to aid in prototyping designs because it can quickly produce real-world results. In addition to this, it must have less direct cost and accounting cost than 3D Design Aided Design (CAD) design of the car engine. Therefore, in order to better the above advantages, one-dimensional special tools are selected to assist the prototype development and design.

WAVE is a design-aided engineering project package developed by Ricardo that dissects the dynamic models of automotive engine piping, increased operating pressure waves, mass flow and kinetic energy losses in the pressure chambers and intake manifolds. It guarantees date-dependent solutions to one-dimensional equations of fluid mechanics and heat. The hardware features

sophisticated subbody models to simulate friction, heat transfer, scavenging, ignition, engine knock and industrial exhaust.

The terminology and definitions used in this section are based on the composition of the engine crankshaft vehicle engine information content obtained by Heywood [22], Blair [223] and Pulkrabek [224].

The engine combustion chamber and cylinder geometry are defined as shown in Figure 3.1 below. The bore of the cylinder is bore (B). Four stroke (S) is defined as the distance of the piston from (bottom dead center) BDC to (bottom dead center) TDC, the volume within the four stroke is called the stroke volume (V_s). For free piston engines, a standard four-stroke (S_{nom}) would be defined as a four-stroke length that is not stable. When the piston is at BDC, the remaining space between the top of the piston and the cylinder head is called the void volume (V_c), and it is included in the clearance distance (c).

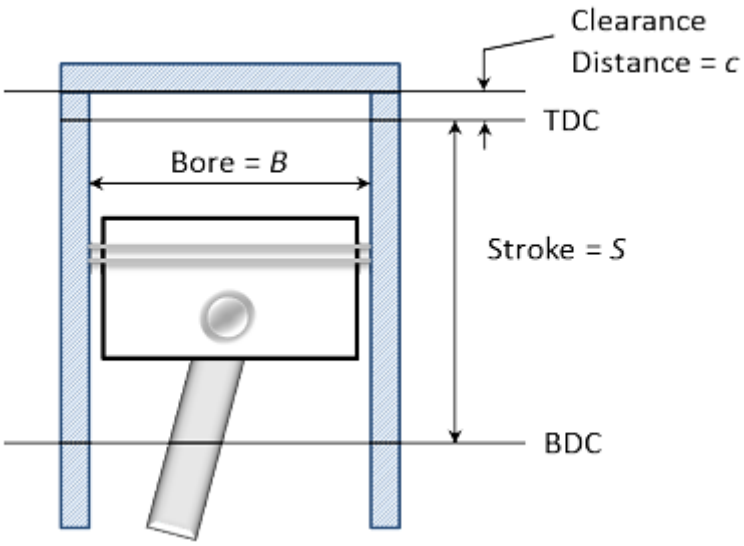

Figure 3.1 Cylinder geometry definitions for an engine with a flat top piston (Without the bowl)

Further parameters and definitions are given by following equations:

- Swept volume, V_S:

$$V_S = \frac{(\pi B^2 S)}{4}[m^3] \tag{3.1}$$

For a known clearance volume (V_c) above the piston at TDC:

- Geometric Compression Ratio, $(CR)_G$ is defined as:

$$(CR)_G = \frac{V_s + V_c}{V_c}[-] \tag{3.2}$$

3.2 Modelling approach and sub-models

Modelling and simulation in the Ricardo WAVE program flow module are carried out using three program segments, as shown in Figure 3.2 below. WaveBuild is a key preparatory handler flow used to simulate the original settings. The program uses its graphical interface design to define the geometric properties and initial conditions of the solid model, which is then transformed into a key-in file format suitable for the solver. WAVE is the solver used in this analysis to obtain all one-dimensional dynamics and thermodynamics time-dependent equations. Finally, after applying WavePost, the CPU can query and express the results in the form of 2D or 3D graphics, photos, text reports or other news media.

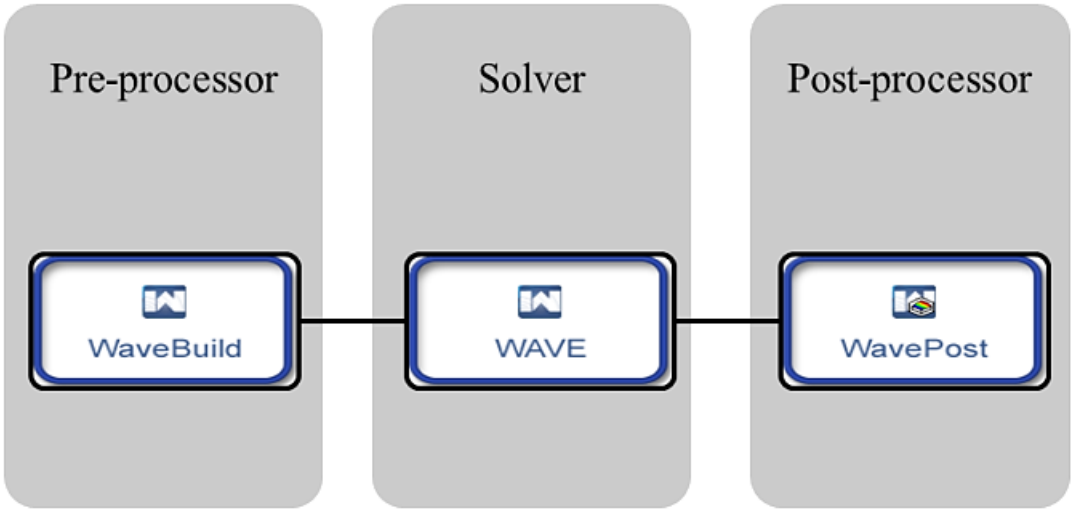

Figure 3.2 Three primary sub-programs in Ricardo WAVE programs suite employed in this research.

The first step in creating an accurate solid model is to gather geometric data information. An automobile engine can be decomposed into key subsystems, namely intake spiral, intake valve passage, cylinder, exhaust valve passage, and exhaust spiral. Specifications and characteristics related to the desired automotive engine are cylinder bore, four stroke, crankshaft length, engine compression ratio, cylinder diameter, cylinder variable valve timing, and cylinder engine timing. The main parameters of automobile engine operation state variables must be defined as automobile

engine operation rate, fuel type, air-fuel ratio and environmental standards (i.e. temperature and working pressure).

The solid model is built in the WaveBuild special tool, and its arguments are shown in Figure 3.3 below. In this basic solid model, the intake side and exhaust pipe side are immediately exposed to the natural environment. As shown in Section 3.3.2, the electronic throttle, intake and exhaust manifold specifications are added to the lift segment of the simulation.

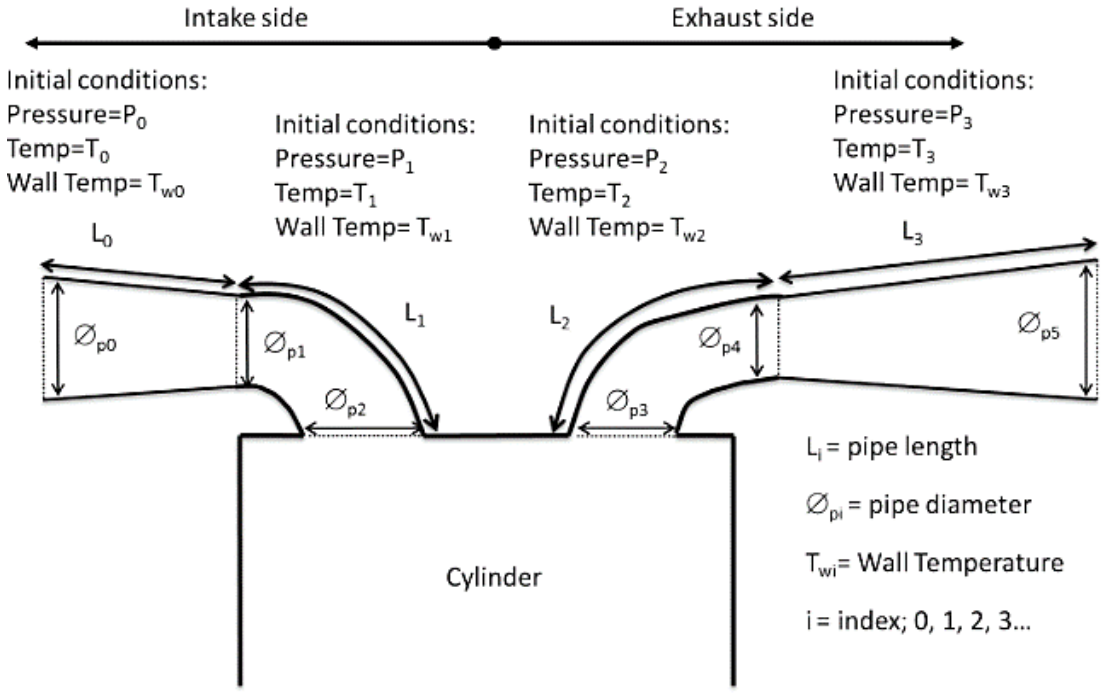

Figure 3.3 Basic model variables and initial conditions

The initial conditions of pressure and temperature were set appropriately and these are recalculated frequently during the simulation. The pipe lengths were centerline lengths. Wall temperature was set appropriately to reflect the actual engine condition based on the correct model building practice guide in the WAVE Help file [225].

3.2.1 Sub-models

The sub-model descriptions presented in this section were obtained from the help file in Ricardo WAVE [225]. Only the relevant sub-models are presented here. By understanding the sub-model, the model can be tuned and optimised by varying the relevant variables. Further, the results can be

efficiently interpreted by understanding the sub-model's capability and limitations thoroughly.

3.2.1.1 Crank/slider piston motion

The crank/slider sub-model represents the relationship between the linear motion of the piston and the rotational motion of the crankshaft as shown in Figure 3.4.

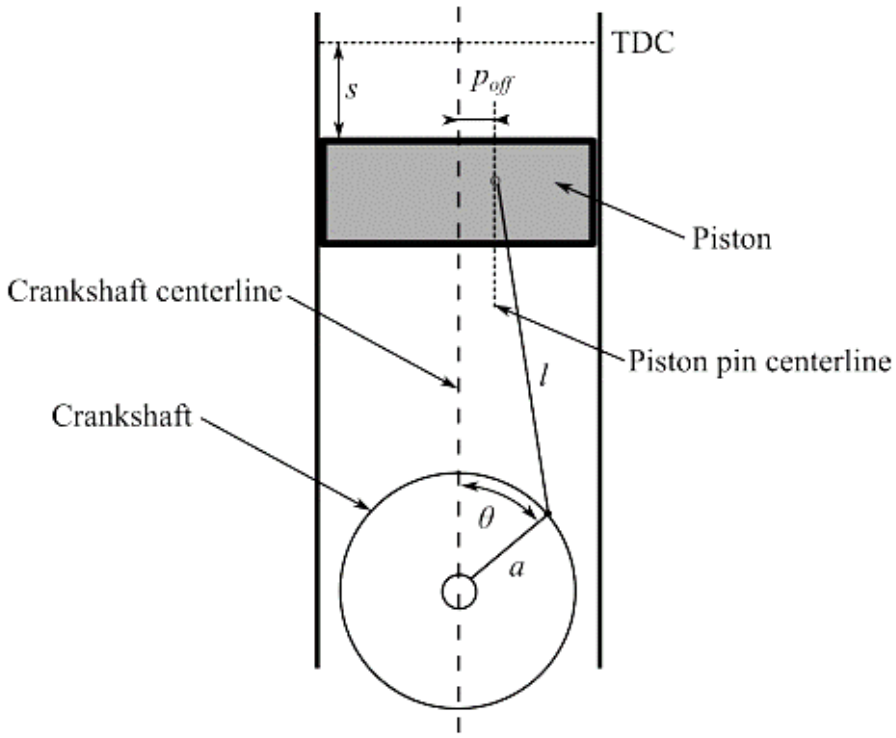

Figure 3.4 Crank-slider mechanism schematic [225]

The formula for this relationship is given by:

$$s = \sqrt{(a+b)^2 - {P_{off}}^2} - a\cos\theta - \sqrt{l^2 - (a\sin\theta + P_{off})^2} \tag{3.3}$$

piston position calculated from the sub-model is used to calculate the volume of the combustion chamber.

The displacement volume of each cylinder is calculated using the same formula given in Equation 3.4.

For a multi-cylinder engine, the total engine displacement volume will be the sum of this individual displacement values.

Next, the clearance volume of each cylinder can be estimated from the geometric compression ratio $(CR)_G$ value input:

$$V_c = \frac{V_s}{(CR)_G - 1} \tag{3.4}$$

Then, the in instantaneous volume in the cylinder at each time step can be calculated:

$$V = V_c + \frac{\pi}{4} B^2 s \tag{3.5}$$

In WAVE, although the clearance distance (c) must be inserted in the geometrical definitions, it is used only for the calculation of heat transfer.

3.2.1.2 Imposed piston sub-model

The reciprocating sub-entity model imposed on is used to cover the gear/roller sub-entity model to simulate automotive engines with novel reciprocating motion profiles, such as rotary, opposed or in this case free piston engines. After being defined, this piston part is used to measure the volume of the combustion chamber of the engine. To apply this sub-entity model in this way, it is important to define a set of gear angle values with corresponding piston parts in the configuration file editor shown in Figure 3.5.

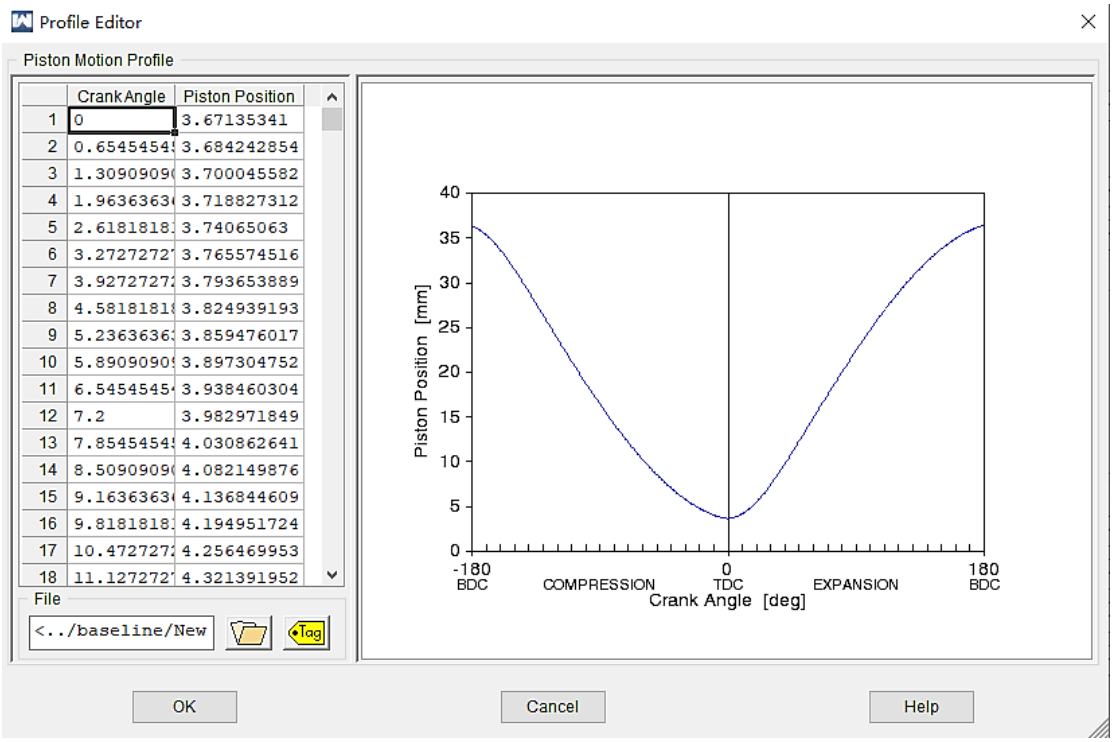

Figure 3.5 Profile editor for piston motion profile to model free-piston engine

The applied gear angle value must encompass the full cycle system of the car engine, while taking care not to exceed the large scale allowed (721 points) and not exceed the four-stroke defined for the car engine to make the results more meaningful. The implication of this limitation is that the number of values that can be entered determines the linearity of the piston velocity graph, which will be discussed in the relevant section later in the text.

3.2.1.3 Friction

The friction solid model in WAVE applies a modification of the Chen-Flynn correlation [226], as shown in Equation 3.6, where the first term indicates the friction of accessories (e.g., centrifugal pumps, alternators and coolers) and the second term Shifting with the maximum working pressure of the cylinder, the third term means dynamic friction and the fourth term means air resistance damage. In this analysis, the initial values proposed in WAVE are used for all frictional resistance in all solid models.

$$f_{mep} = A_{cf}V_c + \frac{1}{ncyl}\sum_{i=1}^{ncyl}\left[B_{cf}(P_{max})_i + C_{cf} * \left(S_{fact}\right)_i + Q_{cf}\left(S_{fact}\right)_i^{\,2}\right] \qquad (3.6)$$

With:

$$S_{fact} = N_{rpm}\left(\frac{S}{2}\right) \tag{3.7}$$

3.2.1.4 Woschni heat transfer

To better measure the heat transfer into and out of the cylinder, WAVE uses the Woschni heat transfer sub-entity model. In this model, the intake port is assumed to have a uniform distribution of hot gas index and velocity over the entire surface of the hydraulic cylinder.

$$h_g = 0..128B^{-0.2}P^{0.8}T^{-0.53}{v_c}^{0.8}C_{enht} \tag{3.8}$$

The characteristic rates are the sum of the mean piston velocity and the additional firing-related rates in the difference between firings and the driving working pressure. Extensive details on the combination of characteristic velocities and their Woschni correlations can be found in the WAVE help document [225].

3.2.1.5 SI Wiebe combustion

In order to better simulate the ignition generated in the simulated cylinder, the SI Wiebe function formulation was used to analyze the natural material ignition rate observed in all premixed and SI ignitions obtained experimentally.

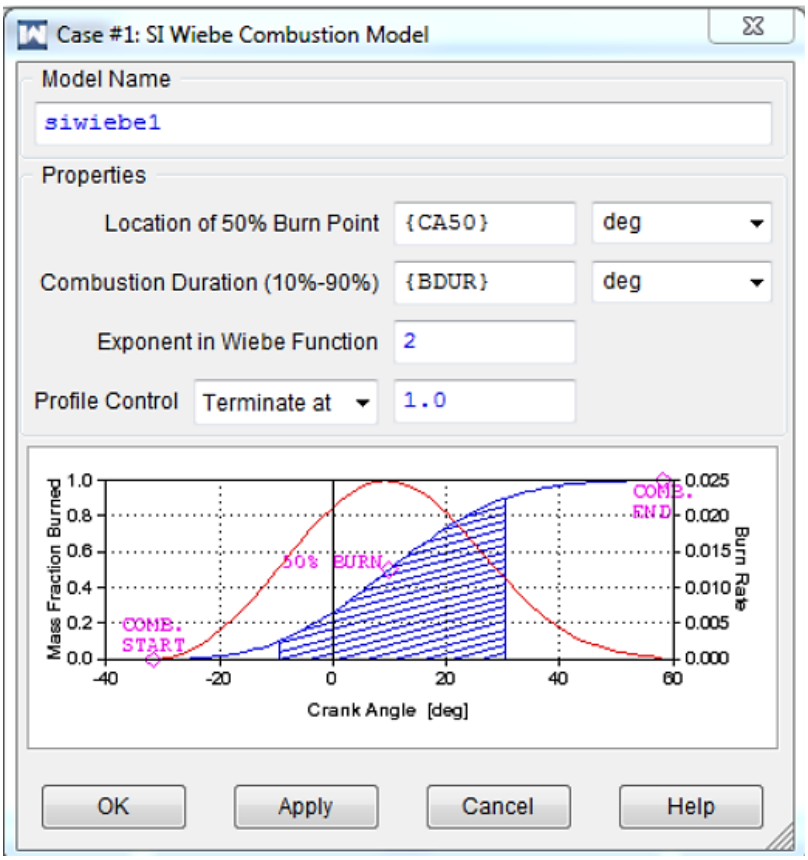

Figure 3.6 SI Wiebe combustion sub-model

The cumulative mass fraction burned ($(MFB)_c$), is given as a function of crank angle by:

$$(MFB)_c = 1.0 - \exp\left(-K_{AWI}\left(\frac{\theta}{\theta_{dur}}\right)^{(W_{exp}+1)}\right) \tag{3.9}$$

With reference to Figure 3.6, the impact of varying 50% burn point will shift the entire curve forward or backward while varying the 10%-90% duration will increase the total combustion duration. Also, varying the Wiebe exponent will change the burn rate profile.

3.3 Modelling and simulation implementation

In order to better reduce the time and cost of development and design, commercial vehicle engines were selected as the basis for prototype development and design. Select a pair of Stihl 4-MIX automotive engines as transmissions to meet the following specifications:

1. Improve emissions and high efficiency of gasoline and diesel

2. Two-stroke lubrication method

3. Equipped with straight-through exhaust pipe raising valve for gas exchange

4. Ease of use of accessories

The car engine is specially designed for the use of garden portable machinery and equipment, which can achieve high power and torque, low exhaust and low noise, and is light in weight and easy to maintain [227]. It operates on a four-stroke cycle car engine using two-stroke lubrication and intake crankcase reduction. In this section, the model and simulation of the selected car engine are presented.

Using Ricardo WAVE to get the final solid model of the free piston engine requires three steps, as shown in Figure 3.7 below. Initially, a baseline mock-up of a 31cc four-stroke engine was certified for the findings reported by Knaus et al [230]. Since there is no baseline characteristic curve for a 65cc engine crankshaft car engine, this certification is essential before a 65cc physical model is developed and designed.

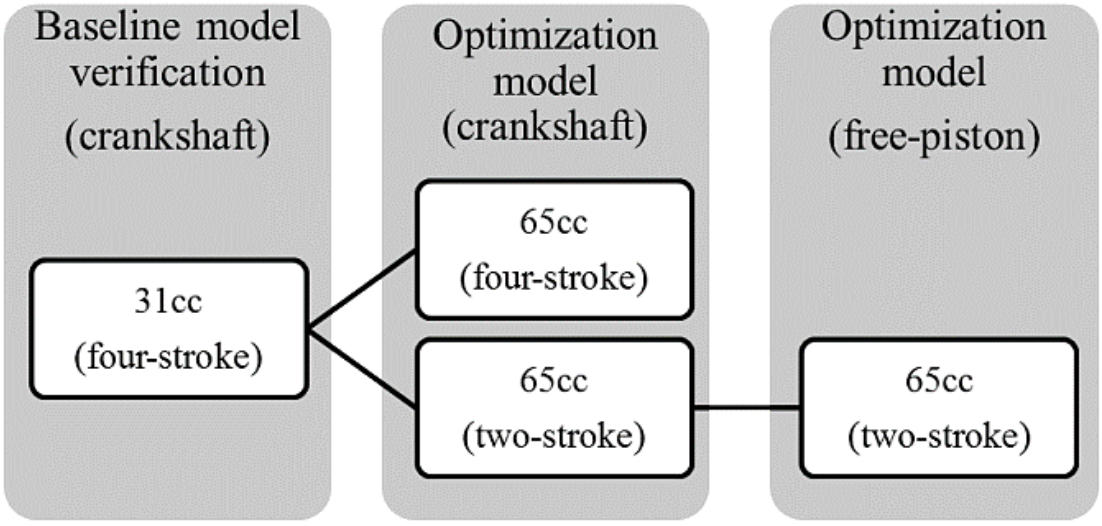

Figure 3.7 Types of models developed for the research

Changes to the baseline mockup allowed the development and design of a mockup of a 65cc engine crankshaft car engine. Since the 65cc version numbers usually have a similar design, it is assumed that the car engine mockup can be resized appropriately from the 31cc car engine version number. In order to better ensure that this assumption is reasonable, the maximum power of the car engine in the manufacturer's specification model is compared with the output power curve shown in Figure 3.9, which is obtained from simulation research. of. Maximum power and corresponding efficiency

are found to be closely paired with the manufacturer-spec model (2.3kW at 7200rpm).

This kind of 65cc automobile engine four-stroke engine crankshaft solid model is converted to the two-stroke cycle system version number according to the following method:

1. Simply change the 4 strokes to 2 for each circulatory system in the WAVE equipment (indicating a 2-stroke circulatory system)
2. Change and adjust intake and exhaust engine timing
3. Lift crankcase and scavenging sub-entity models

The mock-up was then tuned to achieve the highest braking system thermal efficiency and power output in the lower vehicle speed range (i.e., from 600 to 3600rpm). This particular speed range was chosen because the standby speed of the free piston engine is estimated to be 10Hz (equivalent to 600rpm), while the maximum power generation capacity is estimated to be around 50~60Hz (equivalent to 3000~3600rpm). The choice of this operating rate lies in the motor design reported by Arshad [229]. Therefore, it was rated as the basic policy of this scientific research.

Finally, the lifted 65cc two-stroke engine crankshaft car engine solid model was transformed into a free piston engine operation based on the mandatory piston sprout model described above in Section 3.2.1.2. The next section is devoted to detailing the engine crankshaft car engine model and simulation along with the results and discussion, while the free piston engine model will be presented in Section 3.4.

3.3.1 Baseline modelling, simulation and validations

The baseline model was developed from the information obtained in the paper by Knaus, et al. [230] for a 31cc version of the Stihl 4-MIX engine which inherit similar design to the 65cc version selected for the prototype. The engine specifications are shown in Table A-1 in Appendix A.
shows the model developed in Ricardo WAVE which includes the Figure 3.8 crankcase element (labelled as cyl2). The engine uses a carburetor while in the model a proportional fuel injector was used instead, enabling air-fuel ratio control to be implemented. A proportional injector will always inject sufficient fuel to the intake air stream to match a targeted air-fuel ratio and similar to the

carburettor principle.

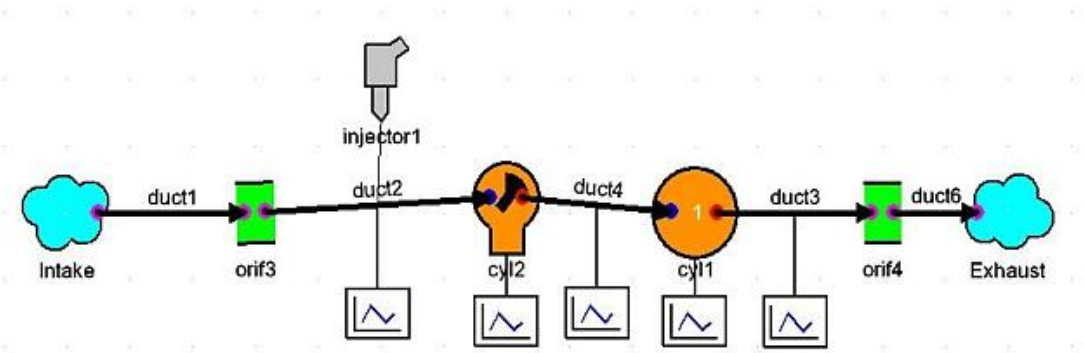

Figure 3.8 Baseline model of 31cc Stihl 4MIX engine in Ricardo WAVE.

The model was validated using the reported power curve by Knaus, et al. [230] and the results are shown in Figure 3.9 which shows excellent correlation between the simulation and experimental for the engine speed from 5000 to 8000 rpm.

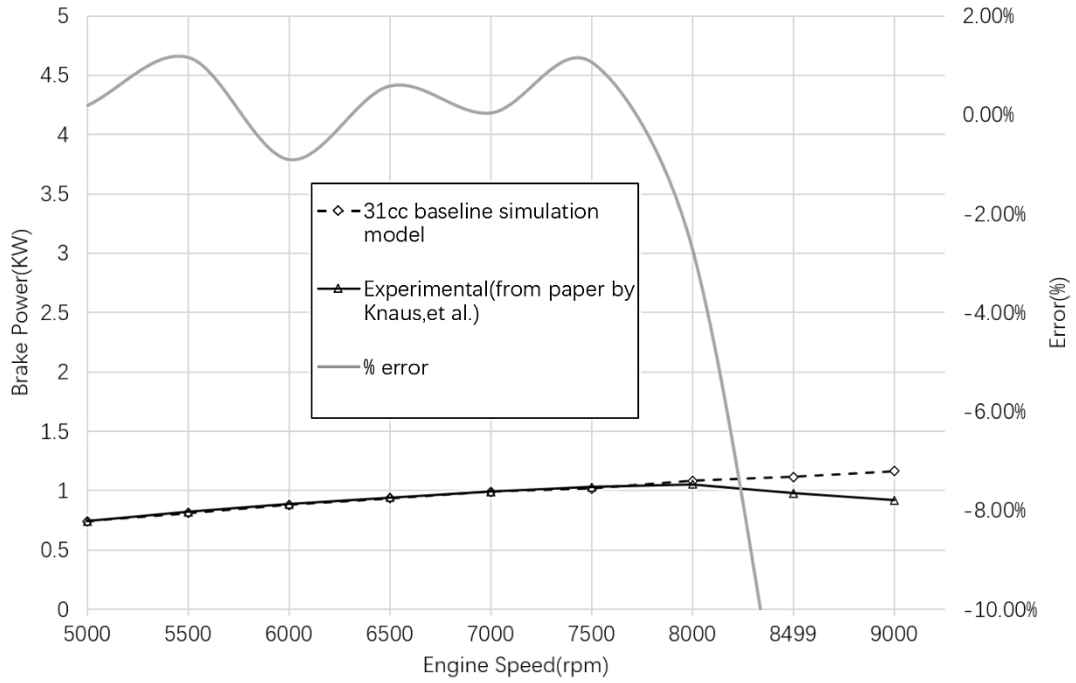

Figure 3.9 Power curves comparison from experimental result and as obtained from Ricardo WAVE simulation

The error between the reported experimental results and the simulation using WAVE was less than 2% for engine speeds below 9000rpm while at the speeds beyond 8500rpm the error increased sharply to 8 %.

The HC+NOx emission between the 31cc baseline WAVE model and the experimental data from Knaus, et al. [230] is illustrated in Figure 3.10. The errors are constantly less than 5%, and emission result is a vital factor in this research, therefore, this baseline model could be considered suitable and reliable.

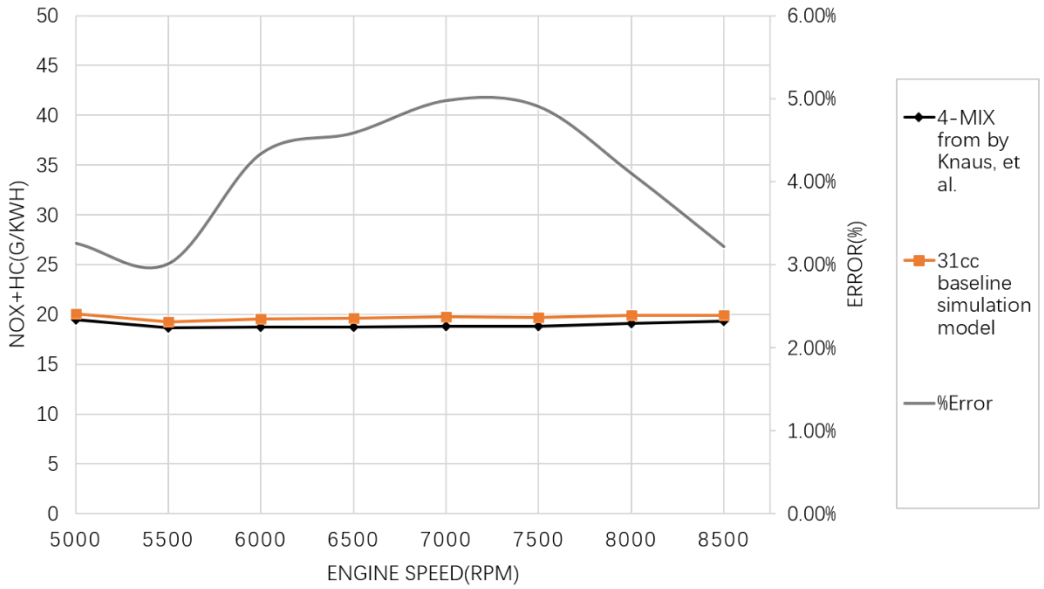

Figure 3.10 HC+NOx emissions comparison from experimental result and as obtained from Ricardo WAVE simulation

3.3.2 Crankshaft engine model optimisation

The optimized model contains a 65cc Stihl 4MIX car engine developed and designed from a standard solid model. As shown in Table A-2 in Appendix A, a similar camshaft-based cylinder variable valve timing curve was selected to modify the variable valve timing for automotive engines and other automotive engine specifications. The entire lifting process can be divided into four-stroke and two-stroke, as shown in the following sections.

3.3.2.1 Four-stroke model up-scaling and validation

Generally speaking, the 31cc solid model becomes larger to the 65cc solid model, due to the similar design of the car engine in these two categories. In addition, the ratio of the total cylinder area of the two engines is in line with the data information of the design scheme based on the work

experience of Taylor [231] for the flat cylinder head. The experience with the cylinder geometry values for the two engine types is given in Table 3.1 for a small to medium sized four-stroke engine with 2 cylinders and a flat head design.

Table 3.1 Empirical design data for valve capacity and head design in relation to the actual design for the 31cc and 65cc Stihl 4MIX engines

Parameter	Empirical design data	31cc	65cc
Inlet valve outside diameter/bore	0.44	0.36*	0.40*
Exhaust valve outside diameter/bore	0.38	0.36*	0.36
Inlet valve nominal area/Piston area	0.19	0.13	0.16

*Similar valve diameter was chosen by the manufacturer due to limited space and for ease of service as mentioned in the paper by Knaus, et al. [230]

The work experience data information is the result of the 31cc car engine obtained in the basic section 3.3.1 of the 65cc version number of the mock-up enlargement and the characteristic investigation certification. In addition to this, the initial 65cc Stihl 4MIX has a peak output of 2.3kW at 7200rpm from the manufacturer's data information, which can be used to certify the physical model. The output power curve of a 65cc car engine obtained from the simulation is shown in Figure 3.11 below, which outlines a typical output power curve outline. In addition to this, the maximum power is 2.4kW, which occurs around 6500rpm, which is almost consistent with the manufacturer's data.

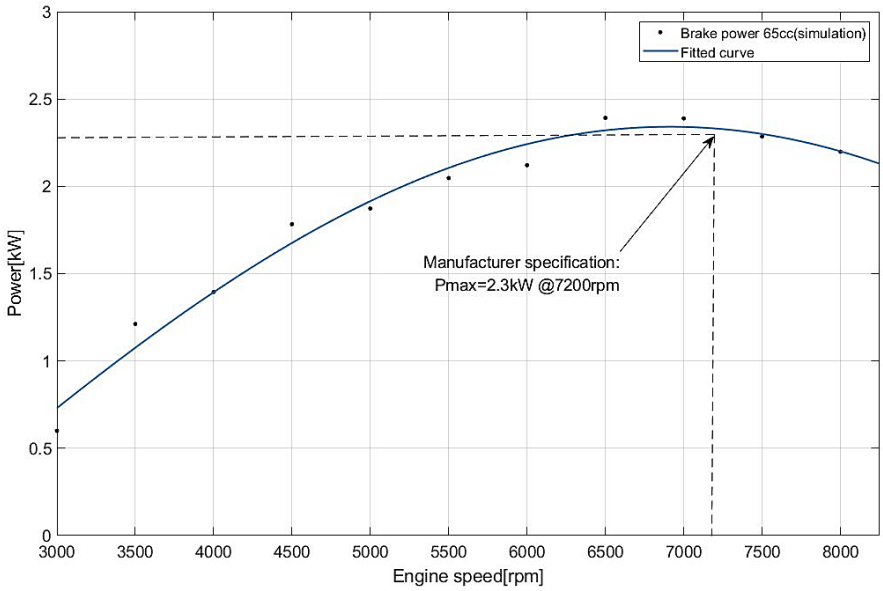

Figure 3.11 Fitted power curve of the four-stroke 65cc engine as obtained from Ricardo WAVE simulation

3.3.3 Two-stroke model performance optimisation

The proven four-stroke mock-up was transformed into a two-stroke mock-up, and further mock-up enhancements were made in terms of intake and exhaust valve engine timing and its intake port increase pressure working pressure. This process is especially important because the prototype's selected car engine was formulated for a four-stroke cycle, while the prototype was run on a two-stroke cycle.

The general gate valve state diagram of the two-stroke solid model is shown in Figure 3.12 below. In the cylinder engine timing improvement process, there are four independent variables that must be improved, namely the exhaust valve opening angle (θ_{EVO}), the exhaust valve closing angle (θ_{EVC}), the intake valve opening angle (θ_{IVO}), and the intake valve opening angle (θ_{IVO}). Door closing angle (θ_{IVC}). Important criteria are profit maximizing output power derivation, improved gas exchange characteristics (according to lift gate valve engine timing) and reduced compression work.

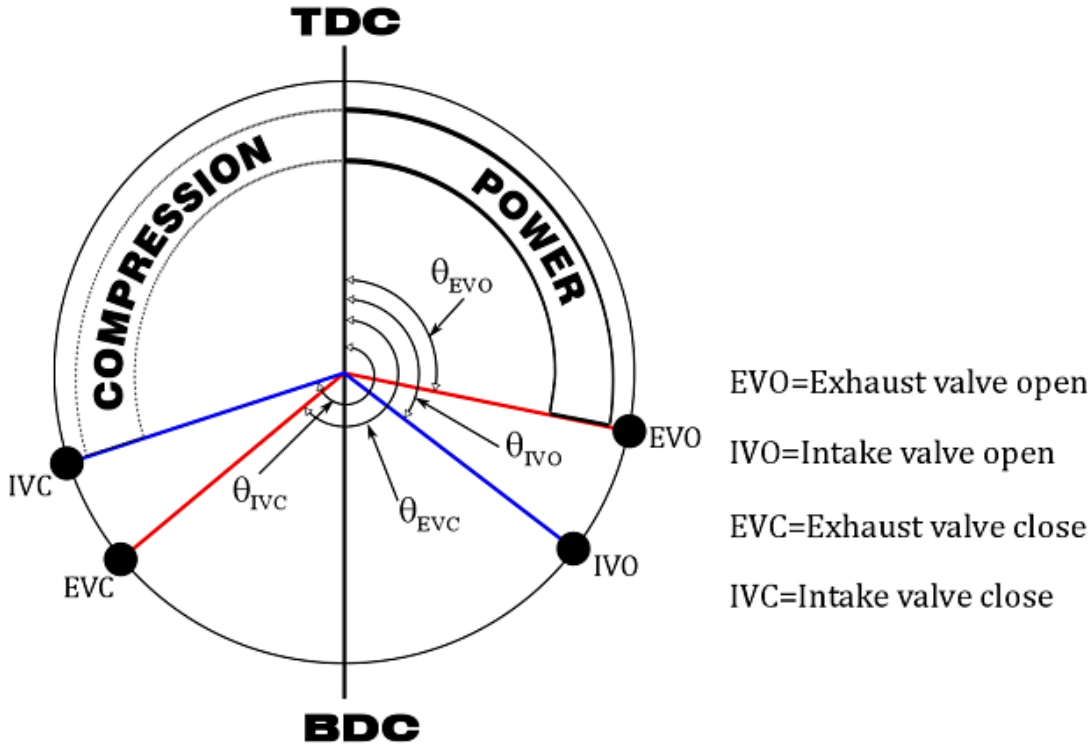

Figure 3.12 General timing diagram for two-stroke cycle

3.3.3.1 Parametric study

In the two-stroke version of the 65cc automotive engine, the program flow for cylinder engine timing boost is based on a scientific study of the main parameters using the test control panel shown in Figure 3.13. Carrying out the experiment will give an export drainage matrix that can be used to indicate how changing one or several key parameters will harm one or several of WAVE's predictive analysis exports. In this way, the harm of each independent variable to the characteristics of the automobile engine can be quickly observed without realizing the specific automobile engine performance indicators.

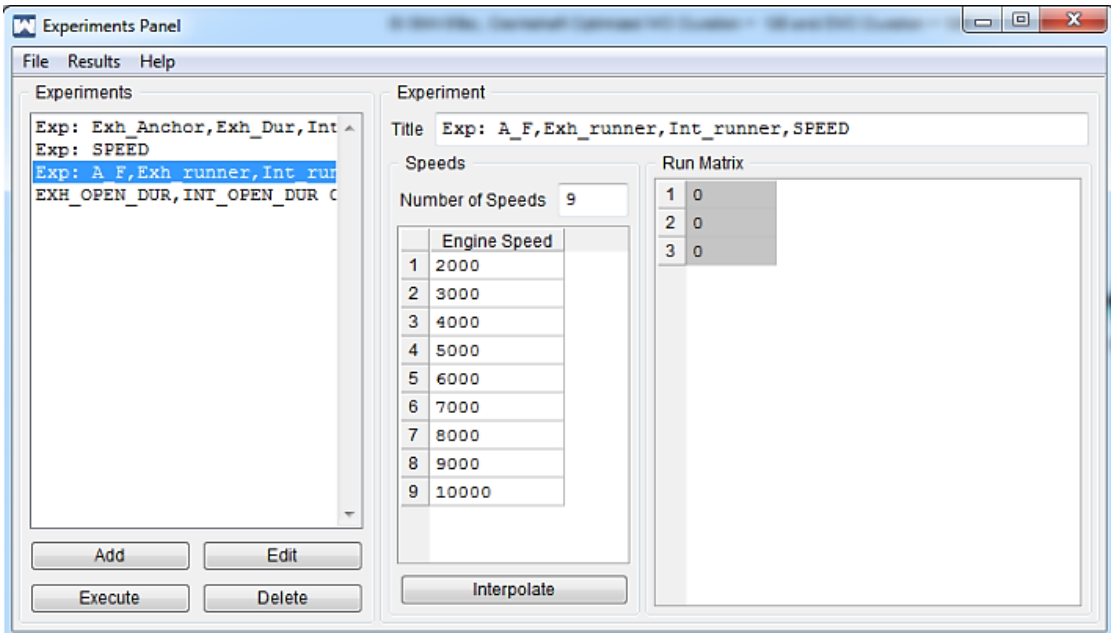

Figure 3.13 The experiments panel in Ricardo WAVE which was used during the parametric investigations for model tuning

The test results are shown in Figure 3.14 below. Several overall objectives in WAVE were made, namely braking power (bpowkw), torque (torqsi), maximum cylinder pressure (pmaxsi1) and capacity high efficiency (volefd) for evaluation. Then, the elements of Figure 3.14(b) are defined by setting the appropriate overall target in the Fitting Curve dialog box, namely the best exhaust pipe valve ps pen position (Exh_{Anchor}), exhaust pipe delay time (Exh_{Dur}), intake air The gate ps pen location (Int_{Anchor}) and intake valve delay time (Int_{Dur}) are shown in Figure 3.14 (c). For example, if the maximum torque speed is set in the operating vehicle speed range from 600rpm to 8,000rpm, the corresponding value of the gate valve setting is automatically adjusted to reflect this overall goal.

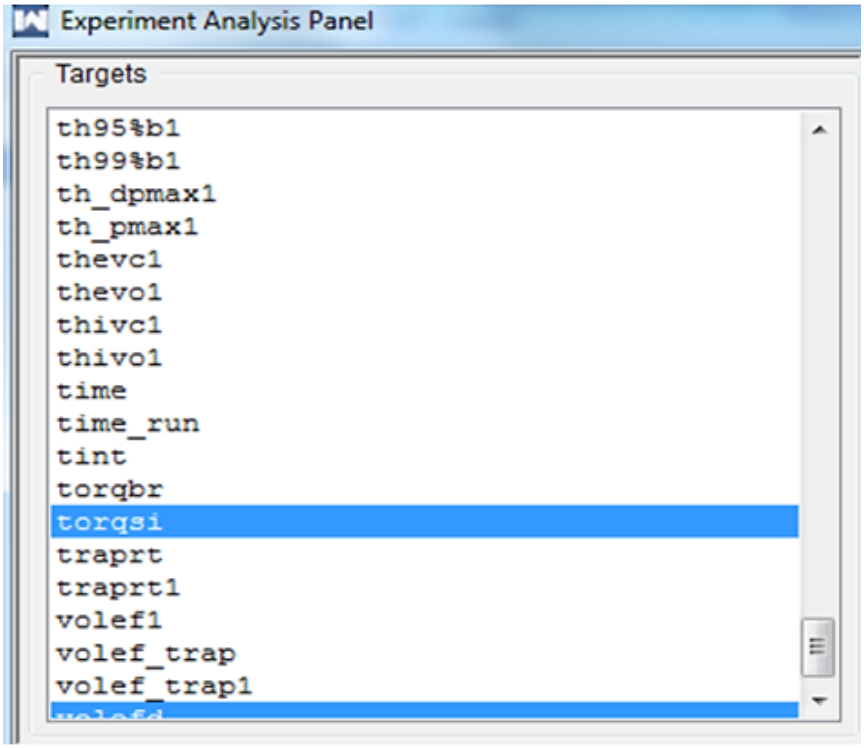
Experiment Analysis Panel
Targets
th95%b1
th99%b1
th_dpmax1
th_pmax1
thevc1
thevo1
thivc1
thivo1
time
time_run
tint
torqbr
torqsi
traprt
traprt1
volef1
volef_trap
volef_trap1

(a)

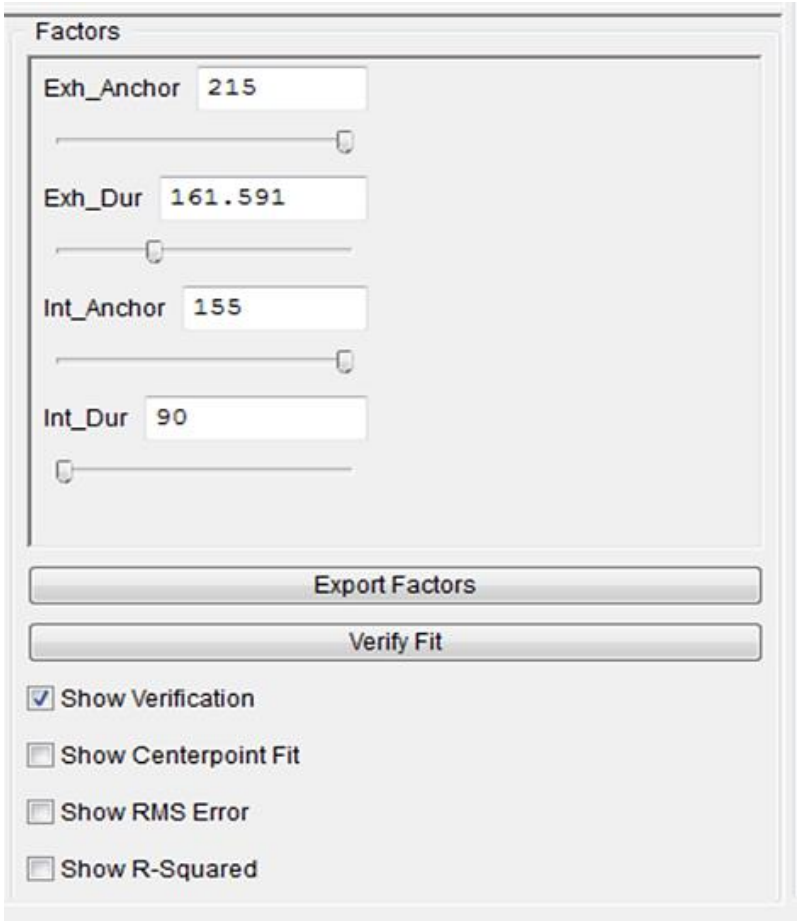
Factors
Exh_Anchor 215
Exh_Dur 161.591
Int_Anchor 155
Int_Dur 90
Export Factors
Verify Fit
Show Verification
Show Centerpoint Fit
Show RMS Error
Show R-Squared

(b)

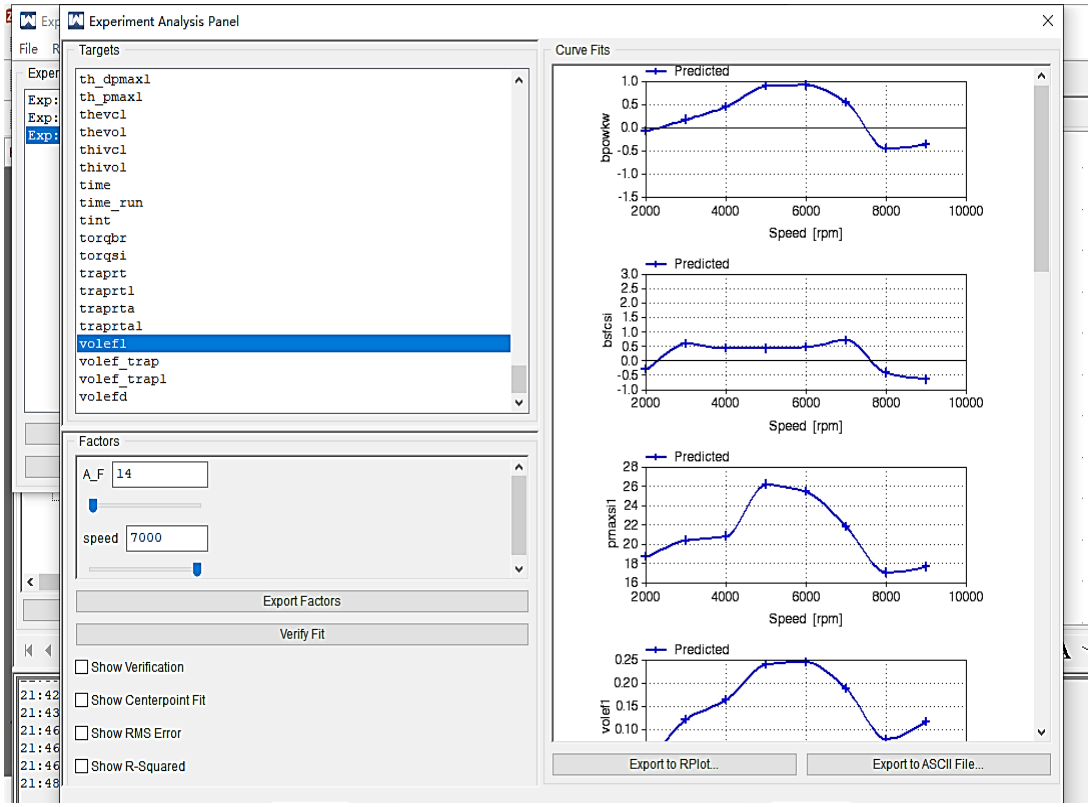

(c)

Figure 3.14 The experiment analysis panel showed-up at the end of the experiments in Ricardo WAVE

In Ricardo WAVE, the anchor position (for intake and exhaust valves) is defined as the crank angle (°) position where the lift is at its maximum value while the valve duration (for intake and exhaust valves) is how long (in crank angle degree) the valve will remain open. The relationship between WAVE's valves parameters and the valves timing variables is summarised in the following equations:

For exhaust valve:

$$\theta_{EVO} = Exh_{Anchor} - \frac{Exh_{Dur}}{2} \tag{3.10}$$

$$\theta_{EVC} = \theta_{EVO} + Exh_{Dur} \tag{3.11}$$

For intake valve:

$$\theta_{IVO} = Int_{Anchor} - \frac{Int_{Dur}}{2} \tag{3.12}$$

$$\theta_{IVC} = \theta_{IVC} + Int_{Dur} \tag{3.13}$$

3.3.3.2 Final optimisation

The limitations of the experimental control panel depend on final precision; it only gives a rough idea of how the independent variables compromise the technical parameters. Therefore, as shown in Figure 3.15 below, a detailed investigation was carried out based on the secondary primary parameter investigation of the scanner generator control panel application. In the final boost, 5 height instances were run at each car speed. Gate valve settings are added as arguments with default and final values are set and then linearly interpolated to create sub-instances. Boost sub-instances at more car RPMs to improve the accuracy of the effect. This simulation has to run for a longer period of time, so it is used for the final part of the improvement when the original settings have been clarified from Section 3.3.3.1.

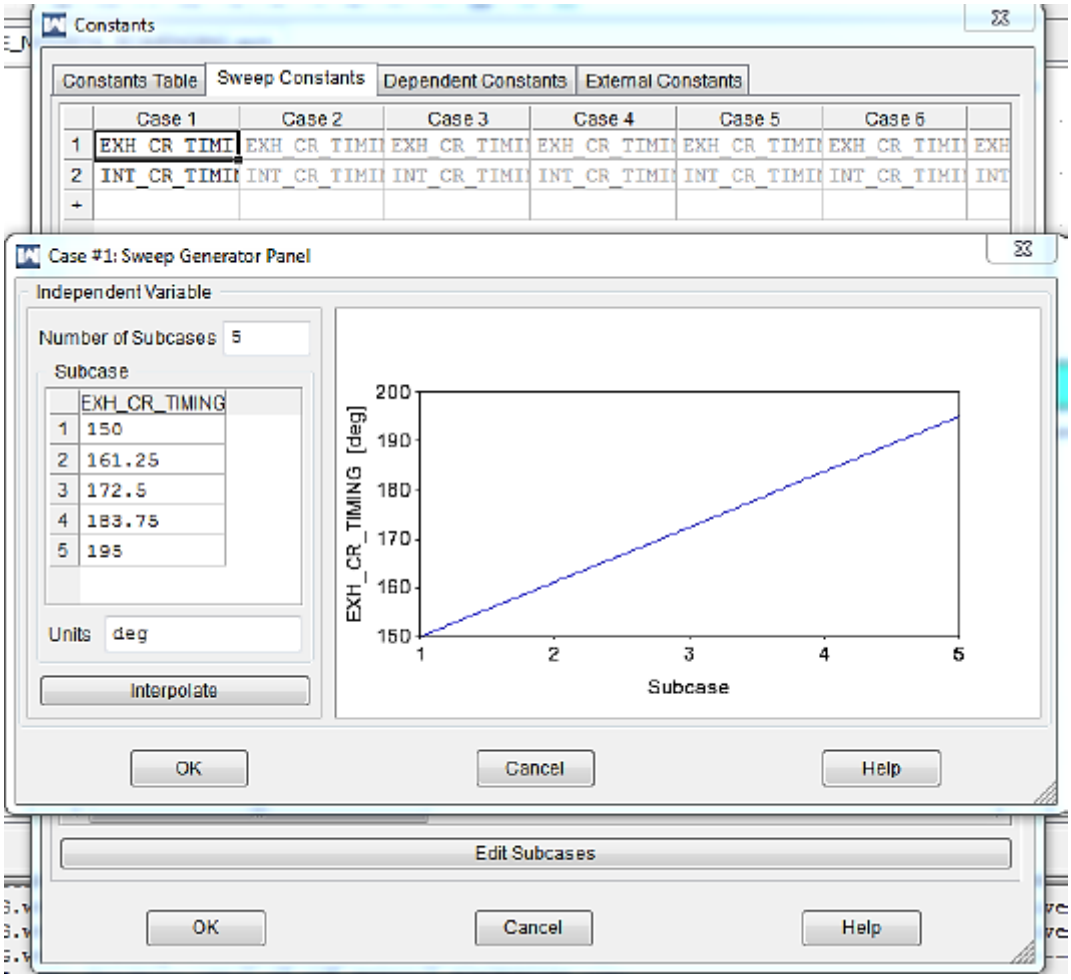

Figure 3.15 The sweep case generator panel used for refined optimizations

3.3.4 Two-stroke optimization results and discussions

The two-stroke engine characterization results are derived from a scientific study of the main parameters detailed in Section 3.3.3. The hazards of the following independent variables on the characteristics of automobile engines are investigated:

1. Increased supply

When the solid model was converted to a two-stroke cycle system, the first observation was that the scavenging characteristics were poor, resulting in no ignition. Therefore, it is necessary to consider the harm of the increased pressure working pressure of the intake port to the characteristics of the automobile engine.

2. Intake and exhaust door rebar anchorages

In the four-stroke cycle system, each four-stroke is completely different, and the intake and exhaust pipes are separate for the four-stroke, so the ps pens of the intake and exhaust valves are far apart. The Stihl 4MIX is designed for the practical operation of a four-stroke cycle system with the required intake and exhaust valve layouts. Therefore, for the two-stroke conversion, it is particularly important to clarify the best cylinder ps fountain pen for the characteristics of the automobile engine.

3. Intake and exhaust valve delay times

The delay time of the intake and exhaust pipes of a two-stroke cycle vehicle engine is very short. The longer the delay time, the worse the collection rate because the gas-fuel mixture short-circuits into the exhaust spinner. In turn, a shorter delay time results in a weaker scavenging efficiency due to residual organic exhaust gas remaining in the cylinder. In both cases, car engine characteristics are severely affected.

3.3.4.1 The effect of intake boost pressure

The boost pressure investigation involved 13 variations, linearly interpolated from 1.1 bar to 2.0 bar, at various vehicle speeds from 600 to 3000 rpm, the anchor values and delay times for the intake and exhaust valves were all numerical value. Figure 3.16 shows the detriment to brake system thermal efficiency (bte) of increased working pressure. At lower car speeds, increasing the pressure

working pressure is not harmful to the bte. Significant damage to bte occurs after 2500rpm until 6000rpm. At speeds above 4000rpm, weaker bte (i.e., less than 10%) was observed for lower incremental pressure working pressures.

The goal is to minimize the increase in pressure gas pressure while obtaining high braking system thermal efficiency and adequate scavenging.

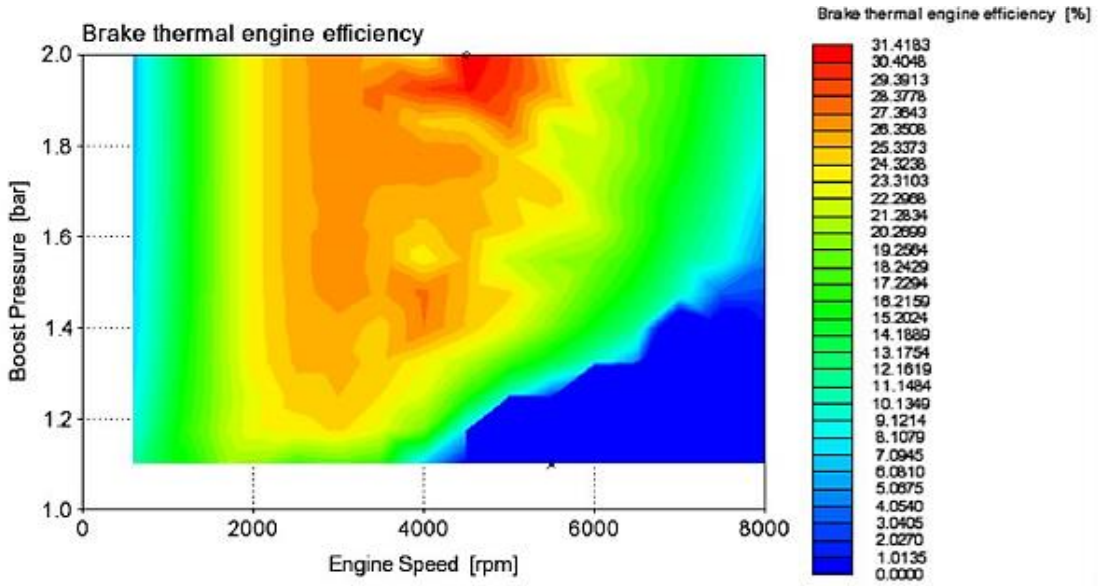

Figure 3.16 Boost pressure effect on brake thermal efficiency(bte)

Figure 3.17 shows how increasing the working pressure immediately compromises the braking power derivation; higher working pressure increases the working pressure causing higher braking power, with a significant detriment to vehicle speeds from 2000rpm to 5500rpm. When the car speed exceeds 4000rpm, the pressure must be increased more.

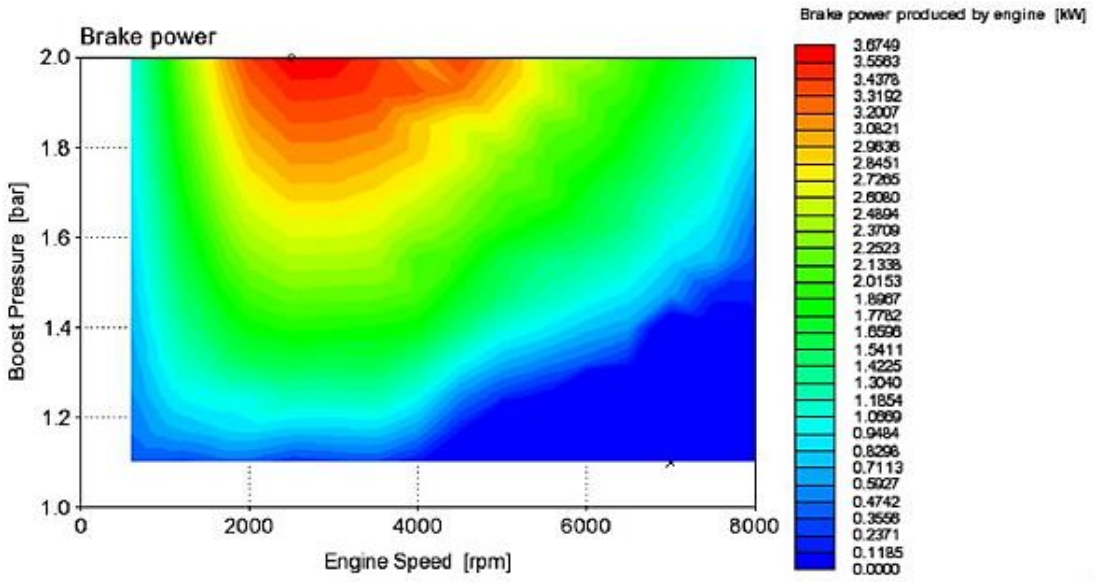

Figure 3.17 Boost pressure effect on brake power

Figure 3.18 shows the brake system mean reasonable working pressure (bmep) response to increasing pressure working pressure. Higher bmep occurs at lower car speeds and is immediately compromised by increased stress working pressure. This hazard is lessened when the car revs above 3000rpm, and the bmep no longer increases due to increased pressure working pressure.

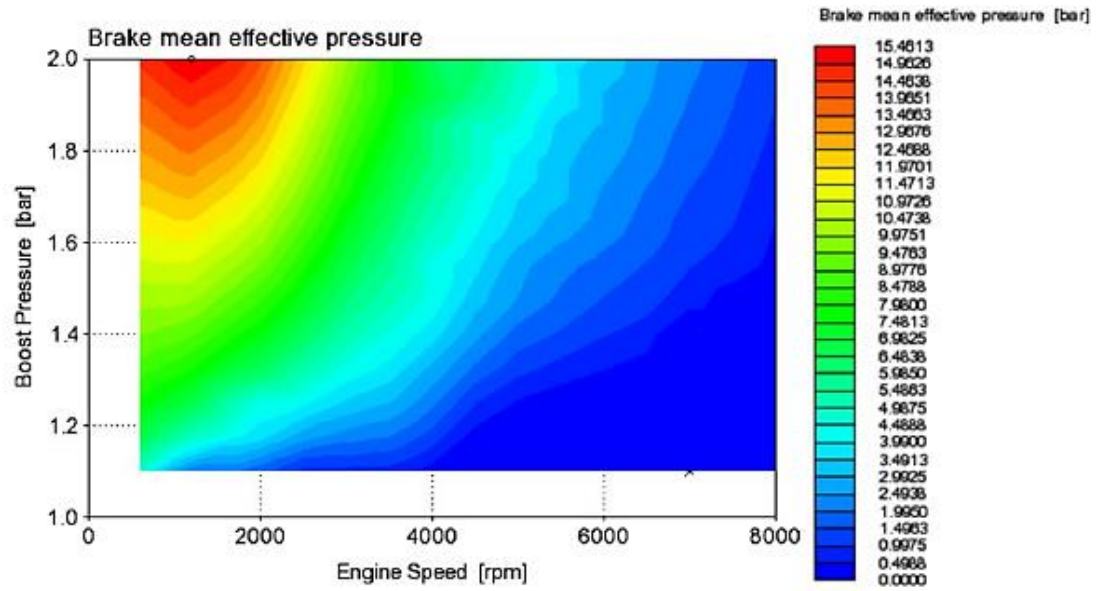

Figure 3.18 Boost pressure effect on brake mean effective pressure(bmep)

3.3.4.2 The effect of intake and exhaust valves anchor

In the main parameter scientific study detailed in Section 3.3.3, various compositions of intake and exhaust valve anchors were studied, depending on where the anchors were changed (defined in Section 3.3.3). Each transition includes several rate data messages, while the intake and exhaust delay times are fixed at 100° CA. There are 25 permutations generated through the combinations of intake anchor from 160°CA to 200°CA and exhaust anchor from 140°CA to 180°CA.

Figure 3.18 shows the optimum valves anchor during which high bte region is observed. For the best bte output, the optimum anchor lies along imaginary diagonal line connecting 140/160° CA (exhaust anchor/intake anchor) to 180/200° CA.

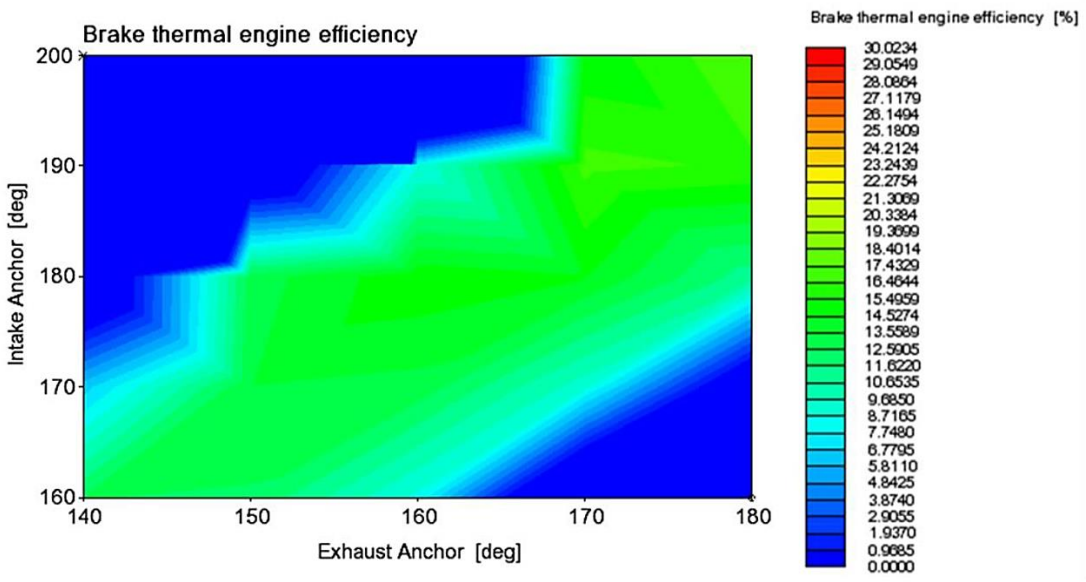

Figure 3.19 Valves anchor positions effect on brake thermal efficiency(bte)

Similar response is observed for brake power as shown in Figure 3.20 and *bmep* as shown in Figure 3.21.

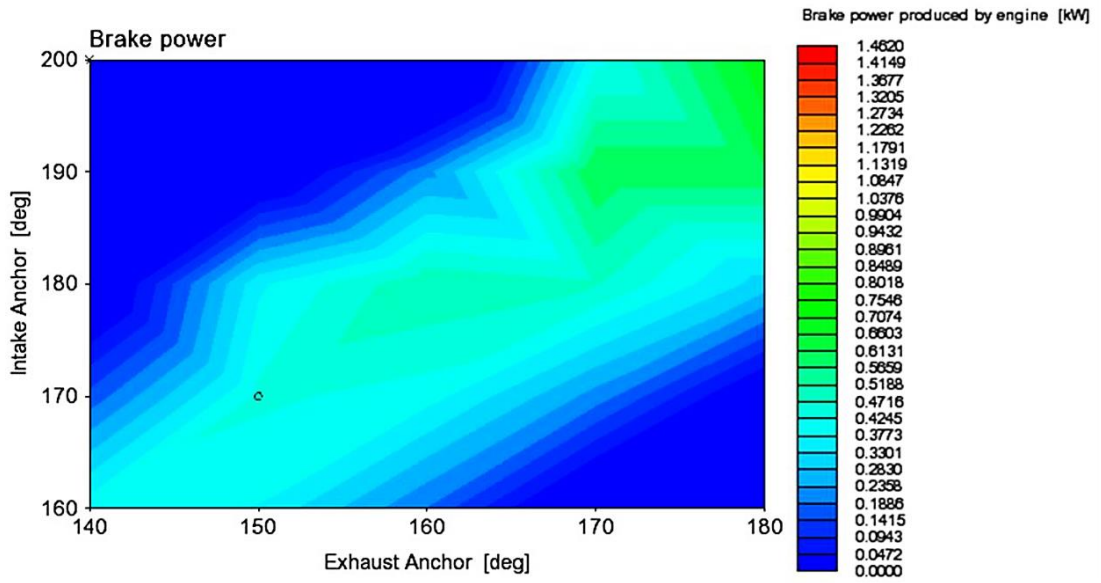

Figure 3.20 Valves anchor positions effect on brake power

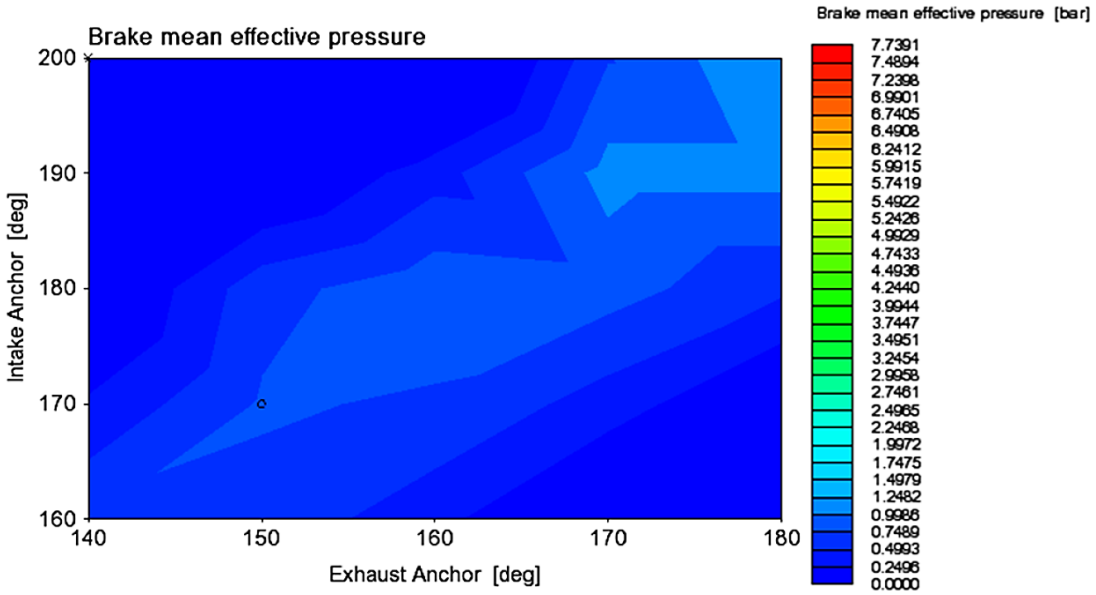

Figure 3.21 Valves anchor positions effect on brake mean effective pressure(bmep)

3.3.4.3 The effect of intake and exhaust valves duration

After getting the best settings for the inlet and exhaust pipe anchors, it is necessary to further increase how long each gate valve should be open (delay time). A similar approach was chosen based on setting the value of the cylinder anchor and changing the delay times of the intake and exhaust at different car engine speeds.

From Figure 3.22 to Figure 3.24, it can be seen that the gate valve delay time is not as sensitive to the hazards of technical parameters (i.e. bte, braking power and bmep) as previously observed gate valve anchors. However, as shown in the figure below, a longer intake valve delay time will result in poor characteristics. The specification of the opening delay time must be further considered, such as driving the organization's formulation and selection of design preferences that increase stress working pressure.

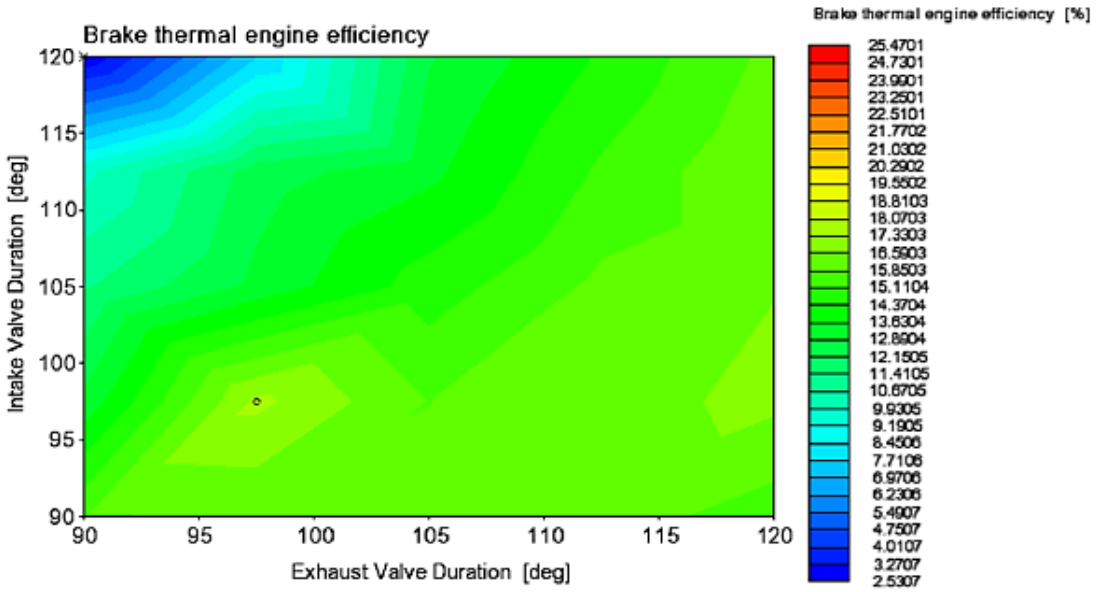

Figure 3.22 Valves duration effect on brake thermal efficiency(bte)

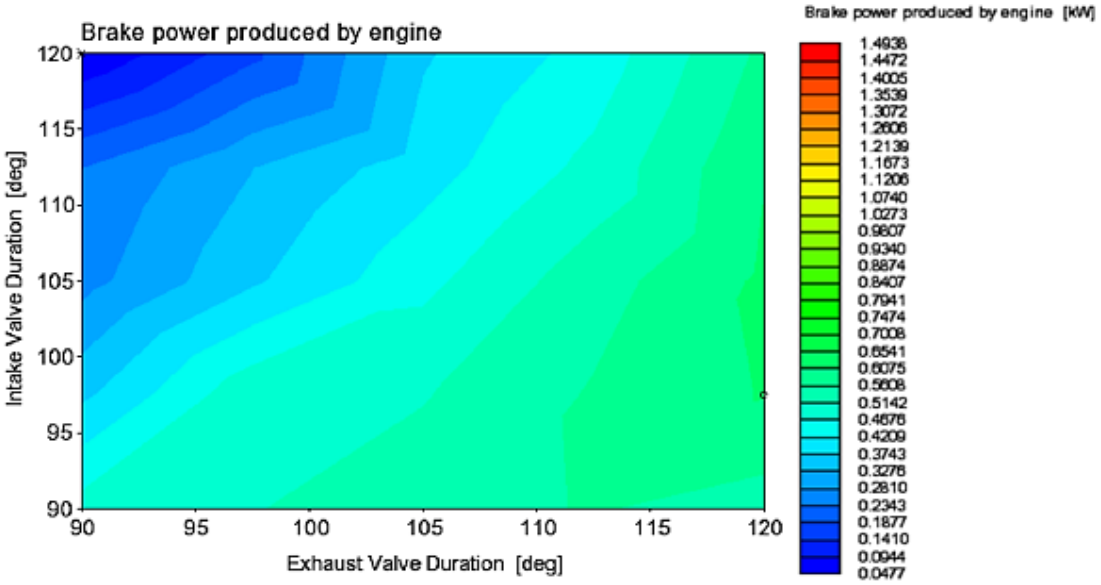

Figure 3.23 Valves duration effect on brake power

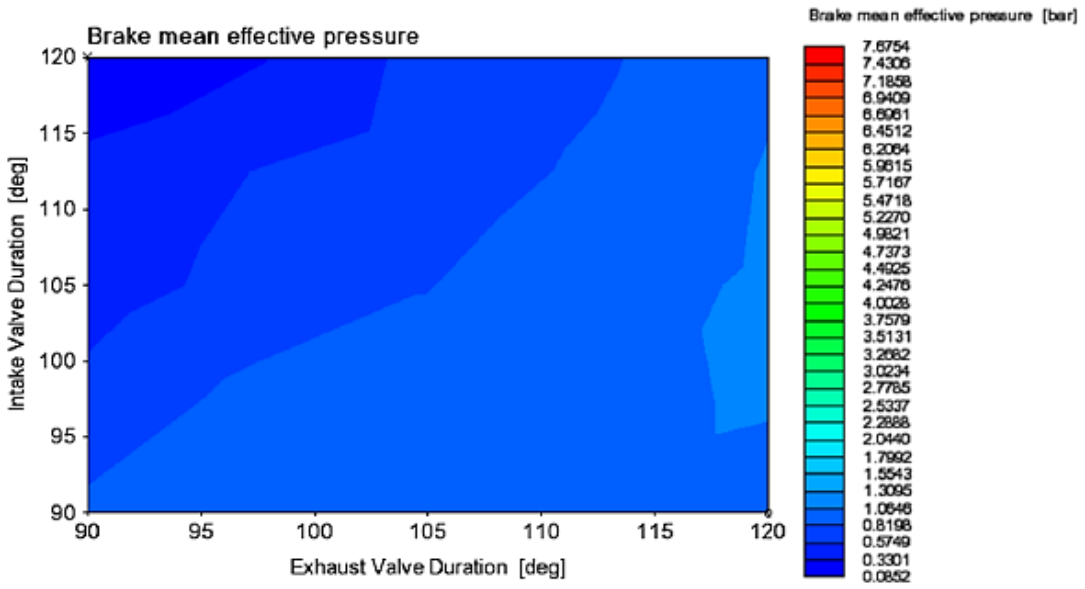

Figure 3.24 Valves duration effect on brake mean effective pressure(bmep)

3.3.5 Summary

Three crankshaft engine models were developed: two models using a four-stroke cycle and the last model being a two-stroke cycle. The first model was a 31cc version and was used for verification purposes since there was no experimental data available for the 65cc engine. The second model was for a 65cc four-stroke engine used as a baseline before converting this model into a two-stroke cycle. The third model was for a 65cc engine using a two-stroke cycle and was used as a baseline for the free-piston engine simulation. The performance parameters for this model are presented and the final valves anchors of the optimized model are shown in Figure 3.25. At optimized valves anchor, the exhaust valve is open at 80°CA before BDC followed by intake valve 25°CA later. Shortly after BDC, i.e., at 20° CA after BDC, the exhaust valve is closed followed by intake valve 15°CA later.

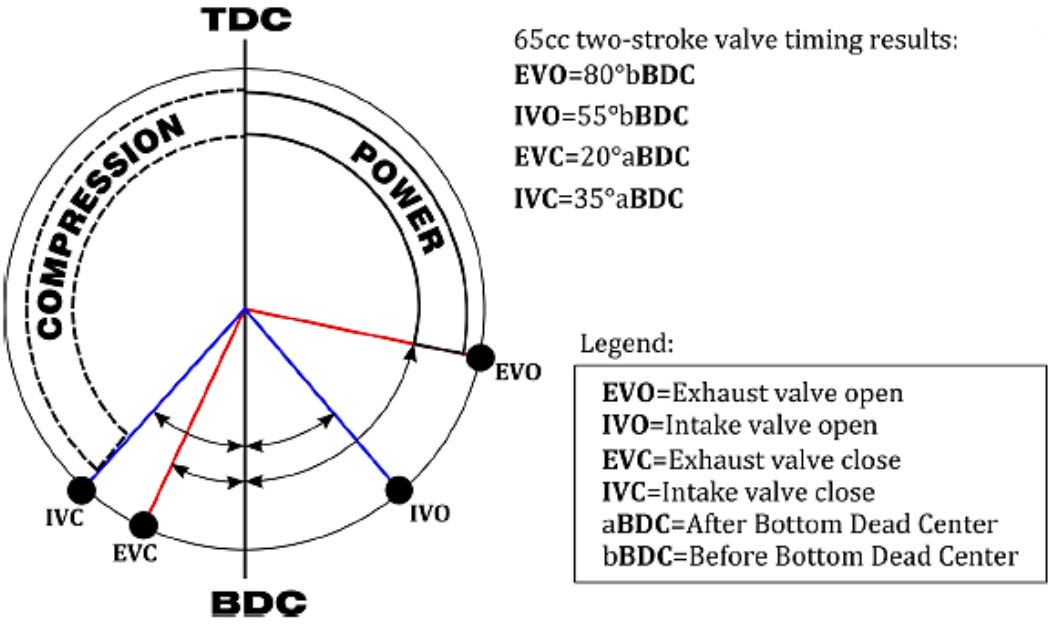

Figure 3.25 Final valves timings for the 65cc two-stroke crankshaft engine

3.4 The free-piston engine modelling and validations

The fitness motion profile of a free-piston engine is governed by a stable balance of forces acting on the individual fitness motion components (i.e., mover components). For an engine crankshaft car engine, the fitness motion graph depends on the engine crankshaft, with known equations and distinctive features based on the design of the car engine geometry. This section details the mathematical model of the free piston engine dynamics model.

The purpose of the dynamic model is to give the 1D solid model in Ricardo WAVE the values of the piston position during driving to allow gas exchange and ignition simulation simulations for the scientific study of free piston engine characteristics. The results are used for cylinder lift and predictive analysis of the characteristics of a prototype of a free piston engine.

3.4.1 Dynamic balance equation of motion

The novelty of free-piston engine generator lies in the piston dynamics where only one moving translator assembly converts the chemical energy via the combustion process into kinetic energy of the moving mass and finally into electrical energy through the generator.

In order to obtain the motion profiles, each of the forces which contribute to the equation of motion must be identified and its mathematical formulation used in the dynamic model. This allows a close form solution to be found thus enabling the motion trajectory to be obtained.

The free-body diagram of the forces acting on a dual-piston type free-piston engine generator is shown in Figure 3.26 and comprises of the following forces:

1. in-cylinder pressure forces acting on both cylinders, $F_{p1}$and F_{p2}
2. frictional forces due to contact surfaces on the moving part of the engine, F_f
3. cogging force acting on the permanent magnet assembly of the generator, F_{cog}
4. motoring force, which is energised during starting, F_{mot}
5. net force or inertial load of the moving mass, $m\ddot{x}$

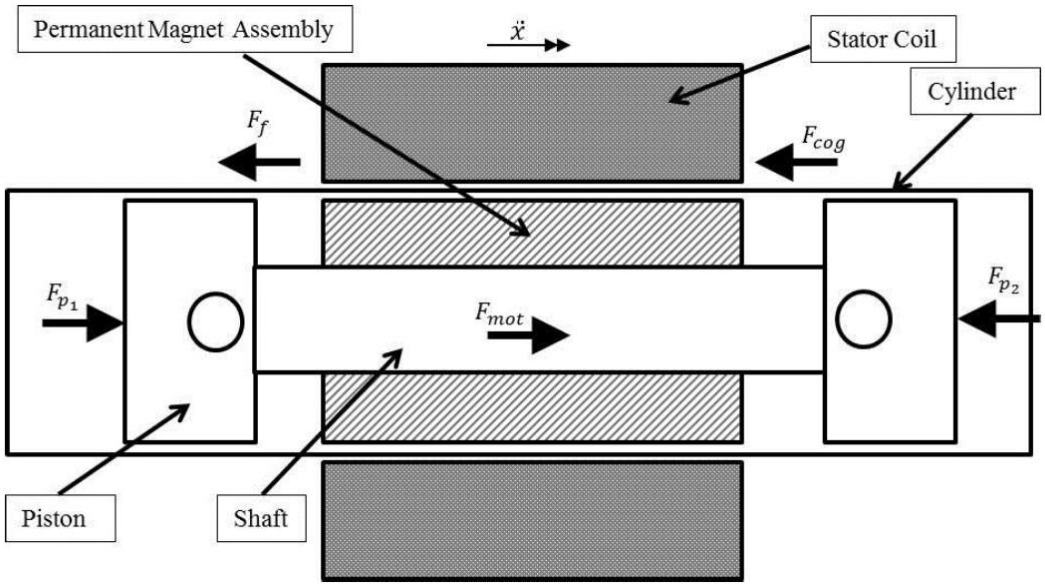

Figure 3.26 Free-body diagram of the dual piston free-piston engine generator dynamic model

Because the motion of the moving mass is related with the longitudinal axis only, and in order to simplify this analysis, the vector treatment of the dynamics analysis has been deleted. By convention, the right-side motion is positive while the left-side motion is negative. Equation 3.14 is a summarised form of Newton second law of motion of net forces:

$$\sum F = F_{mot} + F_p - F_f - F_{cog} = m\ddot{x} \tag{3.14}$$

Where $\ddot{x}$ is the acceleration of the piston in the direction of motion and m is the moving mass

which mainly comprises the piston assembly set and linear generator shaft (with the permanent magnet assembly). F_p is the resulting in-cylinder pressure forces acting on the translator and can be expressed as in Equation 3.15:

$$F_p = F_{p1} - F_{p2} = (p_1 - p_2) \times \frac{\pi B^2}{4} \tag{3.15}$$

Generally speaking, there are three basic principles for the operation of free piston engine generator sets, namely electric type, standby speed and power generation. In the electric mode caused during operation, the electric driving force is the most important force. When ignition occurs, the ignition force $(F_p)_c$ becomes primary. In this manner, the driving force should be slowly reduced until a sustainable repetitive motion is achieved.

These modes are important during the transient phase of the free-piston engine generator operation and the forces can be modelled differently as demonstrated by several researchers; i.e., Goldsborough and Blarigan [142] considered the magnetic force as resisting the motion during combustion proportionally to the translator speed. Mao, et al. [232] included electromagnetic force which depends on motor constants for the motion during electrical power generation. In the following subsection these forces will be discussed thoroughly.

3.4.1.1 Linear electrical machine

In the free-piston linear generator, the linear generator can be operated as linear motor by supplying an electrical current to its driver using a dedicated commutation method to produce the reciprocation motion. During this process, the switching between each coil is determined from the linear position reading and must occur at precise timing and position to produce a smooth motoring force during starting.

Saiful Azrin [298] simulated and tested several commutation methods to energize the linear motor during the starting mode of the free-piston engine generator. It was shown through simulation that, in order to obtain maximum amplitude (and thus, compression ratio) for combustion to occur, the generator could be reciprocated with gradual increasing amplitude until it reaches its resonant frequency [106]. The simulation had successfully demonstrated full stroke motoring during starting

by applying low motoring force using this method [298].

Similarly, Mikalsen [299] suggested this starting method with the concern around control strategy and motor capacity. Mao, et al. [232] proposed a similar reciprocation technique for starting, namely to utilize the air-spring behavior in the cylinder to achieve the required compression ratio.

The motoring force is determined from the linear motor force constant (K_f) which inherit on the stator coil and depends on the winding type. There are three main types of linear generator [58]:

- Moving coil- The coils move to create the power thus requires flexible coils which are prone to wear and tear.
- Moving magnet- Large magnetic field leakage and air gap issue with prolong vibrations and risk of demagnetisation.
- Moving iron- This is the most rugged but relatively the heaviest configuration.

Based on Lorentz law, the motoring force generated for delta (Δ) and wye (Y) winding respectively can be evaluated as follows [298]:

$$F_{mot} = I_{phase} \times K_{f-\Delta} \tag{3.16}$$

$$F_{mot} = \sqrt{3} I_{phase} \times K_{f-Y} \tag{3.17}$$

This required motoring force is determined from the desired compression ratio [299] as well as cyclic speed [106]. Both of these requirements must be met to achieve sufficient compression pressure. It has been estimated via experimental testing that the minimum compression pressure must be around 5-7 bar to produce significant combustion pressure [298]. This is difficult to achieve at slower cyclic speed due to air leakage through piston rings during compression stroke is higher hence reducing the compression pressure. Faster cyclic speed requires higher motoring force that draws uneconomically high electrical power during starting.

3.4.1.2 Cogging force

Cogging forces are generated in linear motors with moving magnet designs and cause wear, vibration and noise [233]. This force is the result of the interaction between the electromagnetic field of the linear motor and the back iron, and the force is usually transformed along the linear part

of the mover, as shown in Figure 3.27 below.

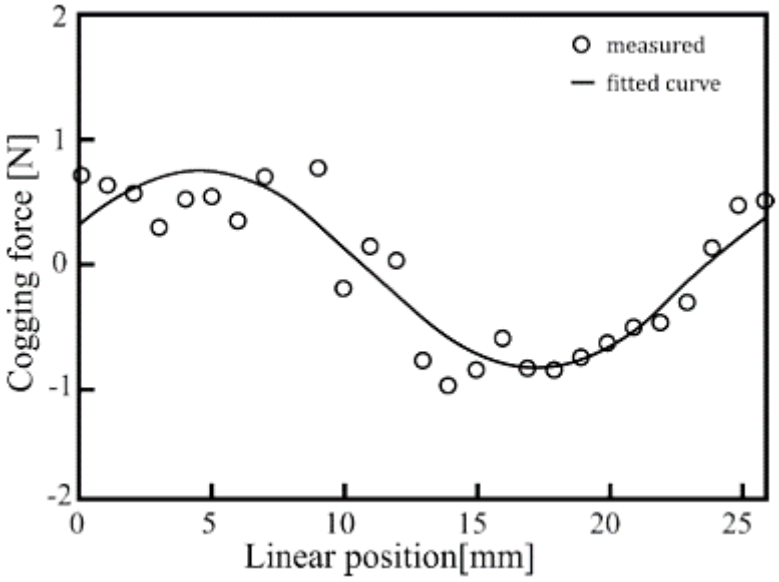

Figure 3.27 Typical profile of cogging force vs. position of a linear motor

Some scientific researchers have ignored the alveolar force because it is relatively ineffective compared to another force on exercise quality. Arshad et al. [235] proposed to introduce a high amount of current during driving to counteract the cogging force effect, assuming that this force can be ignored at ignition. For the entity model developed and designed, the cogging force from the specific linear motor and the sliding friction force of the linear motion bearing are concentrated together and used as a constant standard value.

3.4.1.3 Frictional force

The frictional force in a free-piston engine generator is often simplified in models and is claimed to be very low due to the absence of the crank mechanism. The frictional force is assumed to be constant throughout the cycle by most researchers but a more accurate model has been provided by Atkinson, et al. [11] from an empirical formula provided by Blair [236] which can express as:

$$F_f = 3150 \cdot V_s \cdot f \tag{3.18}$$

From this equation, the frictional force is seemed to be small and thus can be combined as retardation force together with the linear motor cogging and linear bearing.

3.4.1.4 Compression-expansion process

In this calculation, the compression process was considered to be governed by a thermodynamic equation for a polytropic process with a constant index. The pressure and temperature at the beginning of the compression have the same values as the corresponding parameters at the end of the scavenging process or ambient conditions. In the two-stroke engine model, the intake valve closes last during compression whereas its exhaust valve opens first during expansion. The pressure, p, during the compression process is given as a function of piston position, x.

The pressure in cylinder 1 at any time t during compression, $p_1(t)$, is:

$$p_1(t) = p_a \cdot \left(\frac{x_{ivc1}}{x_1(t)}\right)^{\gamma_c} \tag{3.19}$$

Similarly, the pressure in cylinder 2 at any time during compression, $p_2(t)$, is:

$$p_2(t) = p_a \cdot \left(\frac{L - x_{ivc1}}{x_2(t) - x_{ivc2}}\right)^{\gamma_c} \tag{3.20}$$

3.4.2 The imposed piston motion modelling

According to the obtained motion equation, a set of pistons offset values according to time period are obtained. Such trajectories are characteristic of the operation of free piston engine gensets and are unique to the prototype.

The final optimized model of the 65cc two-stroke engine crankshaft car engine obtained in Section 3.3.4 was transformed into a free piston engine by applying the mandatory piston sprout model in Ricardo WAVE. This sub-entity model is used to cover the reciprocating motion of the crank slider with the default settings and to measure the volume of the engine combustion chamber. The WAVE operation panel of the sub-entity model is shown in the following Figure 3.28:

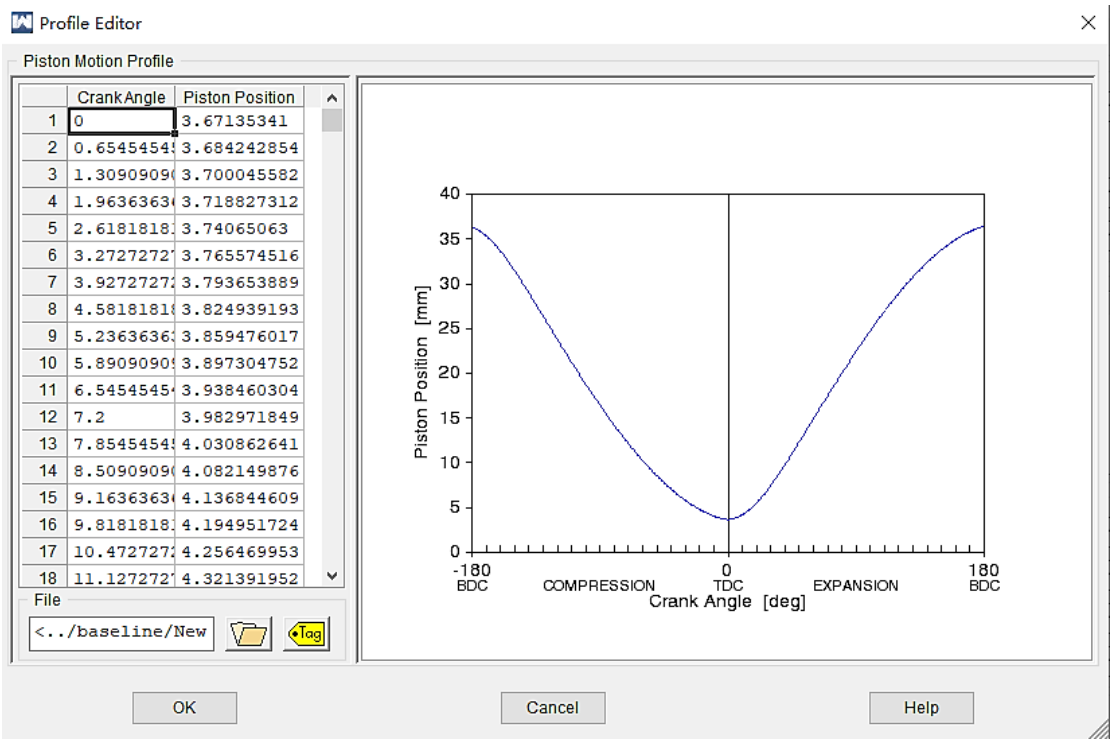

Figure 3.28 The input panel for imposed piston sub-model

Free piston revision numbers for the same automotive engine were modeled based on the application of the mandatory piston sprout model to the improved 65cc two-stroke engine crankshaft solid model obtained from Section 3.3.4. It can be predicted that the gas exchange individual behavior of the free piston solid model is not the same as that of the corresponding engine crankshaft solid model. Therefore, the close cylinder engine timing boost detailed in Section 3.3.3 is implemented to optimize its gas exchange characteristics as shown above.

3.4.3 Valve timing optimisation

The 65cc two-stroke free-piston engine model was subjected to further valve timing optimisation with similar parametric study as presented in Section 3.3.3. The following parameters were varied:

1. Vary intake valve anchor from 160°CA to 200°CA
2. Vary exhaust valve anchor from 140°CA to 180°CA
3. Vary valve duration from 90°CA to 120°CA

The purpose of this optimisation was to finalise the model before comparison with 65cc two-stroke

crankshaft engine model was made.

3.5 Discussion

While developing the models and simulations, several key findings were observed. This discovery has the benefit of accelerating the prototyping design and experimental science detailed in Chapters 4 and 5. In addition, the twin-cylinder 65cc two-stroke gasoline engine mock-up will be used to develop and design a 65cc two-stroke hydrogen free-piston engine mock-up, an ethanol car engine and a baseline mock-up for the Miller cycle.

3.5.1 Effect of piston motion

It has been observed that when a lifted two-stroke engine crankshaft car engine mock-up is immediately transformed into a two-stroke free piston engine mock-up (without optimisation), the characteristics are degraded.

The key factor is that; although similar gate valve engine timing is achieved in the 2 modes, the solid model of the piston imposed on it inherits a different fitness motion curve, as shown in Figure 3.29 below from the piston part and gear angle curve as seen in the picture. Because cylinder engine timing is set by the gear angle (°CA), the same gear angle results in a different piston location in most cases when approaching or avoiding BDC (i.e., from ±90 to ±180 °) There is a large difference of almost 5 mm in California). Thus, a similar major parameter science study was carried out on cylinder engine timing improvements to improve the gas exchange characteristics of a solid model of a free piston engine.

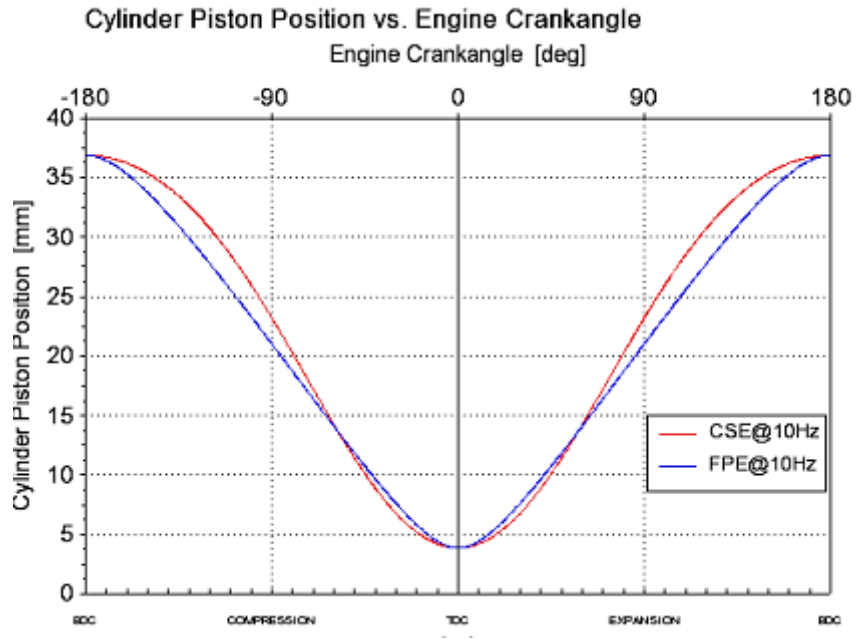

(a)

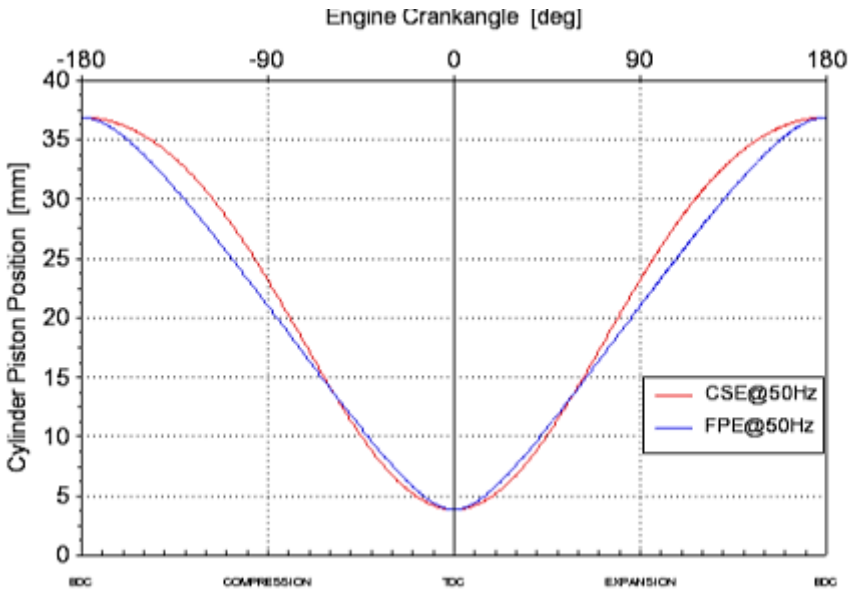

(b)

Figure 3.29 Piston position against crank angle comparison for free-piston engine (FPE) and crankshaft engine (CSE)(a)At 50 Hz and (b) At 10Hz

The piston velocity profiles shown in Figure 3.30 demonstrated typical free-piston engine velocity which is symmetrical along horizontal axis as opposed to oval-shaped profile for crankshaft engine. The crankshaft engine demonstrated higher maximum piston speed although operated at similar

engine speeds. The velocity profile for the free-piston engine was noisy due to data resolution issues highlighted in Section 3.4.2, the piston motion of the free-piston engine was controlled by the imposed piston motion sub-model. The IPM assumed that the motion control had been performed by regulating the piston position around TDC and BDC using linear motor current control whenever the combustion pressure has changed the piston dynamics. In addition, with the IPM, the model was unable to illustrate the impact of knock on the piston trajectory since the motion profile was unchanged during the simulation. This could be improved with an advanced co-simulation, having the plant model and the controller model exchanging information in real-time during the simulation period.

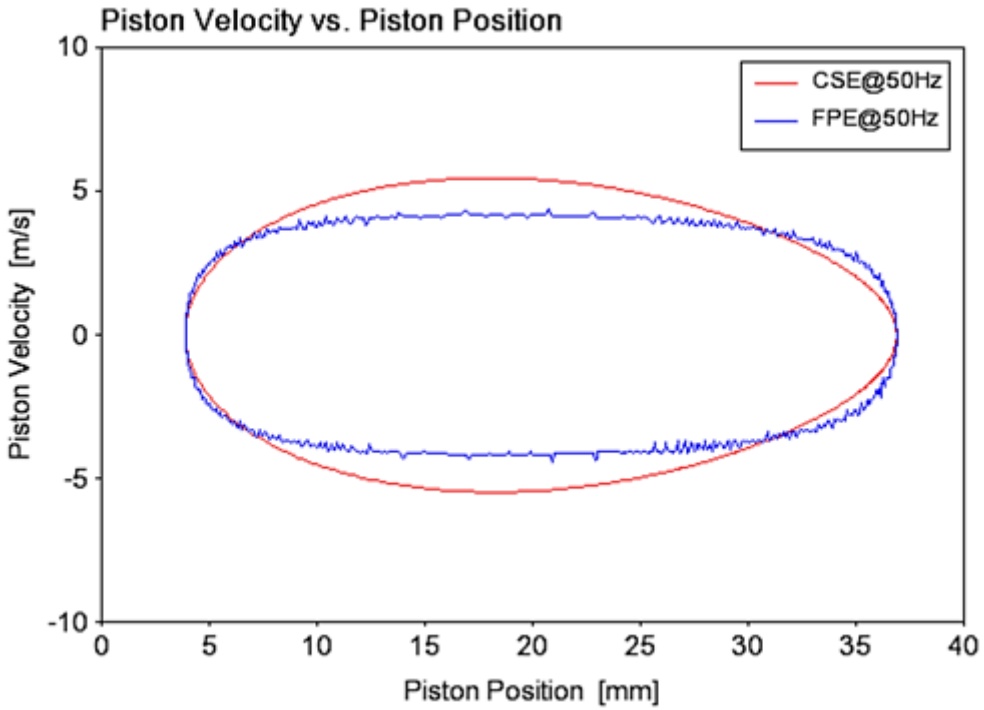

(a)

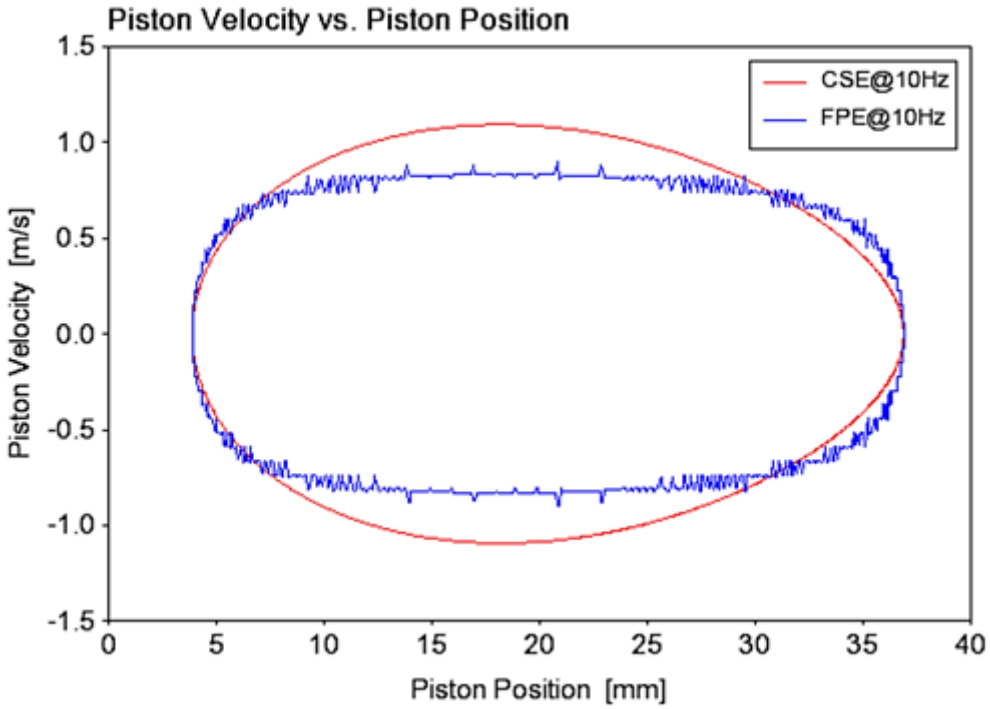

Figure 3.30 Piston velocity against piston position comparison for FPE and CSE(a) At 50Hz and (b) At 10Hz

3.5.2 Valve timings

Figure 3.31 shows the lift-cylinder engine timing for two solid models, fabricated in relation to variable valve timing and gear angle. It was found that for the two model specifications, the EVO parts are the same, while the IVO parts of the optional piston engine are separated by about 10° CA.

This correlates to the reciprocating motion profile described in Section 3.5.1. The error of the piston part of the fitness line of the free piston engine is not large when it is lower than 90°CA (that is, when the EVO is generated), so it is beneficial to the same EVO part. This can be verified when it is produced according to the diagram of the piston part is shown in Figure 3.31 During the 90° CA to 180° CA period, the error was large enough to indicate different IVO sites. In fact, the IVO of a free piston engine is earlier than that of a crankshaft car engine, although its gear corners are later, when made from the piston part. Cylinder engine timing is the primary parameter independent of speed; thus, this discussion applies to other automotive engine speeds.

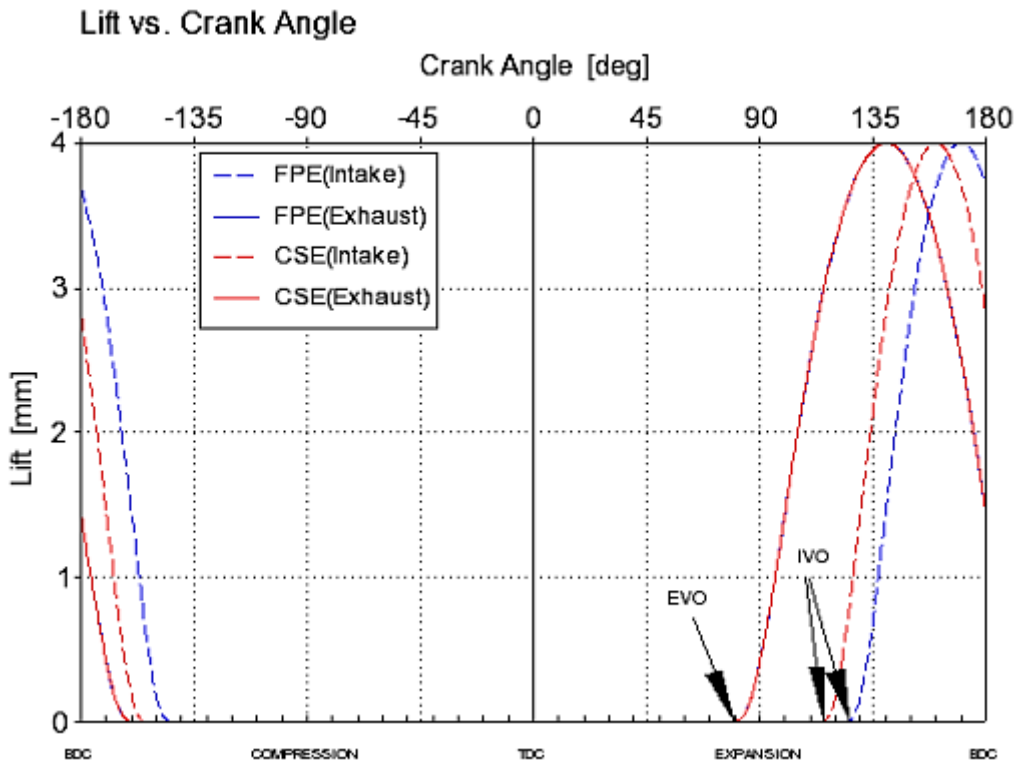

(a)

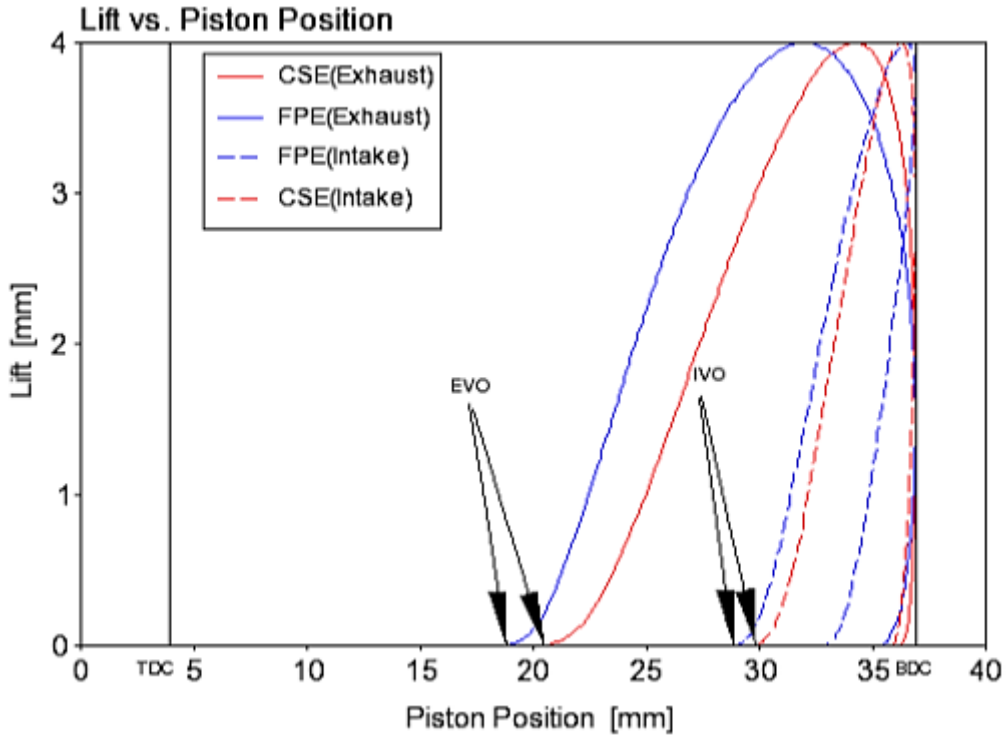

(b)

Figure 3.31 Optimised intake and exhaust valves timing for FPE and CSE(a) Crank angle-based(b) Piston position-based

Figure 3.32 shows the variation valve timing for the free-piston engine for different free-piston engine operating speed. At lower free-piston engine speed, the valve opening occurred later in the cycle and the opening duration was longer while at higher free-piston engine speed both valves opened earlier with shorter duration.

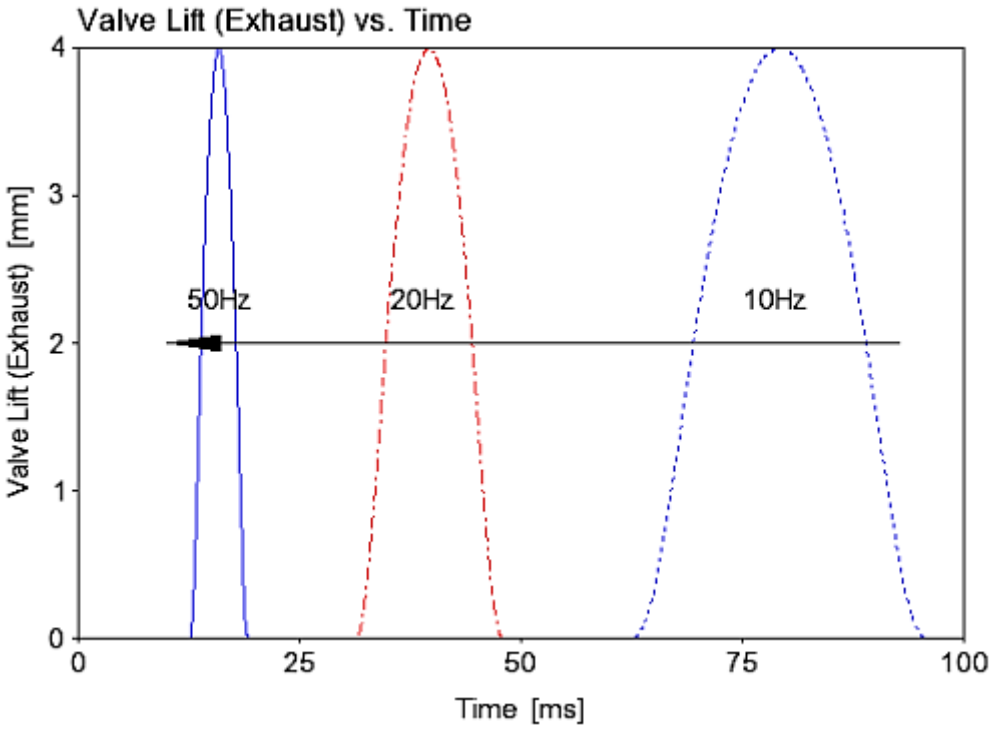

(a)

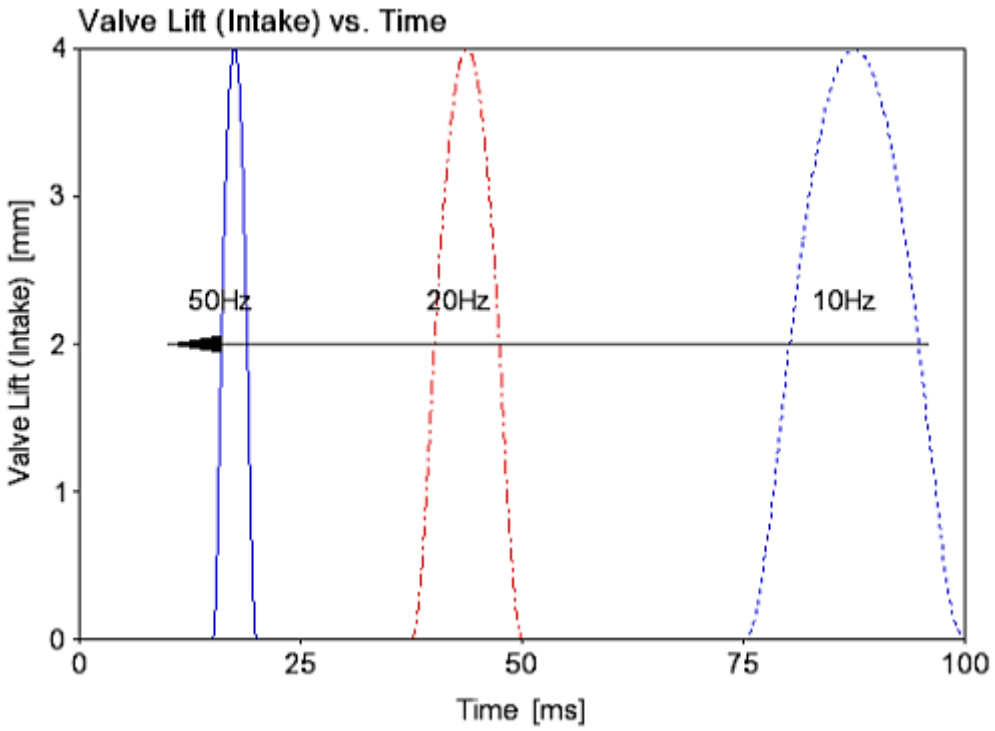

Figure 3.32 Variation of valve opening and closing timing at different speeds for the free-piston engine model(a) Exhaust valve(b) Intake valve

Because in a free piston engine, the cylinder push data signal is based on position, not gear angle, it is interesting to develop an optimization algorithm for cylinder engine timing manipulation. Figure 3.33 shows valve engine timing according to location mode. The exhaust valve closing (EVC) part is 35.7mm after the BDC, nevertheless, in each cycle, the piston will be in this part 2 times; When exercising to TDC Fitness.

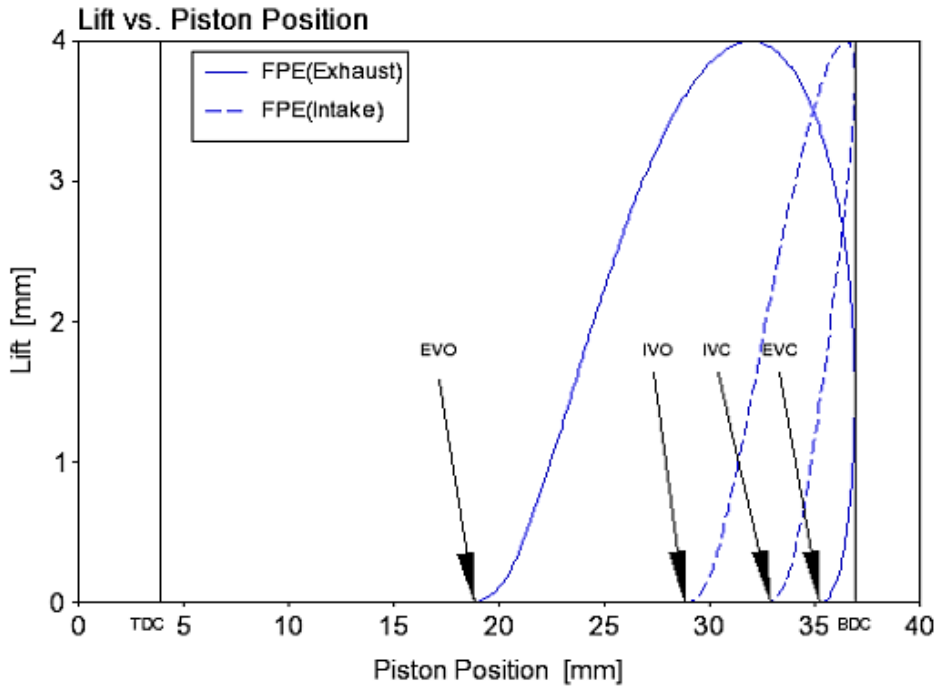

Figure 3.33 Valve opening and closing positions for free-piston engine

Therefore, the practical valve actuation algorithm must be based on the position value and the direction of motion.

3.5.3 In-cylinder pressure

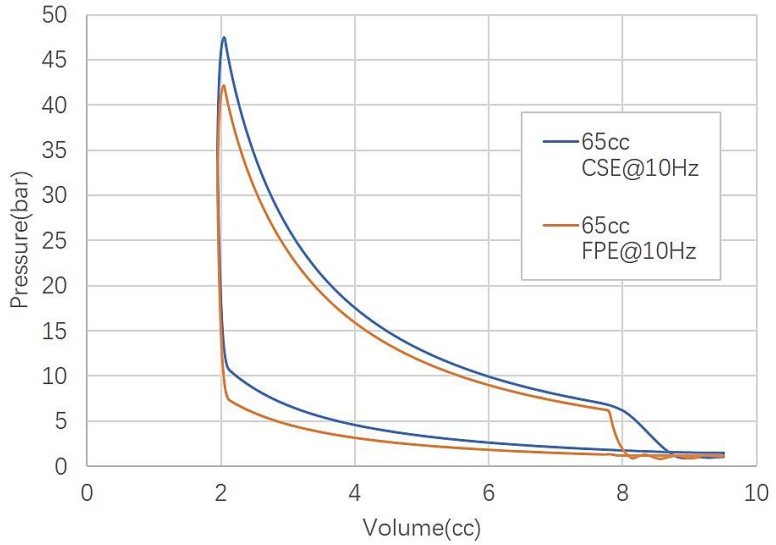

(a)

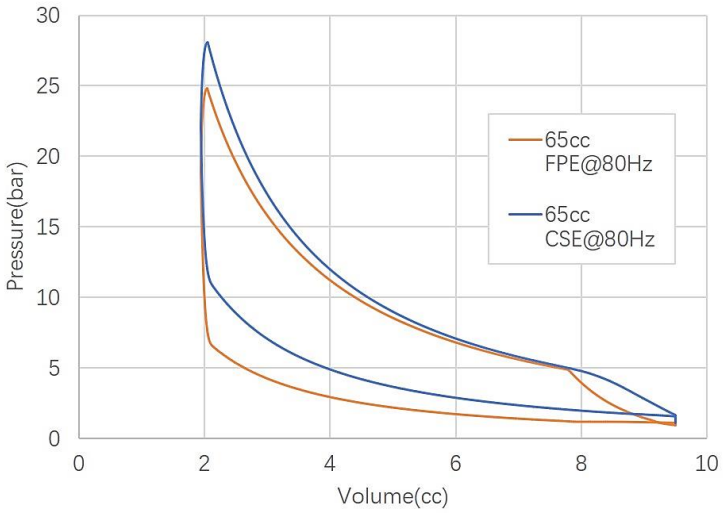

(b)

Figure 3.34 P-V diagram comparison between (a)FPE and (b)CSE at 80Hz

Figure 3.34 (a) and (b) show the P-V diagram comparison between the FPE and the CSE at 10 Hz and 80Hz. For both frequencies, the maximum pressure of the conventional engine is higher than the free-piston engine, and as the engine frequency increases, the maximum pressure decreases.

Lower pressure versus volume profile translated into lower power output as shown in Figure 3.35 where the brake power versus engine cyclic speed (presented in Hz) was plotted. Free-piston engine produced significantly lower power output from 20 to 60 Hz then increased higher than crankshaft engine from 65 to90Hz. The peak power produced by the free-piston engine model was shifted into higher speed. The free-piston engine produced 2.43kW at 50Hz while the crankshaft engine produced 2.42kW at 80Hz.

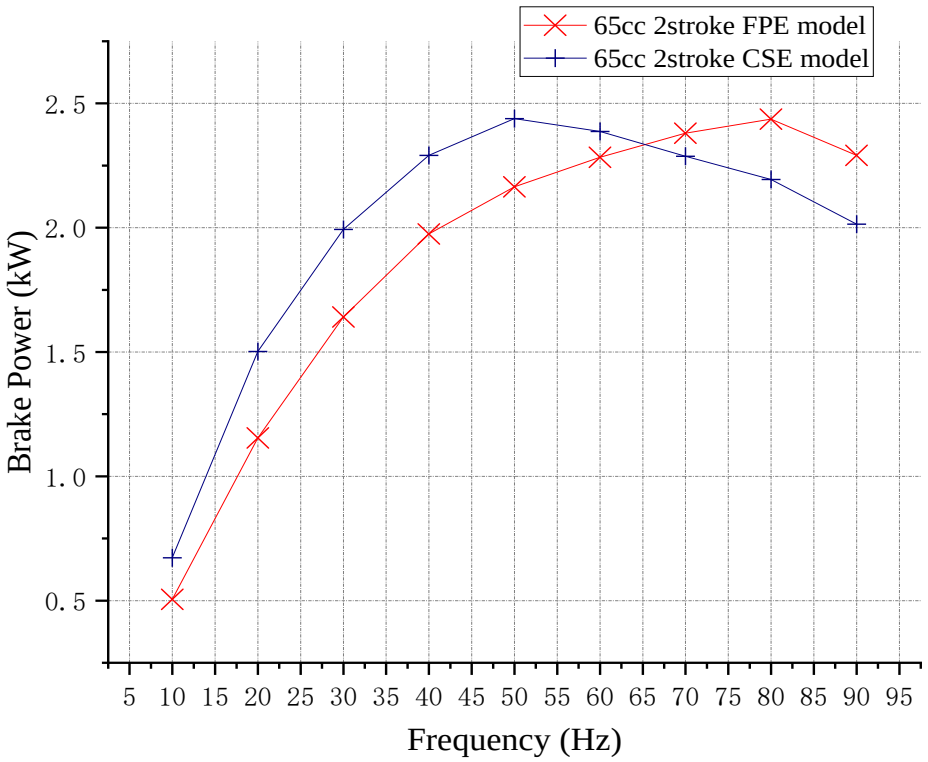

Figure 3.35 Brake power comparison for both models

3.6 Simulation results

The most vital component in Ricardo WAVE for this research is its NOx analysis simulation sub model, and by using which, the NOx emission results along with HC emission results for both 65cc 2stroke FPE model and 65cc 2stroke CSE model have been obtained and the comparisons are illustrated as Figure 3.36 and Figure 3.37.

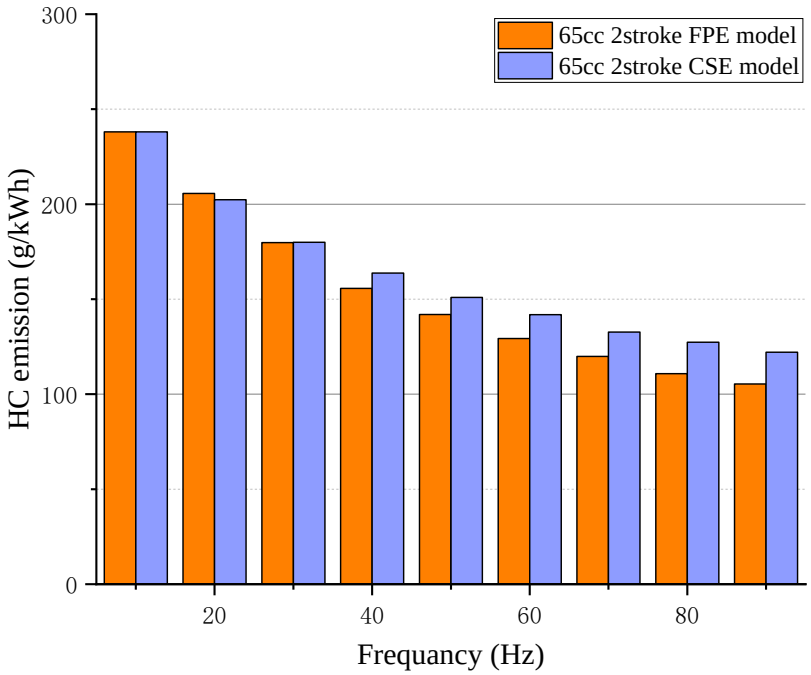

Figure 3.36 HC emission comparison for both models

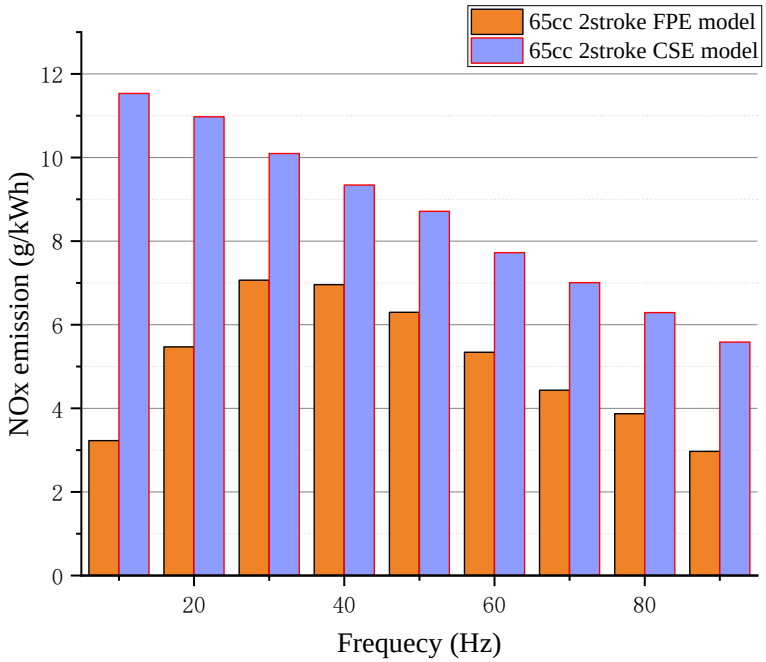

Figure 3.37 NOx emission comparison for both models

It could be concluded that for HC emission, under the same engine condition, there's only slight difference between a free-piston engine and a same scale conventional engine. Due to the formation reason of HC emission is incomplete combustion, together with the brake power varying trend as

showed in figure 3.36, it is not difficult to explain why the HC emission decreases with the increase of engine frequency for both models.

From figure 3.37, there's a significant reduction of NOx emission in the FPE comparing with the CSE, and the highest reduction range is 72.02% which occurs at 10Hz. For the free-piston engine, the average in-cylinder combustion temperature increases from the frequency of 10Hz to 30Hz and decreases afterwards, while the average in-cylinder temperature gradually decreases from 10Hz to 90Hz for the conventional engine. Therefore, the free-piston engine has remarkable ability on NOx reducing.

3.7 Summary

This chapter describes the development and design of the one-dimensional solid model of two versions of the four-stroke flame ignition engine crankshaft automobile engine (31cc and 65cc), and the virtual transformation of the 65cc version number into a two-stroke engine. A four-stroke engine crankshaft mock-up was certified based on torque curve graphs and manufacturer data analysis sheets derived from published studies on the same automotive engine.

This proven mock-up was transformed into a mock-up of a 65cc two-stroke that had to lift the intake and cylinder valves. This type of lifted 65cc two-stroke mockup is transformed into a free-piston engine mockup based on the application of the Forced Reciprocating Motion (IPM) sub-model. The IPM assumes that the motion control of the free piston engine is already in time, resulting in consistent trajectories around the TDC and BDC.

The reciprocating motion graph of the IPM sub model is converted from the equations of motion of the free piston engine dynamics model. This dynamic equation is derived from a mathematical model of the forces that contributes to the exercise of a free piston engine.

It was found that the IPM sub-entity model caused the valve engine timing to be different for the free piston engine mock-up, even though the mock-up is a lift engine crankshaft car engine mock-up and operates at a similar cycle rate. Because of the lack of gear perspective reference, it is recommended that the original valve engine timing must be referenced according to the piston

position and its orientation (house facing TDC or facing BDC). In addition to this, the IPM solid model will be improved in the area of data points, as it was found to be insufficient when applying the kinetic equations to transform into and must be certified before adequate characterization investigations can be carried out.

In conclusion, this chapter has produced a two-stroke free-piston engine model from validated four-stroke crankshaft engine model as explained in Section 3.3. Simulations in following sections were all on the basis of the two-stroke gasoline free-piston engine model.

Chapter 4. Single-cylinder hydrogen FPE modelling and simulation

Emissions of the free-piston engine, especially the hydrogen and renewable fuel free-piston engines has not been widely investigated, and this will be presented chapter 4 and chapter 5 as the most important part and novelty. In order to simulate the operation and exhaust performance of the hydrogen free-piston engine, one single-cylinder hydrogen FPE model is indispensable.

On the basis of chapter 3, a hydrogen free-piston engine WAVE model was developed, and for the purpose of validation, two simulation and calculation models were built by MATLAB and MATLAB/Simulink.

This chapter describes the whole process of emission research including modelling and the theory presents in section 4.1, validation work and simulation presents in section 4.2.

4.1 Theoretical review

An experiment targets on the performance of a hydrogen dual piston 2-stroke and 4-stroke free-piston engine generator was presented by Dr. Smallbone and Ngwaka, et al. [158], which reveals the relationship between equivalence ratio, engine speed and engine operation characteristics, and the scale of his experimental set is the same of this research, therefore, the experimental experience of his could be considered as a perfect comparison to instruct the modelling and validation process.

The specifications of the free-piston engine generator are given in Table 4.1. A conservative approach was adopted in the selection of the prototype piston stroke and engine speed, this was done to minimise the risk of impact between valves, the piston head and the cylinder end and to support the improved control strategy adopted. The linear electric machine was used as an active controller to control the piston movement according to a pre-set sinusoidal displacement profile.

Table 4.1 Hydrogen FPE prototype specifications

Parameters [Unit]	Value

Moving mass [kg]	7.0
Maximum stroke [mm]	40.0
Actual stroke [mm]	34.0
Effective bore [mm]	50.0
Intake valve diameter [mm]	20.0
Exhaust valve diameter [mm]	18.0
Valve lift [mm]	4.0
Number of cylinders [-]	2
Nominal target compression ratio	3.7

The target piston displacement profile is a sinusoidal wave function with amplitudes of 17.0 mm and -17.0 mm. The pre-set piston stroke is 34.0 mm, the clearance from the cylinder head yielded a corresponding compression ratio of 3.7. An operating speed of 5 Hz was selected for the testing, which corresponds to 300 cycles per minute. The FPEG prototype was operated according to both two-stroke and four-stroke thermodynamic cycle; the valve timings and spark ignition initiation were controlled based on piston displacement and velocity feedback. During a series of engine tests, data were collected over 30-60 consecutive sequential combustion cycles and postprocessed. The baseline operating parameters are set out in Table 4.2.

Table 4.2 Baseline model operating parameters

Parameters [Unit]	**Value**
Operational speed [Hz]	5.0

Reference Position (Ref) [mm]	15.0	
	Two-stroke	Four-stroke
Top Dead Center (TDC) [s aRef]	0.059	0.064
Bottom Dead Centre (BDC) [s aRef]	0.160	0.163
Spark Timing [s aTDC]	-0.014	-0.021
Inlet Valve Open (IVO) [s aTDC]	-0.034	-0.017
Inlet Valve Close (IVC) [s aTDC]	0.006	0.114
Exhaust Valve Open (EVO) [s aBDC]	0.039	-0.009
Exhaust Valve Close (EVC) [s aBDC]	0.077	0.112

Thus, a one-cylinder two-stroke hydrogen free-piston engine WAVE model could be developed from the one-cylinder two-stroke gasoline free-piston engine which has been described in section 3 along with the above theoretical basis, and it's not difficult to restore the experiment done by Dr. smallbone perfectly. Once the modelling process completes, the experimental results from Dr. smallbone could be used as control groups for validation work, and the emission performance of the hydrogen FPE model could be investigated.

4.2 Hydrogen FPE modelling/validation and simulation implementation

4.2.1 Hydrogen FPE modelling

There are several kinds of parameters and boundary conditions which differ from gasoline free-piston engine and hydrogen free-piston engine require amendments, such as pre-set piston motion, compression ratio, equivalent air/fuel ratio and valve timing, etc. Figure 4.1 is the diagram of mean

piston motion varies with min time which obtained from experiment, and in the free-piston engine, the crank mechanism is eliminated. Thus, in order to make further comparison of the FPE with CE, an equivalent crank angle (ECA) is adopted for the FPE to describe one operation cycle:

$$ECA = \frac{t}{T} \cdot 360^{\circ} \tag{4.1}$$

The total time of one complete cycle for the two-stroke free-piston engine is 0.2s, while the corresponding crank angle is 360°. As a consequence, the pre-set piston motion applies in Ricardo WAVE engine panel is converted as shown in Figure 4.2.

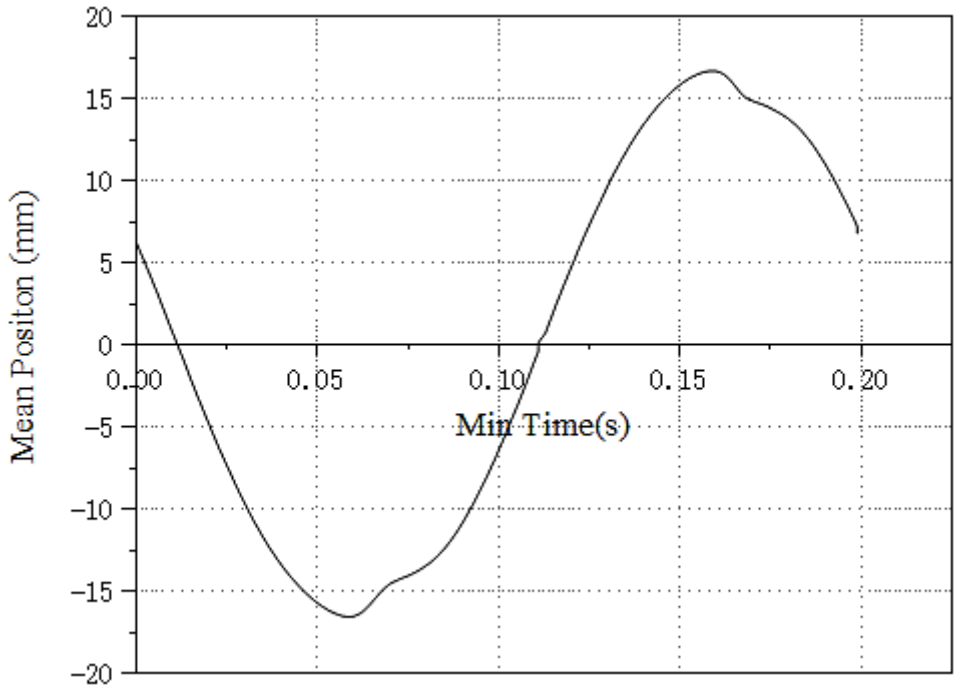

Figure 4.1 Piston motion vs min time in Hydrogen FPE model

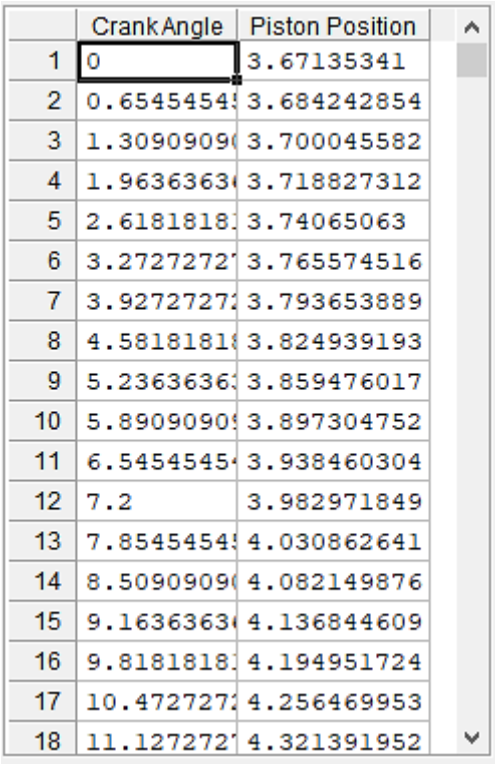

	Crank Angle	Piston Position
1	0	3.67135341
2	0.6545454	3.684242854
3	1.3090909	3.700045582
4	1.9636363	3.718827312
5	2.6181818	3.74065063
6	3.2727272	3.765574516
7	3.9272727	3.793653889
8	4.5818181	3.824939193
9	5.2363636	3.859476017
10	5.8909090	3.897304752
11	6.5454545	3.938460304
12	7.2	3.982971849
13	7.8545454	4.030862641
14	8.5090909	4.082149876
15	9.1636363	4.136844609
16	9.8181818	4.194951724
17	10.472727	4.256469953
18	11.127272	4.321391952

Figure 4.2 Pre-set piston motion data in Ricardo WAVE

The Fuel and Air Properties Panel as shown in Figure 4.3 allows the user to create fuel and air properties files for use in WAVE. It runs the property pre-processor to generate lookup tables of the chemical properties of the fuel-air mixture. It can generate properties for a single fuel, for a blended fuel, and for multiple fuels. Currently up to three fuels are supported in multiple fuels mode [225].

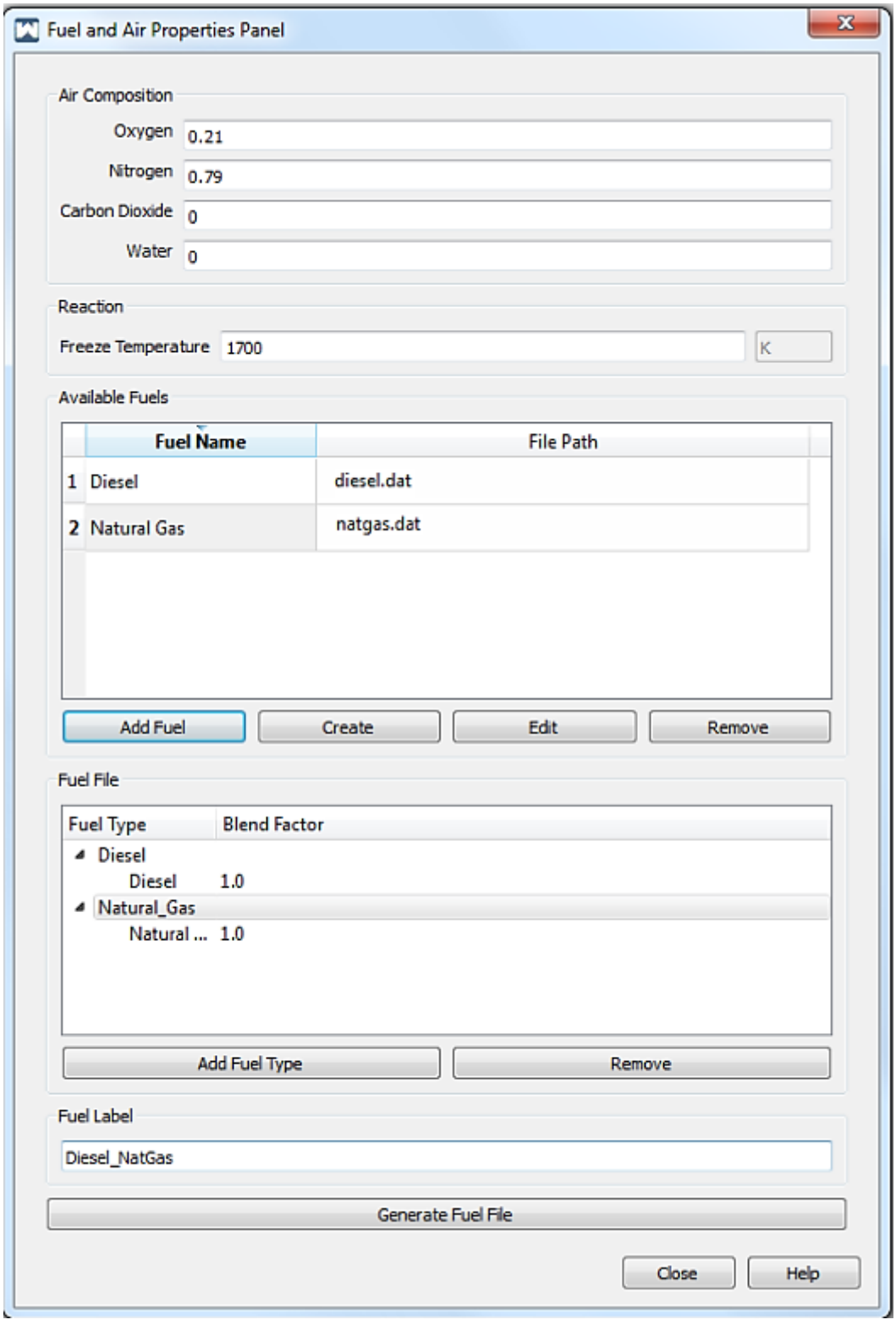

Figure 4.3 Fuel and air properties panel in Ricardo WAVE

And the Fuel Property Tag selector as shown in Figure 4.4 allows the user to choose base fuels that needed. Base fuels are used to build the composition of the fuel to be mapped in a WAVE fuel file.

In this section, a new type of fuel, hydrogen, would be applied to take the place of gasoline, which is set as fuel in the previous free-piston engine model.

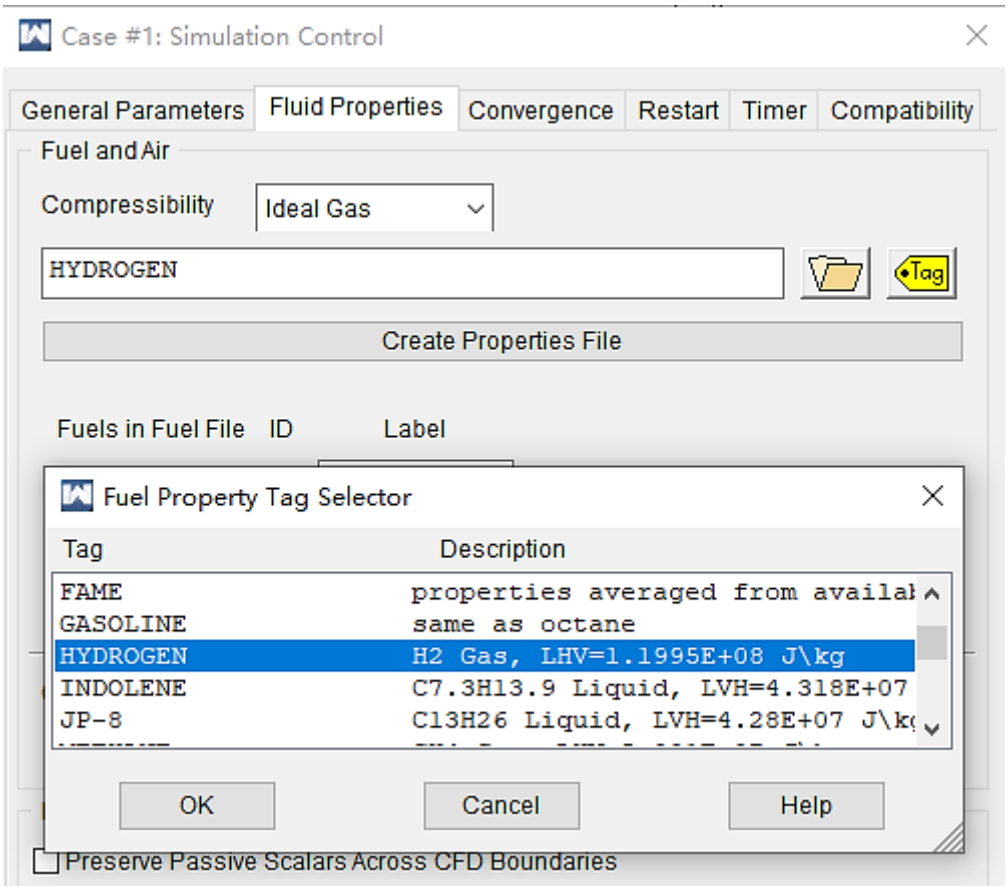

Figure 4.4 Fuel Property Tag Selector in Ricardo WAVE

According to the FPEG prototype specifications in Dr. smallbone's experiment, the compression ratio should be amended from the previous 9.5 to 3.7 as shown in Figure 4.5.

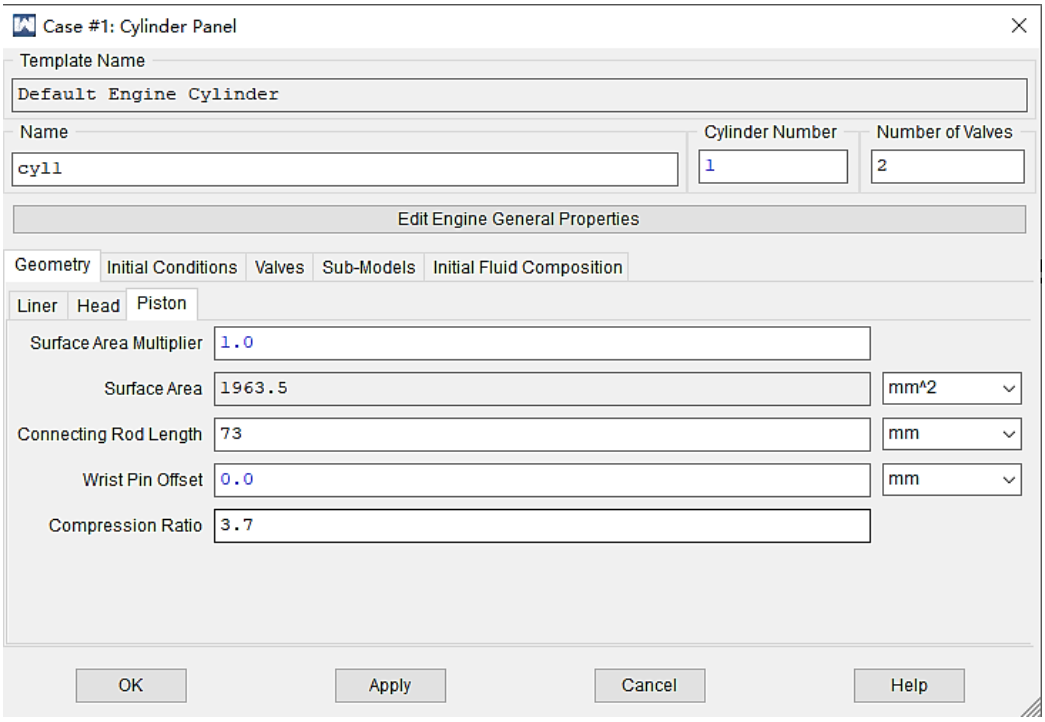

Figure 4.5 Cylinder panel in Ricardo WAVE

The stoichiometric composition of fuel and air is that which provides the chemically precise amount of oxidant to completely burn all the fuel. For hydrogen and oxygen, the stoichiometric combustion equation expressed per mole of fuel and the calculation of the volumetric composition and mass stoichiometric air/fuel ratio (σ), is given below. The actual mass ratio of air to fuel, m_a/m_f, can be expressed as where is called the air excess ratio – the relative amount of mass of air over that required for stoichiometric combustion.

$$\left(m_a/m_f\right)_{actual} = \lambda(m_a/m_f)_s = \lambda \cdot \sigma \tag{4.2}$$

Another commonly used term is the equivalent ratio, denoted φ:

$$\varphi = \lambda^{-1} \tag{4.3}$$

The equivalent ratio is the relative amount of mass of fuel over that required for stoichiometric combustion:

$$\left(m_f/m_a\right)_{actual} = \lambda(m_f/m_a)_s = \lambda \cdot \sigma^{-1} \tag{4.4}$$

Atmospheric air contains 20.95% O_2 and 79.05% atmospheric nitrogen N_2 by Volume. On a molar

basis, since 1 kmol of any perfect gas occupies the same volume ($22.4m^3$) this corresponds to 79.05/20.95=3.773 moles of N_2 per mole of O_2 in atmospheric air. Thus, the stoichiometric combustion equation for hydrogen and atmospheric air is:

$$H_2 + \frac{1}{2}(O_2 + 3.773N_2 \rightarrow H_2O + 1.887N_2$$

$$1 + \frac{1}{2}(1 + 3.773 \rightarrow 1 + 1.887\ or\ 1 + 2.387 \rightarrow 1 + 1.887$$

Thus 2.387 moles of air per mole of H_2 are required to completely burn all the fuel. This corresponds to a stoichiometric volume percent of hydrogen in air of:

100/3.387=29.52%

For the mass stoichiometric air/fuel ratio φ, express the above equation in terms of relative mass, by multiplying by the molecular weight of the species – for atmospheric air, water and atmospheric nitrogen, the molecular weights M, are 28.96 kg/kmol, 18.02 kg/kmol and 28.16kg/kmol respectively giving:

$$(1 \cdot 2.01) + (2.38 \cdot 28.96) \rightarrow (1 \cdot 18.02) + (1.88 \cdot 28.16)$$

Per kilogram of fuel divide through by 2.016

$$1 + 34.3 \rightarrow 8.94 + 26.35$$

The stoichiometric air/fuel ratio is thus φ_{H2} = 34.3kg air per kg fuel. On the basis of this theory, it can be similarly deduced that for gasoline, the stoichiometric volume percent of fuel in air is 1.76%, and $\sigma_{petrol} = 14.6$.

Equation (4.5) shows the relationship between the equivalent ratio, stoichiometric air/fuel ratio and the actual air/fuel ratio:

$$\text{equivalent ratio} = \text{stoichiometric}\frac{\text{air}}{\text{fuel}}\text{ratio} \Big/ \text{actual}\frac{\text{air}}{\text{fuel}}\text{ratio} \tag{4.5}$$

Thus, on the basis of the experiment done by Dr. smallbone, which expressed several different tests with varies equivalent ratio, and for two-stroke hydrogen FPE, when the frequency was set to be 5Hz-11Hz, the equivalent ratio was 0.4365 (at 11 STL/min hydrogen flowrate and 60 STL/min air

flowrate). Therefore, the actual air/fuel ratio that should be pre-set in the Ricardo WAVE model is 78.58 as shown in Figure 4.6.

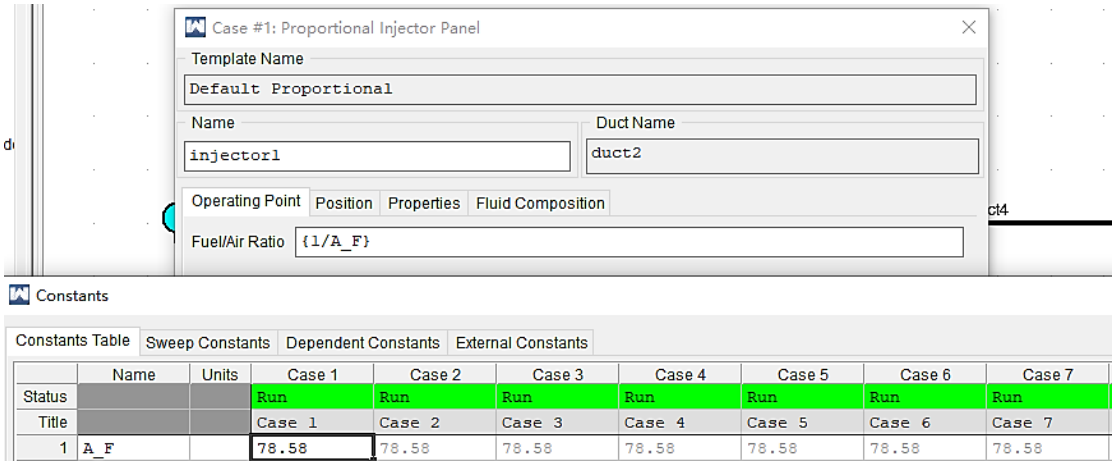

Figure 4.6 Air/fuel ratio pre-set in the injector panel

4.2.2 Model performance optimisation

By utilising the same method which has been described in section 3.3.3, the performance (which especially is the valve timing) of the two-stroke hydrogen free-piston engine model is optimised. As it has been adequately presented in above paragraphs, there's no need to repeat the whole process in details. Optimum exhaust valve anchor position (Exh_{Anchor}), exhaust duration (Exh_{Dur}), intake valve anchor position (Int_{Anchor}) and intake valve duration (Int_{Dur}) were determined by setting the appropriate target in curve fits window in Figure 4.7.

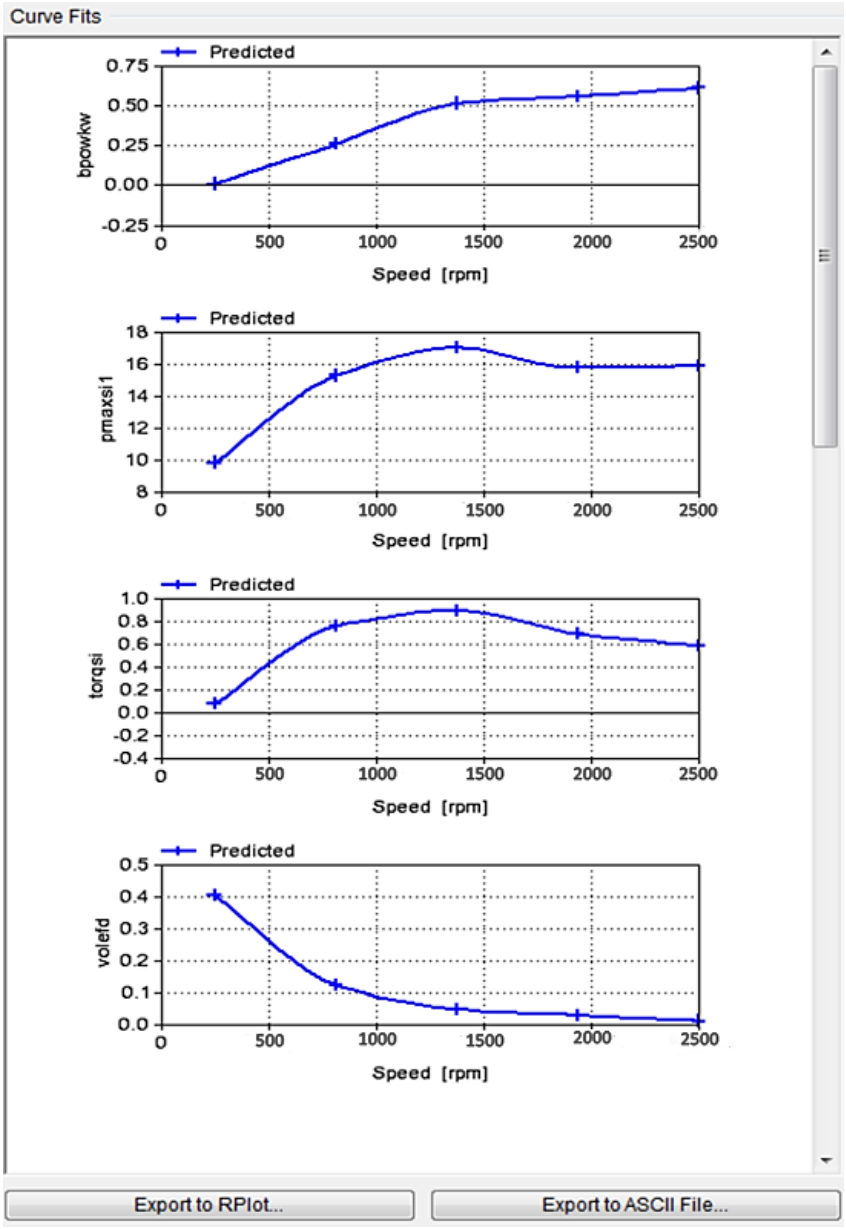

Figure 4.7 The experiment analysis panel showed-up at the end of the experiments in Ricardo WAVE

At optimised valves anchor, the exhaust valve is opened at 116°CA before BDC followed by intake valve 19°CA later. And after BDC, i.e., at 65°CA after BDC, the exhaust valve is closed followed by intake valve 10°CA later. Which means in the free-piston engine model, crank angle has to be converted into particular time:

65cc two-stroke hydrogen FPE model valve timing results:

- EVO=116°bBDC (0.0644s)
- IVO=105°bBDC (0.0583s)

- EVC=65°aBDC (0.1361s)
- IVC=75°aBDC (0.1416s)

Here, the two-stroke hydrogen free-piston engine modelling process is completed, the model has been converted from a two-stroke gasoline free-piston engine model, and factors such as piston motion, compression ratio, equivalent air/fuel ratio and valve timing have been amended.

4.3 Hydrogen free-piston engine model validation

4.3.1 Indicated power

The effects of operational frequency on peak pressure, peak pressure timing, indicated work, indicated power and indicated efficiency at equivalence ratio of 0.4365 (at 11 STL/min hydrogen flowrate and 60 STL/min air flowrate) are all investigated separately in Dr. smallbone's experiment, and this research will take the indicated power results, as shown in Figure 4.8, as control data to validate the WAVE model.

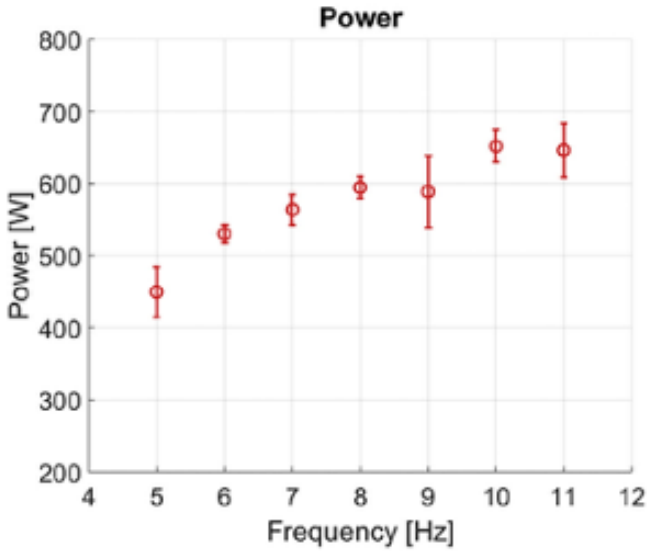

Figure 4.8 Indicated power for four-stroke FPE

As the indicated power result from Dr. smallbone is obtained on a four-stroke cycle mode, an amendment of the two-stroke free-piston engine WAVE model to a four-stroke one is inevitable. And once the model is perfectly changed into a four-stroke model, the indicated power results in WAVEpost can be used for validation, and through the validation work done between two four-

stroke engine data, the two-stroke FPE engine WAVE model is also validated on the indicated power aspect. The comparison between the indicated power result from the experiment of Dr. smallbone and the WAVE model is shown in Figure 4.9. The indicated power increased with increase in operational frequency for both sources, and the error between which is constantly lower than 5% (the biggest error 4.85% accurses at the operational frequency of 8Hz). So far, the indicated power obtained from WAVE is highly consistent with which from the experiment of Dr. smallbone, and this is an important part of the validation process.

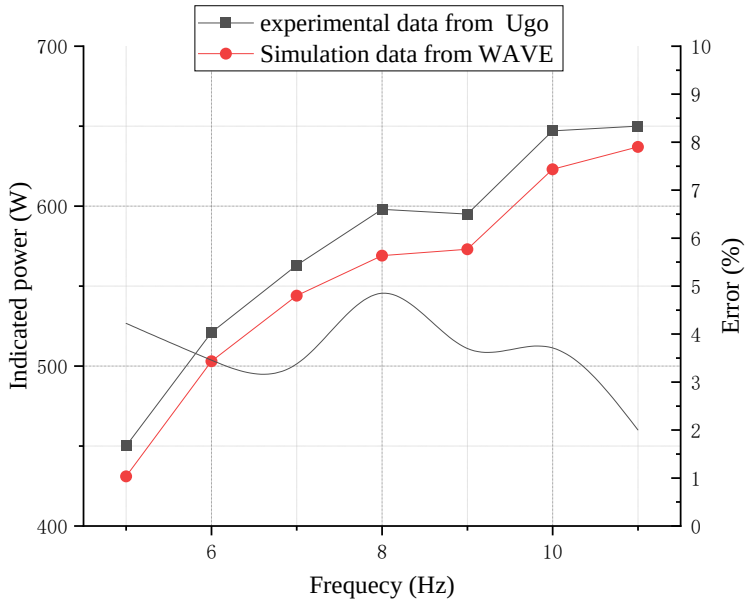

Figure 4.9 Indicated power comparison between WAVE model and experimental data

4.4 Emission performance analysis

4.4.1 NOx emission

Thanks to the fuel speciality of hydrogen (which contains H only), the only one type of emission that require concern is NOx. Figure 4.14 illuminates NOx emission from the two-stroke and four stroke hydrogen free-piston engine WAVE model under the equivalence ratio of 0.4365 and compression ratio of 3.7, and the engine frequency from 5Hz to 11Hz.

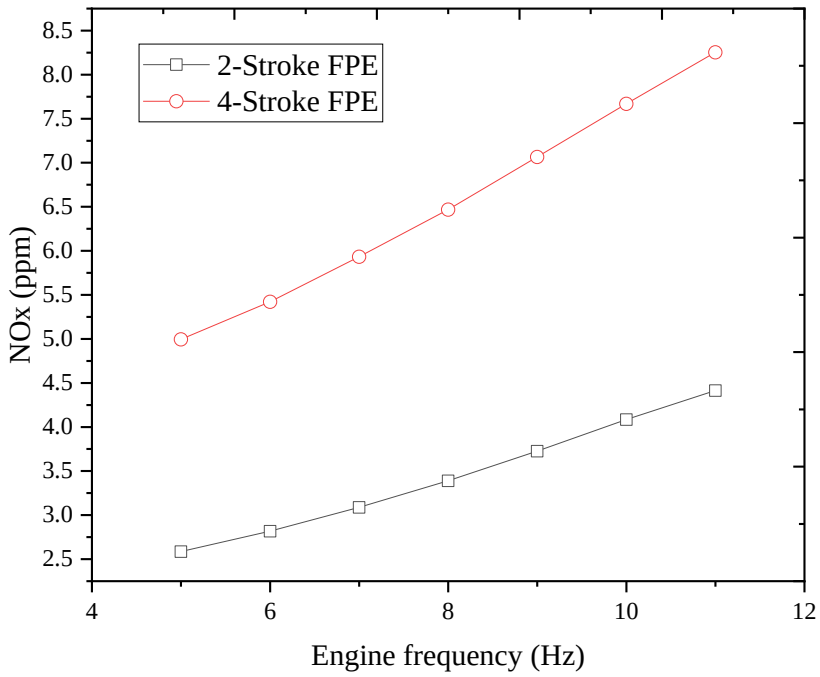

Figure 4.10 NOx emission of two-stroke hydrogen free-piston engine model

As NOx is a type of high temperature emission, and the formation of NOx emission increases with the increase of the combustion temperature when the in-cylinder temperature is higher than 1800K. Therefore when the engine speed (frequency) increases, the value of NOx emission increases simultaneously. NOx emission of the four-stroke FPE model is nearly doubled comparing to the two-stroke FPE model, and this result is slightly lower than what has obtained by Dr. smallbone. A comparison between NOx emission of this two-stroke hydrogen FPE model, the baseline two-stroke gasoline FPE model and the baseline two-stroke gasoline conventional engine model is presented in Figure 4.15.

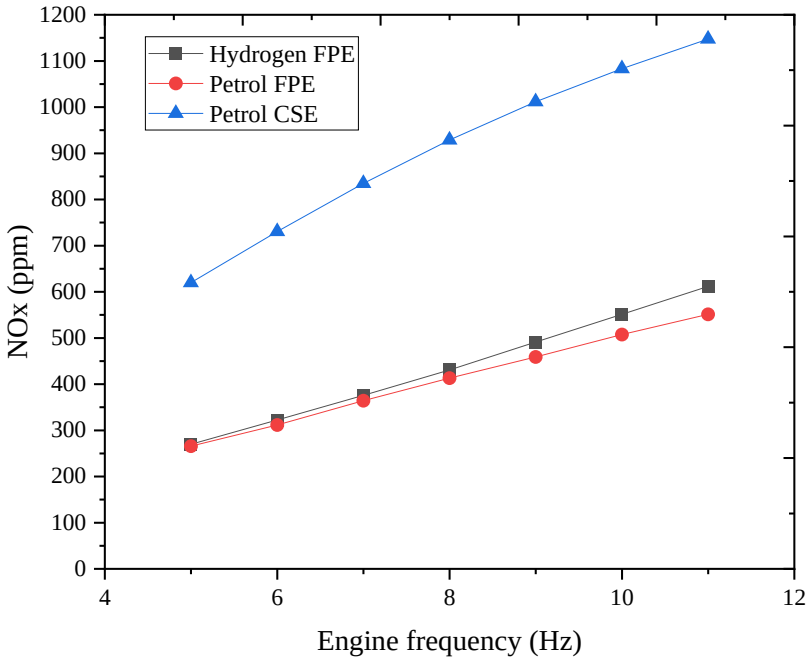

Figure 4.11 NOx emission comparison between three models

Equivalent ratio of the engines shown in Figure 4.15 are pre-set as 1.0, as the stoichiometric air/fuel ratio of gasoline is 14.7 and which of hydrogen is 34.3, so the air/fuel ratio that pre-set in Ricardo WAVE: $AFR_{petrol} = 14.7, AFR_{hydrogen} = 34.3$. It is obvious in Figure 4.15 that conventional spark-ignition gasoline engine produces the largest amount of NOx, and NOx emission produced from gasoline free-piston engine and hydrogen free-piston engine is quite similar. Comparing with conventional spark-ignition gasoline engine and free-piston engine, the NOx reduction potential is remarkable for the FPE, the reduction ranges are all higher than 51% from the engine frequency of 5Hz to 11Hz, and the largest reduction is 57.37% occurs at 6Hz. It is worth mentioning that in the free-piston engine, gasoline produces less NOx emission comparing with hydrogen but the difference is relatively small. The difference of NOx emission of gasoline and hydrogen FPE increases with the increasing engine frequency, and the figure reaches 10.97% at 11Hz.

The reason that NOx emission from hydrogen free-piston engine is higher than gasoline free-piston engine could be known in Figure 4.16. As shown in Figure 4.16 is the highest in-cylinder temperature in the gasoline FPE and Hydrogen FPE under the air/fuel ratio of $AFR_{petrol} = 14.7, AFR_{hydrogen} = 34.3$. For each engine frequency, the highest in-cylinder temperature of hydrogen FPE is slightly higher than what of the gasoline FPE, and the temperatures are all higher

than 2000K which has been mentioned above, NOx emission is strongly affected by temperature.

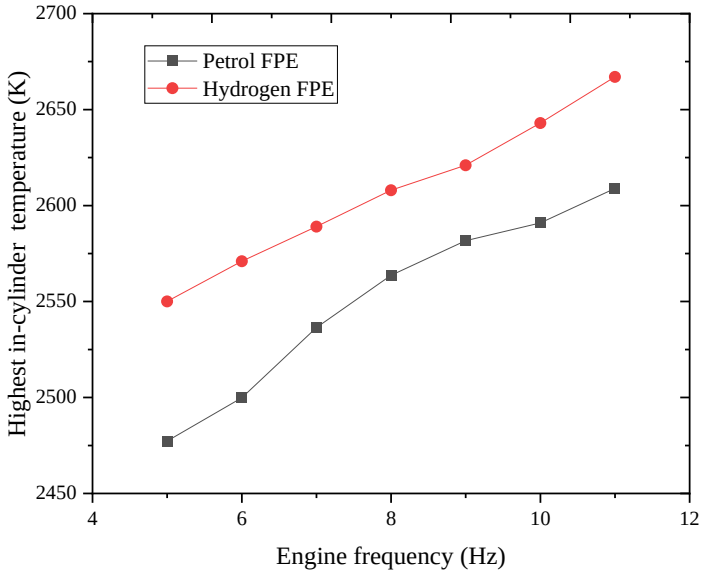

Figure 4.12 Highest in-cylinder temperature of Gasoline FPE and hydrogen FPE

4.4.2 Regulation between NOx emission and equivalent ratio

Figure 4.17 shows the relationship between NOx emission and equivalent ratio (φ) when the ignition advance angle (time) is fixed at 10°CA (0.00583s). As shown: when $\varphi < 0.5$, NOx increases with the increase of φ, but the range is relatively small and the contribution rate of φ is small as well; when $0.5 < \varphi < 0.88$, NOx increases with the increase of φ, but the range is large and the contribution rate of φ is relatively large as well; when $\varphi > 0.88$, NOx sharply decreases with the increase of φ. NOx emission reaches the highest point at $\varphi = 0.88$, and this regulation has highly agreement with what has been mentioned by Safari H, etc. [294-296].

Thermal NOx is the staple NOx emission category in hydrogen internal combustion engine, and the formation of NOx is mainly determined by three factors: high temperature, oxygen enrichment and duration of high temperature, while temperature affects the most. The stagnation temperature of the formation of thermal NOx is 1800K, when temperature is higher than 1800K, the formation of NOx increases exponentially with increasing temperature. When in-cylinder temperature is higher than 2000K, the contribution rate of temperature will become extremely obvious. The highest mean in-cylinder temperature in this thesis was calculated by Ricardo WAVE.

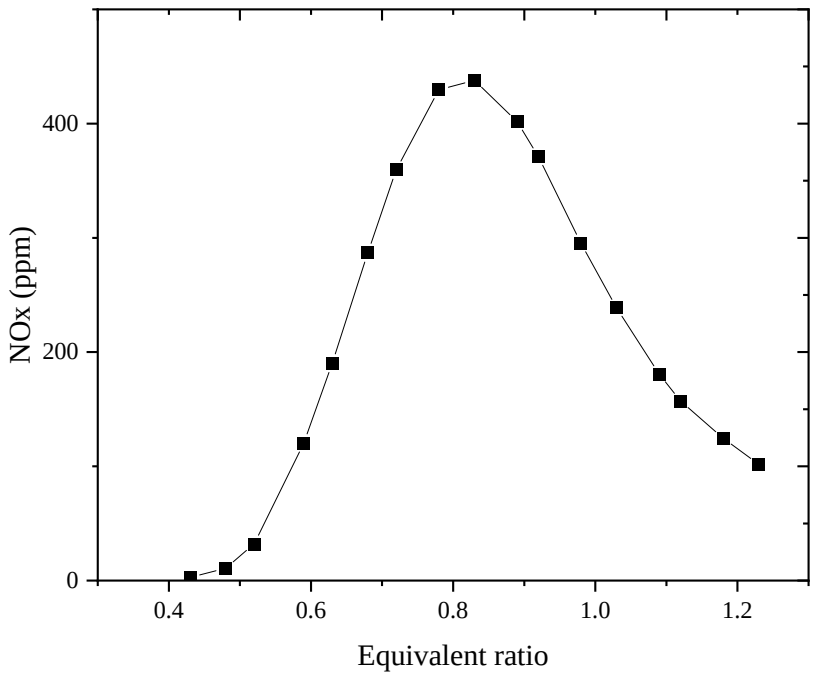

Figure 4.13 NOx emission with different equivalent ratio

Figure 4.18 illustrates the highest mean in-cylinder temperature under different equivalent ratio. It could be seen that: when φ is between the range of 0.33-0.5, the highest mean in-cylinder temperature increases from 1412K to 1972K and reaches the stagnation temperature of the formation of NOx, moreover, part of in-cylinder temperature could be higher than 1800K, therefore, NOx emission slightly increases with the increase of temperature, but generally, the effect of φ on NOx formation is small; when $\varphi = 0.52$, the highest in-cylinder temperature is 2109K, which is obviously higher than the stagnation temperature of NOx formation, and temperature contribution rate become extremely high; when φ increases from 0.48 to 0.52, NOx increases with temperature from 10.76ppm to 31.82ppm.

In the range of φ from 0.52 to 1.2, the highest mean in-cylinder temperature increases with the increase of φ, but NOx does not constantly increase, but reaches the highest point at $\varphi = 0.88$ and decreases with the increase of φ afterwards. The reason of this phenomenon is at the range of φ from 0.52 to 0.88, there's sufficient oxygen in the mixture, which makes temperature the most important factor that affects NOx formation, the higher in-cylinder temperature is, more NOx is produced and high temperature causes the formation of large amount of NOx. When $\varphi > 0.88$, with

the increase of φ, the highest mean in-cylinder temperature increases continuously, but the amount of air in the cylinder is becoming less and less, and there's less and less oxygen to bond with nitrogen. Moreover, due to the higher burning speed of hydrogen, the retention time of high temperature gas in the cylinder is shortened, less oxygen and shorter retention time restricted the formation of NOx together. When $\varphi > 1$, excess hydrogen will not only reduce some of NO, but also absorbs heat in the cylinder and decreases the in-cylinder temperature, lower in-cylinder temperature and insufficient oxygen restricts the formation of NOx simultaneously.

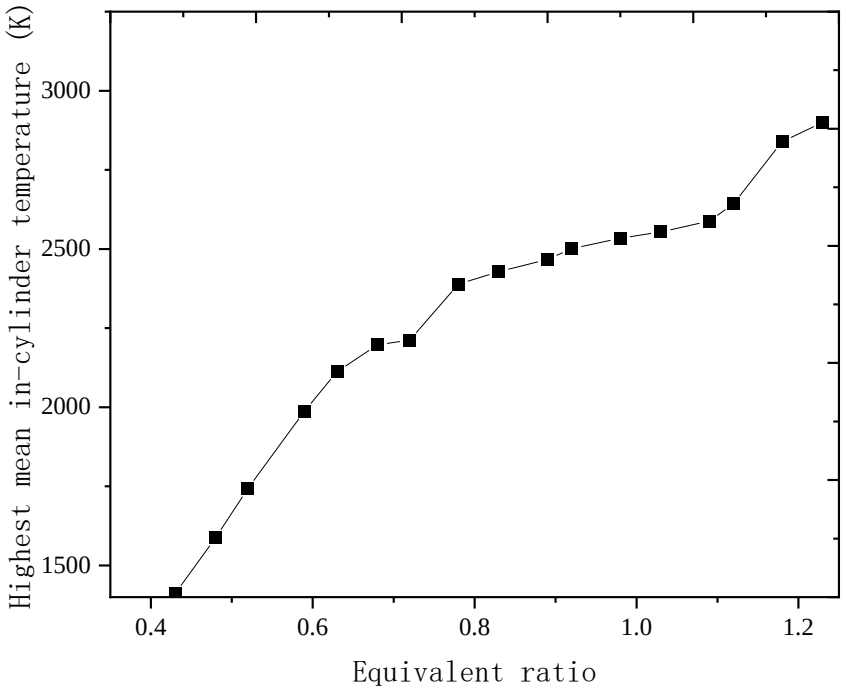

Figure 4.14 Highest mean in-cylinder temperature with equivalent ratio

4.5 Summary

This section presented a two-stroke and a four-stroke hydrogen free-piston engine WAVE model which were developed from two models that described in section 3, and one heat release analysis model was also built by MATLAB. The hydrogen FPE model was validated through four aspects: indicated power, NOx emission, heat release rate and cumulative heat release.

Through the analysis of NOx emission performance of each engine model, it could be concluded

that the free-piston engine possesses remarkable NOx reduction potential comparing with conventional spark-ignition engine. After calculation, the highest NOx reduction could reach 57.37% at the engine frequency of 6Hz. However, hydrogen, which is considered as a high-functioning environmental-friendly renewable fuel, produces more NOx than gasoline in the free-piston engine, though the range is relatively small especially at low engine frequency stage (1.4% at 5Hz and 10.97% at 11Hz). Above all, thanks to the fuel speciality of hydrogen, NOx is only emission that require consideration in hydrogen engines, though hydrogen produces more NOx than gasoline, the range is not considerable, in addition the engine characteristics of hydrogen free-piston engine are as good as those of gasoline free-piston engine.

NOx emission in hydrogen free-piston engine has been deeply investigated. The relationship between NOx formation and equivalent ratio obtained by simulation is: $\varphi = 0.5$ is the obvious demarcation point of the formation of NOx; when $\varphi < 0.5$, it doesn't affect NOx much; when $0.5 < \varphi < 0.88$, NOx increases with the increase of φ and reaches the highest point at $\varphi = 0.88$; when $0.88 < \varphi < 1.2$, NOx sharply decreases with the increasing φ.

Chapter 5. Single-cylinder Ethanol FPE modelling and simulation

The free-piston engine is known to be a type of non-crankshaft engine, which provides it the ability to adapt different fuel types. And it is already a common sense that applying biofuel such as ethanol and methanol on a free-piston engine has countless advantages facing this changing society and environmental requirements, however, no one has really done it practically yet.

An ethanol free-piston engine model built by Ricardo WAVE is presented in this chapter, and engine performance, efficiency and especially emission performance are investigated for the first time.

5.1 Theoretical review

Physical and organic chemistry characteristics indicate the quality of the fuel ignited in a car engine. Car engine ignition qualities, characteristics and emissions are characterized by them. Some characteristics related to diesel and ethanol combustion are compared in Table 5.1. The comparative characteristics of ethanol and motor gasoline are as follows [237,245]:

1. The heat of ethanol is about 1/3 times lower than that of motor gasoline. Therefore, in order to better achieve the same engine output power export, more and more ethanol must be used.

2. The oxygen content in ethanol is 34.7wt%, the ignition efficiency is high, and the ignition temperature is high. 3.

The heat of vaporization of ethanol is higher than that of motor gasoline. Therefore, more and more heat energy must be volatilized for pumping, and this heat is digested and absorbed in the natural environment of the main tank. This in turn increases the capacity and efficiency of the car engine.

4. The density of ethanol is slightly lower than that of automotive gasoline, so the quality of ethanol ejected by the volumetric high-pressure fuel pump is lower than that of automotive gasoline.

5. Ethanol has no nonaliphatic or polyaromatic hydrocarbons.

6. Lower ethanol C/H molecular ratio reduces heat transfer flame temperature.

7. The gasoline octane number (ON) of ethanol is higher than that of motor gasoline. The higher the octane rating of the gasoline, the more shrinkage it can afford before it hits. Too early gasoline and diesel ignition can damage the car engine, which is also a common condition for lower ON gasoline and diesel.

8. Ethanol has a higher layer than automotive gasoline. The flame spreads quickly, so that the entire ignition process is completed earlier, thereby improving the thermal efficiency of the car engine.

9. The use of ethanol and motor gasoline can reduce the cost of smelters because they can produce low-end motor gasoline with low fuel consumption.

Table 5.1 Comparison of gasoline and ethanol fuel properties [246]

Property	**Unit**	**Gasoline**	**Ethanol**
Chemical formula	-	$C_5 - C_{12}$	C_2H_5OH
Molecular weight	$kg/kmol$	114.15	46.07
C-fraction	Mass%	87.4	52.2
O-fraction	Mass%	0	34.7
H-fraction	Mass%	12.6	13.0
Stoichiometric air/fuel ratio	w/w	14.2-15.1	8.97
Higher heating value	MJ/kg	47.3	29.7
Lower heating value	MJ/kg	44.0	26.9

Vapor flammability limits	Vol%	0.6-8	3.5-15

5.1.1 Ethanol effects of engine parameters

5.1.1.1 Effect of compression ratio

In the free-piston engines, the position of the piston in the TDC is not determined by the fixed dimensions of a kinematic system. This means that the compression ratio can be varied. By means of the variation of this ratio, exhaust gas emissions can be reduced and the fuel consumption can be lowered. Furthermore, the variable compression ratio can be used in starting the engine under cold circumstances. These advantages however can only be gained if it is possible to control the compression ratio very precisely. In a free-piston engine, which has no geometrically defined compression ratio, this means that the compression energy (the energy that is delivered by the hydraulic system to the combustion gases during the compression stroke) has to be controlled.

Measurement data information from free piston engine tests show that the shrinking kinetic energy can be converted precisely with a deviation of 2% for positive and negative [247]. In this way, high labeling efficiency (50% or more) can be tightly coupled with low Nox emissions and low ash emissions. Manipulation of the engine compression ratio is also essential to reduce ignition noise. A high engine compression ratio results in a large increase in the working pressure in the engine's combustion chamber (i.e., a high rate of heat release). In addition to the high noise caused by a large increase in working pressure, it will continue to cause knocking and corrosion of the engine that ignites the piston, which in turn has a negative impact on the service life of the car engine or maintenance costs.

The reduction of kinetic energy lies in reducing the working pressure level in the accumulator, reducing the area of the plunger pump, the four-stroke of the piston and the time when the ignition or material is ejected. In a free piston engine, the total area of the piston four-stroke and plunger pump is constant and cannot be changed. This leaves two main parameters, namely reducing the working pressure of the accumulator and the injection time of gasoline and diesel, so as to clarify

the engine compression ratio. Figure 5.1 [247] shows the hazards of such primary parameters as they are precisely measured for free piston engines. It can be seen from the figure that the injection engine timing (gasoline and diesel injection gradually) does little harm to the engine compression ratio, while the harm to the working pressure in the accumulator is very obvious.

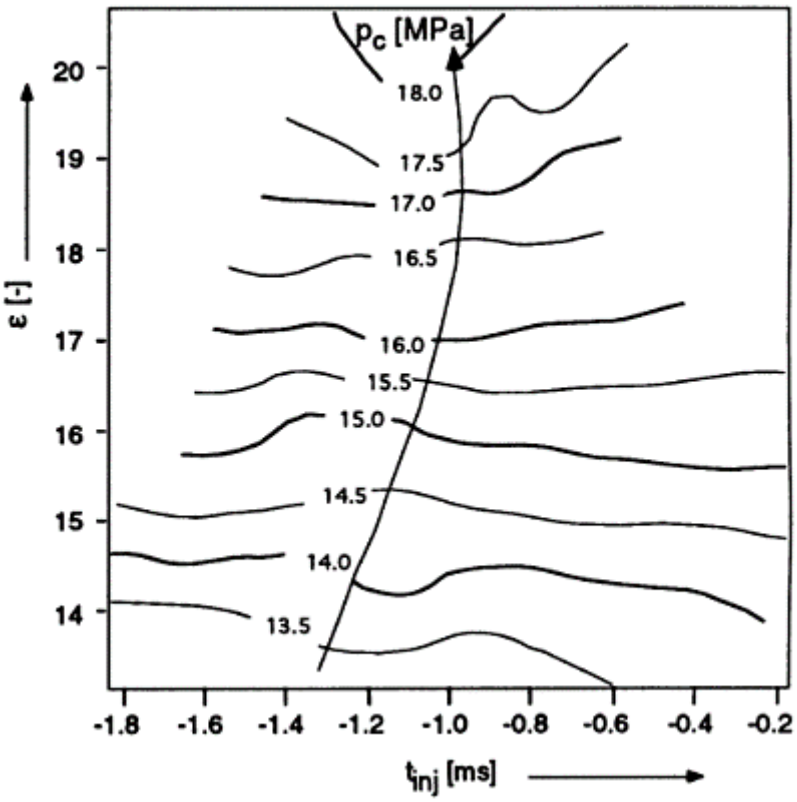

Figure 5.1 Relation between compression ratio accumulator pressure P_c, injection timing t_{inj} and the effective compression ratio ε [247]

A reasonable engine compression ratio is defined relative to the cylinder capacity when the outlet is closed. The injection engine timing is the injection gradually with respect to TDC moment by moment. The graph is constructed based on data detected on a free piston engine, where the hydraulic load remains stable (19.5Mpa). Figure 5.2 shows the detriment of reducing accumulator operating pressure and jetting engine timing to marked high efficiency and its Nox and soot emissions. The graph shows that high efficiency and low discharge can only be achieved by precise manipulation of accumulator working pressure and injection engine timing. Precision is increasingly critical as high efficiency and emission standards become more stringent (e.g., Figure 5.2 from Zone

I to Zone II).

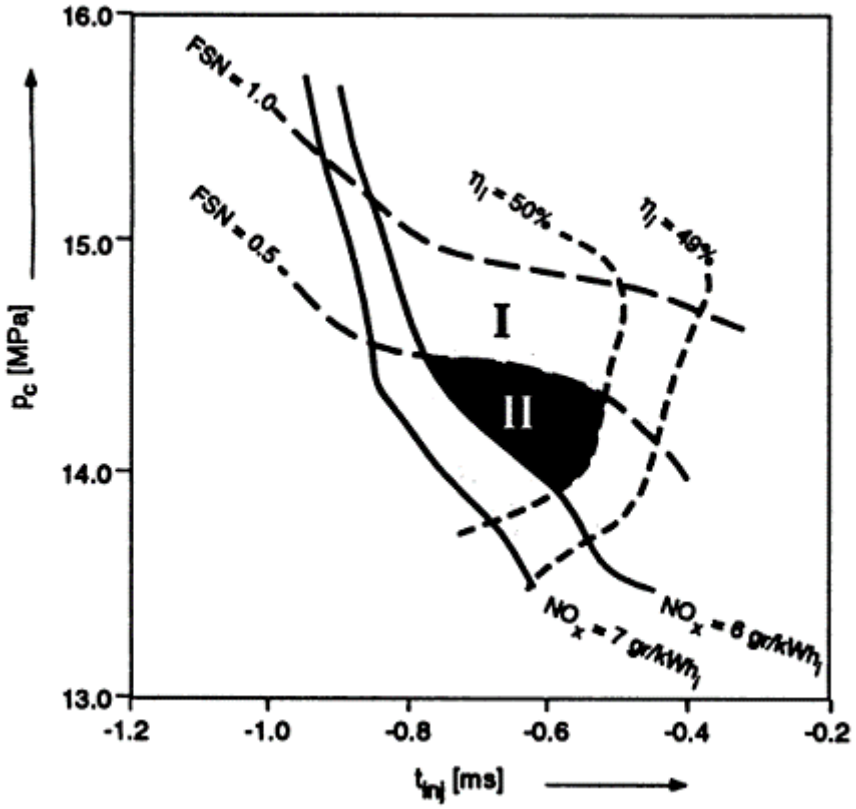

Figure 5.2 The influences of the compression accumulator pressure and the start of fuel injection [247]

A high engine compression ratio (CR) is available because it allows the car engine to extract a lot of kinetic energy from a given quality gas-fuel mixture because it is more thermally efficient. Higher CR allows the same ignition temperature to be achieved with less and less fuel, while giving longer expansion cycles. Engine knock is increased when low gasoline octane numbers are expected to be used in high engine compression ratio automotive engines [248]. The gasoline octane number of ethanol is 108.6, which is higher than that of motor gasoline. The high-octane number of gasolines gives a high engine compression ratio that is less prone to engine knock and improves knock resistance. It was also found that high CR can enhance the high efficiency of ethanol fuel blends, and thus, the gasoline and diesel plausibility impairments associated with the lower kinetic components of E85 can be reduced by about 20% [249]. Higher ignition temperatures result in higher NOx emissions, so forced air intakes can result in more NOx production. Especially at high vehicle engine loads, NOx emissions are boosted with an increase in CR. The relatively high ignition

speed and high temperature natural environment of the overall rich mixture ignition cause the NOx emission to increase with the increase of the CR of the automobile engine under long-term load [250].

To better boost engine output, Al-Baghdadi [251] applied a High Effective Engine Compression Ratio (HUCR), a variable compression ratio that is positively related to the percentage of ethanol in the mixture. The engine compression ratio was shifted from 8 to 9.25 as the percentage of ethanol increased from 0% to 30%. Although CR increased, NOx emissions decreased with increased ethanol. It was also observed that the thermal efficiency, power output, HC and CO emissions of ethanol with HUCR were better than motor gasoline with a stable CR of 8:1. Celik et al. [252] based on adding 50% ethanol to motor gasoline to increase engine compression ratio from 6:1 to 10:1. When operating with E50 at a high engine compression ratio (10:1), there is a 19% reduction in NOx compared to the E0 fuel with an engine compression ratio of 6:1. Since the calorific value of ethanol is lower than that of motor gasoline, NOx emissions are reduced here. Kirk et al. [253] using 0%, 50% and 85% ethanol to motor gasoline, engine compression ratios were 10:1 and 11:1. NOx consumption decreased with increasing ethanol usage. Motor gasoline with a CR of 10:1 also has higher NOx emissions than ethanol-motor gasoline blends with a CR of 11:1. The high latent heat of ethanol reduces the flame temperature, which in turn reduces NOx emissions. However, NOx emissions are likely to vary depending on the percentage of ethanol in the mix and the actual operating standards. Oxygen concentration, ignition temperature and ignition delay time are the basic parameters that endanger NOx emission. Nevertheless, for the same mixture, the NOx with higher CR is higher.

5.1.1.2 Effect of engine load

Automotive engine load plays a particularly critical role in NOx production. More and more fuel or a thicker mixture must be used to increase vehicle engine load, which results in higher master cylinder temperatures and higher NOx production. However, the flame rate of the feed is a major factor in complete ignition under rich mix conditions and high vehicle engine loads.

Melo et al. used a 1.4 L dexterity to feed an automotive engine [254] tested 0-100% water content ethanol and motor gasoline under 2 different loads. At low load (60 Nm), NOx emissions decreased

with the addition of ethanol. However, at the same efficiency and more load (105 Nm), NOx increases with the addition of ethanol. They stated that the higher ignition rate of ethanol compared to fuel oil was due to the increase in NOx emissions when ethanol was used under prolonged loads. A higher flame rate favors complete ignition. It can also be seen that the CO energy saving and emission reduction of adding ethanol under long-term load is higher than that under low load. Keskin and Guru [255] also found that the addition of ethanol resulted in more NOx excretion under prolonged loads. They did experiment with 0%, 4%, 8%, 12%, 16% and 20% ethanol in motor gasoline at different loads (800, 1600, 2400 kW). At lower loads, the NOx consumption is the same for all mixtures. However, the NOx consumption of the ethanol blend was higher at higher loads.

Gomez et al. [256] worked on the practical operation of ethanol blends up to E100 at prolonged loads up to 30 bar IMEP. At relatively low loads, the NOx consumption of the high ethanol content mixture was lower. They stated that ethanol slightly lowered the maximum temperature, which in turn lowered NOx at lower loads. However, at relatively higher loads, NOx emissions are the same for all blends, with similar valley temperatures due to the high ignition rate of the ethanol fuel. Pang et al. did not observe significant shifts in NOx emissions at different vehicle engine loads (3-161 Nm torque) [256], when they compared motor gasoline with 10% ethanol blended with motor gasoline. Nevertheless, for lower calorific value, the fuel consumption of ethanol mixture is higher.

5.1.1.3 Effect of equivalence ratio

The organic stoichiometric air-fuel ratio of motor gasoline is 1.6 times that of ethanol. Because the amount of air intake and supply is constant under a certain electronic throttle opening degree and a certain vehicle speed Base car gasoline for skew utility is higher. However, the skew in the feed/gas ratio results in a sufficiently low flame temperature to reduce NOx and other exhaust emissions [258]. Theoretically, the most flammable flames come from the gas/gas mixtures verified by organic stoichiometry; nevertheless, NOx reaches the highest value when the gas/gas ratio is slightly lower. The skew in the fuel/gas ratio results in a sufficiently low flame temperature to reduce NOx and other exhaust emissions.

Najafi et al. [258] reported that the oxygen content of ethanol could lead to a more dilute practical effect under the premise that the material was rich and colorful. The actual effect of this leaner shifts

the air-fuel ratio to an organic stoichiometric calibration standard and facilitates ignition, which in turn increases NOx emissions. Xie et al. [259] also found higher NOx consumption for organic stoichiometric air-fuel ratios due to high ignition temperatures due to full ignition. However, when the equivalence ratio is less than 1.0, the direct effect of adding ethanol on NOx emission is negligible. The rationale they got was that NOx emissions were due to car engine operating criteria rather than ethanol components. Using six cylinders to examine a car engine, Al-Farayedhi [260] found that applying car gasoline, E10, E15 and E20 as energy sources resulted in a larger NOx emission at an equivalence ratio of 0.9. NOx emissions increased with increasing ethanol concentration in the mixture, except when the equivalence ratio was 0.8. The ease of use and high ignition temperature of the o2 are the reasons for this NOx emission. However, for very dilute mixed substances, the NOx concentration value decreases with the increase of ethanol content.

Ze CBM et al. [262] studied the hazard of industrial waste gas with different equivalence ratios (λ=0.83–1.25). They found that differences in equivalence ratios were less likely to result in relatively large shifts in NOx consumption. NOx varies from 15% to 30% for different λ values. Reduced CO consumption at organic stoichiometry and leaner standards. Plus oxygenates are more critical than the percentage of o2 in the feed, which means less carbon dioxide emissions due to higher oxygen concentrations. Nevertheless, for the E5 material, HC emission is almost irrelevant to λ. For E20, there are two regions: 9-28% reduction in HC consumption at lean standards and 46-48% reduction in HC consumption at organic stoichiometric and rich standards.

Different engine compression ratios and their hazards to free piston engines have been analyzed and described in detail in the following sections.

5.1.1.4 Effect of engine frequency (speed)

Vehicle speed can also harm NOx emissions. Some authors [261,259] reported that with the ignition of a large amount of fuel, NOx will increase with the increase of the car speed, resulting in high master cylinder temperature at fast speeds. Very few creators [253,264] also report low NOx emissions due to less available time for fast ignition.

At higher velocities, shorter ignition times can be used to ignite larger quantities of fuel compared

to lower velocities. Flame rate is a major factor in igniting in a short period of time. Because ethanol has a higher ignition rate than motor gasoline, it favours fast ignition, resulting in higher nitrogen oxide consumption in ethanol. Costa and Sodré [263] found that 100% water content ethanol had higher NOx emissions under fast conditions than E22 because of its higher ethanol content than E22. Nevertheless, in low gears (2500–3000 rpm), there is no significant shift in this material. Koch et al. [252] The mixed results of ethanol were found to be different at a rapid rate. They found that in the speed range of 1500-5000 rpm, the E0, E50 and E85 increased NOx by 42%, 41% and 11% respectively. Compared with E0, the increase in NOx emission with rate is relatively lower for E85. The lower calorific value coupled with the shorter ignition time may be the reason for the lower NOx of ethanol under fast conditions [246].

This scientific study defines the car engine load in frequency, picking the 5-11Hz range. The investigation of ethanol fuel frequency for each vehicle engine is detailed in Section 5.2.

5.1.2 Ethanol-gasoline blend

Scientific researchers have already tested ethanol-vehicle gasoline blends from 5 vol% up to 100 vol% in SI car engines, i.e. pure ethanol. Table 5.2 summarizes the physical properties of different ethanol-motor gasoline compositions. The results presented are based on different test standards performed by scientific researchers. As can be seen from Table 5.2, the addition of ethanol to motor gasoline simultaneously increases gasoline octane number, relative density, and latent heat, and reduces the calorific value of the ethanol-motor gasoline composition. Numerous scientific studies have long been carried out to clarify the harm of this change to the emission characteristics, especially because of the conversion of the ethanol composition to the harm of NOx emission [246].

Table 5.2 Properties of different ethanol–gasoline blended fuels [246]

Property	E0	E5	E10	E15	E20	E25	E30	E40	E50	E60	E85
Density (kg/m^3)	757.5	759.1	760.8	776	764.5	775	768.2	780.6	751	789.5	
RVP (kPa)	53.7	59.3	59.6	58.8	58.3		56.8	63	45.3	57.4	37.85
RON	95.4	96.7	98.1	98.5	100.7	100	102.4	90.9	101.2	92.7	101.7

Sulfur(wt%)	0.0061	0.0059	0.0055	0.0063	0.0049	0.0246	0.0045	0.026	<0.001	0.032	<0.001
Distillation temperature (°C)											
(a) Initial boiling point	35.5–38.8	36.5	37.8	37.9	36.7–38.6		37.2–39.5	39.6	328.3		
(b) 10vol%	54.5–56.1	49.7	50.8–52.9	51.7	51.3–52.8	58.1	52.1–54.8	53.4			73.9
(c) 50vol%	94.4–109.6	88	71.1–95.8	72.6	70.3–73.8	71.7	72.4–74.6	72.5	521		78.0
(d) 90vol%	167.3–206.3	167.7	157–166.4	165.3	165.2–163		154.6–159.3	152.7	547		78.7
(e) End point	197.0	202.5	197.5–208.4	198.1	198.6–203.6	177.9	198.3–205.1	204.1			79.9
Heating value (MJ/kg)	42.58–42.7	40.55–41.78	39.79–41	41.61	38.98–39.5	38.2	36.32–37.8	33.34–36.2	33.34	26.74	29.2

where RVP is the Reid vapor pressure and RON is the scientific research gasoline octane number. Table 5.2 is regarded as a guideline for the ethanol-motor gasoline blend settings in Ricardo WAVE. Much literature shows that NOx consumption decreases with increasing ethanol content. Turner et al. [245] A scientific study investigated the NOx emissions from an ethanol-motor gasoline composition applied to an ethanol-motor gasoline combination from a vehicle engine with immediate flame ignition (DISI) at 1500 rpm and 3.4 bar indicated mean reasonable working pressure (IMEP). When the ethanol fraction in the mixture was raised to 85%, NOx emissions

decreased. They attribute this reduction to a reduction in flame temperature, which is confirmed by a reduction in exhaust pipe temperature. The NOx level of pure ethanol then increased slightly, due to earlier ignition, the master cylinder operating pressure and temperature were higher compared to 85% ethanol. Here, the larger master tank working pressure was reduced by applying ethanol blends up to 85%, and pure ethanol was subsequently boosted. Bielaczyc et al. [241] NOx reductions were also found for 10-85% ethanol mixtures. They assessed the probability of using a gasoline-ethanol blend in a contemporary Euro 4 car without much modification to the car's engine. A good linear fit between the NOx emissions from the automotive engine and the ethanol content of the mixed material was found in the range of 10-85%. Scientific studies have investigated DISI automotive engines with 25%, 50%, and 85% ethanol-motor gasoline compositions. They found that HC consumption increased and NOx consumption decreased with an increase in the percentage of ethanol in the mix due to a decrease in the master tank maximum temperature due to ignition delay time [244].

Joann Molt et al. [265] The NOx emissions of different mixtures were studied for a speed ratio of 2000 rpm at electronic full throttle (WOT). As can be seen from Figure 5.3, NOx emissions decreased with increasing ethanol concentration. Because the heat of vaporization of ethanol is higher than that of fuel oil, the ignition temperature of the mixture decreases. In the case of HC discharge, a certain concentration value is achieved. In ethanol, the HC expulsion decreased, reflecting a trend towards complete ignition due to the oxygen content in the ethanol. Nevertheless, the higher concentration of ethanol in motor gasoline will reduce the flame temperature, thereby increasing the HC emission. It can be seen that E40 is a better choice for reducing HC emission, and E80 is suitable for reducing NOx emission.

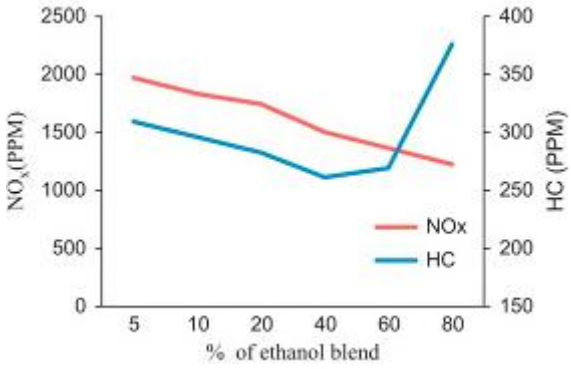

Figure 5.3 Correlation of NOx and HC emission with ethanol percentage at 2000 rpm [265]

In a four-cylinder multi-port number injection system hardware car engine, Canakci et al. [238] found that NOx consumption decreased with an increase in the percentage of ethanol in the mixture. With the use of alcohol in automotive gasoline, because the heat of vaporization is high, the calorific value is low, the ignition temperature is reduced, and NOx emissions are reduced. When comparing industrial exhaust gas from motor gasoline to pure ethanol, Balki et al. [265] found that the NOx consumption of ethanol was lower than that of motor gasoline. They attribute this reduction to the higher heat of vaporization of ethanol, which in turn reduces ignition temperature. Nevertheless, the oxygen content ethanol fuel improves the combustion efficiency. Compared with the fuel oil, the CO2 consumption of ethanol is lower, and the HC and CO emissions are higher. Yao et al. applied a lower percentage of ethanol [262] found similar results. They attribute this to the lower flame temperature due to the higher heat of vaporization of ethanol.

With full consideration of the DISI module, Storey et al. [266] analyzed the hazard of ethanol addition and concluded that NOx emissions decreased with increasing ethanol concentration because of the lower power density of the ethanol mixture. Lin et al. [267] Experiments were carried out on a small engine generator set to observe the hazards of ethanol-motor gasoline blends on industrial exhaust gases and rates. The ethanol-motor gasoline blend significantly reduced the average NOx consumption of E3, E6 and E9 feedstocks by approximately 35%, 86% and 77%, respectively. The best results were obtained with E6 at the exhaust emission level and E9 at the automotive engine characteristic level.

Wu et al. [241] stated that NOx emissions decreased with an increase in the H/C molecular ratio in

the feed. It can be seen from Table 5.2 that the H/C molecular ratio of ethanol is higher than that of motor gasoline. In his findings, the NOx consumption of ethanol was lower than that of motor gasoline. Brewster et al. [268] found a slight reduction in NOx with ethanol and motor gasoline compared to pure motor gasoline.

Applied Motorcycle Engine designed by Chen et al. [248], a scientific study investigated the hazard to emissions from ethanol-motor gasoline blends (E3, E5, E10, E15, E20, E25, and E30). With the increase of ethanol concentration, the particle size of the accumulation mode decreased. The atmospheric aerosol number concentration value decreased with the increase of ethanol concentration, resulting in more and more complete ignition. Thus, CO and NOx production decreased with increasing ethanol concentration. Compared with the high ethanol concentration mixture (>E20), the low ethanol concentration mixture (<E15) has a higher energy saving and emission reduction rate. Applying E3 data, Yang et al. [269] also found a 5.22% increase in NOx compared to fuel.

In turn, some scientific researchers have found an increase in NOx emissions. Schifter et al. applied a two-cylinder SI automotive engine [270]. A scientific study investigated the effects of the application of automotive gasoline-ethanol primary blends (0-20% ethanol) on automotive engine characteristics and industrial exhaust gas hazards. It can be seen that the addition of ethanol to motor gasoline increases NOx emissions compared to fuel. After adding ethanol, compared with fuel oil, the calorific value released by ethanol is higher, so the NOx consumption is higher. However, when ethanol is added to the mixture, the HC consumption will increase due to the shorter ignition delay time compared to pure motor gasoline. Najafi et al. studied the service performance and pollutant emissions of four-stroke SI automotive engines operating with 0%, 5%, 10%, 15%, and 20% ethanol-motor gasoline blends [258]. They also found that as the percentage of ethanol increased, the NOx concentration values were higher, as shown in Figure 5.4 below. Another key factor for this type of improvement is that the oxygen content in the ethanol blend energy increases the oxygen-to-fuel ratio in the rich and colorful regions of the natural material. The most important basic parameter that affects the NOx concentration value is the relative air-fuel ratio. With the improvement of the ethanol content in the mixed energy, the specific air-fuel ratio is close to the organic stoichiometric verification ratio, so the ignition is more and more thorough. This type of

outright ignition increases master cylinder temperature and its NOx emissions, while HC emissions decrease.

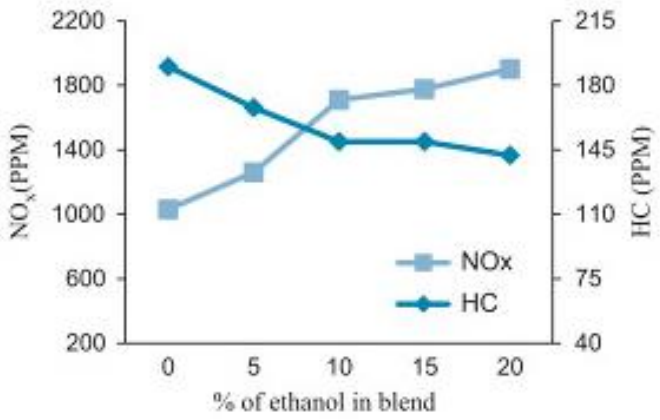

Figure 5.4 Correlation of NOx and HC with the percentage of ethanol at 3500 rpm [258]

Zhuang et al. [271] Changed the ethanol/motor gasoline power ratio from 0% to 60.1%. NOx emissions increased with the addition of ethanol to motor gasoline up to 24.3%, and then decreased with an increase in the percentage of ethanol. With regard to raising NOx, they reported that ethanol improved ignition in the hydraulic cylinder, causing the temperature inside the cylinder to rise. In the case of NOx reduction, they stated that the higher percentage of ethanol in motor gasoline reduces master cylinder temperature. They attribute this reduction to two factors. One is the high latent heat of ethanol fuel, which reduces the master cylinder temperature during gasification. Another factor is that there are more triatomic molecules in the ethanol fuel ignited material than in motor gasoline. The more triatomic molecules are created, the higher the thermal conductivity of the vapor and the lower the temperature of the ignited vapor. Nevertheless, low master cylinder temperatures can also cause unignited combustion substances to rise.

5.1.3 Formation of NOx

NOx is a mixture of such compounds: nitric oxide (NO), nitrogen dioxide (NO_2), nitrous oxide (N_2O), dinitrogen trioxide (N_2O_3), dinitrogen tetroxide (N_2O_4), and dinitrogen pentoxide (N_2O_5) [272]. Among them, nitric oxide (NO) and nitrogen dioxide (NO_2) are most prominent [273]. The other five nitrogen oxides are known to exist, but in very small quantities. Nitric oxide is a colorless, odorless gas. Its ambient concentration is usually far less than 0.5 ppm. Nitrogen dioxide is a

corrosive, toxic, and reddish-brown gas. It is quite visible in sufficient amounts [274][275]. Oxidation of nitrogen molecules at high temperature inside the cylinder is the cause of NOx formation as a product [276]. The pathways of formation of oxides of nitrogen such as Thermal, Prompt, Fuel NOx and N_2O intermediate mechanisms are discussed here [248].

5.1.3.1 Thermal NOx

During combustion, at temperatures above 1800 K, atmospheric nitrogen reacts with oxygen through a series of chemical steps known as the Zeldovich mechanism [277]. This mechanism of thermal NOx formation is believed to be the predominant contributor of total NOx [278]. The equations 3.21 to 3.23 are the basic kinetic equations for thermal NOx formation.

$$O + N_2 \leftrightarrow NO + N$$

$$N + O_2 \leftrightarrow NO + O$$

$$N + OH \leftrightarrow NO + H$$

The first step determines the NOx formation as it requires high temperatures to proceed due to its high activation energy (314 KJ/mole). NO production by thermal mechanism proceeds at a slower rate than the oxidation of hydrocarbons. The NO formation rate can be written using equation (5.1) [279].

$$\frac{d[NO]}{dt} = \kappa e^{-K/T}[N_2][O_2]^{\frac{1}{2}}t^{-\frac{1}{2}} \quad (5.1)$$

Where k and K is reaction constants, t is time and T is absolute temperature [280]. Equation (5.1) represents a strong dependence of NO formation rate on temperature. High temperatures, high oxygen concentrations, and longer residence time results in high NO formation rate.

5.1.3.2 Prompt NOx

Fenimore [281] was the first to identify the existence of a second regime responsible for NOx production and called it "rapid NOx". In the ignition stage of nitrogen compound oil, in the laminar-flow premixed flame zone, some NOx is produced rapidly before the thermal NOx is generated, which is called prompt NOx [282]. There is ample evidence that prompt NOx production is

substantial in some ignition environments; for example, at ultra-low temperatures, rich oil levels and short dwell times. Alert NOx is more widespread in heavy fires. The specific production involves a series of intricate reactions and many possible intermediate chemicals. Generally, at ultra-low temperature (below 750°C) and oil-rich standard, nitrogen molecules react with hydrocarbon radicals to convert into amine or sulfonic acid-based chemicals. Later, this nitrogen highlight reacts with nitrogen in the air and converts it into NO. Prompt NOx is generally generated by the following reactions (5.2) - (5.6).

$$CH + N_2 \leftrightarrow HCN + N \tag{5.2}$$

$$CH_2 + N_2 \leftrightarrow HCN + NH \tag{5.3}$$

$$N + 0_2 \leftrightarrow NO + O \tag{5.4}$$

$$HCN + OH \leftrightarrow CN + H_2O \tag{5.5}$$

$$CN + O_2 \leftrightarrow NO + CO \tag{5.6}$$

Here, CH and CH2 are key enablers for timely NOx generation. Prompt NOx is more sensitive to natural organic chemistry than heat capacity NOx because of its dependence on NOx debris. The amount of HCN increases with the increase of the concentration of hydrocarbon oxygen radicals, and increases with the increase of the dosage ratio. With the increase of the equivalence ratio, the rapid NOx production increased, then reached the highest value and decreased due to hypoxia. In contrast to thermal NOx production, prompt NOx contributes less to the overall ignition system hardware. Nevertheless, in the scientific research of ignition model, the total NOx is underestimated without considering the principle of rapid NOx [283].

5.1.3.3 Intermediate N_2O

The NOx formation by this pathway is another essential mechanism in a combustion process under high pressure and lean air–fuel ratio or low temperature condition compared to Fenimore NO, and a minor contribution to the formation of NOx related to the thermal NO mechanism [284]. Three steps of this NOx formation mechanism are shown in Equations (5.7) (5.8) (5.9).

$$O + N_2 + M \leftrightarrow N_2O + M \tag{5.7}$$

$$H + N_2O \leftrightarrow NO + NH \tag{5.8}$$

$$O + N_2O \leftrightarrow NO + NO \tag{5.9}$$

Here, M is a general third body that is required to complete this reaction [276]. Reaction rates strongly depend on O, OH and H radial concentrations, which makes the mechanism favored for oxygen-rich conditions or lean condition [285].

5.1.3.4 Fuel NOx

When nitrogen-based chemicals are oxidized to NOx during the incineration process, NOx is generated [286]. Fuel NOx increases with the increase of nitrogen content in the fuel. Among other things, it is related to air oxidation of nitrogen oxides as well as chemical kinetics. Nevertheless, the nitrogen content in gasoline or ethanol fuel is extremely low; therefore, the production of NOx can be ignored.

5.2 Ethanol free-piston engine modelling and simulation implementation

5.2.1 Base parameters setting

On the basis of Chapter 3 and Chapter 4, the whole modelling process of one-dimensional simulation WAVE model of the FPE has been fully described, and it is similar that applying ethanol as fuel taking the place of gasoline with applying hydrogen as fuel. Parameters such as compression ratio, air/fuel ratio (equivalence ratio), valve timing, piston motion, etc., were amended on the basis of the gasoline FPE model in Chapter 3.

Similar as the method of changing fuel from gasoline to hydrogen, ethanol is chosen as the substitution fuel running in this free-piston engine model as shown in Figure 5.5.

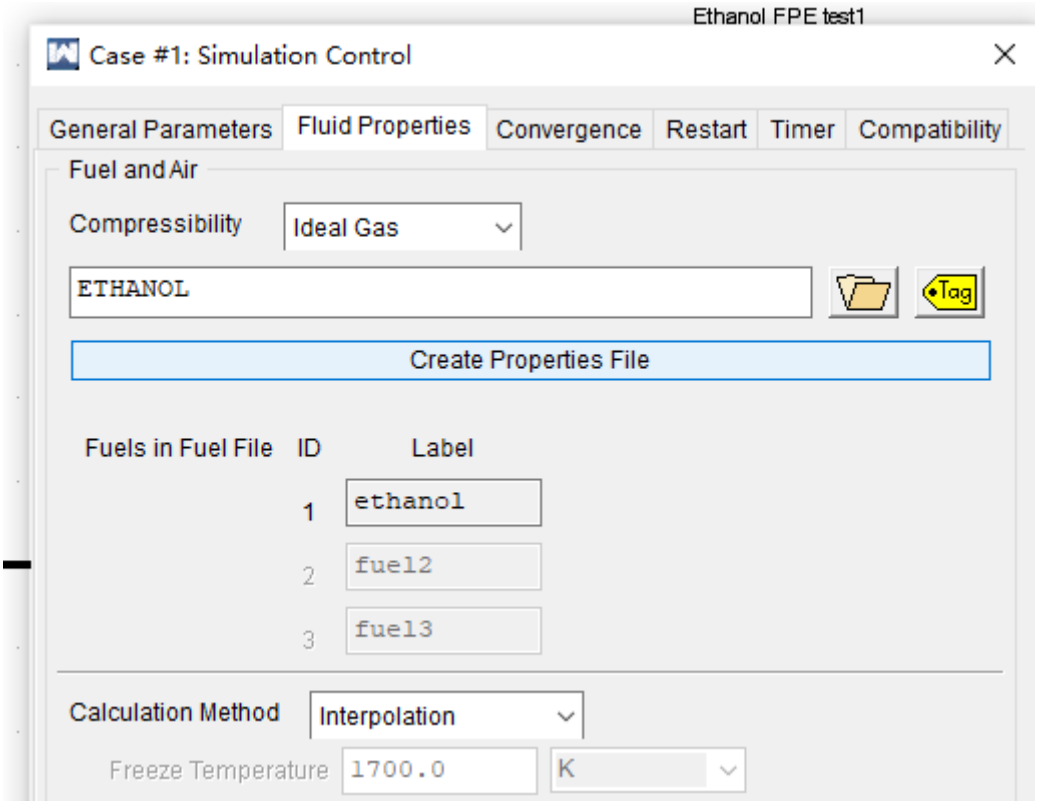

Figure 5.5 Fuel panel in Ricardo WAVE

The simulation of the free-piston engine heat release in combustion process is one of the factors with the highest degree of uncertainty in this model. The piston motion of the free-piston engines differs significantly from that of conventional engines, and very little research results has been reported on how this influences the combustion process [124]. According to previous research, the energy released in the combustion is modelled using a modified Wiebe function. Generally, the Wiebe function is related to the crankshaft angle, however this is not suitable for a linear engine. Therefore, a time-based Wiebe function is used to express the mass fraction burned in the combustion process as:

$$\lambda = 1 - \exp\left(-a\left(\frac{t - t_s}{C_d}\right)^{b+1}\right) \tag{5.10}$$

$$\frac{dQ_c}{dt} = Q_{in}\frac{d\lambda(t)}{dt} \tag{5.11}$$

Where λ is the fuel mass fraction burned; a and b are shape factors in Wiebe function, with the fitting value of 5 and 2 respectively; C_d is the combustion duration with a constant value of 5 ms; t_s is the time at which the combustion process starts. Q_{in} is the overall heat input for each cylinder

in one running cycle. Combing Equations (5.10) and (5.11)., we have:

$$\frac{dQ_c}{dt} = a\frac{b+1}{C_d}\left(\frac{t-t_s^b}{C_d}\right)\exp\left(-a\left(\frac{t-t_s}{C_d}\right)^{b+1}\right)Q_{in} \tag{5.12}$$

Eq. is used to predict the thermal energy delivered to the gas and the resulting pressure in the cylinder.

Figure 5.6 and Figure 5.7 show a MATLAB/Simulink simulation model that used to obtain the suitable piston motion data for the Ethanol free-piston engine model.

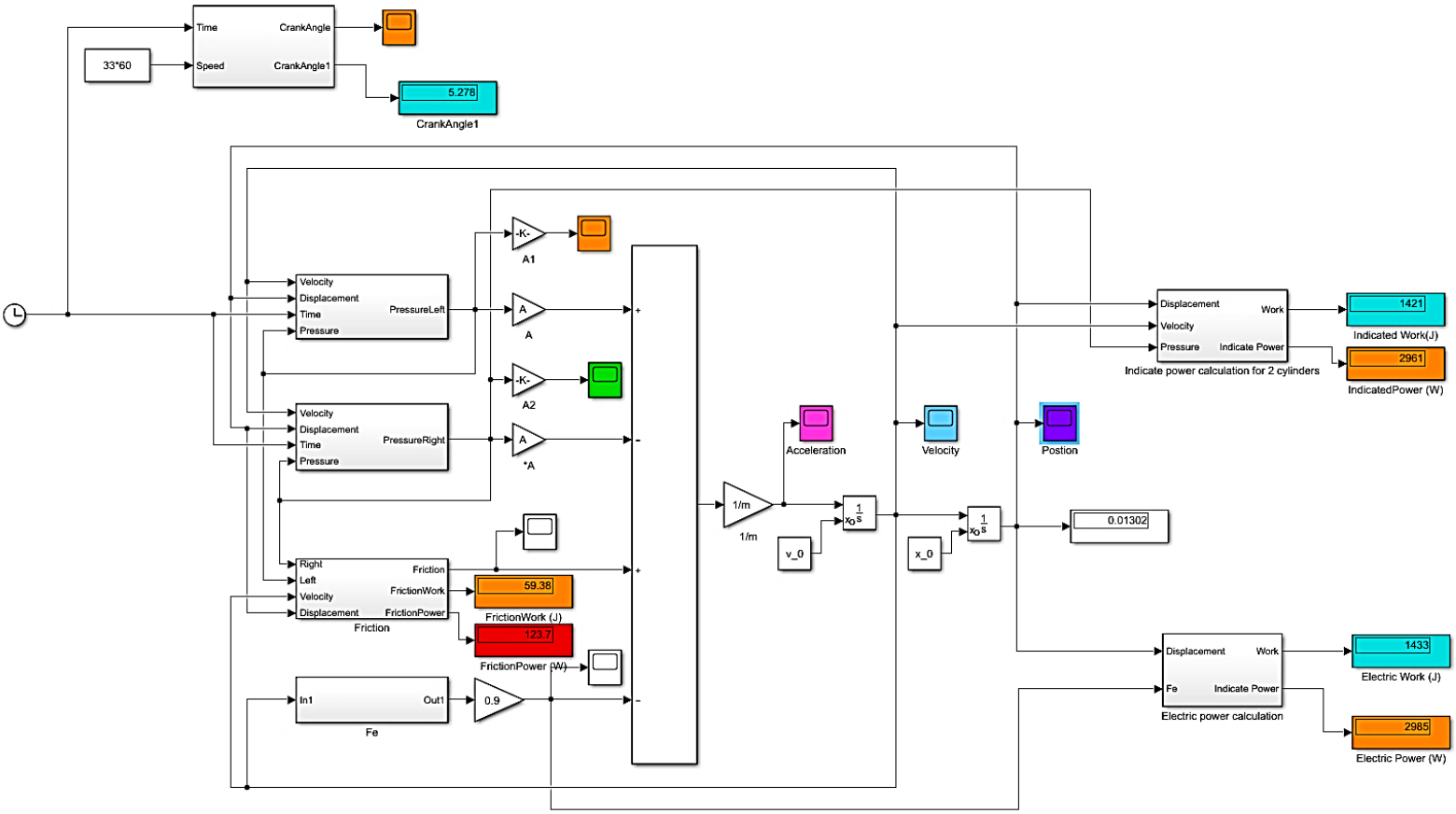

Figure 5.6 Simulink model for the ethanol FPE model

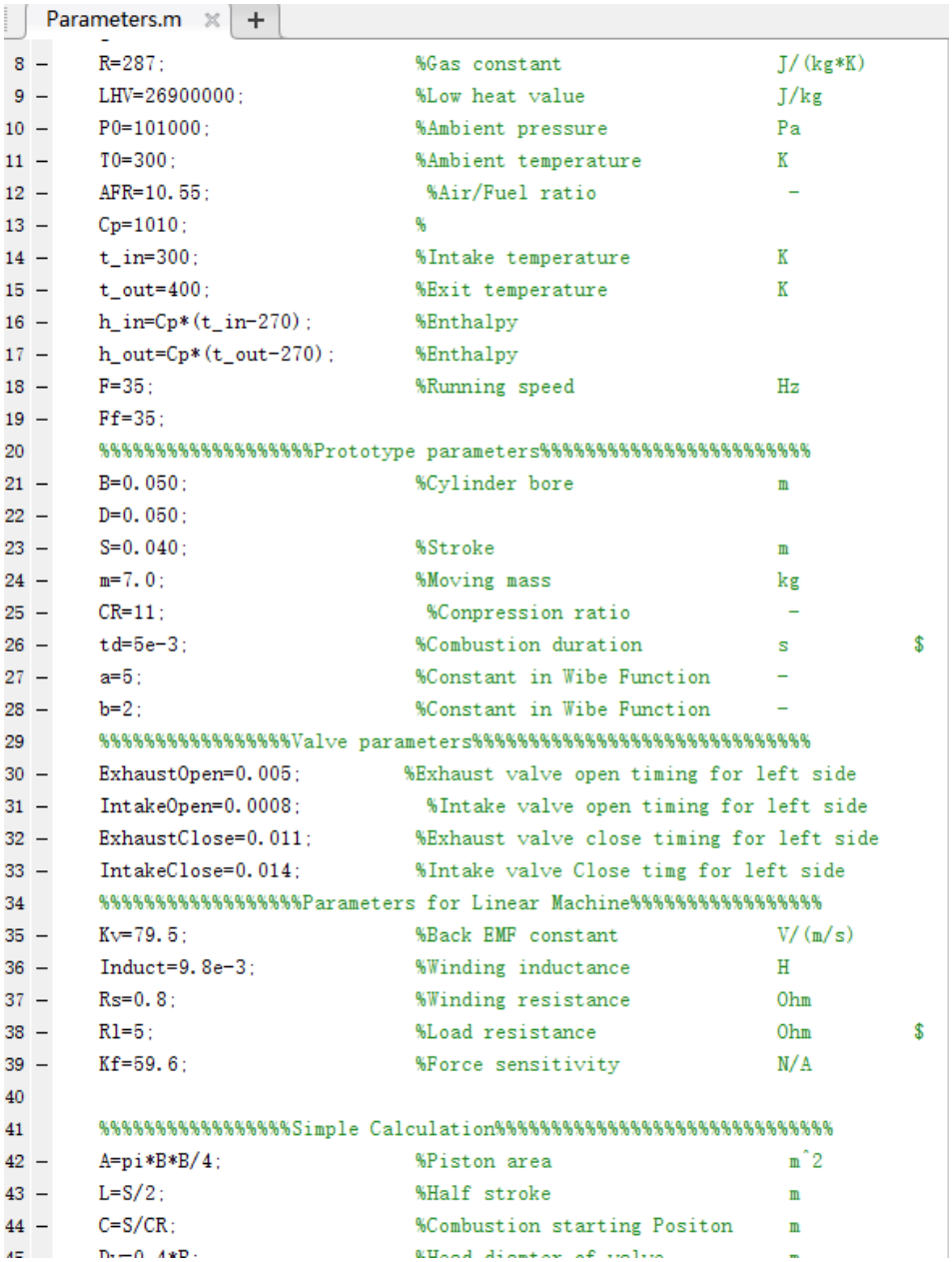

Parameters.m

```
R=287;                          %Gas constant                   J/(kg*K)
LHV=26900000;                   %Low heat value                 J/kg
P0=101000;                      %Ambient pressure               Pa
T0=300;                         %Ambient temperature            K
AFR=10.55;                       %Air/Fuel ratio                 -
Cp=1010;                        %
t_in=300;                       %Intake temperature             K
t_out=400;                      %Exit temperature               K
h_in=Cp*(t_in-270);             %Enthalpy
h_out=Cp*(t_out-270);           %Enthalpy
F=35;                           %Running speed                  Hz
Ff=35;
%%%%%%%%%%%%%%%%%%Prototype parameters%%%%%%%%%%%%%%%%%%%%%%%
B=0.050;                        %Cylinder bore                  m
D=0.050;
S=0.040;                        %Stroke                         m
m=7.0;                          %Moving mass                    kg
CR=11;                           %Conpression ratio              -
td=6e-3;                        %Combustion duration            s           $
a=5;                            %Constant in Wibe Function      -
b=2;                            %Constant in Wibe Function      -
%%%%%%%%%%%%%%%%%Valve parameters%%%%%%%%%%%%%%%%%%%%%%%%%%%%
ExhaustOpen=0.005;             %Exhaust valve open timing for left side
IntakeOpen=0.0008;              %Intake valve open timing for left side
ExhaustClose=0.011;             %Exhaust valve close timing for left side
IntakeClose=0.014;              %Intake valve Close timg for left side
%%%%%%%%%%%%%%%%%Parameters for Linear Machine%%%%%%%%%%%%%%%%%
Kv=79.5;                        %Back EMF constant              V/(m/s)
Induct=9.8e-3;                  %Winding inductance             H
Rs=0.8;                         %Winding resistance             Ohm
Rl=5;                           %Load resistance                Ohm         $
Kf=69.6;                        %Force sensitivity              N/A

%%%%%%%%%%%%%%%%%Simple Calculation%%%%%%%%%%%%%%%%%%%%%%%%%%%
A=pi*B*B/4;                     %Piston area                     m^2
L=S/2;                          %Half stroke                    m
C=S/CR;                         %Combustion starting Positon    m
D=0.4*B;                        %Head diamter of valve          m
```

Figure 5.7 Parameters in MATLAB

According to the above theories, the compression ratio and equivalence ratio were determined, and the lower heating value is also amended in Table 5.1. Figure 5.8 shows the piston motion data obtained from this Simulink model applied into the Ricardo WAVE model.

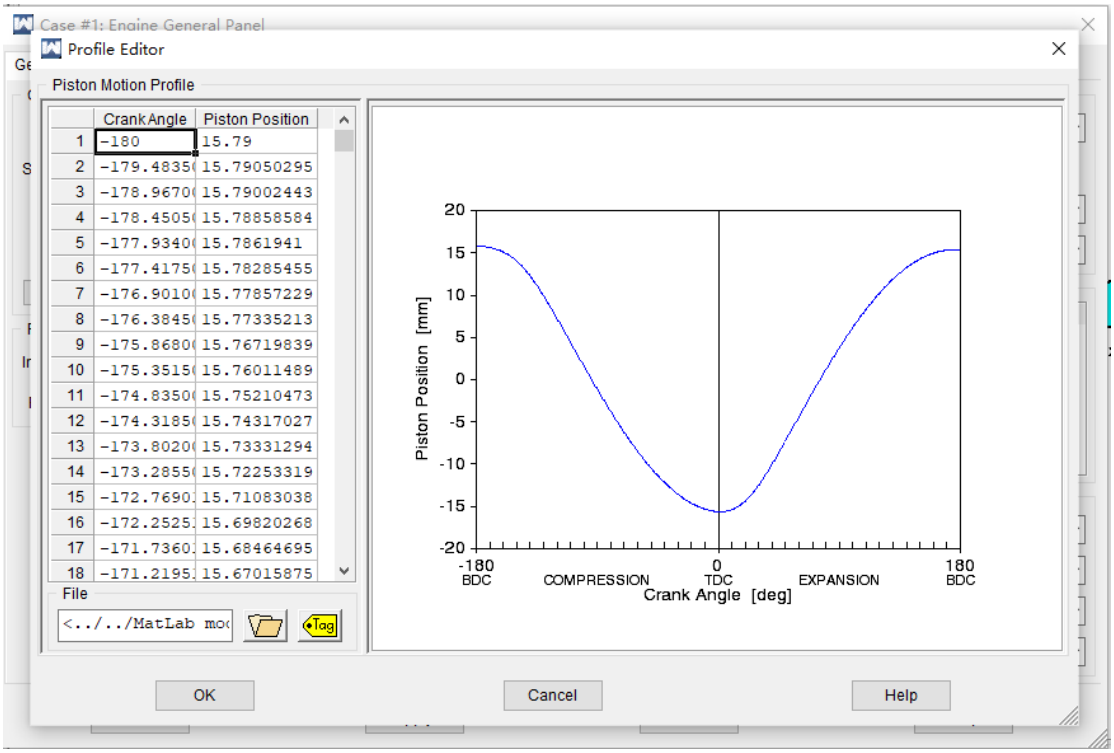

Figure 5.8 Piston motion pre-set in Ricardo WAVE

With the amendment of the compression ratio, equivalence ratio (air/fuel ratio in Ricardo WAVE) and piston motion, the basic scheme of this two-stroke ethanol-gasoline blend simulation model has been successfully built. And the final target await is the valve timing optimisation.

5.2.2 Parametric study

The procedure for valves timing optimisation in the two-stroke ethanol-gasoline blend free-piston engine was done via parametric study using experiments panel shown in Figure 5.9 and this experimental setting was implemented under the fuel choose of pure ethanol. Performing an experiment delivers a matrix of outputs that can be used to show what effect one or more input parameters will have on one or more of WAVE's predicted outputs. Same with the method used and described in section 3, the impact of each variable on the engine performance can be observed quickly without the need of actual engine performance testing.

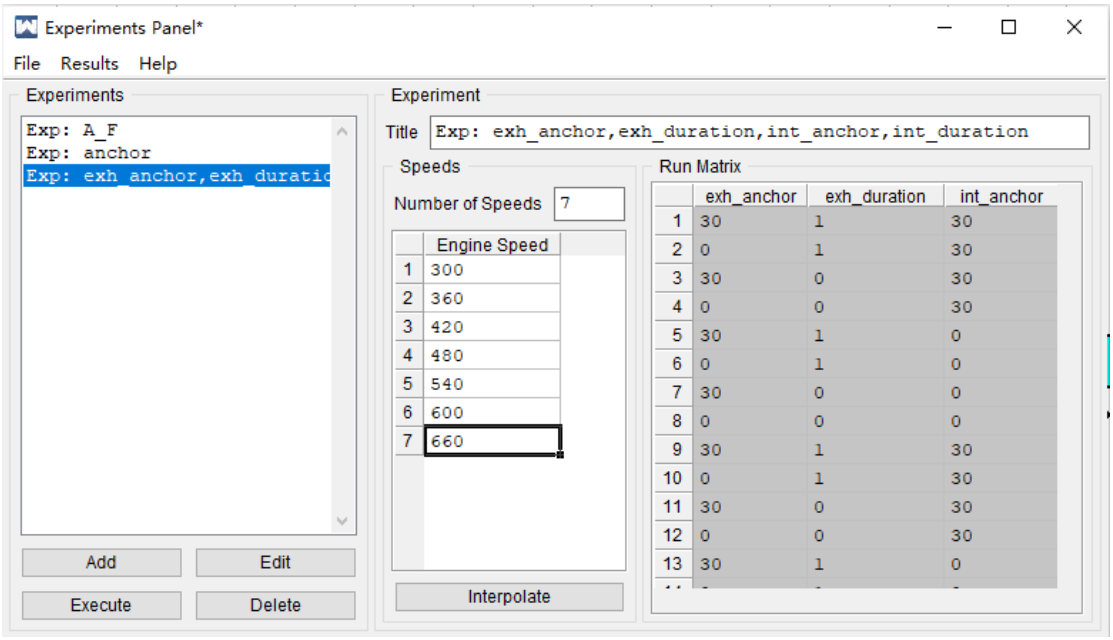

Figure 5.9 The experiments panel in Ricardo WAVE which was used during the parametric investigations for model tuning

The results of the experiments are shown in Figure 5.10. Several targets in Figure 5.10 (a) were plotted, i.e., brake power (bpowkw), torque (torqsi), maximum cylinder pressure (pmaxsi1) and brake specific fuel consumption (bsfcsi) for assessment. Then the factors Figure 5.10 (b), i.e., optimum exhaust valve anchor position (exh_{anchor}), exhaust duration ($exh_{duration}$), intake valve anchor position (int_{anchor}) and intake valve duration ($int_{duration}$) were determined by setting the appropriate target in curve fits window in Figure 5.10 (c). For example, maximum torque was set across the operating engine speed from 300rpm to 660rpm the corresponding values of valves settings were automatically adjusted to reflect this target.

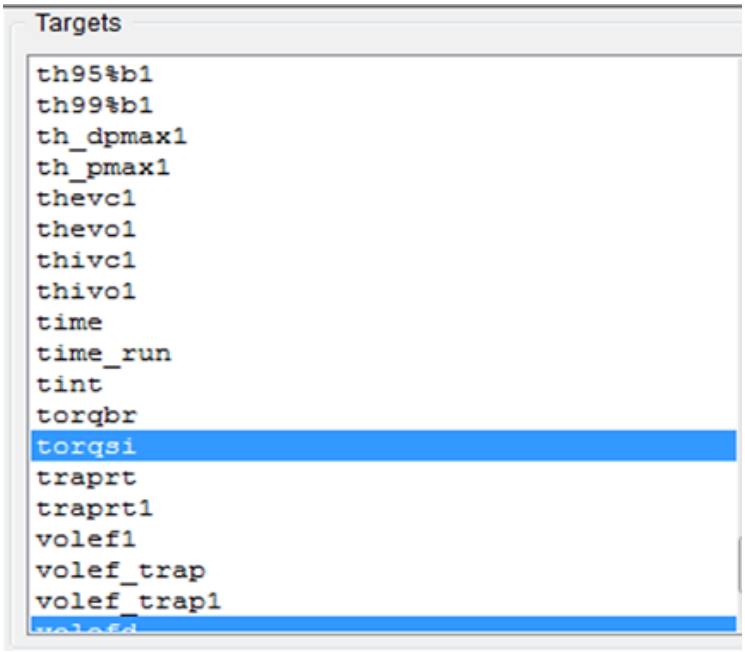
Targets
th95%b1
th99%b1
th_dpmax1
th_pmax1
thevc1
thevo1
thivc1
thivo1
time
time_run
tint
torqbr
torqsi
traprt
traprt1
volef1
volef_trap
volef_trap1

(a)

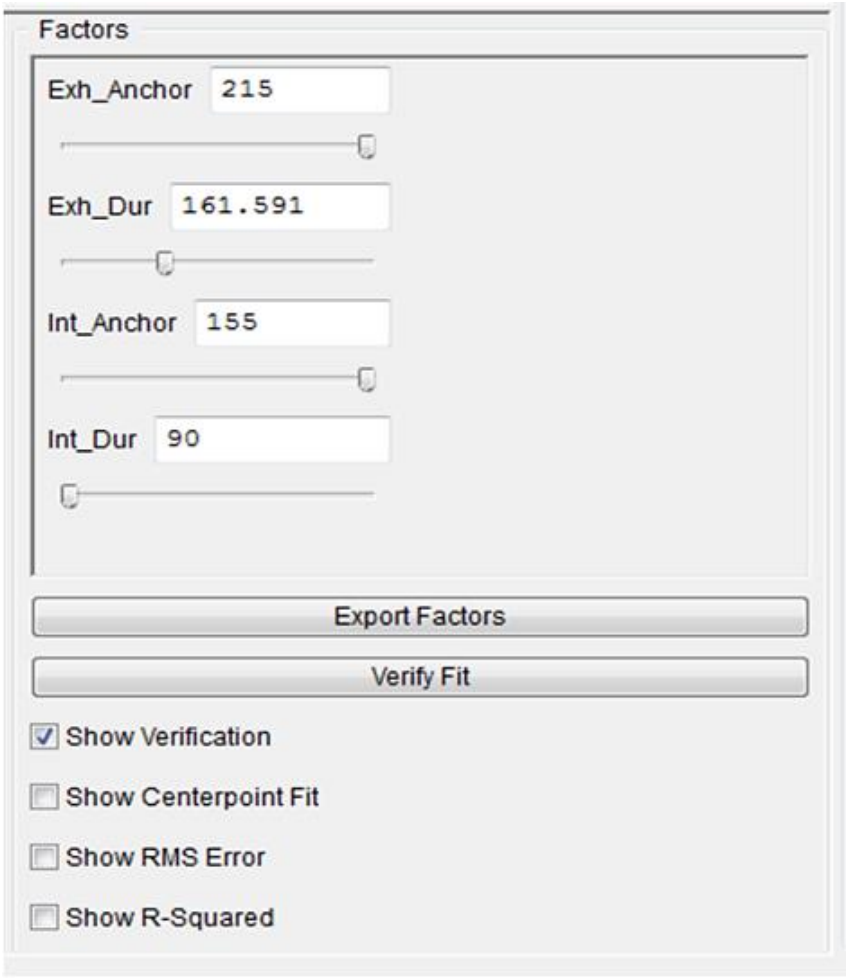
Factors
Exh_Anchor
215
Exh_Dur
161.591
Int_Anchor
155
Int_Dur
90
Export Factors
Verify Fit
Show Verification
Show Centerpoint Fit
Show RMS Error
Show R-Squared

(b)

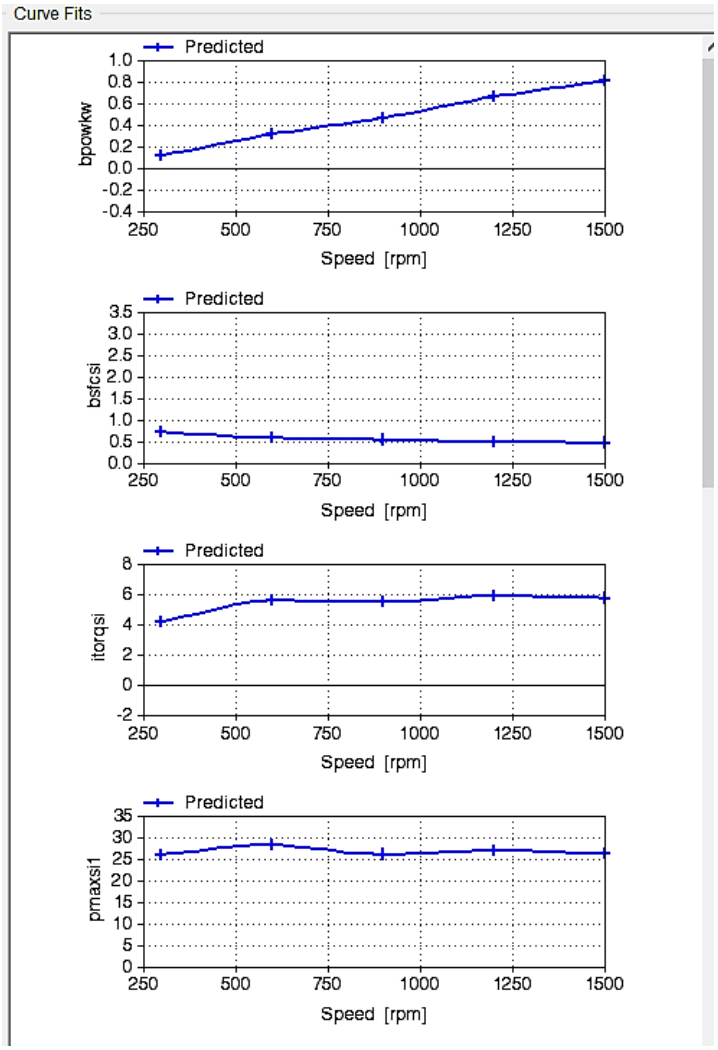

(c)

Figure 5.10 The experiment analysis panel simulation processes and results

As described in section 3, in Ricardo WAVE, the anchor position (for intake and exhaust valves) is defined as the crank angle (°) position where the lift is at its maximum value while the valve duration (for intake and exhaust valves) is how long (in crank angle degree) the valve will remain open. The relationship between WAVE's valves parameters and the valves timing variables is summarised in the following equations:

For exhaust valve:

$$\theta_{EVO} = Exh_{Anchor} - \frac{Exh_{Dur}}{2}$$

$$\theta_{EVC} = \theta_{EVO} + Exh_{Dur}$$

For intake valve:

$$\theta_{IVO} = Int_{Anchor} - \frac{Int_{Dur}}{2}$$

$$\theta_{IVC} = \theta_{IVC} + Int_{Dur}$$

According to the above, at optimised valves anchor, the exhaust valve is opened at 110°CA before BDC followed by intake valve 15°CA later. And after BDC, i.e., at 57°CA after BDC, the exhaust valve is closed followed by intake valve 10°CA later. Which means in this pure ethanol free-piston engine model, crank angle has to be converted into particular time:

Two-stroke ethanol free-piston engine valve timing results:

- EVO=110°bBDC (0.0611s)
- IVO=95°bBDC (0.0527s)
- EVC=57°aBDC (0.1317s)
- IVC=67°aBDC (0.1372s)

Base on the above modelling process description, a two-stroke ethanol-gasoline free-piston engine model has been developed from the previous gasoline FPE model. For investigations in follow sections, parameters such specific ethanol-gasoline blend concentration (E5, E10, E15, E20, E25, E30, E35, E40, E50, E60, E70, E80, E90, E100 (pure ethanol)), corresponding compression ratio, equivalence ratio, etc, are all suitably amended respectively.

5.3 Modelling results

5.3.1 Engine performance

Figure 5.11 illustrates varied brake power with corresponding ethanol-gasoline blend concentrations at different engine frequency. In general, for each engine frequency, the brake power increases with the decrease of the ethanol concentration and also with the increase of engine frequency, and E5 generates the highest brake power while which of E100 is the lowest. It is worthy to mention that the increase range of brake power from 5Hz to 11Hz also increases with the engine frequency, for instant, for the comparison between E100 and E50, the former generates 0.1372kW while the later

generates 0.1456kW at the frequency of 5Hz, however, the brake power generates by E100 is 0.4245kW while which of E50 is 0.5242kW at 11Hz. The increase range is 5.72% at 5Hz and 19.02% at 11Hz, which means the concentration of ethanol-gasoline blend could affect brake power more heavily at higher engine frequency. Figure 5.12 shows BSFC (brake specific fuel consumption) with corresponding ethanol-gasoline blend concentrations at different engine frequency. The fuel consumption decreases with the increase of engine frequency at a low frequency condition. Likewise, fuel consumption increases with the increase of ethanol concentration and E100 consumes the highest fuel amount. Figure 5.13 shows the brake thermal efficiency with corresponding ethanol-gasoline blend concentrations at different engine frequency. No doubt that ethanol-gasoline blend fuel shows a significant thermal efficiency increase for all concentrations, E5 achieved a 0.72% efficiency increase to 35.6% at peak.

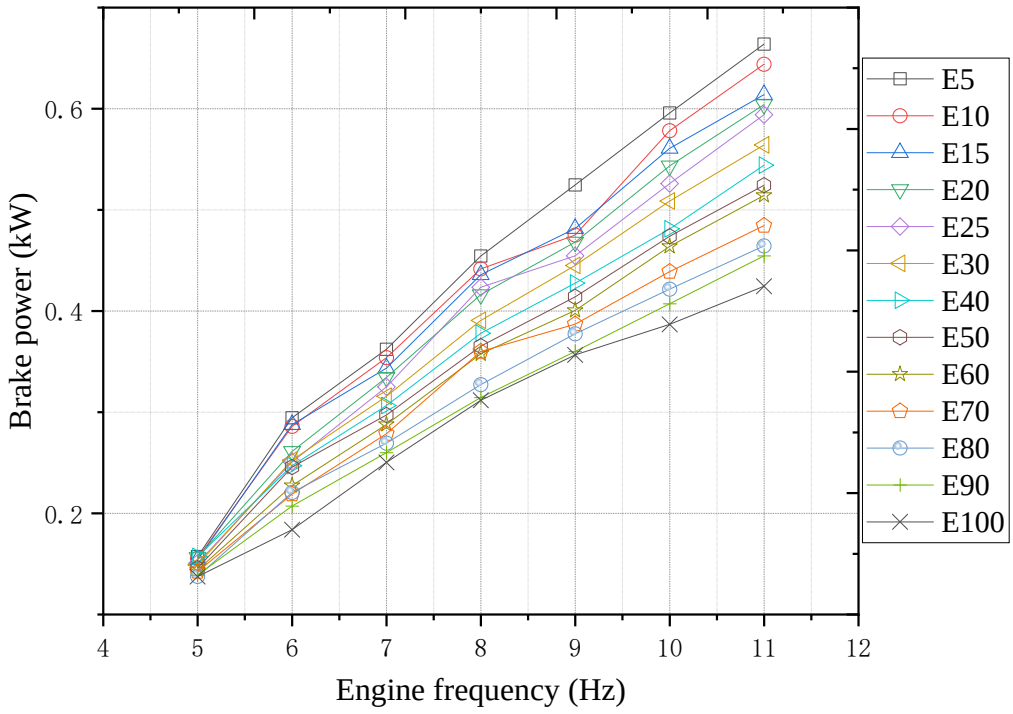

Figure 5.11 Brake power of different ethanol-gasoline blend concentration

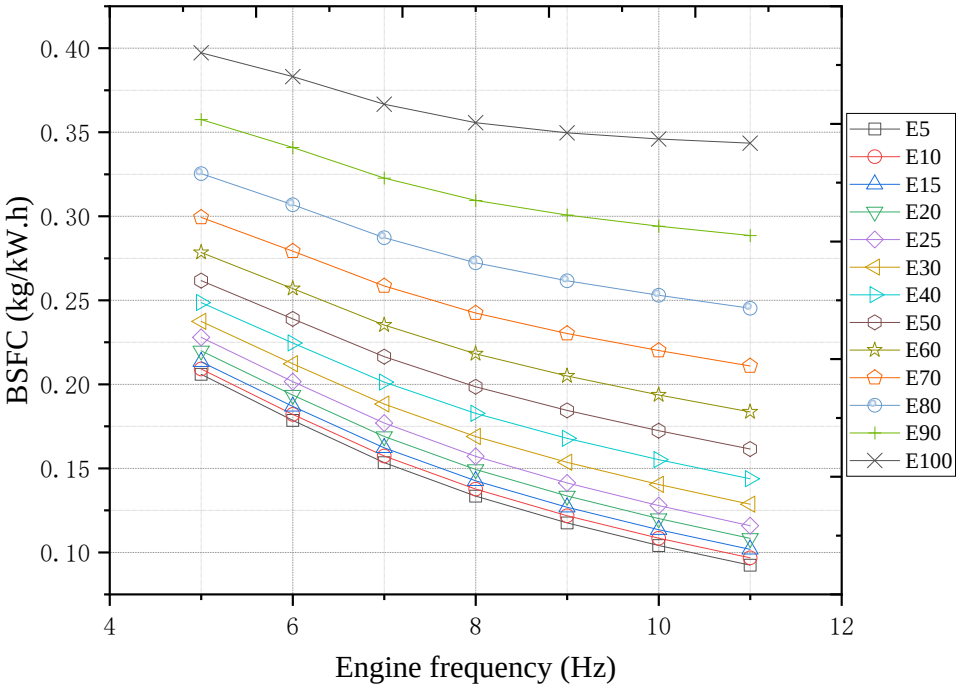

Figure 5.12 BSFC of different ethanol-gasoline blend concentration

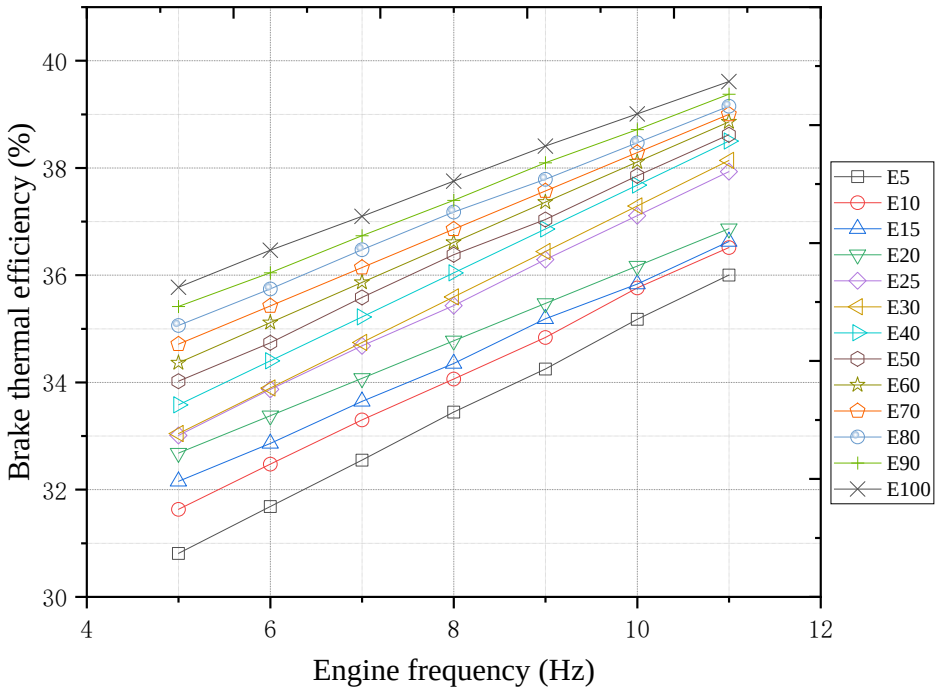

Figure 5.13 Brake thermal efficiency of different ethanol-gasoline blend concentration

5.3.2 Emission performance

Emissions that concerned in this ethanol free-piston engine research are NOx, CO and HC. Since NOx is a type of high-temperature emission, higher temperature is the most important reason of its formation. As presented in Figure 5.14 is the in-cylinder combustion temperature comparison between gasoline, E50 and E100, and it is obvious that burning pure ethanol produce the lowest in-cylinder temperature which is even 21% lower than gasoline and E50. Consequently, it is not difficult to explain the extremely low NOx emission produced by E100 burning.

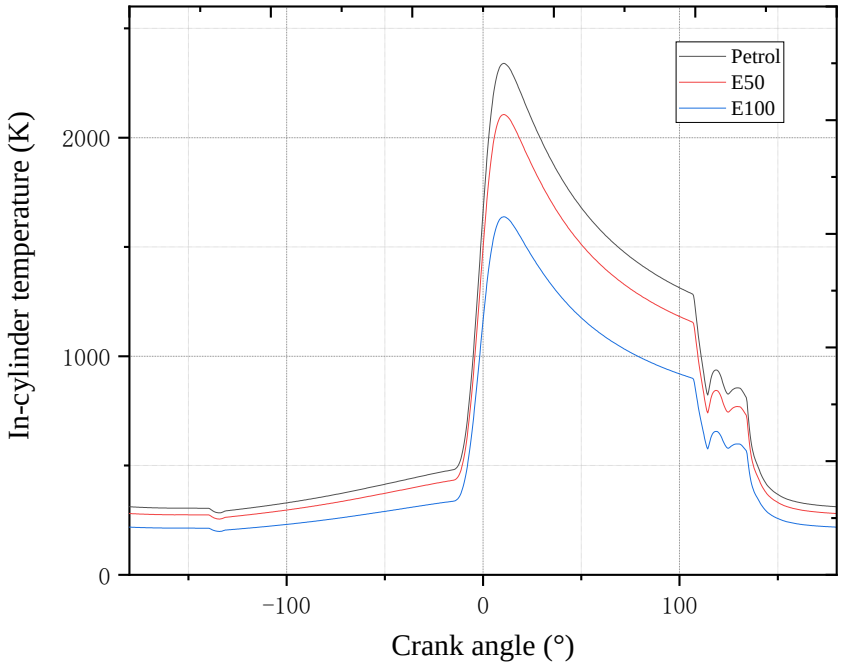

Figure 5.14 In-cylinder temperature comparison

Figure 5.15 illustrates NOx emission of this ethanol-gasoline blend free-piston engine model. Apparently, comparing with taking gasoline as fuel, NOx has been reduced by ethanol, and the reduction range increases with the increase of ethanol blend concentration. But comparing with the performance of hydrogen fueled, the condition of NOx emission reduction brough by ethanol is not that significant. However, E100 still reduces NOx to a range of 28.72% compared with gasoline, and the highest reduction occurs at the engine frequency of 8Hz. As shown in Figure 5.16, CO

emission also increases with the increase of engine frequency and decrease with ethanol blend concentration. Simultaneously, the highest reduction between gasoline and E100, occurs at the engine frequency of 11Hz, where the error is 75.14%. Figure 5.17 is the HC emissions comparison of different ethanol blend and gasoline. Differ from NOx and CO, the main reason of the formation of hydrocarbon emission is incomplete combustion and further, the main reason of incomplete combustion is lower combustion temperature and insufficient oxygen, and because of the unique characteristic of the free-piston engine, the engine is operated and simulated in a relatively low speed condition, incomplete burning is inevitable. Therefore, hydrocarbon emission decrease with the increase of engine frequency and there seems no regulars between each ethanol blend. E40 produces the highest HC from 5Hz-8Hz while E30 produces the highest HC from 8Hz-11Hz, and still, E100 produces the lowest HC of all engine frequencies and the reduction range between E100 and gasoline is 17.89%

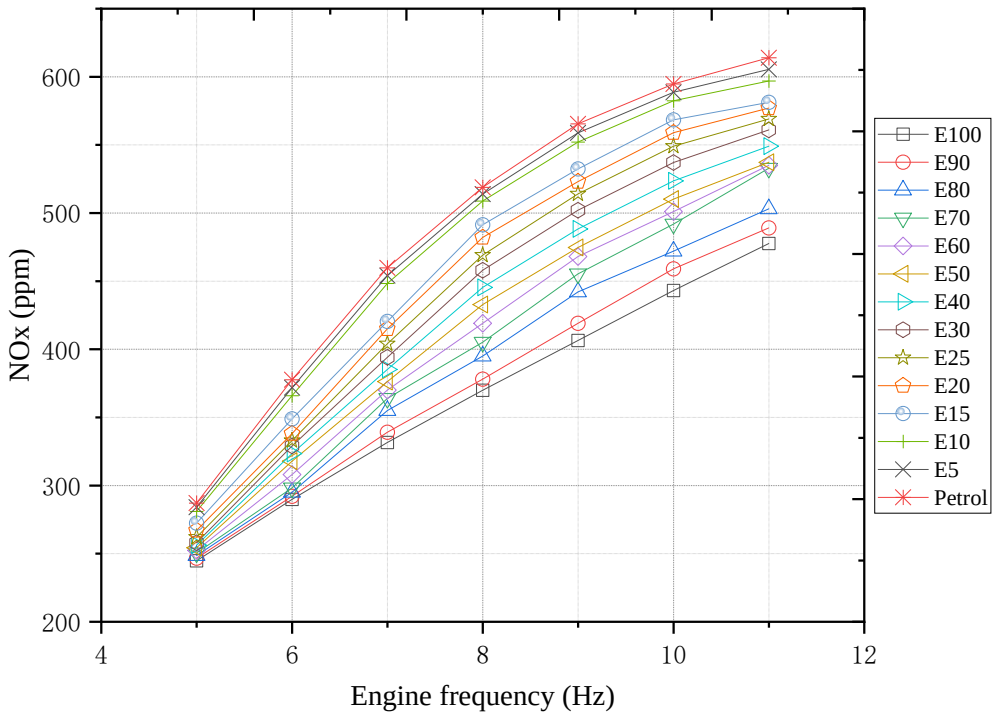

Figure 5.15 NOx emission of different ethanol-gasoline blend concentration and gasoline

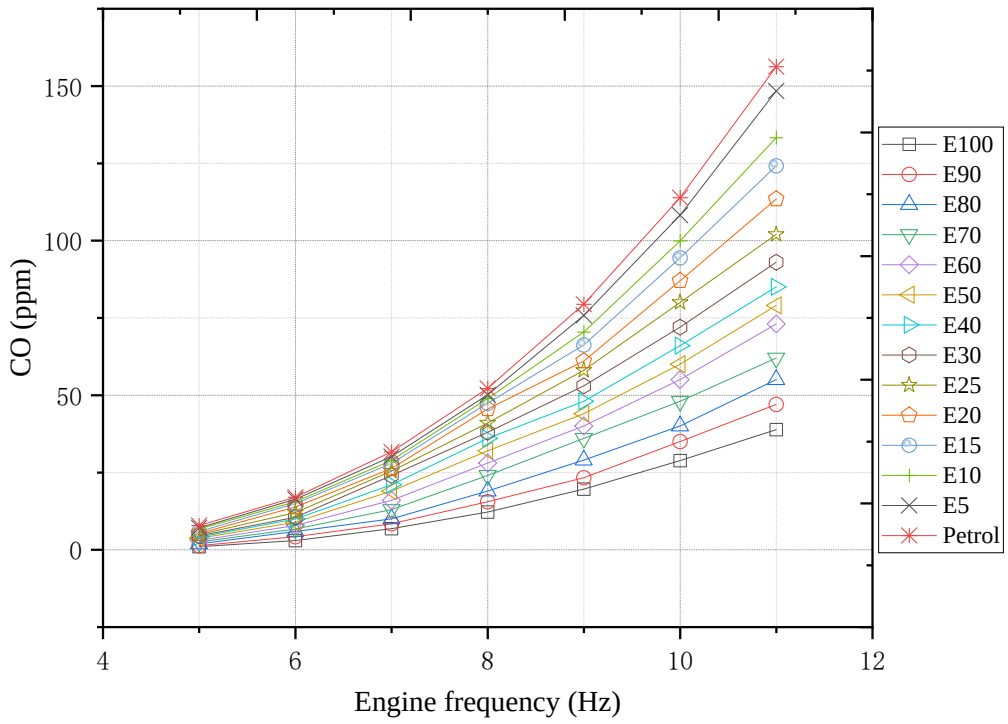

Figure 5.16 CO emission of different ethanol-gasoline blend concentration and gasoline

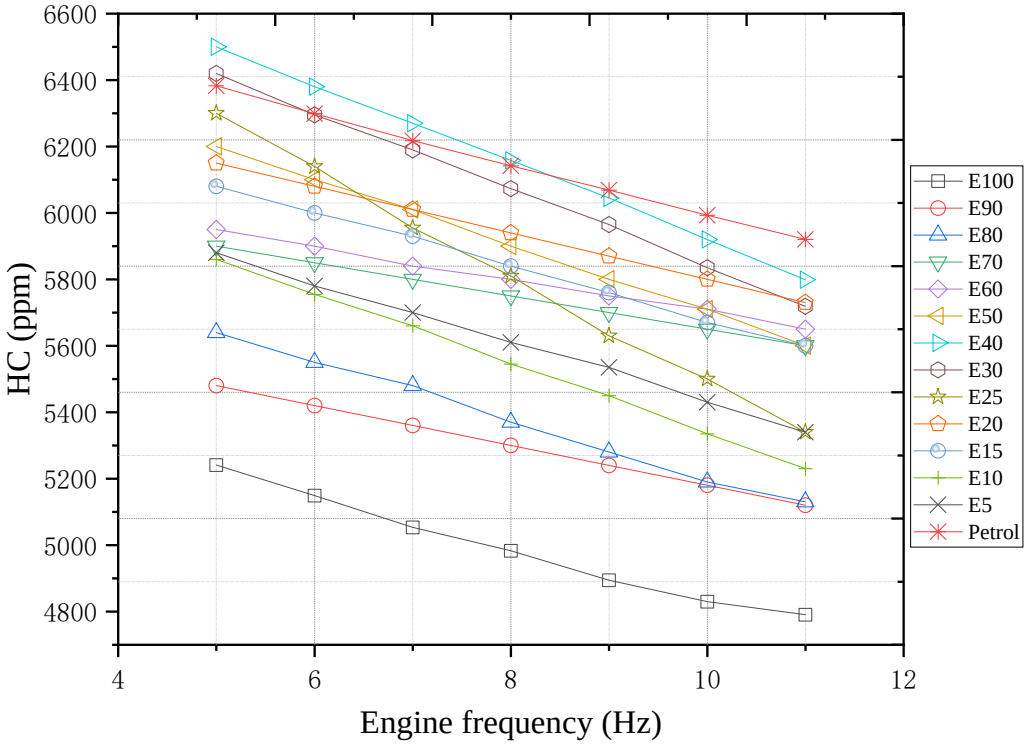

Figure 5.17 HC emission of different ethanol-gasoline blend concentration and gasoline

5.4 Summary

Series of ethanol-gasoline blend free-piston engine models have been developed from the baseline model and presented in this chapter. A MATLAB/Simulink model was used for obtaining the piston motion of these WAVE ethanol-gasoline blend free-piston engine models, and after the amendments of air/fuel ratio (equivalence ratio), compression ratio valve timing, etc., large amount of simulation results towards emission performance was gained. Comparing with gasoline fuel, pure ethanol (E100) presented impressive ability in emission reducing: NOx emission was reduced by 28.72% at the engine frequency of 8Hz, CO emission was significantly reduced by 75.14% at the engine frequency of 11Hz and HC emission was also reduced by 17.89% at the engine frequency of 5Hz.

Chapter 6. Miller cycle and its application on the FPE

The effective compression ratio of Miller cycle is smaller than its expansion ratio, which invests Miller cycle numbers of advantages such as lower exhaust emission and higher thermal efficiency, and Miller cycle is always known as an environmental-friendly evolved thermal cycle today.

Applying Miller cycle in the free-piston engine is a novel task in this research which has not been raised in other researches before. More than ten one-dimensional simulation model built by Ricardo WAVE are presented in this chapter, which contains Late Intake Valve Closure (LIVC) Miller cycle FPE models and Early Intake Valve Closure (EIVC) Miller cycle FPE model. Engine performance and emission performance of each model have been investigated, and the suitable late/early intake valve timing for the gasoline free-piston engine and hydrogen free-piston engine has been found, which provides valuable advices to the application of Miller cycle in the future.

In 2019, a one-cylinder conventional diesel engine model was built for investigating the application of Miller cycle on diesel engines. At that moment, Late Intake Valve Closure (LIVC) was applied and it turned out that emission performance under the application of Miller cycle was impressive.

Theories is presented in Section 6.1 while section 6.2 illustrated the whole modelling process of the previous diesel engine model and several free-piston engine models.

6.1 Theoretical review

6.1.1 Concept of Miller cycle

As mentioned above, the Miller cycle can be regarded as a relatively developed automotive engine cycle system because of its unique intake valve engine timing. Miller cycles can be divided into two different categories: Bypass Valve Delay Time Closure (LIVC) Miller Cycle FPE Mock-ups and Bypass Valve Early Closure (EIVC). The former one is compared with all normal automobile engine cycle systems. The intake valve closes the engine timing delay time, which means that there is less mixed gas entering the cylinder. Compared with the enlarged four-stroke, the reasonable compression stroke is shorter; conversely, the latter increase the intake valve to close the engine timing to facilitate the discharge of a portion of the mixture during the compression stroke, and

result in a reasonably shorter compression stroke compared to the expanded four-stroke. Figure 6.1 shows the P-V plot compared to the LIVC Miller cycle and the diesel cycle system. On this PV diagram, the black bar circulation system (0-1-2-3-3'-4-1-0) means the basic diesel circulation system, the blue line circulation system (0-1-1a-2a-3a- 3 'a-4a-1-0) means Miller cycle. The straight line 1-1a means the uniqueness of the Miller cycle, that is, during the closing phase of the intake valve delay time, the piston is gradually compressed stroke after rising from BDC, during this time the intake valve is still open for a certain period of engine crankshaft corners time (1-1a). Thus, the air volume decreases while the cylinder pressure does not change during this time. Since a portion of the intake port that goes into the cylinder is expelled into the intake port during the compression stroke. The subsequent intake air supply to the cylinder is relatively lower than the diesel cycle system, which reduces the reasonable engine compression ratio. At the end of the compression stroke, the master cylinder working pressure and temperature are less than the standard Otto cycle; then during the ignition four-stroke, the ignition temperature is lower, which may result in less NOx production in the cylinder; finally, in the exhaust four-stroke, it can reduce NOx emissions [288].

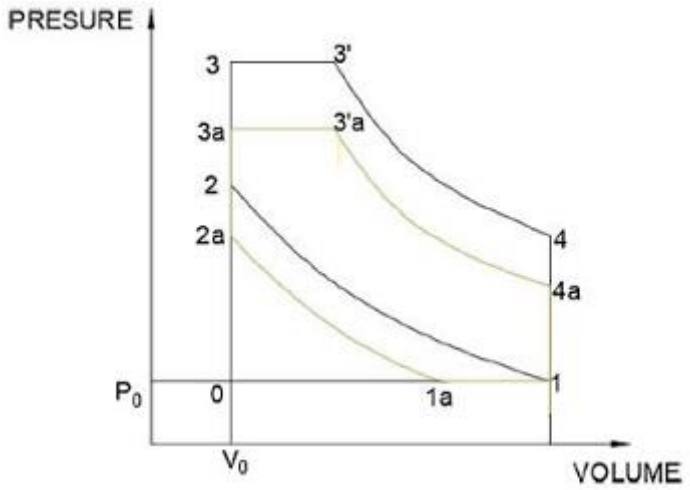

Figure 6.1 P-V diagram compared between LIVC Miller cycle and Diesel cycle.

Compared with the traditional automobile engine, according to the Miller cycle, the engine crankshaft angle usually has a large intake valve closed in the middle and late stages, and part of the mixed gas can be discharged, thereby delaying the time to turn off the engine timing and increasing the working time. Four strokes, which in turn increase the engine compression ratio. lower than the expansion ratio. In addition, discussions on energy issues and air pollution have been under

consideration in recent years. Technical engineers have been focusing on finding new countermeasures that can simultaneously increase the efficiency of gasoline and diesel and improve the emission characteristics. In such a case, the Miller cycle is concerned again. The Miller Cycle, despite its many salient advantages, has been less successful in promotional marketing. There are not many car engines today that can really be considered Miller cycle car engines, and the role of the Miller cycle has not been fully utilized. It can be deduced from the above factors that the driving experience of the customer and the driving characteristics of the Miller cycle automobile engine itself are far from being achieved. In general, under the condition of low and medium working conditions in the whole process of operation, the Miller cycle causes the gas mixture at the intake port to decrease. Therefore, regardless of whether the thermal efficiency of the Miller cycle car engine can be improved, the total torque output will be reduced. Under relatively stable and fast working conditions, the harm of this problem can be ignored to a certain level. Based on this factor, engine companies have little interest in the Miller cycle. Nevertheless, with the continuous development of automobile engines, various new technology applications and methods have been clearly proposed. In particular, some new car engines that are completely different from traditional car engines have been derived. For new automobile engines, the difference between them and traditional automobile engines is not only limited to the key point level, but also exists in the overall design method. The development trend of self-innovating automotive engines has brought numerous opportunities for the use of the Miller cycle [221]. Figure 6.2 shows the PV diagram of the EIVC Miller cycle. It is remarkable that from point 5 to point 1, no large amount of gas-fuel mixture is sucked into the cylinder, and no work is performed according to the reduction during this time, shrink to decrease.

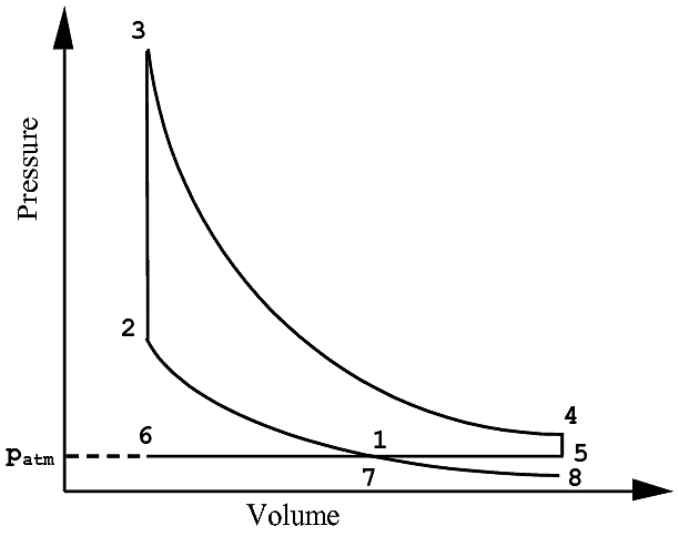

Figure 6.2 EIVC Miller cycle P-V Diagram

In summary, Miller cycle possesses impressive ability on emission reduction, however, due to less air-fuel mixture is burned (no meter less intake or part of intake air-fuel mixture is rejected), Miller cycle application would inevitably cause lower brake torque and output brake power. In order to solve this, turbocharger was considered as the most suitable method to bring back both brake torque and output brake power to the initial level. As shown in Figure 6.3, Figure 6.4 and Figure 6.5 are turbocharger fixed compressor panel, turboshaft panel and turbocharger fixed turbine panel. All kind parameters that required for the whole turbocharger system could be amended in these three panels.

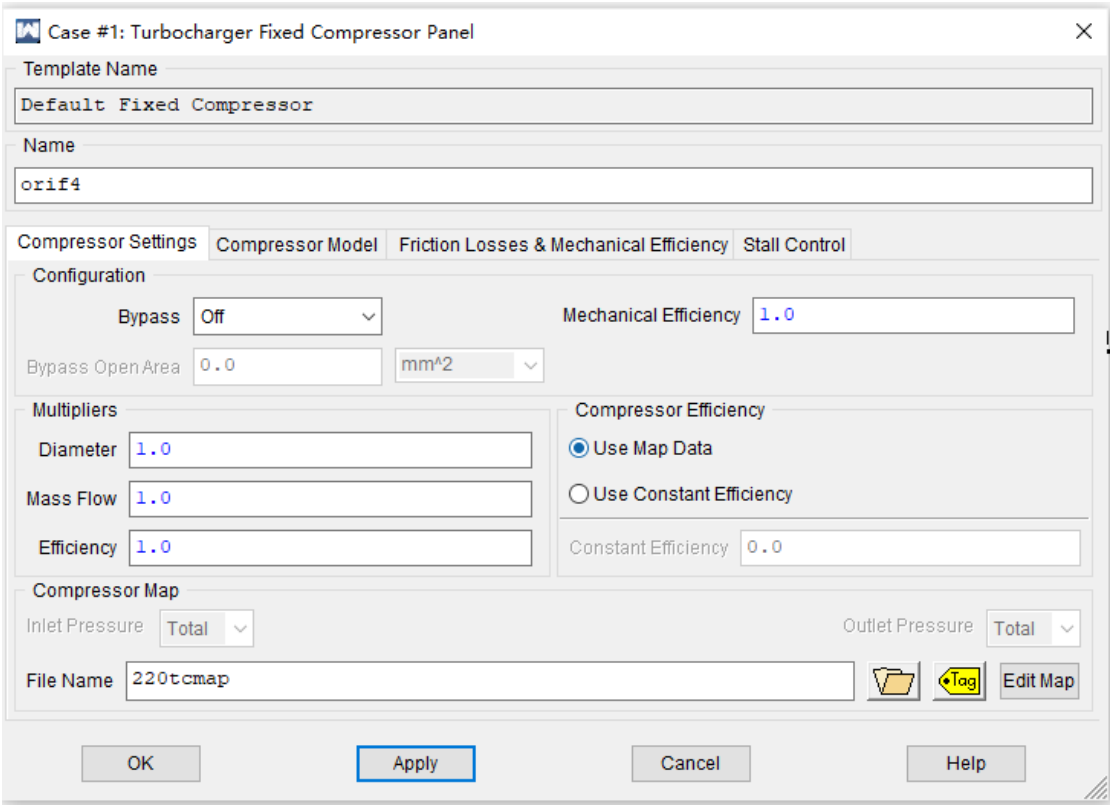

Figure 6.3 Turbocharger fixed compressor panel

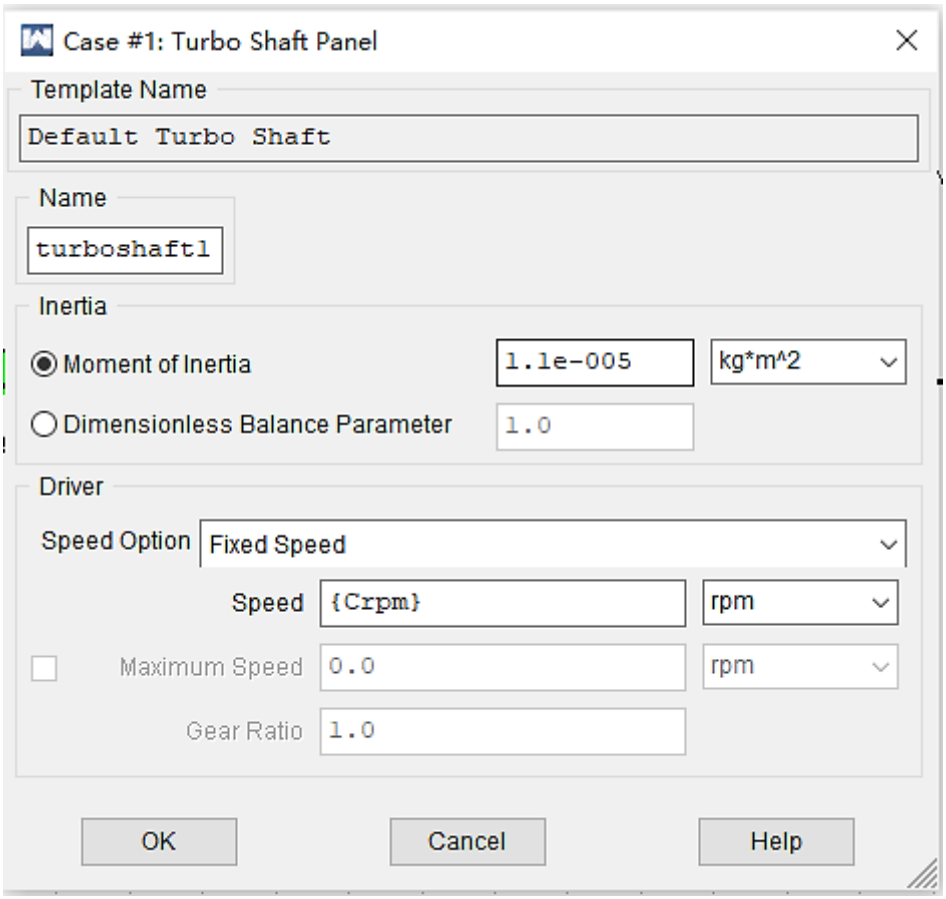

Figure 6.4 Turbo shaft panel

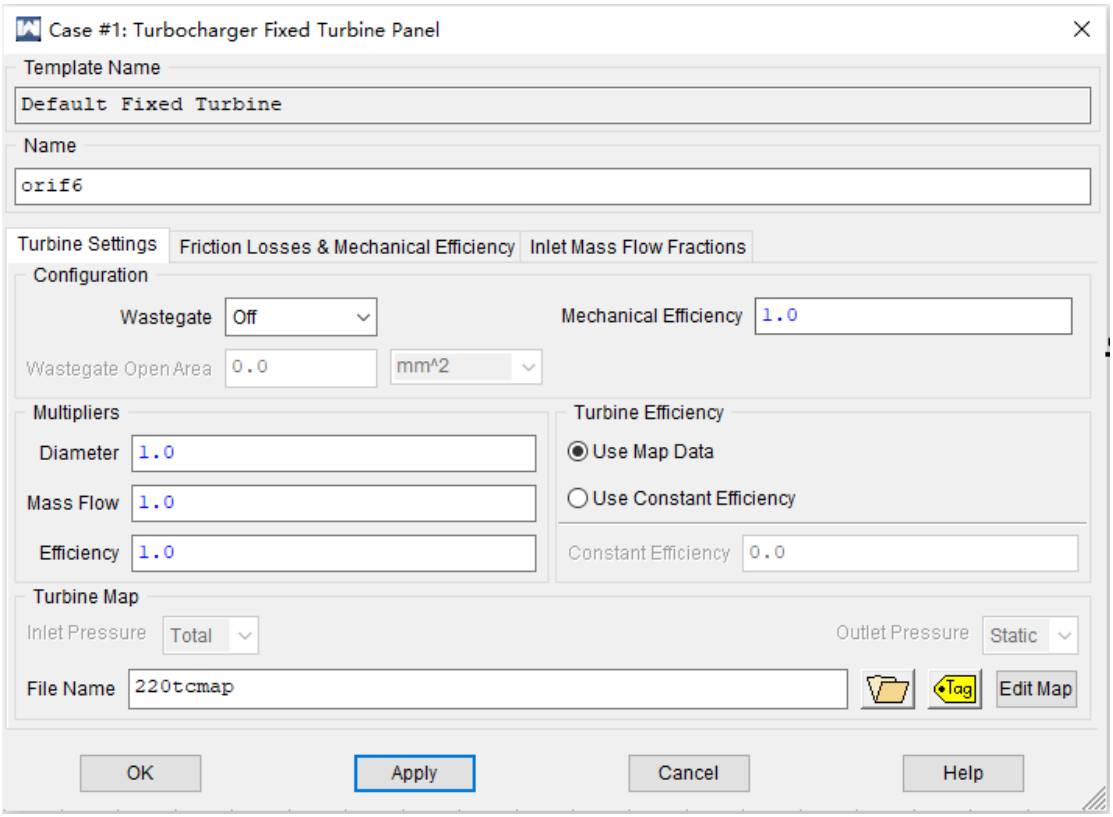

Figure 6.5 Turbocharger fixed turbine panel

6.2 Engine modelling

6.2.1 Miller cycle on the free-piston engine

The two-stroke gasoline and hydrogen free-piston engine model which have been described in Section 3 is taken as baseline models in this Section, and due to the baseline models have been validated before, there's no need to repeat another validation work.

In this section, three types of the free-piston engine (four-stroke gasoline free-piston engine, four-stroke hydrogen free-piston engine and four-stroke ethanol-gasoline blend free-piston engine) that described in previous chapters were amended with the application of Miller cycle. Figure 6.6 shows different intake valve timing of all types of Miller cycle that have been tested on the hydrogen free-piston engine model, following sections will describe the reason of choosing these early or late crank angles. For gasoline and ethanol-gasoline blend free-piston engines, Miller cycle was applied by similar methods. Due to the unique non-crank characteristic of the free-piston engine, all

early/late intake valve closing angles that used in following sections are converted from specific time in the engine cycle correspondingly. For instance, the total time of one cycle in this two-stroke free-piston engine is 2s, therefore, 5°CA equal to 0.00278s and 30°CA equal to 0.1667s, etc. Using crank angle instead to represent the extent of Miller cycle that applied is for Ricardo WAVE amendment only.

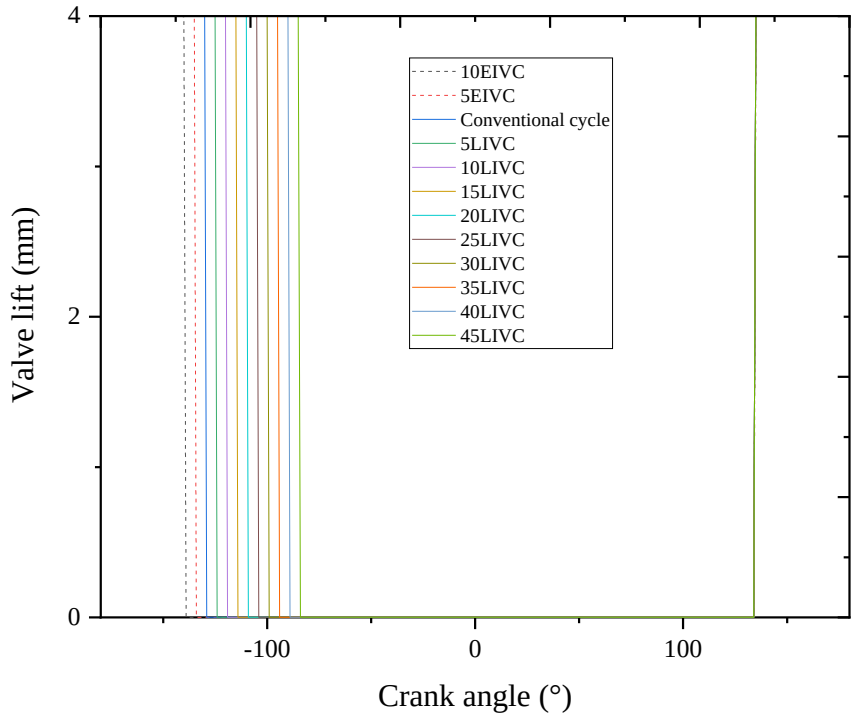

Figure 6.6 Different Miller cycle intake valve timing on hydrogen FPE

6.3 Simulation results

6.3.1 Simulation results on the free-piston engine

Both LIVC and EIVC have been applied into the free-piston engine in order to find out their regulation, but consequences did not always meet the experiments due to the difference between pushing out part of air-fuel mixture and indrawing insufficient air-fuel mixture at the beginning. Details are presented in the following section.

6.3.1.1 Engine performance

6.3.1.1.1 Gasoline free-piston engine

Figure 6.7 shows the comparison of indicated power of different late intake valve closing angles. This is the situation simulated without turbocharger, indicated power of each engine frequency has been significantly decreased, the value decreased from near 1.6kW to under 1.2kW at the engine frequency of 5Hz and from near 2.5kW decreased to near 1.9kW. As mentioned above, the reduction of output power is something unacceptable, therefore, the application of turbocharger is inescapable.

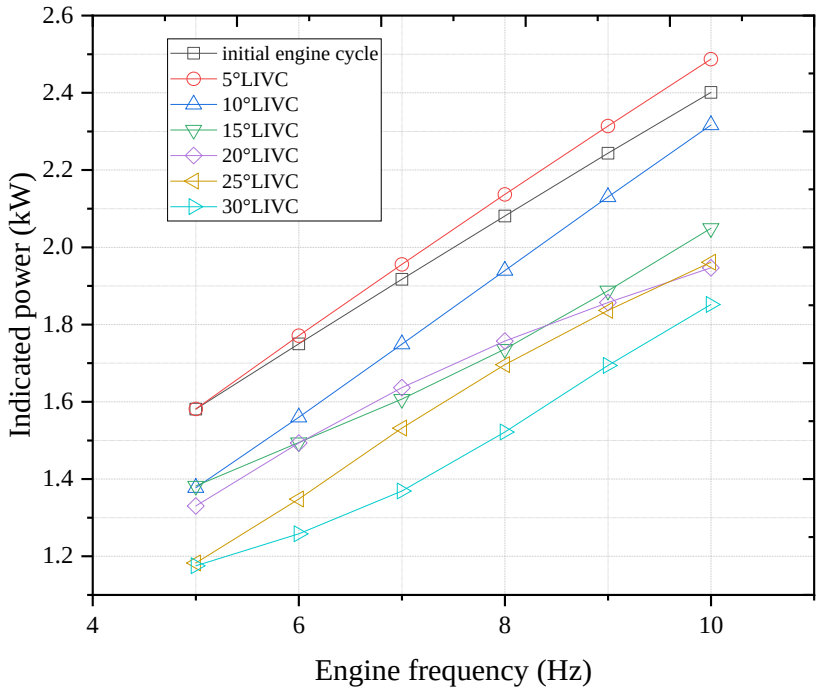

Figure 6.7 Indicated power comparison of different LIVC angles

Table 6.1 Indicated power of different turbo-charged LIVC comparison

Engine Frequency （Hz）	**Indicated power (kW)**						
	Initial engine cycle	**5°T-LIVC**	**10°T-LIVC**	**15°T-LIVC**	**20°T-LIVC**	**25°T-LIVC**	**30°T-LIVC**
5	1.58	1.622	1.570	1.513	1.529	1.502	1.505

6	1.75	1.791	1.734	1.671	1.700	1.672	1.673
7	1.92	1.955	1.891	1.822	1.867	1.833	1.838
8	2.08	2.114	2.058	1.970	2.038	2.002	2.008
9	2.24	2.266	2.210	2.135	2.186	2.169	2.179
10	2.40	2.411	2.358	2.278	2.359	2.328	2.326

Table 6.2 BSFC of different turbo-charged LIVC comparison

Engine Frequency （Hz）	**BSFC (kg/kWh)**						
	Initial engine cycle	**5°T-LIVC**	**10°T-LIVC**	**15°T-LIVC**	**20°T-LIVC**	**25°T-LIVC**	**30°T-LIVC**
5	5	3.458	4.150	4.323	4.496	4.669	4.842
6	6	1.516	1.879	1.955	2.031	2.107	2.183
7	7	1.044	1.336	1.388	1.440	1.493	1.545
8	8	0.862	1.138	1.181	1.224	1.267	1.310
9	9	0.728	0.990	1.027	1.063	1.099	1.136
10	10	0.658	0.921	0.954	0.987	1.020	1.053

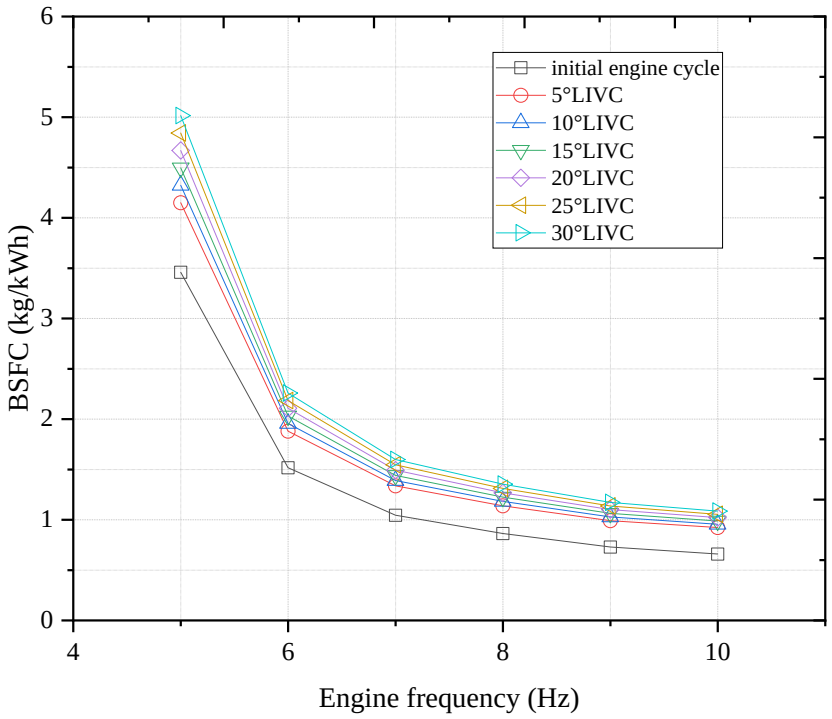

Figure 6.8 BSFC of different turbo-charged LIVC comparison

Figure 6.8 shows the comparison of indicated power of different LIVC late intake valve closing angles on this gasoline free-piston engine model after turbo-charged. It is obvious that thanks to the application of turbocharger, indicated power of each late closing angles has been increased back to a similar value of what produced by the initial engine cycle, and errors of each data is all below 5%. In this case, different parameters such as fixed drive speed of the compressor and turbine have been pre-set for different engine model. Table 6.2 and Figure 6.8 both illustrated the comparison of BSFC of different LIVC late intake valve closing angles on this gasoline free-piston engine model after turbo-charged. Same with predicted above, brake specific fuel consumption was risen inevitably due to the less air-fuel mixture for combustion stroke. However, the extent of the increase of BSFC is still acceptable. 65% more gasoline was consumed at the engine frequency of 5Hz which was the largest extent, and the value of BSFC has still decreased under 2.5kg/kWh, fuel consumption could still be maintained around a relatively low level after 6Hz.

Table 6.3 Indicated power of different EIVC comparison

Engine Frequency （Hz）	Indicated power (kW)						
	Initial engine cycle	5°T-EIVC	10°T-EIVC	15°T-EIVC	20°T-EIVC	25°T-EIVC	30°T-EIVC
5	1.58	1.49	1.29	1.29	1.24	1.09	1.09
6	1.75	1.68	1.47	1.40	1.40	1.26	1.17
7	1.92	1.87	1.66	1.52	1.55	1.44	1.28
8	2.08	2.05	1.85	1.65	1.67	1.61	1.43
9	2.24	2.22	2.04	1.80	1.77	1.75	1.60
10	2.40	2.40	2.23	1.96	1.86	1.87	1.76

The comparison of indicated power of different EIVC early intake valve closing angles is shown in Table 6.3. From which it could be seem that EIVC strongly affected the indicated power and the extent was even larger than what of LIVC, and it was reduced by 33.14% at the engine frequency of 6Hz. As always, turbocharger was necessary to be applied in order to rise the value.

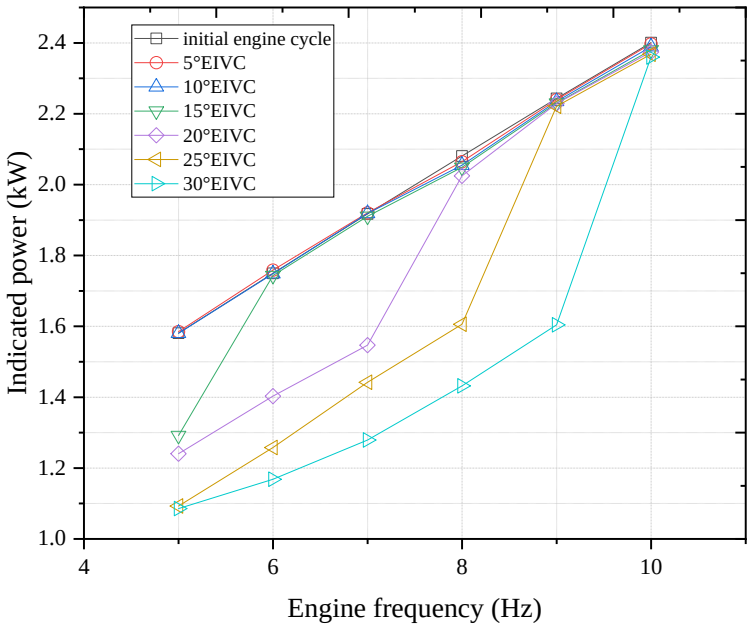

Figure 6.9 Indicated power of different turbo-charged EIVC comparison

Figure 6.9 shows the comparison of indicated power of different turbo-charged EIVC early intake

valve closing angles. Situation is different from LIVC, only the indicated power of 5°CA and 10°CA EIVC could be increased to an equal level as the initial engine cycle. Once the early intake valve closing angle is larger than 10°CA, the indicated power was no longer able to be increased as expected, especially at lower engine frequency period, no matter how the parameters of compressor or turbine were set. Therefore, for the research of EIVC on the gasoline free-piston engine, early intake valve closing angle larger than 10°CA will be taken into consideration no more.

6.3.1.1.2 Hydrogen free-piston engine

For hydrogen free-piston engine, modelling process and Miller cycle application process are similar with what has been implemented on the gasoline free-piston engine model and have been described in above sections. As explained in section 6.4.2.1.1, Miller cycle (no matter EIVC or LIVC) will always causes a unignorable reduction of the indicated power and increases brake specific fuel consumption simultaneously, and turbocharger is a vital opponent that used to increase the indicated power. Therefore, same theory that has been applied on the hydrogen free-piston engine model. For EIVC, turbocharger could only increase the indicated power of 5°CA EIVC back to an equal level of the initial engine cycle, and for cases of the early intake valve closing angle, the indicated power is constantly hugely lower than the initial data. For LIVC, all the models from 5°CA LIVC to 35°CA LIVC could be run as expected. Illustration of indicated power that produced without turbocharger will no longer presented here and in following sections.

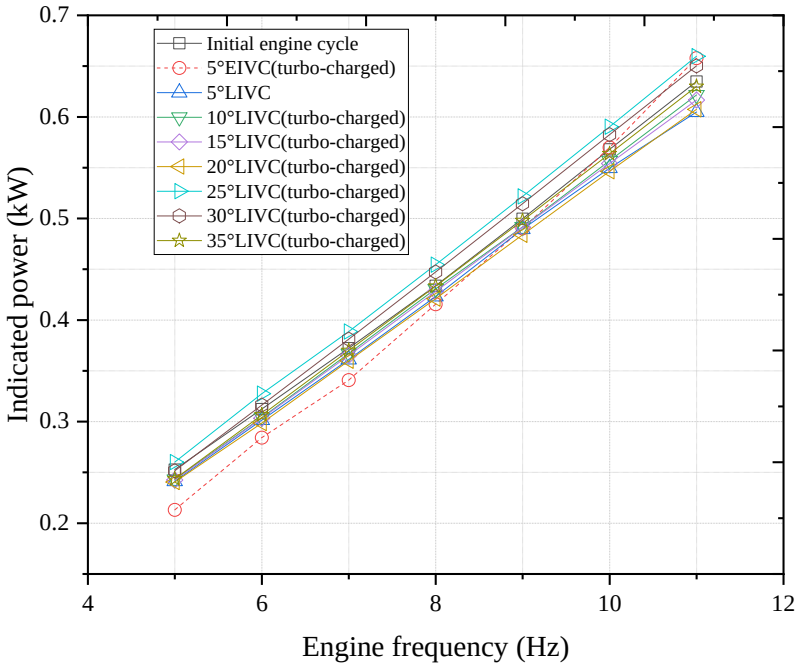

Figure 6.10 Indicated power comparison of different types of Miller cycle

Figure 6.10 shows the comparison of indicated power of both EIVC and LIVC. As shown, for 5°CA EIVC, even after turbo-charged, the indicated power (at low engine frequency from 5Hz to 8Hz) is still relatively low with a minimum error of 8.45%. For LIVC, all types of early intake valve closing angle could be run as expected. Therefore, EIVC would no longer be taken into consideration for the research on the hydrogen free-piston engine. Figure 6.11 and Figure 6.12 show the comparisons of BSFC and indicated efficiency of different early intake valve closing angles. LIVC Miller cycle has brought a certain extent of increase to fuel consumption and decrease to the indicated efficiency, and indicated efficiency at the engine frequency of 11Hz has been reduced 29.7%.

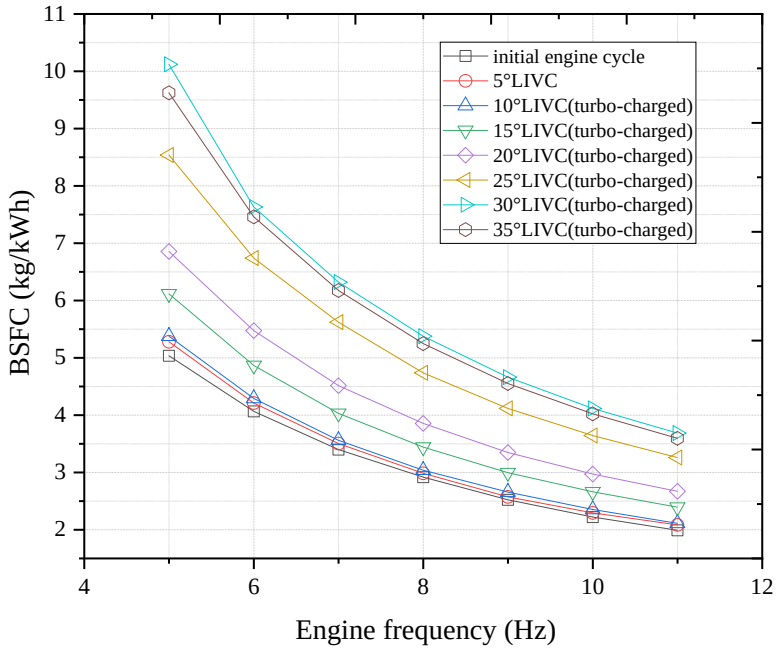

Figure 6.11 BSFC comparison of different types of Miller cycle

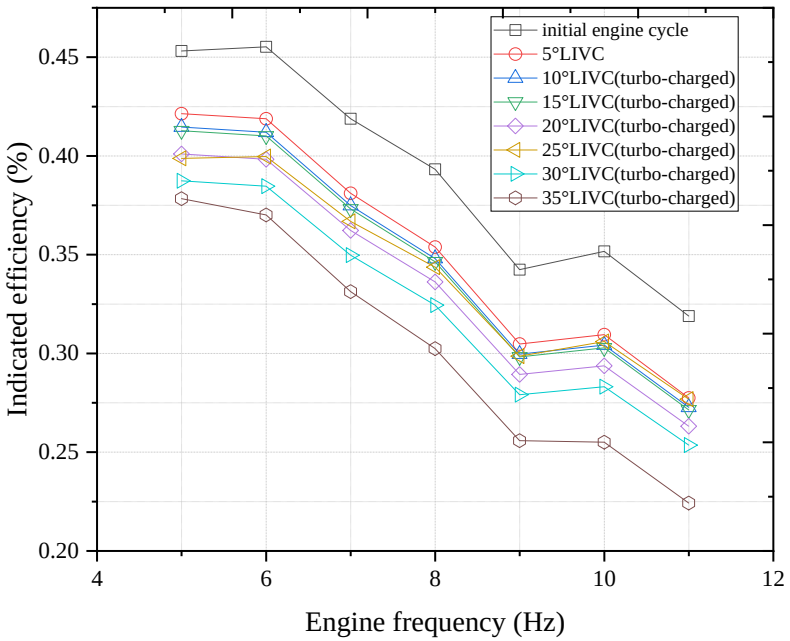

Figure 6.12 Indicated efficiency of different types of Miller cycle

6.3.1.1.3 Ethanol free-piston engine

Different ethanol-gasoline blend engine models have been presented in Chapter 5, however, comparing all kinds of ethanol-blend free-piston engines' engine performance and emission performance under the application of Miller cycle will not only make the research results miscellaneous but also have no occasion to do so. Therefore, only E100 (pure ethanol) has been taken into consideration in this section to discover the effect of Miller cycle and ethanol combination applied on a free-piston engine.

Figure 6.13 shows the comparison of indicated power of EIVC and LIVC. Similar with gasoline free-piston engine, for cases of the early intake valve closing angle smaller than 10°CA EIVC, the indicated power could be increased to an equal level as the initial engine cycle.

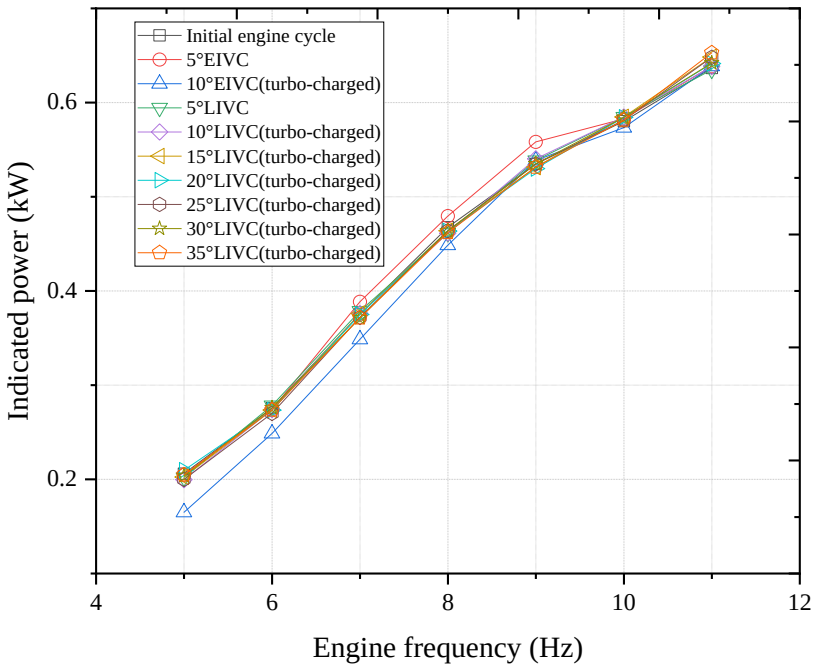

Figure 6.13 Indicated power comparison of different Miller cycle

Figure 6.14 shows the comparison of BSFC of different EIVC and LIVC angles. As previous, both EIVC and LIVC brought a certain extent of increase to fuel consumption, and the range of increase that made by 35°CA LIVC reached 78.3% at the engine frequency of 5Hz. Figure 6.15 shows the comparison of indicated efficiency on each EIVC and LIVC free-piston engine models. Slight larger

of the early/late intake valve closing angle would causes slight reduction on the indicated efficiency, and the largest decrease occurs at the engine frequency of 5Hz as well, indicated efficiency was reduced 21.62% from the value of 40.77% to 31.95%.

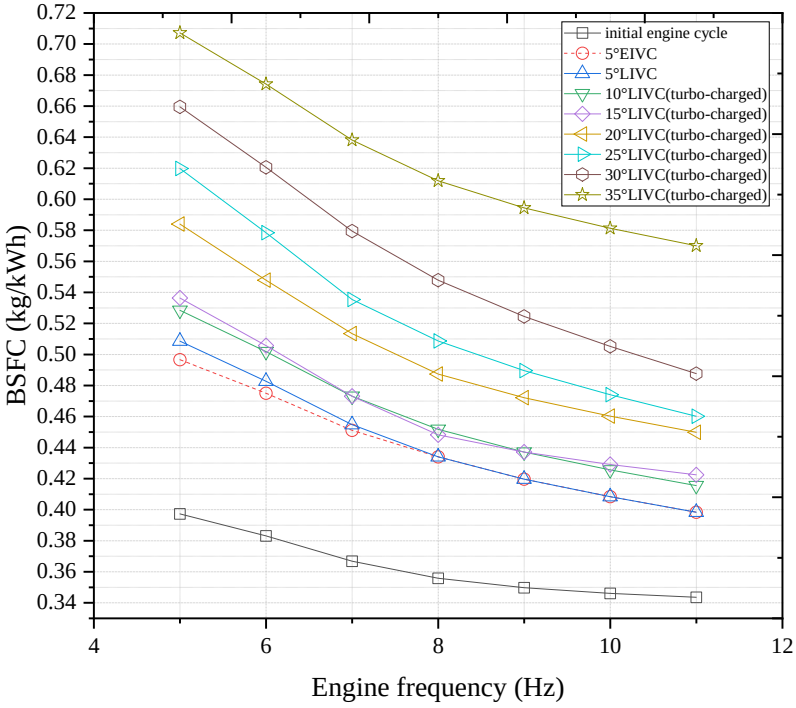

Figure 6.14 BSFC comparison of EIVC and LIVC

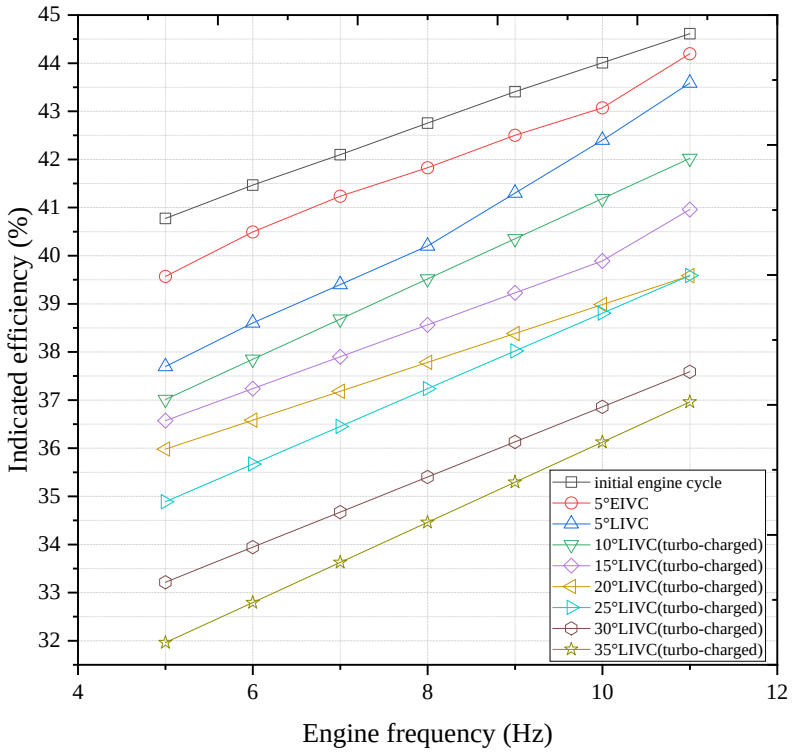

Figure 6.15 Indicated efficiency comparison of EIVC and LIVC

6.3.2.1 Emission performance

6.3.2.1.1 Gasoline free-piston engine

Figure 6.16 shows NOx emission comparison of different EIVC and LIVC Miller cycle on the gasoline free-piston engine. As expected, no matter for EIVC or LIVC, no matter how large the early/late intake valve closing angle is, Miller cycle could significantly reduce NOx emission, and the reduction extent increases with the enlargement of the intake valve closing angle. It is worth mentioning that, though the early intake valve closing angle of EIVC larger than 5°CA would reduce indicated power to an extremely low level, 5°CA EIVC is still working and its NOx reducing ability is even more remarkable than most of conditions of LIVC, which has reduced 30.9% NOx at the engine frequency of 11Hz. Figure 6.17 and Figure 6.18 show the comparisons of HC and CO emission of different EIVC and LIVC Miller cycle on the gasoline free-piston engine. As previously explained, hydrocarbon emission would be increased by the effect of Miller cycle and decreases with the increase of engine frequency. EIVC produced the highest amount of HC emission

(increased 5.5% at 11Hz) even comparing with all types of LIVC while 5°CA LIVC produced the lowest, which was even lower than the amount produced by initial engine cycle. It is worth noticing that CO emission produced in the free-piston engine is extremely low comparing with conventional diesel engine. Generally speaking, the difference between each group of carbon monoxide emission was relatively small and the amount increases with the increase of engine frequency. 15°CA LIVC produced the largest amount of emission while 5°CA EIVC produced the smallest.

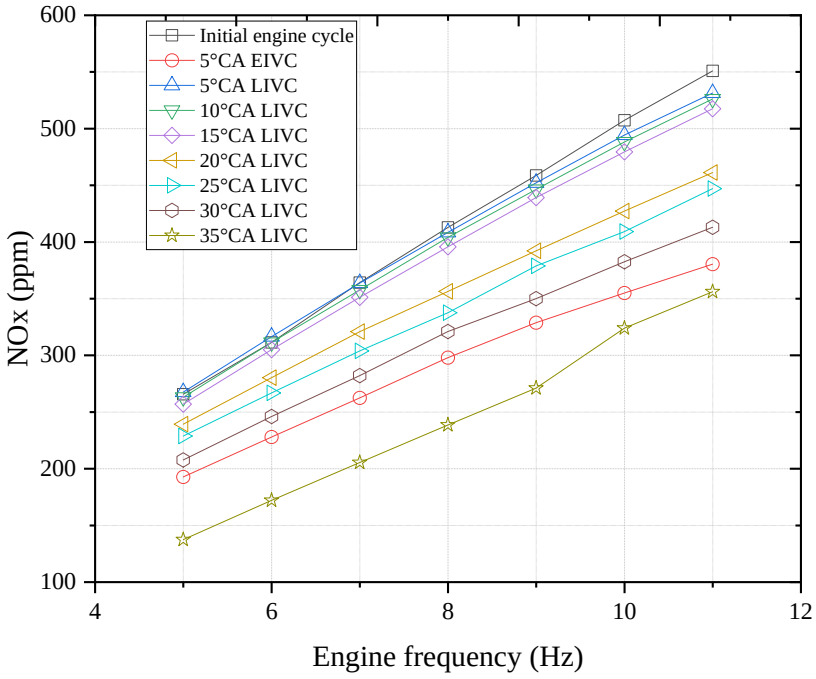

Figure 6.16 NOx emission comparison of different EIVC and LIVC

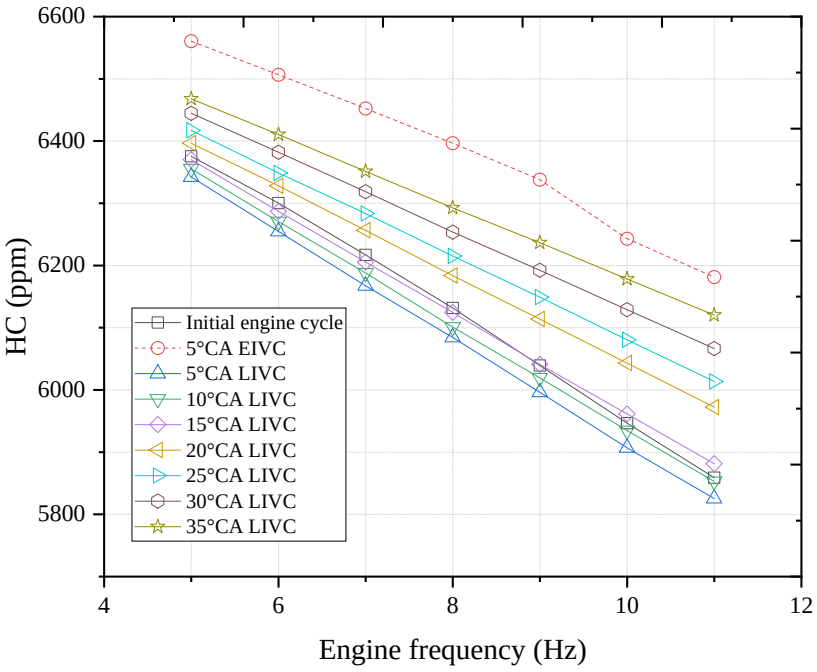

Figure 6.17 HC emission comparison of different EIVC and LIVC

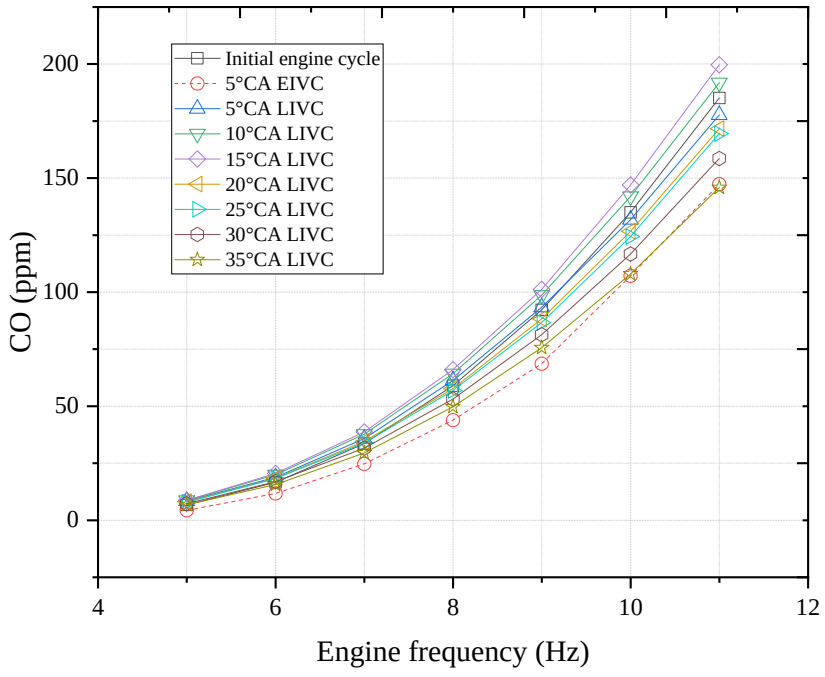

Figure 6.18 CO emission comparison of different EIVC and LIVC

6.3.2.1.2 Hydrogen free-piston engine

Figure 6.19 illustrated the comparison of NOx emission of different LIVC late intake valve closing angles on the hydrogen free-piston engine model. It could be concluded from the figure that for this two-stroke free-piston engine, NOx emission is already at a relatively low level even is run by the initial engine cycle comparing with gasoline FPE. On the basis of this, Miller cycle has brough impressive reduction to NOx and made it almost negligible. For all engine frequencies that have been tested, 30°CA LIVC has constantly presented its remarkable NOx reducing ability and reduced 38.3% NOx emission at the engine frequency of 11Hz. With the late intake valve closing angle continuously risen up, the amount of NOx appears a phenomenon of increase. Due to the fuel speciality of hydrogen, no HC or CO emission would be produced in this free-piston engine.

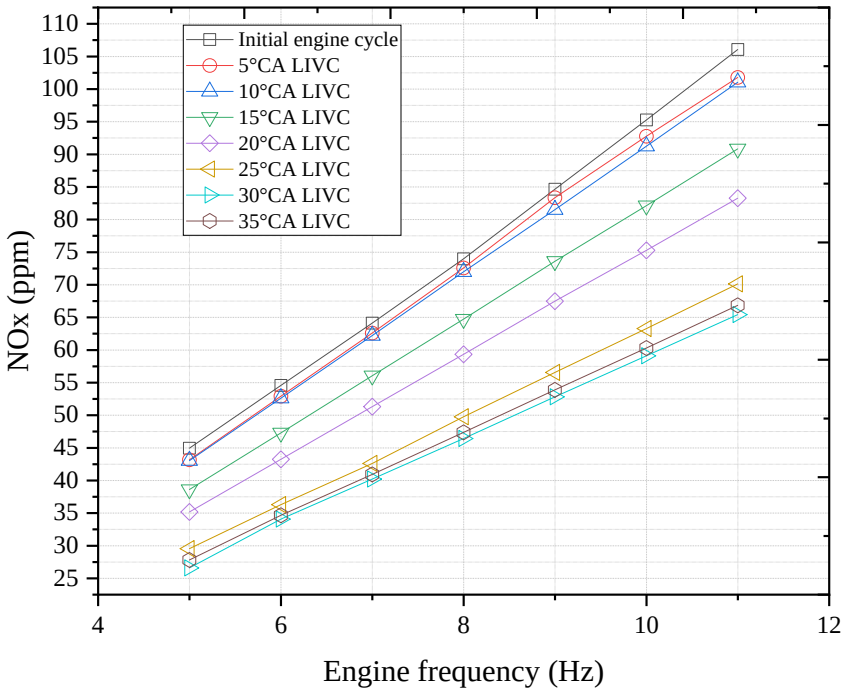

Figure 6.19 NOx emission comparison of different LIVC angles

6.3.2.1.3 Ethanol free-piston engine

Figure 6.20 shows the comparison of NOx of different early/late intake valve closing angles of

EIVC or LIVC. The rising regulation is similar with other engines, NOx emission increases with the increase of engine frequency. However, in this ethanol free-piston engine, 20°CA LIVC produced the lowest amount of NOx and reduced 27.45% emission comparing with what produced by initial engine cycle at the engine frequency of 11Hz.

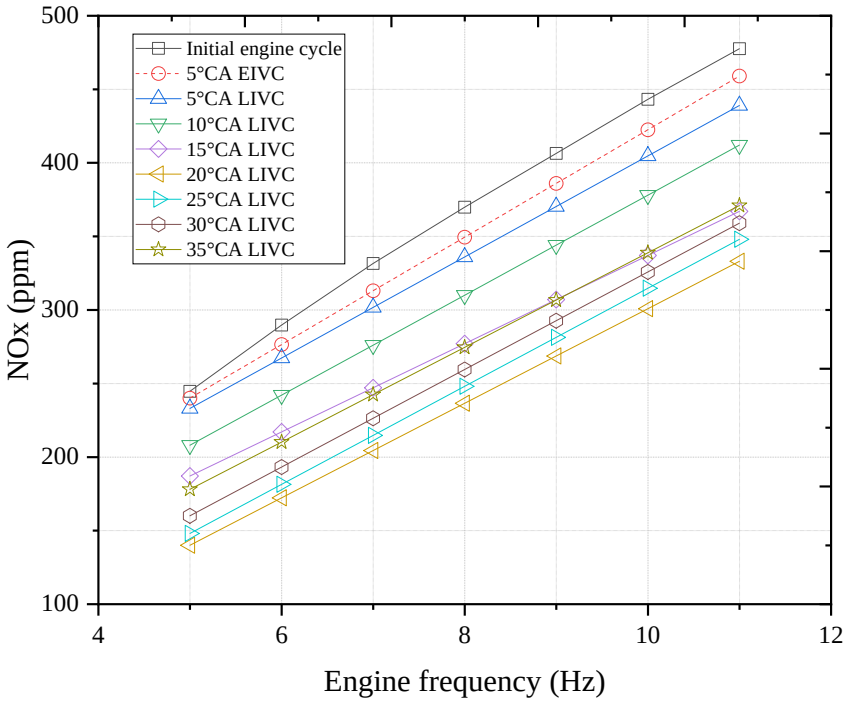

Figure 6.20 NOx emission comparison of different EIVC and LIVC

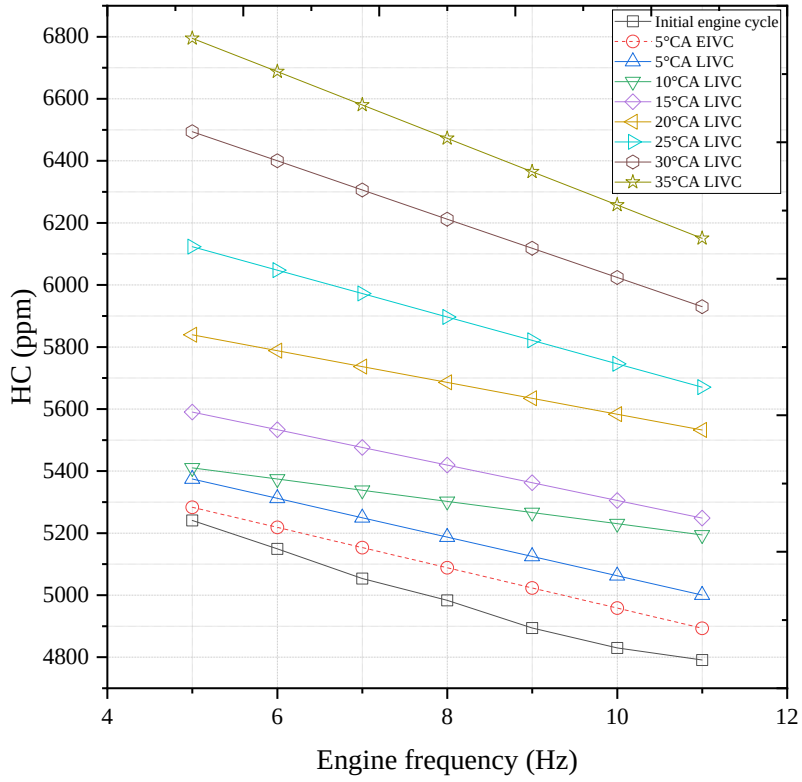

Figure 6.21 HC emission comparison of different EIVC and LIVC

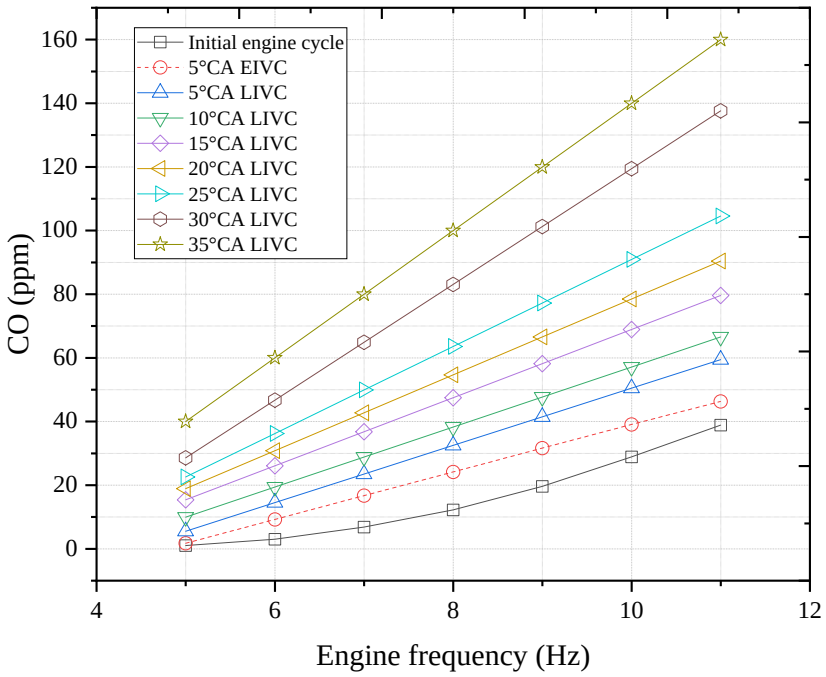

Figure 6.22 CO emission comparison of different EIVC and LIVC

Figure 6.21 and Figure 6.22 illustrated comparisons of HC and CO of different EIVC and LIVC early/late intake valve closing angles. For both hydrocarbon and carbon monoxide emissions, Miller cycle would always cause negative effects. For instance, 35°CA LIVC has brought an increase of 29.67% to HC emission at the engine frequency of 5Hz and 311.72% to CO emission at the engine frequency of 11Hz. Nothing is given without a disadvantage in it, while the benefit like significant reduction to NOx is obtained, disadvantages such as slightly lower indicated efficiency, higher fuel consumption, higher hydrocarbon and carbon monoxide emission would have to accept simultaneously.

6.4 Summary

A series of Miller cycle engine models including gasoline free-piston engine, hydrogen free-piston engine and ethanol free-piston engine have been presented in this Chapter, and different Miller cycle types including early intake valve closure (EIVC) and late intake valve closure (LIVC) have been tested separately. On the aspect of engine performance, Miller cycle would inevitably cause a decrease to output power and increase brake specific fuel consumption simultaneously, therefore, turbocharger, in purpose of increase output power back to the initial level has been applied.

On the two-stroke gasoline free-piston engine, brake specific fuel consumption has been risen 65% at the late intake valve closing angle of 35°CA. Though the early intake valve closing angle of EIVC larger than 5°CA would reduce indicated power to an extremely low level, 5°CA EIVC is still working and its NOx reducing ability is even more remarkable than most of conditions of LIVC, which has reduced 30.9% NOx at the engine frequency of 11Hz. EIVC produced the highest amount of HC emission (increased 5.5% at 11Hz) even comparing with all types of LIVC while 5°CA LIVC produced the lowest, which was even lower than the amount produced by initial engine cycle. 15°CA LIVC produced the largest amount of emission while 5°CA EIVC produced the smallest.

On the hydrogen free-piston engine, 29.7% indicated efficiency was reduced at the late intake valve closing angle of 35°CA. For all engine frequencies that have been tested, 30°CA LIVC has constantly presented its remarkable NOx reducing ability and reduced 38.3% NOx emission at the engine frequency of 11Hz. With the late intake valve closing angle continuously risen up, the amount of NOx appears a phenomenon of increase. Due to the fuel speciality of hydrogen, no HC or CO

emission would be produced in this free-piston engine.

On the ethanol free-piston engine, both EIVC and LIVC brought a certain extent of increase to fuel consumption, and the range of increase that made by 35°CA LIVC reached 78.3% at the engine frequency of 5Hz. Slight larger of the early/late intake valve closing angle would causes slight reduction on the indicated efficiency, and the largest decrease occurs at the engine frequency of 5Hz as well, indicated efficiency was reduced 21.62% from the value of 40.77% to 31.95%. 20°CA LIVC produced the lowest amount of NOx and reduced 27.45% emission comparing with what produced by initial engine cycle at the engine frequency of 11Hz. 35°CA LIVC has brought an increase of 29.67% to HC emission at the engine frequency of 5Hz and 311.72% to CO emission at the engine frequency of 11Hz.

In summary, Miller cycle is only a remarkable tool to reduce NOx emission, but a series of negative effect such as lower output power, higher fuel consumption and higher carbon emission would follow. For hydrogen free-piston engine, the advantage of Miller cycle could be enlarged to the best since there's no carbon emission but only NOx to concern. For gasoline/ethanol engines, the advantage of applying Miller cycle is slightly smaller due to its cost. However, if turbocharger and suitable Miller cycle application could be matched up, Miller cycle is still valuable because of its incredibly NOx emission reducing ability.

Chapter 7. Conclusions and future research

This thesis has presented and described different types of free-piston engine model and the effect of Miller cycle application on these different engine models. In this chapter, the important findings and contributions will be summarised and relevant recommendations for future work will be discussed.

7.1 Summary of the findings

Chapter 2 covered the findings from researchers on free-piston engine technology in terms of its parameters, emission performances and challenges as well as the history and application of Miller cycle. Since investigations on emission is the main purpose of this thesis, categories of common engine emissions such as NOx, HC and CO have been introduced, and series of effects of the free-piston engine and Miller cycle on emission performance have been reviewed and integrated.

In Chapter 3, four main simulation models were developed using one-dimensional simulation tools. Both crankshaft models were validated while the two-stroke crankshaft model was optimised and tuned for performance before being converted into the two-stroke free-piston engine model. This was done by using the imposed-piston motion (IPM) sub-model. It was found that, due to different piston motion profiles, different valves timings are required for this model. Further, it was necessary to have directional tracking (i.e., towards TDC or away from TDC) due to the lack of crank-angle degree positioning in free-piston engine. The motion profiles generated from the dynamic equation were found insufficient to produce optimal resolution for thorough performance investigations.

In Chapter 4, a two-stroke hydrogen free-piston engine has been developed based on the baseline model described in Chapter 3. This Chapter narrated the whole process of modelling, validation, implementation and simulation. Two MATLAB models were built for the purpose of heat release rate and cumulative heat release calculation. The main emission on the hydrogen free-piston engine is NOx only, therefore, NOx emission performance has been emphasized. It has been found that from conventional spark-ignition engine to the free-piston engine, under the same engine scale and operation conditions, NOx emission is hugely reduced by the later and the highest range of 57.37% occurs at the engine frequency of 6Hz. Taking hydrogen as the fuel of the free-piston engine would slightly produce more NOx than gasoline, but the increasing range is relatively small especially at

low engine frequency stage (1.4% at 5Hz and 10.97% at 11Hz). NOx emission in hydrogen free-piston engine has been deeply investigated. The relationship between NOx formation and equivalent ratio was obtained as well: $\varphi = 0.5$ is the obvious demarcation point of the formation of NOx; when $\varphi < 0.5$, it doesn't affect NOx much; when $0.5 < \varphi < 0.88$, NOx increases with the increase of φ and reaches the highest point at $\varphi = 0.88$; when $0.88 < \varphi < 1.2$, NOx sharply decreases with the increasing φ.

In chapter 5, firstly presented essential theories of taking ethanol or ethanol-gasoline blend as fuel on the free-piston engine, vital factors that affected by ethanol like compression ratio, engine loads, engine speed and equivalence ratio have been investigated, secondly, series of ethanol-gasoline blend free-piston engine models have been developed. This Chapter narrated the whole process of modelling, validation, implementation and simulation. One MATLAB/Simulink model has been built in order to obtain the piston motion that could be applied into Ricardo WAVE models. In the end, engine performance along with emission performance on the ethanol-gasoline blend free-piston engine have been investigated. Comparing with gasoline fuel, pure ethanol (E100) presented impressive ability in emission reducing: NOx emission was reduced by 28.72% at the engine frequency of 8Hz, CO emission was significantly reduced by 75.14% at the engine frequency of 11Hz and HC emission was also reduced by 17.89% at the engine frequency of 5Hz.

In Chapter 6, the conception of Miller cycle and its implementation methods on conventional engine and the free-piston engine have been presented. Also, huge amount of simulation models has been built by Ricardo WAVE, and Miller cycle on conventional diesel engine, gasoline free-piston engine, hydrogen free-piston engine and ethanol free-piston engine has been investigated separately. Method of applying turbocharger has been described. On the two-stroke gasoline free-piston engine, brake specific fuel consumption has been risen 65% at the late intake valve closing angle of 35°CA. Though the early intake valve closing angle of EIVC larger than 5°CA would reduce indicated power to an extremely low level, 5°CA EIVC is still working and its NOx reducing ability is even more remarkable than most of conditions of LIVC, which has reduced 30.9% NOx at the engine frequency of 11Hz. On the hydrogen free-piston engine, 29.7% indicated efficiency was reduced at the late intake valve closing angle of 35°CA. For all engine frequencies that have been tested, 30°CA LIVC has constantly presented its remarkable NOx reducing ability and reduced 38.3% NOx

emission at the engine frequency of 11Hz. On the ethanol free-piston engine, both EIVC and LIVC brought a certain extent of increase to fuel consumption, and the range of increase that made by 35°CA LIVC reached 78.3% at the engine frequency of 5Hz. In summary, Miller cycle is only a remarkable tool to reduce NOx emission, but a series of negative effect such as lower output power, higher fuel consumption and higher carbon emission would follow. For hydrogen free-piston engine, the advantage of Miller cycle could be enlarged to the best since there's no carbon emission but only NOx to concern. For gasoline/ethanol engines, the advantage of applying Miller cycle is slightly smaller due to its cost. However, if turbocharger and suitable Miller cycle application could be matched up, Miller cycle is still valuable because of its incredibly NOx emission reducing ability.

7.2 Significant contributions and findings

Through careful readings on huge number of existing literatures, it has been found though plenty of researches have been done on the free-piston engine, investigation on the emission performance of the free-piston engine, investigation on the ethanol free-piston engine is still blank, moreover, Miller cycle has barely been applied on the free-piston engine. Thus, these specific areas have been considered as the core focus in this thesis. Through descriptions in Chapter 5 and Chapter 6, engine performance along with emission performance on the ethanol-gasoline blend free-piston engine and the effects of Miller cycle have been obtained. Ethanol, because of its fuel specialty, could significantly reduce NOx and maintain the same engine output simultaneously. And since the valve timing of each model were pre-set to a relatively most suitable condition, Miller cycle has not presented much advantages, but if we focus on the NOx emission, Miller cycle could be considered as the best method of NOx reduction.

7.3 Recommendations for further research

7.3.1 Practice experiment

The whole researches in this thesis were done by computational simulation work, though models have all been validated by experiments, all conditions have been considered as ideal, real conditions in experiments and errors might occur are something that can't be considered in simulation, thus, results will not as precise as in real experiments.

7.3.2 Co-simulation

The limitations of using the imposed piston motion sub-model (IPM) were highlighted in Section 5.2.2. Therefore, it is proposed that a co-simulation model is developed by coupling the dynamics model with the one-dimensional engine model. In this way, the free-piston engine generator motion trajectory is continuously updated from dynamics model while the cyclic speed and stroke is being updated in the engine model. The co-simulation will enable the study of motion control, misfire and knock to be conducted.

7.3.3 Miller cycle valve timing

Methodology on applying Miller cycle in the free-piston engine was to consider the free-piston engine a conventional crank engine, then convert its early/late valve closing angle to corresponding time in a free-piston engine cycle. This was due to the limitation of Ricardo WAVE: valve timing has to been defined as crank angles.

Reference

[1]Bae C, Kim J. Alternative fuels for internal combustion engines. Proc Combust Inst 2017;36(3):3389-413.

[2]Dimitriou P, Tsujimura T. A review of hydrogen as a compression ignition engine fuel Int J Hydrogen Energy 2017;42(38):24470-86.

[3]Sun ZY, Liu FS, Liu XH, Sun BG, Sun DW. Research and development of hydrogen fuelled engines in China. Int J Hydrogen Energy 2012; 23:664-81.

[4]Elkelawy M, Bastawissi HA. Numerical study on the hydrogen fueled SI engine combustion optimization through a combined operation of DI and PFI strategies. Energy Power Eng 2013; 5:513-22.

[5]transport@eti.co.uk. (2013, 05 December). An insight report by the Energy Technologies Institute. Available: www.eti.co.uk

[6]R. Mikalsen and A. P. Roskilly, "A review of free-piston engine history and applications," Applied Thermal Engineering, vol. 27, pp. 2339-2352, Oct 2007.

[7]J. Hansson and M. Leksell., "Performance of a Series Hybrid Electric Vehicle with a Free-Piston Energy Converter," 2006.

[8]R. Stone, Introduction to Internal Combustion Engines, Third Edition ed. Warrendale, Pa.: Society of Automotive Engineers, Inc., 1999.

[9]J. B. Heywood, McGraw-Hill International, 1988.

[10]Peter Van Blarigan, Nicholas Paradiso, Scott Goldsborough, Homogeneous charge compression ignition with a free piston: A new approach to ideal otto cycle performance. 1998, SAE Technical Paper, No. 982484.

[11]Christopher M. Atkinson, Sorin Petreanu, Nigel Clark, Richard J. Atkinson, Thomas I. McDaniel, Subhash Nandkumar, Parviz Famouri, Numerical simulation of a two-stroke linear engine-alternator combination. 1999, SAE Technical Paper, No. 1999-01-0921.

[12]S. Scott Goldsborough, Peter Van Blarigan, Optimizing the scavenging system for a two-stroke cycle, free piston engine for high efficiency and low emissions: A computational approach. 2003, SAE Technical Paper, No. 2003-01-0001.

[13]Qingfeng Li, Jin Xiao, Zhen Huang, Simulation of a two-stroke free-piston engine for electrical power generation. Energy & fuels, 2008. 22(5): p. 3443-3449.

[14]Researcher Seppo Tikkanen, Professor Matti Vilenius. Hydraulic free piston engine-the power unit of the future? in Proceedings of the JFPS International Symposium on Fluid Power. 1999. The Japan Fluid Power System Society.

[15]Gautam Kalghatgi, Is it really the end of internal combustion engines and gasolineeum in transport? Appl. Energy 225 (2018) 965–974.

[16]Jinxing Zhao, Research and application of over-expansion cycle (Atkinson and Miller) engines-A review, Appl. Energy 185 (2017) 300–319.

[17]Nguyen Ba Hung, Ocktaeck Lim, A review of free-piston linear engines, Appl. Energy 178 (2016) 78–97.

[18]M. Razali Hanipah, R. Mikalsen, A.P. Roskilly, Recent commercial free-piston engine developments for automotive applications, Appl. Thermal Eng. 75 (2015) 493–503.

[19]Yingcong Zhou, Aimilios Sofianopoulos, Benjamin Lawler, Sotirios Mamalis, Advanced combustion free-piston engines A comprehensive review, Int. J. Engine Res. 21 (2018) 1205–1230.

[20]Zhenfeng Zhao, Fujun Zhang, Ying Huang, Changlu Zhao, An experimental study of the cycle stability of hydraulic free-piston engines, Appl. Therm. Eng. 54 (2013) 365–371.

[21]Shahryar Zare, AliReza Tavakolpour-Saleh, Free piston Stirling engines A review, Int. J. Energy Res. (2019) 1–32.

[22]Chris Mi, M. Abul Masrur, and D. W. Gao., Hybrid Electric Vehicles: Principles and Applications with Practical Perspectives: John Wiley & Sons, Ltd, 2011.

[23]W. Arshad, "A Low-Leakage Linear Transverse-Flux Machine for a Free-Piston Generator,"

Elektrotekniska system, Stockholm, 2003.

[24]H. T. Aichlmayr, "Design Considerations, Modelling and Analysis of Micro-Homogeneous Charge Compression Ignition Combustion Free-Piston Engines.," Ph.D. Thesis, UNIVERSITY OF MINNESOTA, 2002.

[25]P. A. J. Achten, "A review of free piston engine concepts," Society of Automotive Engineers Transactions, 1994.

[26]T. J. Callahan1 and S. K. Ingram2, "Free-piston Engine Linear Generator for Hybrid vehicles modelling study," 1Southwest Research Institute, San Antonio, Texas & 2UT/Center for Electromechanics, The University of Texas, Austin, Texas, Interim Report, 1995.

[27]P. V. Blarigan, N. Paradiso, and S. S. Goldsborough, "Homogeneous Charge Compression Ignition with a Free Piston: A New Approach to Ideal Otto Cycle Performance," SAE International, vol. 982484, 1998.

[28]Alternative fuels data center, reported by U.S. department of energy. Available at: www.afdc.energy.gov/fuels/hydrogen.html

[29]R. Mikalsen, A. P. Roskilly, The design and simulation of a two-stroke free-piston compression ignition engine for electrical power generation. Applied Thermal Engineering, 2008. 28(5): p. 589-600.

[30]H.O. Farmer, Free-piston compressor-engines, Proceedings of Institute of Mechanical Engineering 156 (1947) 253–271.

[31]R.P. Pescara, Motor compressor of the free piston type, US Patent 2,241,957, 1941.

[32]R.P. Pescara, Motor compressor apparatus, US Patent 1657641, 1928.

[33]A.L. London, A.A. Oppenheim, The free-piston engine development-present status and design aspects, Trans. ASME 74 (1952) 1349–1361.

[34]W.T. Toutant, The WorthingTon-Junkers free-piston air compressor, 64(1952) 583–594.

[35]Norman H. Beachley, Frank J.Fronczak, Design of a free-piston engine-pump, SAE paper, 1992,

921740.

[36]D.H. Specht, Evalutaion of free piston-gas turbine marine propulsion machinery in GTS William Patterson, SAE National Powerplant Meeting 620280, 1962.

[37]Donald N. Frey, Paul Klotsch, Adolph Egli, The automotive free-piston-turbine engine, SAE Trans. 65 (1957) 628–634.

[38]Huber, Present state and future outlook of the free-piston engine, Trans. ASME 80 (1958) 1779–1790.

[39]Chendong Guo, et al., Advances in free-piston internal combustion engines: A comprehensive review, Applied Thermal Engineering 189 (2021) 116679

[40]Guo, C., Feng, H., Jia, B., Zuo, Z., Guo, Y. and Roskilly, T., 2017. Research on the operation characteristics of a free-piston linear generator: Numerical model and experimental results. Energy Conversion and Management, 131, pp.32-43.

[41]Feng, H., Guo, C., Jia, B., Zuo, Z., Guo, Y. and Roskilly, T., 2016. Research on the intermediate process of a free-piston linear generator from cold start-up to stable operation: Numerical model and experimental results. Energy Conversion and Management, 122, pp.153-164.

[42]Feng, H., Guo, C., Yuan, C., Guo, Y., Zuo, Z., Roskilly, A. and Jia, B., 2016. Research on combustion process of a free piston diesel linear generator. Applied Energy, 161, pp.395-403.

[43]P. Famouri et al., "Design and testing of a novel linear alternator and engine system for remote electrical power generation," IEEE Power Engineering Society. 1999 Winter Meeting (Cat. No.99CH36233), 1999, pp. 108-112 vol.1, doi: 10.1109/PESW.1999.747434.

[44]Cawthorne, W., Famouri, P., Jingdong Chen, Clark, N., McDaniel, T., Atkinson, R., Nandkumar, S., Atkinson, C. and Petreanu, S., 1999. Development of a linear alternator-engine for hybrid electric vehicle applications. IEEE Transactions on Vehicular Technology, 48(6), pp.1797-1802.

[45]W. Cawthorne, P. Famouri and N. Clark, "Integrated design of linear alternator/engine system for HEV auxiliary power unit," IEMDC 2001. IEEE International Electric Machines and Drives Conference (Cat. No.01EX485), 2001, pp. 267-274, Doi:

10.1109/IEMDC.2001.939310.

[46]Talyor, Samuel, Free-Piston Diesel-Fuelled Linear Alternator for Auxiliary Power Unit Applications, Report, West Virginia University, 1996.

[47]E. Shoukry, S. Taylor, N. Clark, and P. Famouri, "Numerical Simulation for Parametric Study of a Two-Stroke Direct Injection Linear Engine," Engine Modeling Techniques: SI and Diesel, SAE TECHNICAL, vol. 2002-01-1739, 2002.

[48]Mattew C. Robinson, Nigel N. Clark, Study on the use of springs in a dual free piston engine alternator, SAE Technical Paper Series, 2016-01-2233.

[49]Mattew C. Robinson, Nigel N. Clark Effect of combustion timing and heat loss on spring-assisted linear engine translator motion SAE Int. J. Engines, 9 (2016), pp. 546-564

[50]Mehar Bade, Nigel Clark, Parviz Famouri, PriyaankaDevi Guggilapu, Feasibility of Multiple Piston Motion Control Approaches in a Free Piston Engine Generator, SAE Technical Paper Series, 2019-01-2599.

[51]Peter Van Blarigan, Advanced internal combustion engine research, in: Proceedings of the 2000 DOE Hydrogen Program Review, 2000, pp. 19.

[52]Peter Vam Blarigan, Aadvanced internal combustion electric generator, in: Proceedings of the 2002 U.S. DOE Hydrogen Program Review, 2002.

[53]S. Scott Goldsborough, Peter Van Blarigan A numerical study of a free piston IC engine operating on homogeneous charge compression ignition combustion SAE Trans. (1999), p. 990619

[54]Peter Van Blarigan Developing a Thermodynamic Fuel Cell, Hydrogen Fuel Cells, and Infrastructure Technologies (2003)

[55]S. Scott Goldsborough, Peter Van Blarigan, Optimizing the Scavenging System for a Two-Stroke Cycle, Free Piston Engine for High Efficiency and Low Emissions, SAE Transactions, 2003-01-0001.

[56]Peter Van Blarigan, Nicholas Paradiso, Scott Goldsborough Homogeneous charge compression

ignition with a free piston_ a new approach to ideal otto cycle performance SAE Trans. (1998), p. 982484

[57]Terry A. Johnson, Michael T. Leick, Ronald.W. Moses, Experimental Evaluation of a Prototype Free Piston Engine - Linear Alternator (FPLA) System, SAE Technical Paper Series, 2016-01-0677.

[58]Jörgen Hansson, Mats Leksell, Fredrik Carlsson, Minimizing Power Pulsations in a Free Piston Energy Converter, in: 2005 European Conference on Power Electronics and Applications, 2005.

[59]Jakob Fredriksson, Ingemar Denbratt, Simulation of a two-stroke free piston engine, SAE Technical Paper Series, 2004-01-1871.

[60]D. Svechkarenko, A. Cosic, J. Soulard, C. Sadarangani Transverse flux machines for sustainable development - road transportation and power generation Proceeding 7th International Conference on Power Electronics and Drive Systems (2007), pp. 1108-1114

[61]Alija Cosic, Chandur Sadarangani, Fredrik Carlsson, A novel concept of a Transverse Flux Linear Free Piston Generator. Proc. of LDIA2005 318-321.

[62]Zheng Ping, Anyuan Chen, Peter Thelin, Waqas M. Arshad, Chandur Sadarangani Research on a tubular longitudinal flux PM linear generator used for free-piston energy converter IEEE Trans. Magn., 43 (2007), pp. 447-449

[63]Anyuan Chen, Waqas M. Arshad, Peter Thelin, Ping Zheng, Analysis and optimization of a longitudinal flux linear generator for hybrid electric vehicle applications, in: IEEE Symp. Vehicle Power and Propulsion, 2004.

[64]Jiabin Wang, David Howe A linear permanent magnet generator for a free-piston energy converter 2005 IEEE International Conference on Electric Machines and Drives (2005), pp. 1521-1528

[65]M. Jiabin Wang, David Howe West, Hector Zelaya-De La Parra, Waqas M. Arshad Design and experimental verification of a linear permanent magnet generator for a free-piston energy converter IEEE Trans. Energy Convers., 22 (2007), pp. 299-306

[66]J. Wang, W. Wang, R. Clark, K. Atallah, D. Howe A tubular flux-switching permanent magnet machine J. Appl. Phys., 103 (2008), p. 07F105

[67]J. Wang, D. Howe, Y. Amara Armature reaction field and inductances of tubular modular permanent magnet machines J. Appl. Phys., 97 (2005), p. 10Q504

[68]Jörgen Hansson, Mata Leksell, Fredrik Carlsso, Chandur Sadarangani, Operational Strategies for a free piston energy converter, in: Proceedings of the fifth International Symposium on Linear Drives for Industry Applications, Kobe-Awaji, Japan, 2005.

[69]Jörgen Hansson, Mats Leksell, Performance of a series hybrid electric vehicle with a free-piston energy converter, in: Proceedings of the 2006 IEEE Vehicle Power and Propulsion Conference 2006.

[70]Yimin Lu, Xiaofeng Huang, Z. Q. Zhu, Direct power control of a permanent magnet linear generator in a free piston energy converter, in: Electrical Machines and Systems, 2008, pp. 3636–3639.

[71]A. Cosic, J.Lindback, W. M. Arshad, M. Leksell, P. Thelin, E. Nordlun, Application of a free-piston generator in a series hybrid vehicle, in: Proceedings of the 4th International Symposium on Linear Drives for Industry Applications, 2003.

[72]Němeček, Pavel, Šindelka Michal, Vysoký Ondrej, Modeling and control of free piston generator, in: IFAC Symposium on Advances in Automotive Control, 2004, pp. 320–325.

[73]S. Plsek, P. Deutsch, O. Vysoky, Validation of the linear combustion engine model, Bratislava, 2007.

[74]P. Němeček, O. Vysoký, Control of two stroke free piston generator, in: Proceedings of the 6th Asian Control Conference, 2006.

[75]Pavel Němeček, Michal Sindelka, O. Vysoký Ensuring steady operation of free piston generator Systemics, Cybernetics Informat., 4 (2003), pp. 19-23

[76]R. Mikalsen, A.P. Roskilly Performance simulation of a spark ignited free-piston engine generator Appl. Therm. Eng., 28 (2008), pp. 1726-1733

[77]R. Mikalsen, A.P. Roskilly Coupled dynamic–multidimensional modelling of free-piston engine combustion Appl. Energy, 86 (2009), pp. 89-95

[78]R. Mikalsen, A.P. Roskilly, The fuel efficiency and exhaust gas emissions of a low heat rejection free-piston diesel engine Proc. Inst. Mech. Eng., Part A J. Power Energy, 223 (2009) (2009), pp. 379-386

[79]Boru Jia, Rikard Mikalsen, Andrew Smallbone, Anthony Paul Roskilly A study and comparison of frictional losses in free-piston engine and crankshaft engines Appl. Therm. Eng., 140 (2018), pp. 217-224

[80]Boru Jia, Andrew Smallbone, Zhengxing Zuo, Huihua Feng, Anthony Paul Roskilly Design and simulation of a two- or four-stroke free-piston engine generator for range extender applications Energy Convers. Manage., 111 (2016), pp. 289-298

[81]R. Mikalsen, E. Jones, A.P. Roskilly Predictive piston motion control in a free-piston internal combustion engine Appl. Energy, 87 (2010), pp. 1722-1728

[82]R. Mikalsen, A.P. Roskilly, The control of a free-piston engine generator. Part 1 Fundamental analyses Appl. Energy, 87 (2010), pp. 1273-1280

[83]R. Mikalsen, A.P. Roskilly, The control of a free-piston engine generator. Part 2 Engine dynamics and piston motion control Appl. Energy, 87 (2010), pp. 1281-1287

[84]Boru Jia Andrew Smallbone Huihua Feng Guohong Tian Zhengxing Zuo A.P. Roskilly A fast response free-piston engine generator numerical model for control applications Applied Energy 162 2016 321-329.

[85]Boru Jia, Rikard Mikalsen, Andrew Smallbone, Zhengxing Zuo, Huihua Feng, Anthony Paul Roskilly Piston motion control of a free-piston engine generator A new approach using cascade control Appl. Energy, 179 (2016), pp. 1166-1175

[86]Florian Kock, Johannes Haag, Horst E. Friedrich, The Free Piston Linear Generator - Development of an Innovative, Compact, Highly Efficient Range-Extender Module, SAE Technical Paper Series, 2013-01-1727.

[87]Johannes Haag, Cornelius Ferrari, Jan Hendrik Starcke, Michael Stohr, Uwe Riedel, Numerical and Experimental Investigation of In-Cylinder Flow in a Loop-Scavenged Two-Stroke Free Piston Engine, SAE Technical Paper Series, 2012-32-0114.

[88]Johannes Haag, Florian Kock, Marco Chiodi, Olive Mack, Michael Bargende, Development Approach for the Investigation of Homogeneous Charge Compression Ignition in a Free-Piston Engine, SAE Technical Paper Series, 2013-24-0047.

[89]Stephan Schneider, Horst. E. Friedrich, Experimental Investigation and Analysis of Homogeneous Charge Compression Ignition in a Two-Stroke Free-Piston Engine, SAE Technical Paper Series, 2015-32-0706.

[90]Schneider Schneider, Marco Chiodi, Michael Bargende, Development and Experimental Investigation of a Two-Stroke Opposed-Piston Free-Piston Engine, SAE Technical Paper Series, 2016-32-0046.

[91]Stephan Schneider, Horst Friedrich, Marco Chiodi, Michael Bargende, Analysis of SI and HCCI Combustion in a Two-Stroke Opposed-Piston Free-Piston Engine, SAE Technical Paper Series, 2017-32-0037.

[92]Douglas Carter, Edward Wechner, The Free Piston Power Pack_ Sustainable Power for Hybrid Electric Vehicles, SAE technical paper series, 2003-01-3277.

[93]Jaeheun Kim, Choongsik Bae, Gangchul Kim, The Effects of Spark Timing and Equivalence Ratio on Spark-Ignition Linear Engine Operation with Liquefied Gasolineeum Gas, SAE Technical Paper Series, 2012-01-0424.

[94]Nguyen Ba Hung, Ocktaech Lim, Norimasa Iida, The effects of key parameters on the transition from SI combustion to HCCI combustion in a two-stroke free piston linear engine Appl. Energy, 137 (2015), pp. 385-401

[95]Ocktaeck Lim, Nguyen Ba Hung, Oh Seokyoung, Gangchul Kim, Hanho Song, Norimasa Iida A study of operating parameters on the linear spark ignition engine Appl. Energy, 160 (2015), pp. 746-760

[96]Nguyen Ba Hung, Sung Jaewon, Ocktaeck Lim A study of the scavenging process in a two-stroke free piston linear engine using CFD Energy Procedia, 142 (2017), pp. 1353-1360

[97]Hung Nguyen Ba, Ocktaeck Lim, Simulation Study of SI-HCCI Transition in a Two-Stroke Free Piston Engine Fuelled with Propane, SAE Technical Paper Series, 2014-01-1104.

[98]Hidemasa Kosaka, Tomoyuki Akita, Kazunari Moriya, Shigeaki Goto, Yoshihiro Hotta, Takaji Umeno, Kiyomi Nakakita, Development of Free Piston Engine Linear Generator System Part 1 - Investigation of Fundamental Characteristics, SAE Technical Paper Series, 2014-01-1203.

[99]Hidemasa Kosaka, Tomoyuki Akita, Kazunari Moriya, Shigeaki Goto, Yoshihiro Hotta, Takaji Umeno, Kiyomi Nakakita, Development of Free Piston Engine Linear Generator System Part 1 - Investigation of Fundamental Characteristics, SAE Technical Paper Series, 2014-01-1203.

[100]Shigeaki Got, Kaznunari Moriya, Hidemasa Kosaka, Tomoyuki Aktita, Yoshihiro Hotta, Takaji Umeno, Kiyomi Nakakita, Development of Free Piston Engine Linear Generator System Part 2 - Investigation of Control System for Generator, SAE Technical Paper Series, 2014-01-1193.

[101]Kaznunari Moriya, Shigeaki Gota, Tomoyuki Akita, Hidemase Kosaka, Yoshihiro Hotta, Kiyomi Nakakita, Development of Free Piston Engine Linear Generator System Part3 -Novel Control Method of Linear Generator for to Improve Efficiency and Stability, SAE Technical Paper Series, 2016-01-0685.

[102]Chia-Jui Chiang, Jing-Long Yang, Shao-ya Lan, Tsung-Wei Shei, Wen-She Chiang, Bo-Liang Chen Dynamic modeling of a SI/HCCI free-piston engine generator with electric mechanical valves Appl. Energy, 102 (2013), pp. 336-346

[103]N.A.N. Mohamed, A.K. Ariffin, S. Fonna Simulation of a two-stroke spark ignition free piston linear engine motion Jurnal Teknologi (2006), pp. 27-40

[104]Ahmad Kamal Ariffin, Nik Abdullah Nik Mohamed, Syarizal Fonna Simulation of free piston linear engine motion with different intake and exhaust port positions Jurnal Kejuruteraan (2005), pp. 97-106

[105]M.M. Rahman, A.K. Ariffin, N. Jamaludin, C.H.C. Haron Duribility assement of a new free

piston spark ignition linear engine a computational approach Jurnal Teknologi (2006), pp. 81-102

[106]Saiful A. Zulkifli, Mohd N. Karsiti, A. Rashid, A. Aziz Starting of a free-piston linear engine-generator by mechanical resonance and rectangular current commutation IEEE Vehicle Power and Propulsion Conference (VPPC) (2008)

[107]Abdulwehab A. Ibrahim, A. Rashid, A. Aziz, Ezran Zharif B. Zainal Abidin, Saiful A. Zulkifli The operation of free piston linear generator engine using MOSFET and IGBT drivers J. Appl. Sci., 11 (2011), pp. 1791-1796

[108]Ezrann Zharif Zainal Abidin, Abdulwehab A. Ibrahim, A. Rashid, A. Aziz, Saiful A. Zulkifli Investigation of starting behaviour of a free-piston linear generator J. Appl. Sci., 12 (2012), pp. 2592-2594

[109]Abdulwehab A. Ibrahim, Zharif B. Ezrann, A. Zainal Abidin, Rashid A. Aziz, Saiful A. Zulkifli, Mohd N. Karsiti, A. Rashid, A. Aziz Effect of injection timing on the operation of hydrogen-fuelled free-piston linear generator engine during starting Int. J. Automotive Eng., 4 (2011), pp. 47-53

[110]Peng Sun, Fei Zhao, Chi Zhang, Jie Zhang, Jinhua Chen, Dynamic simulation of a novel free-piston linear generator, in: IEEE International Conference on Advanced Intelligent Mechatronics (AIM), 2015, pp. 1641–1646.

[111]Peng Sun, Chi Zhang, Jinhua Chen, Fei Zhao, Youyong Liao, Guilin Yang, Chinying Chen Decoupling design and verification of a free-piston linear generator Energies, 9 (12) (2016)

[112]Peng Sun, Chi Zhang, Lianlian Mao, Dequan Zen, Fei Zhao, Jinhua Chen, Coupling thermodynamics modelling and analysis of a free piston linear generator range extender for HEVs, in: IEEE 11th Conference on Industrial Electronics and Applications, 2016, pp. 405–410.

[113]Peng Sun, Chi Zhang, Lianlian Mao, Dequan Zeng, Fei Zhao, Jinhua Chen, Fault recovery control strategy of a two-stroke free piston linear generator, in: 2016 Eleventh International Conference on Ecological Vehicles and Renewable Energies (EVER), 2016.

[114]Peng Sun, Chi Zhang, Jinhua Chen, Fei Zhao, Youyong Liao, Gulin Yang, Chinyin Chen Hybrid system modeling and full cycle operation analysis of a two-stroke free-piston linear generator Energies, 10 (2) (2017)

[115]Chenheng Yuan, Xu. Jing, Yituan He Performance characteristics analysis of a hydrogen fueled free-piston engine generator Int. J. Hydrogen Energy, 41 (2016), pp. 3259-3271

[116]Chenheng Yuan, Yuan Jing, Chunzhi Liu, Yituan He, Effect of variable stroke on fuel combustion and heat release of a free piston linear hydrogen engine Int. J. Hydrogen Energy, 44 (2016), pp. 20416-20425

[117]Chenheng Yuan, Cuijie Han, Yang Liu, Yituan He, Yiming Shao, Xiaochun Jian Effect of hydrogen addition on the combustion and emission of a diesel free-piston engine Int. J. Hydrogen Energy, 44 (2018), pp. 13583-13593

[118]Jin Xiao, Qingfeng Li, Zhen Huang Motion characteristic of a free piston linear engine Appl. Energy, 87 (2010), pp. 1288-1294

[119]Jiming Lin, Xu. Zhaoping, Siqin Chang, Hao Yan Finite-time thermodynamic modeling and analysis of an irreversible Miller cycle working on a four-stroke engine Int. Commun. Heat Mass Transfer, 54 (2014), pp. 54-59

[120]Xu. Zhaoping, Siqin Chang Prototype testing and analysis of a novel internal combustion linear generator integrated power system Appl. Energy, 87 (2010), pp. 1342-1348

[121]Xu Zhaoping, Chang Siqin, Lin Jiming Piston motion control method of four-stroke free-piston generator Trans. Chinese Soc. Agric. Mach., 44 (2013), pp. 6-12

[122]Hao Yan, Dengqiang Wang, Zhaoping Xu, Design and Simulation of Opposed-Piston Four-Stroke Free-Piston Linear Generator, SAE Technical Paper Series, 2015-01-1277.

[123]Chendong Guo, Yu Song, Huihua Feng, Zhengxing Zuo, Boru Jia, Ziwei Zhang, A.P. Roskilly Effect of fuel injection characteristics on the performance of a free-piston diesel engine linear generator CFD simulation and experimental results Energy Convers. Manage., 160 (2018), pp. 302-312

[124]Boru Jia, Zhengxing Zuo, Guohong Tian, Huihua Feng, A.P. Roskilly Development and validation of a free-piston engine generator numerical model Energy Convers. Manage., 91 (2015), pp. 333-341

[125]Jinlong Mao, Zhengxing Zuo, Wen Li, Huihua Feng Multi-dimensional scavenging analysis of a free-piston linear alternator based on numerical simulation Appl. Energy, 88 (2011), pp. 1140-1152

[126]Yuxi Miao, Zhengxing Zuo, Huihua Feng, Yu. Chendong Guo, Boru Jia Song, Yuyao Guo Research on the combustion characteristics of a free-piston gasoline engine linear generator during the stable generating process Energies, 655 (2016), p. 9

[127]Chenheng Yuan, Huihua Feng, Yituan He, An experimental research on the combustion and heat release characteristics of a free-piston diesel engine generator Fuel, 188 (2017), pp. 390-400

[128]Boru Jia, Zhengxing Zuo, Huihua Feng, Guohong Tian, Andrew Smallbone, A.P. Roskilly Effect of closed-loop controlled resonance-based mechanism to start free piston engine generator Simulation and test results Appl. Energy, 164 (2016), pp. 532-539

[129]Boru Jia, Guohong Tian, Huihua Feng, Zhengxing Zuo, A.P. Roskilly, An experimental investigation into the starting process of free-piston engine generator Appl. Energy, 157 (2015), pp. 798-804

[130]Chunlai Tian, Huihua Feng, Zhengxing Zuo Load following controller for single free-piston generator Appl. Mech. Mater., 157 (2012), pp. 617-621

[131]C. Yuan, H. Feng, Y. He, J. Xu Combustion characteristics analysis of a free-piston engine generator coupling with dynamic and scavenging Energy, 102 (2016), pp. 637-649

[132]R. Mikalsen and A. P. Roskilly, The fuel efficiency and exhaust gas emissions of a low heat rejection free-piston diesel engine, Vol. 223 Part A: J. Power and Energy, DOI: 10.1243/09576509JPE653

[133]S.M. Sangeeta, M. Pande, M. Rani, R. Gakhar, M. Sharma, J. Rani, et al. Alternative fuels: an

overview of current trends and scope for future Renew Sustain Energy Rev, 32 (2014), pp. 697-712

[134]Y. Kalinci, A. Hepbasli, I. Dincer Biomass-based hydrogen production: a review and analysis Int J Hydrogen Energy, 34 (2008), pp. 8799-8817

[135]E. Kirtay Recent advances in production of hydrogen from biomass Energy Convers Manage, 52 (2011), pp. 1778-1789

[136]B.L. Salvi, K.A. Subramanian, N.L. Panwar alternative fuels for transpiration vehicles: a technical review Renew Sustain Energy Rev, 25 (2013), pp. 404-419

[137]S.M. Sangeeta, M. Pande, M. Rani, R. Gakhar, M. Sharma, J. Rani, et al. Alternative fuels: an overview of current trends and scope for future Renew Sustain Energy Rev, 32 (2014), pp. 697-712

[138]Afdc.energy.gov. 2022. Alternative Fuels Data Center: Hydrogen Basics. [online] Available at: <https://afdc.energy.gov/fuels/hydrogen_basics.html> [Accessed 9 February 2022].

[139]Woo Y, Lee Y, Lee Y. The performance characteristics of a hydrogen-fuelled free piston internal combustion engine and linear generator system. Int J Low-Carbon Technol2009;4(1):36-41.

[140]Woo Y, Lee Y. Free piston engine generator: technology review and an experimental evaluation with hydrogen fuel. Int J Automot Technol 2014;15(s):229-35.

[141]Blarigan PV, Paradiso N, Goldsborough S. Homogeneous charge compression ignition with a free piston: a new approach to ideal Otto cycle performance. In: SAE paper, No. 982484; 1998.

[142]Goldsborough S, Blarigan PV. A numerical study of a free piston IC engine operating on homogeneous charge compression ignition combustion. In: SAE paper, No. 990619; 1999.

[143]Zhang C, Sun Z. Trajectory-based combustion control for renewable fuels in free piston engines. Appl Energy 2017; 187:72-83.

[144]Zhang C, Li K, Sun Z. Modeling of piston trajectory-based HCCI combustion enabled by a free piston engine. Appl Energy 2015; 139:313-26.

[145]Yuan C, Xu J, He Y. Performance characteristics analysis of a hydrogen fueled free-piston engine generator. Int J Hydrog Energy 2016;41(4):3259-71.

[146]Miao Y, Zuo Z, Feng H, Guo C, Song Y, Jia B, et al. Research on the combustion characteristics of a free-piston gasoline engine linear generator during the stable generating process.

[147]Yuan C, Feng H, He Y, An experimental research on the combustion and heat release characteristics of a free-piston diesel engine generator. Fuel 2017; 188:390-400.

[148]Yuan C, Feng H, He Y, Xu J. Combustion characteristics analysis of a free-piston engine generator coupling with dynamic and scavenging. Energy 2016; 102:637-49.

[149]Aksu C, Kawahara N, Tsuboi K, Kondo M, Tomita E. Extension of PREMIER combustion operation range using split micro pilot fuel injection in a dual fuel natural gas compression ignition engine: a performance-based and visual investigation. Fuel 2016; 185:243-53.

[150]Wang Z, Zhao Z, Wang D, Tan M, Han Y, Liu Z, et al. Impact of pilot diesel ignition mode on combustion and emissions characteristics of a diesel/natural gas dual fuel heavy-duty engine. Fuel 2016; 167:248-56.

[151]Papagiannakis RG, Rakopoulos CD, Hountalas DT. Emission characteristics of high speed, dual fuel, compression ignition engine operating in a wide range of natural gas/diesel fuel proportions. Fuel 2010; 89:1397-406.

[152]Li W, Liu Z, Wang Z, Dou H, Wang C, Li J. Experimental and theoretical analysis of effects of equivalence ratio on mixture properties, combustion, thermal efficiency and exhaust emissions of a pilot-ignited NG engine at low loads. Fuel 2016; 171:125-35.

[153]H. Machrafi, S. Cavadias, J. Amouroux A parametric study on the emissions from an HCCI alternative combustion engine resulting from the auto-ignition of primary reference fuels Appl Energy, 85 (8) (2008), pp. 755-764

[154]S. Mousavi, R. Saray, K. Poorghasemi, A. Maghbouli A numerical investigation on combustion and emission characteristics of a dual fuel engine at part load condition Fuel, 166 (2016), pp. 309-319

[155]S. Cordiner, V. Rocco, R. Scarcelli, M. Gambino, S. Lannaccone Experiments and multi-dimensional simulation of dual-fuel diesel/natural gas engines SAE paper, No. 2007-24-0124 (2007)

[156]Yuan, C., Han, C. and Xu, J., 2017. Numerical evaluation of pilot-ignition technology used for a hydrogen fuelled free piston engine generator. International Journal of Hydrogen Energy, 42(47), pp.28599-28611.

[157]Yuan C, Feng H, He Y, Xu J. Effect of hydrogen addition on the combustion and emission of a diesel free-piston engine, international journal of hydrogen energy 43 (2018) 13583-13593

[158]Ngwaka, U., Smallbone, A., Jia, B., Lawrence, C., Towell, B., Roy, S., KV, S. and Roskilly, A., 2021. Evaluation of performance characteristics of a novel hydrogen-fuelled free-piston engine generator. International Journal of Hydrogen Energy, 46(66), pp.33314-33324.

[159]Van Blarigan P, Paradiso N, Goldsborough S. Homogeneous charge compression ignition with a free piston: a new approach to ideal otto cycle performance. SAE technic paper 982484; October 1998.

[160]DieselNet Technology Guide. What are diesel emissions. Available at https:// www.dieselnet.com/tech/emi_gas.php.

[161]Zeldovich YB, Sadovnikov PY, Frank-kamenetskii DA. Oxidation of nitrogen in combustion. Moscow-Leningrad: Academy of Sciences of USSR, Institute of Chemical Physics; 1947.

[162]Lehman, Clarence and Selin, Noelle Eckley. "biofuel". Encyclopedia Britannica, 15 Sep. 2021, https://www.britannica.com/technology/biofuel. Accessed 6 February 2022.

[163]"Transport biofuels". IEA. Archived from the original on 17 October 2020. Retrieved 18 October 2020.

[164]Afdc.energy.gov. 2022. Alternative Fuels Data Center: Ethanol Fuel Basics. [online] Available at: <https://afdc.energy.gov/fuels/ethanol_fuel_basics.html> [Accessed 9 February 2022].

[165]M. Balat, H. Balat Recent trends in global production and utilization of bio-ethanol fuel Appl Energy, 86 (2009), pp. 2273-2282

[166]A.K. Agarwal Biofuel (alcohols and biodiesel) applications as fuels for internal combustion engine Prog Energy Combust Sci, 33 (2007), pp. 233-271

[167]Hahn-Hägerdal, B., Galbe, M., Gorwa-Grauslund, M., Lidén, G. and Zacchi, G., 2006. Bio-ethanol – the fuel of tomorrow from the residues of today. Trends in Biotechnology, 24(12), pp.549-556.

[168]Guo, M., Song, W. and Buhain, J., 2015. Bioenergy and biofuels: History, status, and perspective. Renewable and Sustainable Energy Reviews, 42, pp.712-725.

[169]R. Stone, "Introduction to internal combustion engines," Basingstoke, UK, 1999.

[170]J. B. Heywood, Internal combustion engine fundamentals vol. 930: Mcgraw hill New York, 1988.

[171]T. Ma and H. Rajabu, "Computer Simulation of a Diesel-Atkinson Cycle Engine with Variable Timing Multi-Intake Valves and Variable Compression Ratio," IMechE C53/88, pp. 273-277, 1988.

[172]S. C. Blakey, R. J. Saunders, T. H. Ma, and A. Chopra, "A design and experimental study of a Diesel Atkinson cycle engine using late intake valve closing," SAE Technical Paper1991.

[173]D. L. Boggs, H. S. Hilbert, and M. M. Schechter, "The Diesel-Atkinson cycle engine-fuel economy and emissions results and hardware design," SAE Technical Paper1995.

[174]Y. Ge, L. Chen, F. Sun, and C. Wu, "Performance of an Atkinson cycle with heat transfer, friction and variable specific-heats of the working fluid," Applied Energy, vol. 83, pp. 1210-1221, 2006.

[175]Y. L. Ge, L. G. Chen, F. R. Sun, and C. Wu, "Performance of end reversible Atkinson cycle," Journal of the Energy Institute, vol. 80, pp. 52-54, 2007.

[176]S.-S. Hou, "Comparison of performances of air standard Atkinson and Diesel cycles with heat transfer considerations," Energy conversion and Management, vol. 48, pp. 1683-1690, 2007.

[177]J. Benajes, J. R. Serrano, S. Molina, and R. Novella, "Potential of Atkinson cycle combined with EGR for pollutant control in a HD diesel engine," Energy Conversion and Management,

vol. 50, pp. 174-183, 2009.

[178]A. Mozaffari, A. Ramiar , and A. Fathi, "Optimal design of classic Atkinson engine with dynamic specific heat using adaptive neuro-fuzzy inference system and mutable smart bee algorithm," Swarm and Evolutionary Computation, vol. 12, pp. 74-91, 2013.

[179]J. Zhao and M. Xu, "Fuel economy optimization of an Atkinson cycle engine using genetic algorithm," Applied Energy, vol. 105, pp. 335-348, 2013.

[180]P. Capaldi, "A high efficiency 10 kWe micro co-generator based on an Atkinson cycle internal combustion engine," Applied Thermal Engineering, vol. 71, pp. 913-920, 2014.

[181]R. H. Miller, "Supercharging and internal cooling cycle for high output," ASME Transactions, vol. 69, pp. 453-457, 1947.

[182]R. Miller and H. U. Lieberherr , "The Miller supercharging system for diesel and gas engines operating characteristics," in International Congress of Combustion Engine Conference, CIMAC, 1957, pp. 787-803.

[183]T. Ahmad and M. A. Theobald, "A survey of variable-valve-actuation technology," SAE Technical Paper1989.

[184]B. Bates, J. M. Dosdall, and D. H. Smith, "Variable Displacement by Engine Valve Control," SAE Technical Paper1978.

[185]T. W. Asmus, "Valve events and engine operation," SAE Technical Paper1982.

[186]M. Imperato, E. Antila, T . Sarjovaara, O. Kaario, M. Larmi, I. Kallio, et al., "NOx Reduction in a Medium-Speed Single-Cylinder Diesel Engine using Miller Cycle with Very Advanced Valve Timing," SAE Technical Paper2009.

[187]S. Niemi, J. Tö rnvall, M. Lauré n, and P. Nousiainen, "Optimization of Some Injection Parameters in a Common-Rail Non-Road Diesel Engine," SAE Technical Paper2009.

[188]O. M. Franç a, "Impact of the Miller Cycle in the Efficiency of an FVVT (Fully Variable Valve Train) Engine during Part Load Operation," SAE Technical Paper2009.

[189]L. Zhu, D.-x. Xue, and X.-g. Song, "Simulation of Working Process on a Medium speed High-power Diesel Engine," Science technology and Engineering, vol. 24, p. 013, 2011.

[190]F. Millo, M. G. Bernardi, and D. Delneri, "Computational analysis of internal and external EGR strategies combined with Miller cycle concept for a two-stage turbocharged medium speed marine diesel engine," SAE T echnical Paper2011.

[191]W. Qifu, C. Yi, D. Kangyao, W. Xinquan, and L. Xiang, "Design of Miller Cycle and Two Stage Turbocharging System on Marine Diesel," Diesel Engine, vol. 2, p. 010, 2012.

[192]K. Payrhuber , C. Trapp, and D. Chvatal, "The new J920 gas engine," PowerGen Europe, Milan, 2011.

[193]J. Blair and G. Bower, "Development of a Miller Cycle Powersports Engine," SAE T echnical Paper2014.

[194]D.-I. C.-P. Stö ber-Schmidt, D.-I. M. Pü schel, and D.-I. M. Drescher, "Exhaust gas recirculation for medium-speed diesel engines," MTZ industrial, vol. 1, pp. 72-77, 2011.

[195]D. Branyon and D. Simpson, "Miller cycle application to the scuderi split cycle engine (by downsizing the compressor cylinder)," SAE Technical Paper2012.

[196]M. Riess, A. Benz, M. Wö bke, and M. Sens, "Intake Valve Lift Strategies for Turbulence Generation," MTZ worldwide, vol. 74, pp. 42-47, 2013.

[197]E. Codan and T. Huber, "Application of two stage turbocharging systems on large engines," in 10th International Conference on Turbochargers and Turbocharging, 2012, p. 55.

[198]L. Miklanek, O. Vitek, O. Gotfryd, and V. Klir , "Study of unconventional cycles (Atkinson and Miller) with mixture heating as a means for the fuel economy improvement of a throttled SI engine at part load," SAE T echnical Paper2012.

[199]R. Ebrahimi, "Performance analysis of an irreversible Miller cycle with considerations of relative air–fuel ratio and stroke length," Applied Mathematical Modelling, vol. 36, pp. 4073-4079, 2012.

[200]R. Ebrahimi, "Thermodynamic modelling of performance of a Miller cycle with engine speed

and variable specific heat ratio of working fluid," Computers & Mathematics with Applications, vol. 62, pp. 2169-2176, 2011.

[201]K. Lehto, A. Elonheimo, H. Kari, T. Sarjovaara, and M. Larmi, "Emission reduction using hydro-treated vegetable oil (HVO) with Miller timing and EGR in diesel combustion," SAE Technical Paper2011.

[202]M. Imperato, A. Tilli, T. Sarjovaara, and M. Larmi, "Large-bore compression-ignition engines: high NOx reduction achieved at low load with hydro-treated vegetable oil," SAE Technical Paper2011.

[203]J. Heikkilä , M. Happonen, T . Murtonen, K. Lehto, T. Sarjovaara, M. Larmi, et al., "Study of Miller timing on exhaust emissions of a hydrotreated vegetable oil (HVO)- fuelled diesel engine," Journal of the Air & Waste Management Association, vol. 62, pp. 1305-1312, 2012.

[204]C. Wang, R. Daniel, and X. Ma, "Comparison of Gasoline (ULG), 2, 5-Dimethylfuran (DMF) and Bio-Ethanol in a DISI Miller Cycle with Late Inlet Valve Closing Time," SAE Technical Paper2012.

[205]W. Gottschalk, U. Lezius, and L. Mathusall, "Investigations on the potential of a variable Miller cycle for SI knock control," SAE Technical Paper2013.

[206]M.L.Birt and G. W . Davis, "Developing Best Available Technology in a Flex-Fuel Snowmobile by Using a Lean-Burn Miller Cycle," SAE Technical Paper2013.

[207]C.A. Rinaldini, E. Mattarelli, and V. I. Golovitchev, "Potential of the Miller cycle on a HSDI diesel automotive engine," Applied Energy, vol. 112, pp. 102-119, 2013.

[208]G. Gonca, B. Sahin, and Y. Ust, "Performance maps for an air-standard irreversible Dual–Miller cycle (DMC) with late inlet valve closing (LIVC) version," Energy, vol. 54, pp. 285-290, 2013.

[209]C. Verraes, M. Uyttendaele, A. Clinquart, G. Daube, M. Sindic, D. Berkvens, et al., "Microbiological safety and quality aspects of the short supply chain: SWOT analysis of the Belgian case study," British Food Journal, vol. 117, pp. 2250-2264, 2015.

[210]J. Benajes, S. Molina, R. Novella, and E. Belarte, "Evaluation of massive exhaust gas recirculation and Miller cycle strategies for mixing-controlled low temperature combustion in a heavy-duty diesel engine," Energy, vol. 71, pp. 355-366, 2014.

[211]C. Zhao, Yu, G., Yang, J., Bai, M. et al., "Achievement of Diesel Low Temperature Combustion through Higher Boost and EGR Control Coupled with Miller Cycle," SAE Technical Paper vol. 2015-01-0383, 2015.

[212]T. Li, Y. Gao, J. Wang, and Z. Chen, "The Miller cycle effects on improvement of fuel economy in a highly boosted, high compression ratio, direct-injection gasoline engine: EIVC vs. LIVC," Energy Conversion and Management, vol. 79, pp. 59-65, 2014.

[213]R. Verschaeren, W. Schaepdryver , T . Serruys, M. Bastiaen, L. Vervaeke, and S. Verhelst, "Experimental study of NO x reduction on a medium speed heavy duty diesel engine by the application of EGR (exhaust gas recirculation) and Miller timing," Energy, vol. 76, pp. 614-621, 2014.

[214]G. Gonca, B. Sahin, A. Parlak, Y. Ust, V. Ayhan, İ. Cesur , et al., "The effects of steam injection on the performance and emission parameters of a Miller cycle diesel engine," Energy, vol. 78, pp. 266-275, 2014.

[215]G. Gonca, B. Sahin, Y. Ust, A. Parlak, and A. Safa, "Comparison of steam injected diesel engine and miller cycled diesel engine by using two zone combustion model," Journal of the Energy Institute, vol. 88, pp. 43-52, 2015.

[216]S. Birch, "Audi evolves the Miller cycle in its new 2.0-L spark-ignition engine," SAE Technical Paper, 2015.

[217]G. Gonca, B. Sahin, A. Parlak, Y. Ust, V. Ayhan, İ. Cesur , et al., "Theoretical and experimental investigation of the Miller cycle diesel engine in terms of performance and emission parameters," Applied Energy, vol. 138, pp. 11-20, 2015.

[218]G.Frankle, "Potential for Reducing Internal Engine Emissions in Modern Commercial Vehicle Diesel Engines," ACEA, Jul, pp. 1-2, 1996.

[219]W. T. Toutant, "THE WORTHINGTON-JUNKERS FREE PISTON AIR COMPRESSOR," Journal of the American Society for Naval Engineers, vol. 64, pp. 583-594, 1952.

[220]C. McMullen, “PERFORMANCE OF FREE PISTON GAS GENERATORS," SAE Technical Paper vol. 540001, 1954.

[221]Chengqian, Yaodong, Boru, Application of Miller cycle with turbocharger and ethanol to reduce NOx and particulates emissions from diesel engine – A numerical approach with model validations, Applied Thermal Engineering 150(2019)904-911

[222]O.A. Ozsoysal Heat loss as a percentage of fuel’s energy in air standard Otto and Diesel cycles Energy Convers Manage, 47 (2006), pp. 1051-1062

[223]R. D. Matthews, "Relationship of brake power to various energy efficiencies and other engine parameters: the efficiency rule," International Journal of Vehicle Design, vol. 4, pp. 491-500, 1983

[224]K. Hidemasa, O. Yuichi, H. Yoshihiro, N. Kiyomi, and A. Kosuke, "Free-piston type Generator (I)," Japan Patent JP2012202385A, 2012.

[225]"Ricardo Wave Help," WaveBuild 2013.3 ed, 2014.

[226]G. P. Merker, C. Schwarz, G. Stiesch, and F. Otto, Simulating Combustion: Springer, 2006.

[227]K. Z. Mendera, A. Spyra, and M. Smereka, "Mass Fraction Burned Analysis," Journal of KONES Internal Combustion Engine 2002, 2002.

[228]D. Sandoval and J. B. Heywood, "An Improved Friction Model for Spark-Ignition Engines," SAE Technical Paper 2003-01-0725, 2003.

[229]W. Arshad, "A Low-Leakage Linear Transverse-Flux Machine for a Free-Piston Generator," Elektrotekniska system, Stockholm, 2003.

[230]K. Knaus, J. Häberlein, G. Becker, and H. Rosskamp, "A New High-Performance Four-Stroke Engine for All-Position Use in Hand-Held Power Tools," SAE Technical Paper vol. 2004-32-0075, 2004.

[231]C. F. Taylor, The Internal Combustion Engine in Theory and Practice: Combustion, Fuels, Materials, Design vol. 2: The M.I.T. Press, 1985.

[232]J. L. Mao, Z. X. Zuo, and H. H. Feng, "Parameters coupling designation of diesel free-piston linear alternator," Applied Energy, vol. 88, pp. 4577-4589, Dec 2011.

[233]A. Cosic, "Analysis of a Novel Transverse Flux Machine with a Tubular Cross-section for Free Piston Energy Converter Application," KTH School of Electrical Engineering, 2010.

[234]W. M. Arshad, T. Bäckström, P. Thelin, and C. Sadarangani, "Integrated Free-Piston Generators: An Overview," 2002.

[235]G. P. Blair, Design and Simulation of Two-Stroke Engines. Warrendale, PA: SAE Inc., 1996.

[236]C. Park, Y. Choi, C. Kim, S. Oh, G. Lim, Y. Moriyoshi Performance and exhaust emission characteristics of a spark ignition engine using ethanol and ethanol-reformed gas Fuel, 89 (8) (2010), pp. 2118-2125

[237]S. Kumar, J.H. Cho, J. Park, I. Moon Advances in diesel–alcohol blends and their effects on the performance and emissions of diesel engines Renewable and Sustainable Energy Reviews, 22 (2013), pp. 46-72

[238]M. Canakci, A.N. Ozsezen, E. Alptekin, M. Eyidogan Impact of alcohol–gasoline fuel blends on the exhaust emission of an SI engine Renewable Energy, 52 (2013), pp. 111-117

[239]W.D. Hsieh, R.H. Chen, T.L. Wu, T.H. Lin Engine performance and pollutant emission of an SI engine using ethanol–gasoline blended fuels Atmospheric Environment, 36 (3) (2002), pp. 403-410

[240]P. Bielaczyc, A. Szczotka, J. Woodburn The effect of various gasoline–ethanol blends on exhaust emissions and fuel consumption of an unmodified light-duty si vehicle SAE Technical Paper (2011), pp. 24-0177

[241]X. Wu, R. Daniel, G. Tian, H. Xu, Z. Huang, D. Richardson Dual-injection: the flexible, bi-fuel concept for spark-ignition engines fueled with various gasoline and biofuel blends Applied Energy, 88 (7) (2011), pp. 2305-2314

[242]R.H. Chen, L.B. Chiang, M.H. Wu, T.H. Lin Gasoline displacement and NOx reduction in an SI engine by aqueous alcohol injection Fuel, 89 (3) (2010), pp. 604-610

[243]H. Oh, C. Bae, K. Min Spray and combustion characteristics of ethanol blended gasoline in a spray guided DISI engine under lean stratified operation SAE International Journal of Engines, 3 (2) (2010), pp. 213-222

[244]D. Turner, H. Xu, R.F. Cracknell, V. Natarajan, X. Chen Combustion performance of bio-ethanol at various blend ratios in a gasoline direct injection engine Fuel, 90 (5) (2011), pp. 1999-2006

[245]Masum, B., Masjuki, H., Kalam, M., Rizwanul Fattah, I., Palash, S. and Abedin, M., 2013. Effect of ethanol–gasoline blend on NOx emission in SI engine. Renewable and Sustainable Energy Reviews, 24, pp.209-222.

[246]Achten, Peter A. J. "A Review of Free Piston Engine Concepts." SAE Transactions, vol. 103, SAE International, 1994, pp. 1836–47, http://www.jstor.org/stable/44632919.

[247]H.S. Yücesu, T. Topgül, C. Çinar, M. Okur Effect of ethanol–gasoline blends on engine performance and exhaust emissions in different compression ratios Applied Thermal Engineering, 26 (17–18) (2006), pp. 2272-2278

[248]Szybist J, Foster M, Moore WConfer K, Youngquist A, and Wagner R, Investigation of knock limited compression ratio of ethanol gasoline blends. SAE Technical Paper; 2010. p. 01–0619.

[249]J. Zheng, J. Wang, B. Wang, Z. Huang Effect of the compression ratio on the performance and combustion of a natural-gas direct-injection engine Proceedings of the Institution of Mechanical Engineers, Part D: Journal of Automobile Engineering, 223 (1) (2009), pp. 85-98

[250]M. Al-Baghdadi Measurement and prediction study of the effect of ethanol blending on the performance and pollutants emission of a four-stroke spark ignition engine Proceedings of the Institution of Mechanical Engineers, Part D: Journal of Automobile Engineering, 222 (5) (2008), pp. 859-873

[251]M.B. Celik Experimental determination of suitable ethanol–gasoline blend rate at high

compression ratio for gasoline engine Applied Thermal Engineering, 28 (5–6) (2008), pp. 396-404

[252]M. Koç, Y. Sekmen, T. Topgül, H.S. Yücesu The effects of ethanol–unleaded gasoline blends on engine performance and exhaust emissions in a spark-ignition engine Renewable Energy, 34 (10) (2009), pp. 2101-2106

[253]Melo TCCd, G.B. Machado, C.R.P. Belchior, M.J. Colaço, J.E.M. Barros, E.J. de Oliveira, et al. Hydrous ethanol–gasoline blends—Combustion and emission investigations on a Flex-Fuel engine Fuel, 97 (2012), pp. 796-804

[254]A. Keskin, M. Gürü The effects of ethanol and propanol additions into unleaded gasoline on exhaust and noise emissions of a spark ignition engine Energy Sources, Part A: Recovery, Utilization, and Environmental Effects, 33 (23) (2011), pp. 2194-2205

[255]Gomes P, Ecker R, Kulzer A, Kufferath A. Study on boosted direct injection si combustion with ethanol blends and the influence on the ignition system. SAE Technical Paper; 2011. p. 36–0196.

[256]X. Pang, Y. Mu, J. Yuan, H. He Carbonyls emission from ethanol-blended gasoline and biodiesel-ethanol-diesel used in engines Atmospheric Environment, 42 (6) (2008), pp. 1349-1358

[257]S. Kumar, N. Singh, R. Prasad Anhydrous ethanol: a renewable source of energy Renewable and Sustainable Energy Reviews, 14 (7) (2010), pp. 1830-1844

[258]G. Najafi, B. Ghobadian, T. Tavakoli, D.R. Buttsworth, T.F. Yusaf, M. Faizollahnejad Performance and exhaust emissions of a gasoline engine with ethanol blended gasoline fuels using artificial neural network Applied Energy, 86 (5) (2009), pp. 630-639

[259]W.D. Hsieh, R.H. Chen, T.L. Wu, T.H. Lin Engine performance and pollutant emission of an SI engine using ethanol–gasoline blended fuels Atmospheric Environment, 36 (3) (2002), pp. 403-410

[260]Al-Farayedhi A, Al-Dawood, A., Gandhidasan, P. Effects of blending crude ethanol with

unleaded gasoline on exhaust emissions of SI engine. SAE Technical Paper 2000-01-2857; 2000.

[261]E. Zervas, X. Montagne, J. Lahaye Emissions of regulated pollutants from a spark ignition engine. Influence of fuel and air/fuel equivalence ratio Environmental Science and Technology, 37 (14) (2003), pp. 3232-3238

[262]Y.-C. Yao, J.-H. Tsai, H.-L. Chiang Effects of ethanol-blended gasoline on air pollutant emissions from motorcycle Science of The Total Environment, 407 (19) (2009), pp. 5257-5262

[263]R.C. Costa, J.R. Sodré Hydrous ethanol vs. gasoline–ethanol blend: engine performance and emissions Fuel, 89 (2) (2010), pp. 287-293

[264]Gravalos I, Moshou D, Gialamas T, Xyradakis P, Kateris D, Tsiropoulos Z. Performance and Emission Characteristics of Spark Ignition Engine Fuelled with Ethanol and Methanol Gasoline Blended Fuels. Alternative Fuel 2011.

[265]M.K. Balki, C. Sayin, M. Canakci The effect of different alcohol fuels on the performance, emission and combustion characteristics of a gasoline engine Fuel (2012)

[266]C.A.C. Alzate, O.J.S. Toro Energy consumption analysis of integrated flowsheets for production of fuel ethanol from lignocellulosic biomass Energy, 31 (13) (2006), pp. 2447-2459

[267]W.Y. Lin, Y.Y. Chang, Y.R. Hsieh Effect of ethanol–gasoline blends on small engine generator energy efficiency and exhaust emission Journal of the Air and Waste Management Association, 60 (2) (2010), pp. 142-148

[268]G. Broustail, F. Halter, P. Seers, G. Moréac, C. Mounaim-Rousselle Comparison of regulated and non-regulated pollutants with iso-octane/butanol and iso-octane/ethanol blends in a port-fuel injection Spark-Ignition engine Fuel, 94 (2012), pp. 251-261

[269]H.-H. Yang, T.-C. Liu, C.-F. Chang, E. Lee Effects of ethanol-blended gasoline on emissions of regulated air pollutants and carbonyls from motorcycles Applied Energy, 89 (1) (2012), pp. 281-286

[270]I. Schifter, L. Diaz, R. Rodriguez, J.P. Gómez, U. Gonzalez Combustion and emissions

behavior for ethanol–gasoline blends in a single cylinder engine Fuel, 90 (12) (2011), pp. 3586-3592

[271]Y. Zhuang, G. Hong Primary investigation to leveraging effect of using ethanol fuel on reducing gasoline fuel consumption Fuel, 105 (2013), pp. 425-431

[272]C. Cooper, F. Alley Air pollution control: a design approach 1994 PWS Inc, Boston (1986)

[273]F. Normann, K. Andersson, B. Leckner, F. Johnsson Emission control of nitrogen oxides in the oxy-fuel process Progress in Energy and Combustion Science, 35 (5) (2009), pp. 385-397

[274]AH. Lefebvre The role of fuel preparation in low-emission combustion ASME Journal of Engineering for Gas Turbines and Power, 117 (1995), pp. 617-654

[275]F.N. Alasfour NOx Emission from a spark ignition engine using 30% Iso-butanol–gasoline blend: Part 1—Preheating inlet air Applied Thermal Engineering, 18 (5) (1998), pp. 245-256

[276]J.J. Chong, A. Tsolakis, S.S. Gill, K. Theinnoi, S.E. Golunski Enhancing the NO2/NOx ratio in compression ignition engines by hydrogen and reformate combustion, for improved aftertreatment performance International Journal of Hydrogen Energy, 35 (16) (2010), pp. 8723-8732

[277]I.M. Rizwanul Fattah, H.H. Masjuki, A.M. Liaquat, R. Ramli, M.A. Kalam, V.N. Riazuddin Impact of various biodiesel fuels obtained from edible and non-edible oils on engine exhaust gas and noise emissions Renewable and Sustainable Energy Reviews, 18 (2013), pp. 552-567

[278]K. Varatharajan, M. Cheralathan Influence of fuel properties and composition on NOx emissions from biodiesel powered diesel engines: a review Renewable and Sustainable Energy Reviews, 16 (6) (2012), pp. 3702-3710

[279]Heywood JB. Internal combustion engine fundamentals. New York: McGraw-Hill Book Co; 1988.

[280]C.T. Bowman Kinetics of pollutant formation and destruction in combustion Progress in Energy and Combustion Science, 1 (1) (1975), pp. 33-45

[281]Fenimore CP, Formation of nitric oxide in premixed hydrocarbon flames. In: Proceedings of

the 13th international symposium on combustion. The Combustion Institute; 1971. p. 373–80.

[282]Fluent Inc. Prompt NOx formation; 2001. Available from: 〈http://combust.hit.edu.cn:8080/fluent/Fluent60_help/html/ug/node582.htm〉.

[283]J.A. Miller, C.T. Bowman Mechanism and modeling of nitrogen chemistry in combustion Progress in Energy and Combustion Science, 15 (4) (1989), pp. 287-338

[284]Gardiner WC. Gas-Phase Combustion Chemistry. 175, Fifth Avenue, New York, NY 10010, USA: Springer-Verlag New York, Inc.; 2000.

[285]W. Yang, W. Blasiak Mathematical modelling of NO emissions from high-temperature air combustion with nitrous oxide mechanism Fuel Processing Technology, 86 (9) (2005), pp. 943-957

[286]M.A. Galbiati, A. Cavigiolo, A. Effuggi, D. Gelosa, R. Rota Mild Combustion For Fuel-Nox Reduction Combustion Science and Technology, 176 (7) (2004), pp. 1035-1054

[287]Wang, Y., Lin, L., Roskilly, A., Zeng, S., Huang, J., He, Y., Huang, X., Huang, H., Wei, H., Li, S. and Yang, J., 2007. An analytic study of applying Miller cycle to reduce NOx emission from gasoline engine. Applied Thermal Engineering, 27(11-12), pp.1779-1789.

[288]Y. Moskov, "Trainable Mathematical Model of Fuel Supply of a Ship Diesel Engine as an Element of a Synergetic System," 2020 International Conference Automatics and Informatics (ICAI), 2020, pp. 1-3, doi: 10.1109/ICAI50593.2020.9311352.

[289]Y. Moskov, "Trainable Mathematical Model of Gas Exchange of a Ship Diesel Engine as an Element of a Synergetic System," 2020 International Conference Automatics and Informatics (ICAI), 2020, pp. 1-4, doi: 10.1109/ICAI50593.2020.9311356.

[290]J. Moskov, “Mathematical model of turbocharger as part of intelligent system component designed for technical operation of diesel engines and for training”, 2018 IOP Conference Series: Earth and Environmental Science 172(1),012006

[291]H. Milushev, “Advanced mathematical model of slow speed diesel engine”, 2021 International Conference Automatics and Informatics (ICAI), 2021

[292]G. Enchev, “Analysis of gas exchange of marine diesel engine by equilibration and minimization of deviations in the equilibrium states”, 2021 International Conference Automatics and Informatics (ICAI), 2021

[293]H. Milushev, “Digital evaluation of the accuracy and sensitivity of a mathematical model of a slow speed marine diesel engine”, 2021 International Conference Automatics and Informatics (ICAI), 2021

[294]Tang, Xiaoguo, et al. “Ford P2000 Hydrogen Engine Dynamometer Development.” SAE Transactions, vol. 111, SAE International, 2002, pp. 631–42, http://www.jstor.org/stable/44743090.

[295]SAFARI, H., JAZAYERI, S. and EBRAHIMI, R., 2009. Potentials of NOX emission reduction methods in SI hydrogen engines: Simulation study. International Journal of Hydrogen Energy, 34(2), pp.1015-1025.

[296]Subramanian, V., Mallikarjuna, J. and Ramesh, A., 2007. Intake charge dilution effects on control of nitric oxide emission in a hydrogen fueled SI engine. International Journal of Hydrogen Energy, 32(12), pp.2043-2056.

[297]Hohenberg Günter F. Advanced approaches for heat transfer calculations. SAE technical paper, No. 790825; 1979. http://dx.doi.org/10.4271/790825.

[298]M. Z. Saiful Azrin, "Modelling, Simulation and Implementation of Rectangular Commutation for Starting of Free-Piston Linear Generator," Masters Of Science In Electrical And Electronic Engineering, Electrical and Electronic Engineering Department, Universiti Teknologi PETRONAS, 2007.

[299]R. Mikalsen, "An Investigation into the Free-Piston Engine Concept and its Potential for High Efficiency and Low Emissions Power Generation," Doctor of Philosophy, Newcastle University, 2008.

Appendix

Parameter	Value
Bore	40 mm
Stroke	25 mm
Swept volume	31.4 cc
Geometric compression ratio	9.5:1
Maximum Valve lift	3.2 mm
Intake valve diameter	14.5 mm
Exhaust valve diameter	14.5 mm

Table A-1: The engine specifications of the 31cc version of the Stihl 4MIX engine

Parameter	Value
Capacity	65cc
Bore	50mm
Stroke	33mm
Geometric compression ratio	9.5:1
Valve lift	4.0mm
Intake valve diameter	20mm
Exhaust valve diameter	18mm
Max. Power	2.3 kW @ 7200rpm

Table A-2: The 65cc version of the Stihl 4MIX engine selected for the design